A new transform approach to biharmonic boundary value problems in circular domains with applications to Stokes flows

A thesis presented for the degree of

Doctor of Philosophy of the University of London

and the

Diploma of Imperial College

by

Elena Louca

Department of Mathematics

Imperial College

180 Queen's Gate, London SW7 2BZ

NOVEMBER 30, 2016

I certify that this thesis, and the research to which it refers, are the product of my own work, and that any ideas or quotations from the work of other people, published or otherwise, are fully acknowledged in accordance with the standard referencing practices of the discipline.

Elena Louca

Copyright

The copyright of this thesis rests with the author and is made available under a Creative Commons Attribution Non-Commercial No Derivatives licence. Researchers are free to copy, distribute or transmit the thesis on the condition that they attribute it, that they do not use it for commercial purposes and that they do not alter, transform or build upon it. For any reuse or redistribution, researchers must make clear to others the licence terms of this work.

Abstract

In this thesis, we present a new transform approach for solving biharmonic boundary value problems in two-dimensional polygonal and circular domains. Our approach provides a unified general approach to finding quasi-analytical solutions to a wide range of problems in Stokes flows and plane elasticity.

We have chosen to analyze various Stokes flow problems in different geometries which have been solved using other techniques and present our transform approach to solve them. Our approach adapts mathematical ideas underlying the Unified transform method, also known as the Fokas method, due to Fokas and collaborators in recent years.

We first consider Stokes flow problems in polygonal domains whose boundaries consist of straight line edges. We show how to solve problems in the half-plane subject to different boundary conditions along the real axis and we are able to retrieve analytical results found using other techniques. Next, we present our transform approach to solve for a flow past a periodic array of semi-infinite plates and for a periodic array of point singularities in a channel, followed by a brief discussion on how to systematically solve problems in more complex channel geometries.

Next, we show how to solve problems in circular domains whose boundaries consist of a combination of straight line and circular edges. We analyze the problems of a flow past a semicircular ridge in the half-plane, a translating and rotating cylinder above a wall and a translating and rotating cylinder in a channel.

Acknowledgements

I would like to thank my supervisor, Darren Crowdy, for the guidance and supervision. I wish to thank the Leverhulme Trust and the Department of Mathematics, Imperial College London for funding my studies. I would like to thank Vikas Krishnamurthy, Christopher Green and Samuel Brzezicki for their support and useful discussions. I acknowledge helpful discussions with Jonathan Marshall. Finally, I would like to thank Everett Kropf for discussions on the numerical implementation of the transform method.

Table of contents

Abstract **4**

1 Introduction **15**
1.1 Methods and techniques 16
1.1.1 The Fourier transform 16
1.1.2 The Mellin transform 17
1.1.3 The Wiener-Hopf method 17
1.1.4 The method of images 18
1.1.5 Bipolar coordinates 19
1.1.6 Conformal mapping 20
1.1.7 Streamfunction and Papkovich-Fadle eigenfunctions 20
1.1.8 Boundary integral method 21
1.2 The Unified transform method 21
1.3 Structure of the thesis 22

2 The Unified transform method **23**
2.1 The transform method for polygonal domains 23
2.1.1 The global relations 27
2.1.2 Unbounded polygonal regions 28
2.2 The transform method for circular domains 28
2.2.1 Transform pair for interior of unit disc 31
2.2.2 Transform pair for exterior of unit disc 32
2.2.3 Domains with both straight and circular edges 33
2.3 Summary 33

3 Complex variable formulation of Stokes flows **35**
3.1 Stokes equations in two dimensions 35
3.1.1 Velocity 37
3.1.2 Pressure and vorticity 38
3.1.3 Fluid stress 39
3.1.4 Force 41
3.1.5 Torque 42

3.1.6 Remark . . . 42
3.2 Goursat functions representations for flows of interest . . . 42
3.2.1 Pressure-driven flow in a channel . . . 43
3.2.2 Shear flow . . . 44
3.2.3 Stagnation point flow . . . 45
3.3 Fundamental singularities of Stokes flows . . . 46
3.3.1 Stokeslet (point force) . . . 47
3.3.2 Force dipole (stresslet) . . . 47
3.3.3 Force quadrupole . . . 47
3.3.4 Source/sink . . . 48
3.3.5 Rotlet (rotational torque) . . . 48
3.3.6 Source dipole . . . 48
3.3.7 Source quadrupole . . . 48

4 Stokes flows in the half-plane **49**
4.1 Introduction . . . 49
4.2 A point stresslet above a no-slip boundary . . . 51
4.2.1 Problem formulation . . . 51
4.2.2 Transform approach . . . 52
4.2.3 Method of images . . . 56
4.3 A point stresslet above a boundary with mixed boundary conditions . . . 57
4.3.1 Problem formulation . . . 57
4.3.2 Problem I . . . 59
4.3.3 Problem II . . . 65
4.3.4 Conformal mapping (full problem) . . . 72
4.4 Summary . . . 73

5 Shear flow past a periodic array of semi-infinite plates **75**
5.1 Introduction . . . 75
5.2 The slip length λ . . . 77
5.3 Longitudinal flow problem . . . 78
5.3.1 Domain splitting: left and right semi-strips . . . 79
5.3.2 Boundary conditions . . . 81
5.3.3 Spectral analysis . . . 82
5.3.4 Solution scheme and function representation . . . 84
5.3.5 Comparison with Jeong [54] and Luchini *et al.* [78] . . . 87
5.3.6 Conformal geometric approach . . . 88
5.4 Transverse flow problem . . . 90
5.4.1 Domain splitting: left and right semi-strips . . . 91
5.4.2 Boundary conditions . . . 94
5.4.3 Spectral analysis . . . 96
5.4.4 Solution scheme and function representation . . . 99

5.4.5 Comparison with solution of Jeong [54] . . . 102
5.5 Summary . . . 103

6 Periodic array of point singularities in a channel 106
6.1 Introduction . . . 106
6.2 Problem formulation . . . 107
6.3 Goursat functions and transform representation . . . 108
6.4 Boundary conditions . . . 110
6.5 Spectral analysis . . . 111
6.6 Solution scheme . . . 113
6.6.1 Function representations . . . 115
6.6.2 Formulation of a linear system . . . 116
6.7 Comparison to an alternative method . . . 117
6.8 Summary . . . 117

7 Applications in polygonal domains 119
7.1 Introduction . . . 119
7.2 Flow in a 'partitioned' channel (or symmetric channel divider) . . . 121
7.3 Flow in an asymmetric channel divider . . . 122
7.4 Flow through a shunt between two channels . . . 124
7.5 Flow past a plate located midway in a channel . . . 125
7.6 Summary . . . 127

8 Stagnation point flow past a semicircular ridge 128
8.1 Introduction . . . 128
8.2 Problem formulation . . . 129
8.3 Davis & O'Neill's [30] solution . . . 130
8.4 Approach I: Transform method for circular domains . . . 131
8.4.1 Goursat functions and transform representation . . . 131
8.4.2 Boundary conditions . . . 133
8.4.3 Spectral analysis . . . 134
8.4.4 Solution scheme . . . 135
8.5 Approach II: Transform method for polygons . . . 139
8.5.1 Conformal mapping and function representation . . . 139
8.5.2 Boundary conditions . . . 141
8.5.3 Spectral analysis . . . 142
8.5.4 Solution scheme . . . 143
8.6 Results and comparison to Davis & O'Neill's solution [30] . . . 145
8.7 Summary . . . 147

9 A translating and rotating cylinder near a wall 155
9.1 Introduction . . . 155
9.2 Problem formulation . . . 156
9.3 Jeffrey & Onishi's [53] solution . . . 157
9.4 Goursat functions and transform representation . . . 158
9.5 Boundary conditions . . . 160
9.6 Spectral analysis . . . 161
9.6.1 Fourier transform . . . 161
9.6.2 Mellin-type transforms . . . 162
9.7 Solution scheme . . . 164
9.7.1 Function representation . . . 164
9.7.2 Formulation of the linear system . . . 165
9.8 Computation of the mobility matrix . . . 167
9.9 Comparison to Jeffrey & Onishi's [53] solution . . . 168
9.10 Summary . . . 168

10 A translating and rotating cylinder in a channel 173
10.1 Introduction . . . 173
10.2 Problem formulation . . . 174
10.3 Goursat functions and transform representation . . . 174
10.4 Boundary conditions . . . 177
10.5 Spectral analysis . . . 178
10.5.1 Fourier transforms . . . 178
10.5.2 Mellin-type transforms . . . 180
10.6 Solution scheme . . . 182
10.6.1 Function representation . . . 183
10.6.2 Formulation of the linear system . . . 184
10.7 Computation of the mobility matrix . . . 187
10.8 Summary . . . 187

11 Conclusion 189

A Spectral representation of the Weierstrass $\mathcal{P}$-function 193
A.1 The Weierstrass $\mathcal{P}$-function . . . 193
A.2 Problem formulation and solution . . . 194
A.3 Alternative solution . . . 199
A.4 Comparison of the two methods . . . 201
A.5 Summary . . . 201

B Calculation of the torque on a cylinder 202

List of Figures

2.1 A point z' on a slit of finite length on the real axis and point z in the upper half-plane. . . . 24
2.2 A point z' on a slit of finite length on the 'rotated' with angle χ real axis and point z in the half-plane to the left of the slit. . . . 25
2.3 A convex polygon P formed from the intersection of $N = 3$ half-planes with angles χ_1, χ_2, χ_3 respectively. . . . 26
2.4 The fundamental contour for circular arc edges with $0 < r < 1$. . . . 29
2.5 A point z' on boundary of the disc and point z in its interior. . . . 29
2.6 Contours L_- and L_+ in the spectral k-plane used to establish (2.18) . . . 31
2.7 The contours $\mathcal{L}_+$ and $\mathcal{L}_-$ . . . 31

3.1 Pressure-driven flow . . . 43
3.2 Shear flow . . . 44
3.3 Stagnation point flow . . . 45
3.4 A collection of some Stokes flow singularities and their local streamlines. . . 46

4.1 Problem configuration: a point stresslet at point z_0 above a wall. . . . 51
4.2 Schematic of the spectral functions along the real axis. . . . 53
4.3 Problem configuration: a point stresslet at z_0 near a boundary with mixed boundary conditions. . . . 58
4.4 Conformal mapping from the upper unit ζ-disc (left) to the unit η-disc (centre) and finally to the fluid region in the upper half-plane (right). The correspondence of the boundaries is illustrated by the solid and dashed lines. . 63
4.5 Schematic of the spectral functions along the real axis. . . . 67

5.1 Shear flow past a periodic array of semi-infinite flat plates in the longitudinal direction: the boundary value problem to be solved is for a harmonic field. This problem was solved by Luchini *et al.* [78] and Jeong [54]. . . . 76
5.2 Shear flow past a periodic array of semi-infinite flat plates in the transverse direction: the boundary value problem to be solved is for a biharmonic field. This problem was solved by Luchini *et al.* [78] and Jeong [54]. . . . 76
5.3 Interpretation of the slip length λ: the fictitious distance below the surface where the no-slip boundary condition would be satisfied. . . . 77

5.4 Schematic of a single period of the longitudinal problem of shear flow past an array of semi-infinite flat plates (extending indefinitely into $y \to \pm\infty$). The no-slip walls of this period window are defined for $x < 0$ and $y = \pm h/2$. The velocity $w(x, y)$, which is into the page (direction is denoted by the two circles), tends to a uniform shear as $x \to +\infty$ and vanishes as $x \to -\infty$. 79
5.5 Domain splitting into two semi-strips and related spectral functions. (the common edge at $x = 0$ is shown separately for each sub-problem). 80
5.6 Schematic illustrating the conditions on $\sigma_3(k)$ from different sectors of the complex k-plane. 86
5.7 The sequence of conformal mappings (5.48). 89
5.8 The sequence of conformal mappings (5.49)–(5.50). 89
5.9 Schematic of a single period of the transverse shear flow problem past an array of semi-infinite plates. 92
5.10 The two semi-strips and assignation of the associated spectral functions. In this problem each edge has two associated spectral functions. 94
5.11 Schematic of the points in the spectral k-plane at which information on the spectral functions is available. 101

6.1 Schematic of the configuration: A periodic array of point stresslets placed at points $z = z_0 + nl$, $n \in \mathbb{Z}$ in a two-dimensional channel $-\infty < x < \infty$, $0 \le y \le h$. 107
6.2 The period window $0 \le x \le l$, $0 \le y \le h$ and associated spectral functions. 108
6.3 Schematic of the points in the spectral k-plane at which information on the spectral functions is available. These points coincide with the eigenvalue set associated with the so-called Papkovich-Fadle eigenfunctions in a semi-strip. 115
6.4 A doubly-periodic array of point singularities placed at points $z = z_0 + nl + \mathrm{i}mh$, $n, m \in \mathbb{Z}$. 118

7.1 Problems presented in Chapters 5 and 6 were solved by decomposing the problem domain into semi-strip and rectangular domains. 119
7.2 Stokes flow in a symmetric channel divider driven by pressure gradient. This problem was solved by Jeong [55] using the Wiener-Hopf technique (scalar case). 121
7.3 Domain decomposition for Jeong's [55] problem. 122
7.4 Stokes flow in an asymmetric channel divider driven by the motion of the upper and lower boundaries with prescribed velocities U_1 and U_2 respectively. This problem was solved by Abrahams, Davis & Llewellyn Smith [4]. 123
7.5 Domain decomposition for Abrahams, Davis & Llewellyn Smith's [4] problem. 124

7.6 Stokes flow through a shunt between two channels; the flow is driven by pressure gradient. This problem was solved by Setchi *et al.* [97] for different inlet and outlet fluxes. 124
7.7 Domain decomposition for the one of the problems considered by Setchi *et al.* [97]: For a flow admitting symmetries with respect to $x = 0$ and $y = 0$, it is sufficient to analyze the problem in the two domains only. 125
7.8 Pressure-driven flow past a plate located midway in a channel; this problem was solved by Kim & Chung [67] using a three-part Wiener-Hopf method. . 126
7.9 Domain decomposition for Kim & Chung's [67] problem. 126

8.1 Schematic of the configuration. A stagnation point flow past a plane with a cylindrical ridge with angle of intersection between the two boundaries equal to $\pi/2$. 129
8.2 Conformal mapping from the physical z-plane to the parametric η-plane. Associated spectral functions are also illustrated (η-plane). 139
8.3 Vorticity ω along the circular boundary in terms of parametrization variable s defined in (8.33) computed using our transform approach (I/II). 146
8.4 Pressure p along the circular boundary in terms of parametrization variable of s defined in (8.33)computed using our transform approach (I/II). 147
8.5 Schematic of the configuration. A point swimmer near a semicircular ridge of unit radius. 149
8.6 A stagnation point flow past a plane with a cylindrical trough. The angle of intersection θ between the plane and cylindrical boundaries is $\theta > \pi$ (here $\theta = 3\pi/2$). This problem was solved by Davis & O'Neill [30] for a general angle of intersection. 150
8.7 Domain splitting for analysis using the transform method for circular domains. 151
8.8 Shear flow past a periodic array of bubbles. This problem was solved by Davis & Lauga [28] in the dilute limit $c/l \ll 1$. 152
8.9 Weinel [114] considered a notched plate under tension for a general angle of intrsection between the planar and circular boundaries. (Figure reproduced from [114]). 153
8.10 Problem configuration considered by Atsumi [7]. This author determined the stresses in a plate under tension containing a periodic row of semicircular nodges. (Figure reproduced from [7]). 154
8.11 In another study, Atsumi [6] analyzed the problem of determining the stresses in an infinite strip under tension containing an infinite row of semicircular notches. (Figure reproduced from [6]). 154

9.1 Schematic of the configuration: a translating and rotating cylinder of unit radius centred at $z_0 = \mathrm{i}y_0$, with $y_0 > 1$, above a straight wall. 156

9.2 Comparison between our transform approach and the exact solution by Jeffrey & Onishi [53]: (a) computation of the force $F = F_x$ when cylinder is moving parallel to the wall (for $U = 1$) as a function of the distance from the wall y_0. 169
9.3 Comparison between our transform approach and the exact solution by Jeffrey & Onishi [53]: (b) computation of the force $F = \mathrm{i}F_y$ when the cylinder is moving away from the wall (for $U = \mathrm{i}$) as a function of the distance from the wall y_0. 170
9.4 Comparison between our transform approach and the exact solution by Jeffrey & Onishi [53]: (c) computation of the torque T when the cylinder is in pure rotation (for $\Omega = 1$) as a function of the distance from the wall y_0. . . . 171

10.1 Schematic of the configuration: a translating and rotating cylinder of unit radius centred at z_0 in a channel geometry. 174
10.2 A translating and rotating cylinder centred at z_0 in a wedge geometry. . . . 188

A.1 Schematic of a period window and associated spectral functions. 194
A.2 Conformal mapping from the annulus $\rho < |\zeta| < 1$ in ζ-plane to the period rectangle in the physical z-plane occupying the region $0 \leq x \leq l, 0 \leq y \leq h$. 199

List of Tables

5.1 Evaluation of the longitudinal slip length λ for $h = 2$ and $U = 1$ for different values of the truncation parameter N of the sum (5.42). 87
5.2 Convergence of slip length λ, for $h = 2$ and $U = 1$, computed using (5.112) and by truncating the infinite product (5.113) to M terms. This formula is generated by the Wiener-Hopf method of [54]. 103
5.3 Convergence of slip length λ, for $h = 2$ and $U = 1$, as computed by truncating the sums (5.110) in the new transform approach. 103

Chapter 1

Introduction

In this thesis we shall be considering a variety of biharmonic boundary value problems in circular domains. The biharmonic equation in two dimensions is given by

$$\nabla^4 \psi(x, y) = 0. \tag{1.1}$$

It arises in Stokes flow problems in which case $\psi(x, y)$ is the associated streamfunction (Langlois [69]), as well as in plane elasticity where $\psi(x, y)$ is the associated Airy stress function (Muskhelishvili [86]). The term 'circular domain' refers to a bounded or unbounded, simply- or multiply- connected domain, whose boundary consists of straight or circular edges or a combination of the two. This term is associated to refer to such domains, even if the boundary consists of straight line edges only (e.g. a rectangle), since straight edges can be thought as circular boundaries of zero curvature.

Our focus in this thesis is to present a systematic approach based on the Unified transform method (Fokas [38, 39], Deconinck, Trogdon & Vasan [32]), also known as the Fokas method, for solving Stokes flow problems in polygonal and circular domains. We shall be using the term 'polygonal' to refer to domains whose boundary consists of straight line edges only and the more general term 'circular' to refer to domains whose boundary consists of a combination of straight and circular edges. All Stokes flow problems to be considered in this thesis have been solved using other techniques. It is therefore instructive,

before presenting our transform approach, to give an overview of the main analytical methods and techniques in the literature which have been used to solve Stokes flow problems.

1.1 Methods and techniques

In this section, we present an overview of the main analytical methods for solving biharmonic boundary value problems with main focus on Stokes flow problems, including all techniques which were used to solve the problems to be presented in this thesis.

1.1.1 The Fourier transform

The general approach for solving a partial differential equation, and particularly the biharmonic equation, using this method, is to use the Fourier transform to obtain an ordinary differential equation and then to use the inverse Fourier transform to obtain a representation of the solution. The Fourier transform of an integrable function $f(x)$ defined on $\mathbb{R}$ is given by

$$\hat{f}(\xi) = \int_{-\infty}^{\infty} f(x) e^{\mathrm{i}\xi x} dx. \tag{1.2}$$

The transform of f can be recovered from the inverse Fourier transform, via the inversion formula

$$f(x) = \frac{1}{2\pi} \int_{-\infty}^{\infty} \hat{f}(\xi) e^{-\mathrm{i}\xi x} d\xi. \tag{1.3}$$

Stokes flow problems in the half-plane and in strip/channel geometries, where transform with respect to one variable is required, can be solved using Fourier tranform techniques. Related to the problems to be presented in this thesis, we mention the work by Davis [25] who solved various problems involving distributions of point singularities in a two-dimensional channel using Fourier transforms with respect to the variable along the channel length. Pozrikidis [89], in his monograph, presented a standard Fourier transform analysis of a two-dimensional point singularity in a channel. Crowdy & Davis [20] solved, among others, for point singularities in a channel using standard Fourier transform techniques.

1.1.2 The Mellin transform

The Mellin transform of a function $f(x)$ (Ablowitz & Fokas [1]) is given by

$$\phi(s) = \int_0^\infty x^{s-1} f(x) dx \tag{1.4}$$

and the inverse Mellin transform is

$$f(x) = \frac{1}{2\pi \mathrm{i}} \int_{c-\mathrm{i}\infty}^{c+\mathrm{i}\infty} x^{-s} \phi(s) ds. \tag{1.5}$$

The Mellin transform method can be used to solve problems in wedge geometries. We mention the work by Davis & Crowdy [27] used Mellin transform techniques and obtained analytical results for the dynamics of a circular microswimmer in Stokes flows near an angle of $\pi/2$, as well as in other fractional angles.

1.1.3 The Wiener-Hopf method

The Wiener-Hopf technique is a method first put forward [115] for the solution $f(x)$ of the integral equation on the half-plane

$$\int_0^\infty k(x-y) f(y) dy = g(x), \;\; 0 < x < \infty, \tag{1.6}$$

where $k(x-y)$ is a given difference kernel and $g(x)$ a specified function for the positive real axis $x > 0$; the essence of the method is to extend the given equation into the negative axis $x < 0$ to a similar one for which the "forcing" on the right side for $x < 0$ is unknown. Therefore,

$$\int_0^\infty k(x-y) f(y) dy = \begin{cases} g(x), & 0 < x < \infty, \\ h(x), & -\infty < x < 0, \end{cases} \tag{1.7}$$

where $h(x)$ is unknown. Once the equation is defined over the whole real axis, it is natural to take a Fourier transform with respect to x, with α as the spectral variable. This will then result to a typical Wiener-Hopf functional equation of the form

$$G_+(\alpha) + H_-(\alpha) = F_+(\alpha) K(\alpha), \tag{1.8}$$

where

$$H_-(\alpha) = \int_{-\infty}^{0} h(x)e^{\mathrm{i}\alpha x}dx, \quad F_+(\alpha) = \int_0^{\infty} f(x)e^{\mathrm{i}\alpha x}dx \tag{1.9}$$

and

$$G_+(\alpha) = \int_0^{\infty} g(x)e^{\mathrm{i}\alpha x}dx, \quad K(\alpha) = \int_{-\infty}^{\infty} k(x)e^{\mathrm{i}\alpha x}dx. \tag{1.10}$$

The quantities $H_-(\alpha)$ and $F_+(\alpha)$ are half-range Fourier transforms of the unknown functions $h(x)$ (along the negative real axis) and $f(x)$ (along the positive real axis) respectively, while $G_+(\alpha)$ and $K(\alpha)$ are transforms of known functions. The Wiener-Hopf method relies on being able to factorize $K(\alpha)$ into a product of upper and lower analytic functions in the spectral plane.

The Wiener-Hopf technique, in both scalar and matrix (Noble [87]), has proven very useful when solving mixed boundary value problems for Stokes flows. Richardson [92] considered a two-dimensional pressure-driven fluid flow confined between two parallel stick-slip boundaries which transforms to a uniform flow downstream in response to no-stress boundary conditions and obtained analytical solutions using the Wiener-Hopf method. Luchini [78] used Wiener-Hopf techniques to solve for a shear flow past a periodic array of semi-infinite flat plates. Jeong [54] solved the same boundary value problem with different technical details. Other studies where the Wiener-Hopf method has been employed concern problems in channel dividers: Buchwald & Doran [10] solved the problem of a symmetric channel divider and found the solution of the flow considered using scalar Wiener-Hopf techniques. Abrahams, Davis & Llewellyn-Smith [4] solved for an asymmetric channel divider and obtained a numerical solution using Padé approximant techniques for a matrix Wiener-Hopf system. Other Stokes flow problems which were solved using Wiener-Hopf techniques include the studies by Jeong [55, 56, 57], Jeong & Kim [59, 60, 61], Jeong & Park [62], Kim & Chung [67]. Some of these problems will presented in Chapters 5 and 7.

1.1.4 The method of images

The method of images is a mathematical technique used to solve boundary value problems in certain domains by adding 'images' in the symmetrically extended domain. Therefore,

in certain problems, the addition of these images enforces the required boundary conditions to be satisfied. Blake [8] presented the solution for a point force near a wall using Fourier transforms and obtained the image system required to satisfy the boundary condition along the boundary. More recently, Crowdy & Or [23] present a method of images approach for various point singularities above a wall using complex variable techniques.

1.1.5 Bipolar coordinates

Bipolar coordinates (η, ξ) are a two-dimensional orthogonal coordinate system, such that curves of constant ξ and η are circles that intersect at angles $\pi/2$ (Abramowitz & Stegun [5]). They are defined by

$$x = \frac{c \sinh \xi}{(\cosh \xi - \cos \eta)}, \qquad y = \frac{c \sin \eta}{(\cosh \xi - \cos \eta)}, \tag{1.11}$$

where c is such that the two foci are located at $(-c, 0)$ and $(c, 0)$. These coordinates can be used to solve problems in various geometries, such as

- the exterior of two discs,
- the eccentric annulus,
- a disc and a half-plane,
- half-plane with a semicircular ridge/trough,

as well as other domains which can be mapped to these domains.

There have been many studies in Stokes flow problems, where the bipolar coordinates have been employed. We mention a number of these studies: Dorrepaal & O'Neill [34] solved for a flow past two cylinders which were in contact or not, when the flow direction was perpendicular to the line connecting the centres of the cylinders. Davis & O'Neill [30] considered a stagnation point flow past a ridge or trough with the aim of understanding the separation of the flow near the point of intersection and employed bipolar coordinates to map the fluid domain to a channel geometry and then used Fourier transform techniques.

In another study, Davis & O'Neill [29] solved the problem of a shear flow past a cylinder above a wall using again bipolar coordinates to map the fluid region to a channel geometry and then employ Fourier transform techniques. Jeffrey & Onishi [53] analyzed the problem of a translating and rotating cylinder near a wall and computed forces and torque acting on the cylinder in terms of linear and angular velocities.

1.1.6 Conformal mapping

Conformal mapping (Ablowitz & Fokas [1]) is a useful method in complex variables and analytic functions. For example, if we were to solve Laplace's equation in a given domain in the plane, knowing that the real and imaginary parts of an analytic (complex-differentiable) function satisfy Laplace's equation, it is natural to associate an analytic funtion. Since Laplace's equation is conformally invariant (Ablowitz & Fokas [1]), this implies that to find an expression for the solution in a complicated geometry, it is sufficient to find a conformal mapping from a simpler domain in which the solution can be found.

Although this technique is widely used in potential flow theory, it is not very well used in the literature of Stokes flows problems (in contrast to plane elasticity problems), since the biharmonic equation is not conformally invariant. However, analytical progress can still be made in various geometries. We mention the studies by Crowdy & Samson [24] who presented the solution for flows past a wall with one or two gaps. Philip [88] presented a number of mixed boundary value problems in various geometries. Crowdy [13, 16, 17] presented the solution to Stokes flow problems subject to mixed boundary conditions.

1.1.7 Streamfunction and Papkovich-Fadle eigenfunctions

Streamfunction and Papkovich-Fadle eigenfunctions have extensively been used in the literature for solving Stokes flow problems and they are based on writing series representations for the unknown streamfunction in various geometries and then finding the unknown coefficients using the associated boundary conditions. The Papkovich-Fadle eigenfunctions are eigenfunctions for the biharmonic operator; for special forms of the boundary conditions (those corresponding to so called canonical problems), it is possible to determine the com-

plex expansion coefficients analytically using the biorthogonality conditions among these eigenfunctions (Joseph [64, 65]). Related to the problems to be presented in this thesis, we mention the work by Setchi *et al.* [97] who obtained an analytical solution for Stokes flows through a shunt by matching expansions of Papkovich-Fadle eigenfunctions in rectangular subregions.

1.1.8 Boundary integral method

Although the boundary integral method is a numerical method for solving Stokes flow problems, we have included it in this section, since it is widely used in the literature (Pozrikidis [89]). It is based on use of Green's theorem to obtain an integral equation for the unknown boundary data. Taking the limit as we approach the boundary of the domain, we obtain a linear integral equation for the unknown boundary data whose solution gives the unknown boundary data.

1.2 The Unified transform method

The Unified transform method, known as the Fokas method [38, 39], is a transform method for solving linear and nonlinear integrable partial differential equations introduced by Fokas [39] and developed by Fokas and collaborators during the last twenty years. The Fokas method can be thought as a generalized Fourier transform, since it involves a simultaneous spectral analysis in both x and y variables in contrast to traditional Fourier transform approaches which employ a spectral parameter associated only with the x-variable. A review of the Unified transform method for Laplace's equation in polygonal and circular domains will be given in the next Chapter.

There exists only few studies for biharmonic boundary value problems using the Unified transform method. Crowdy $\&$ Fokas [21] have considered biharmonic boundary value problems in a semi-strip geometry arising in elastostatics. More recently, Crowdy $\&$ Davis [20] have presented the solution to Stokes flow problems in a channel geometry with applications to microswimming. Dimakos $\&$ Fokas [33] have presented a novel integral repre-

sentation of the solution of the biharmonic equation in the interior of a convex polygon.

1.3 Structure of the thesis

This thesis is structured as follows: In Chapter 2, we present an overview of the Unified transform method for polygonal and circular domains. In Chapter 3, we present a complex variable of Stokes flows. In Chapters 4-7, we consider Stokes flow problems in polygonal domains. Specifically, in Chapter 4, we consider two problems in the half-plane: a point singularity above a no-slip wall and a above a boundary with mixed boundary conditions. Next, in Chapter 5, we solve the problem of a shear flow (in both longitudinal and transverse directions) past a periodic array of semi-infinite plates; the material of this chapter forms the content of the paper by Crowdy & Luca [22]. In Chapter 6, we consider a periodic array of point singularities in a channel. We then briefly discuss how to solve Stokes flow problems in more complex channel geometries (Chapter 7). In Chapters 8-10, we solve problems in circular domains: Particularly, we consider the problems of a stagnation point flow past a semicircular ridge (Chapter 8), a translating and rotating cylinder near a wall (Chapter 9) and a translating and rotating cylinder in a channel (Chapter 10).

Chapter 2

The Unified transform method

In this Chapter, we present a review of the Unified transform method, also known as the Fokas method (Fokas [39, 38]) for Laplace's equation in polygonal and circular domains (Fokas & Kapaev [42, 43]). Following recent work by Crowdy [18, 19], we present an alternative derivation of the associated transform pairs, followed by his recent extension of the transform method to simply- and multiply- connected circular domains.

2.1 The transform method for polygonal domains

We begin this section by giving some basic definitions (Ablowitz & Fokas [1]) which we shall refer to from now on. *Laplace's equation* is given by

$$\nabla^2 w(x,y) \equiv \frac{\partial^2 w}{\partial x^2} + \frac{\partial^2 w}{\partial y^2} = 0, \tag{2.1}$$

where function $w(x,y)$ satisfying Laplace's equation is called a *harmonic function*. A function $f(z)$ is *analytic* at a point z_0 if $f(z)$ is differentiable in a neighborhood of z_0 and it is analytic in a domain if it is analytic at every point in the domain. The real and imaginary parts of an analytic function $f(z)$ are harmonic functions. The *Cauchy integral formula* is given by

$$f(z) = \frac{1}{2\pi \mathrm{i}} \oint_{\partial D} \frac{f(z')}{z'-z} dz', \tag{2.2}$$

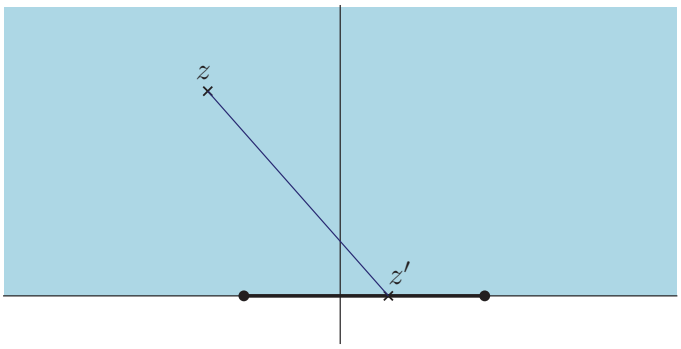

Figure 2.1: A point z' on a slit of finite length on the real axis and point z in the upper half-plane.

which states that the values of an analytic function $f(z)$ on the boundary of a domain D, ∂D, determine the values of $f(z)$ in D.

When solving Laplace's equation $\nabla^2 w(x, y) = 0$ in a given domain, it is natural to associate an analytic function whose real or imaginary part is the unknown function $w(x, y)$. Therefore, finding the associated analytic function is sufficient to give the solution to the harmonic problem considered. Fokas & Kapaev [42, 43] presented a novel method for solving Laplace's equation in polygonal domains. In this section, following Crowdy [18], we present a new and elementary derivation of the transform method for convex polygonal domains first introduced by Fokas & Kapaev [42, 43].

We start with the following geometrical observation. If a point z' lies on some slit of finite length on the real axis and another point z is in the upper half-plane (Figure 2.1), then, clearly,

$$0 < \arg[z - z'] < \pi, \tag{2.3}$$

from which follows that

$$\int_0^\infty e^{\mathrm{i}k(z-z')} dk = \left[\frac{e^{\mathrm{i}k(z-z')}}{\mathrm{i}(z' - z)} \right]_0^\infty = \frac{1}{\mathrm{i}(z' - z)}. \tag{2.4}$$

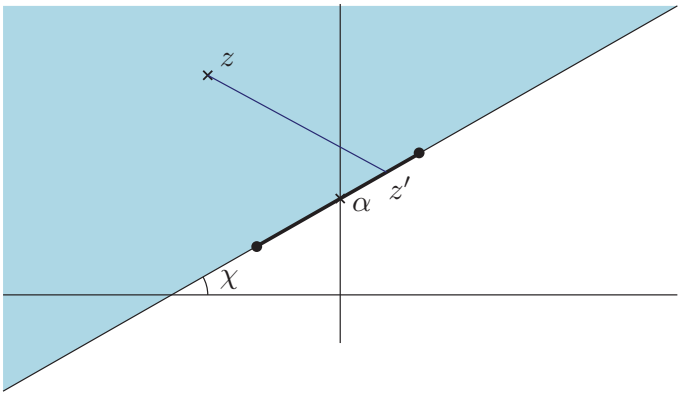

Figure 2.2: A point z' on a slit of finite length on the 'rotated' with angle χ real axis and point z in the half-plane to the left of the slit.

This can equivalently be written as:

$$\frac{1}{z'-z} = \mathrm{i}\int_0^\infty e^{\mathrm{i}k(z-z')}dk, \qquad 0 < \arg[z-z'] < \pi. \tag{2.5}$$

It is straightforward to verify that the upper limit of integration does not have any contribution for the particular choices of z' and z considered above.

Next, we assume that point z' lies again on some other slit of finite length but now rotated with an angle χ with respect to the positive real axis. A point z is now in the half-plane to the left of the slit as one follows its tangent with uniform inclination angle χ, as illustrated in Figure 2.2. The affine transformation given by

$$z' \mapsto e^{-\mathrm{i}\chi}(z'-\alpha), \quad z \mapsto e^{-\mathrm{i}\chi}(z-\alpha), \tag{2.6}$$

where the additive constant α is shown in Figure 2.2, rotates the slit to be on the real axis, and point z to be in the upper half-plane, such that

$$0 < \arg[e^{-\mathrm{i}\chi}(z-\alpha) - e^{-\mathrm{i}\chi}(z'-\alpha)] < \pi. \tag{2.7}$$

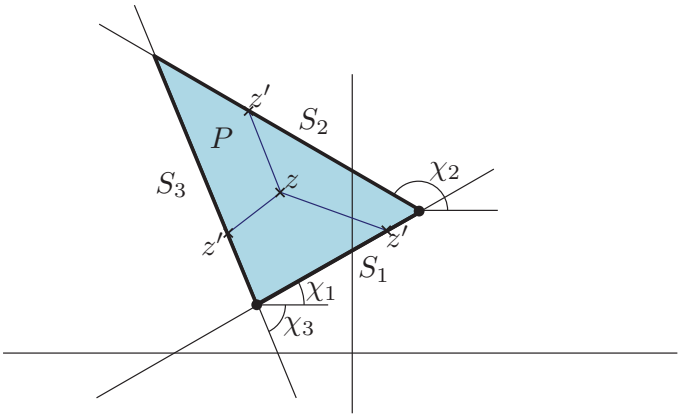

Figure 2.3: A convex polygon P formed from the intersection of $N = 3$ half-planes with angles χ_1, χ_2, χ_3 respectively.

Using (2.5) with (2.6), we can write

$$\frac{1}{e^{-\mathrm{i}\chi}(z'-\alpha) - e^{-\mathrm{i}\chi}(z-\alpha)} = \mathrm{i}\int_0^\infty e^{\mathrm{i}k(e^{-\mathrm{i}\chi}(z-\alpha)-e^{-\mathrm{i}\chi}(z'-\alpha))}dk, \tag{2.8}$$

or, if we cancel constant α and rearrange,

$$\frac{1}{z'-z} = \mathrm{i}\int_0^\infty e^{\mathrm{i}e^{-\mathrm{i}\chi}k(z-z')}e^{-\mathrm{i}\chi}dk. \tag{2.9}$$

It should be noted that this integral expression is valid uniformly for all points z and z' positioning as depicted in Figure 2.2.

The next step is to consider a bounded convex polygon P with N sides $\{S_j | j = 1, ..., N\}$ as shown in Figure 2.3 (for $N = 3$). The bounded convex polygon P can be thought as the intersection of $N = 3$ half-plane regions of the form considered above. We know that for a function $f(z)$ analytic in P, Cauchy's integral formula provides that for $z \in P$,

$$f(z) = \frac{1}{2\pi\mathrm{i}}\oint_{\partial P}\frac{f(z')dz'}{z'-z}. \tag{2.10}$$

If this boundary integral is splitted into a sum over the N sides, then we can write:

$$f(z) = \frac{1}{2\pi \mathrm{i}} \sum_{j=1}^{N} \int_{S_j} f(z') \left[\frac{1}{z'-z} \right] dz'. \tag{2.11}$$

But if side S_j has inclination angle χ_j, we can use (2.9) with $\chi \mapsto \chi_j$, to re-express the Cauchy kernel uniformly for all points z in P and for z' positioned on the respective sides:

$$f(z) = \frac{1}{2\pi \mathrm{i}} \sum_{j=1}^{N} \int_{S_j} f(z') \left[\mathrm{i} \int_0^{\infty} e^{\mathrm{i}e^{-\mathrm{i}\chi_j} k(z-z')} e^{-\mathrm{i}\chi_j} dk \right] dz'. \tag{2.12}$$

Changing the order of integration, this can be written as

$$f(z) = \frac{1}{2\pi} \sum_{j=1}^{N} \int_{\mathcal{L}} \rho_{jj}(k) e^{-\mathrm{i}\chi_j} e^{\mathrm{i}e^{-\mathrm{i}\chi_j} kz} dk, \tag{2.13}$$

where, for integers m, n between 1 and N, the spectral matrix is defined to be given by

$$\rho_{mn}(k) \equiv \int_{S_n} f(z') e^{-\mathrm{i}e^{-\mathrm{i}\chi_m} kz'} dz', \tag{2.14}$$

and with $\mathcal{L} = [0, \infty)$ defined to be the fundamental contour for straight line edges. In summary, the transform pair for polygonal domains can be stated as

$$\begin{cases} f(z) = \frac{1}{2\pi} \sum_{j=1}^{N} \int_{\mathcal{L}} \rho_{jj}(k) e^{-\mathrm{i}\chi_j} e^{\mathrm{i}e^{-\mathrm{i}\chi_j} kz} dk, \\ \rho_{jj}(k) = \int_{S_j} f(z') e^{-\mathrm{i}e^{-\mathrm{i}\chi_j} kz'} dz', \end{cases} \tag{2.15}$$

2.1.1 The global relations

The elements of the spectral matrix, also known as spectral functions, have important features. We observe that,

$$\sum_{n=1}^{N} \rho_{mn}(k) = \sum_{n=1}^{N} \int_{S_n} f(z') e^{-\mathrm{i}e^{-\mathrm{i}\chi_m} kz'} dz' = \int_{\partial P} f(z') e^{-\mathrm{i}e^{-\mathrm{i}\chi_m} kz'} dz' = 0, \tag{2.16}$$

for any point $k \in \mathbb{C}$, and for any $m = 1, ..., N$ and where we have used both the fact that $f(z')e^{-\mathrm{i}e^{-\mathrm{i}\chi_m}kz'}$ (for $m = 1, ..., N$) is analytic inside P, and Cauchy's theorem. It should be noted that there exist N such global relations providing a relation between different elements of the spectral matrix. However, each of these global relations, is an equivalent statement of the analyticity of function $f(z)$ in the polygon P. We also note that for this class of domains (polygonal domains) only the diagonal elements of the spectral matrix appear in the integral representation (2.13).

In a similar manner, we can write transform pairs for unbounded polygonal domains, such as semi-strip, quarter-plane, with the difference that the global relations will be valid in restricted sectors of the k-plane, such that the spectral functions remain well-defined (Fokas & Kapaev [43]). For completeness, we refer to Crowdy [18] for the connection of the above results to those obtained by Fokas & Kapaev [43].

2.1.2 Unbounded polygonal regions

For unbounded domains exterior to some bounded polygons, we observe that it is geometrically impossible to form the entire region from a finite intersection of half-planes. Therefore, we can subdivide the domain into a collection of polygonal subdomains that are the intersection of half-planes and for which we can write an integral representation as shown above. We mention the work by Charalambopoulos, Dassios & Fokas [12] who solved Laplace's equation in the exterior of an equilateral triangle by subdividing the domain to six convex subdomains.

2.2 The transform method for circular domains

To find generalized transform schemes for circular domains (whose boundaries consist of a combination of straight line and circular edges), we first consider D to be the unit disc. It should be clear that, to extend our transform approach to D, we must identify the particular spectral representation of the Cauchy kernel that is uniformly valid for z' on the domain boundary ∂D and for z inside D.

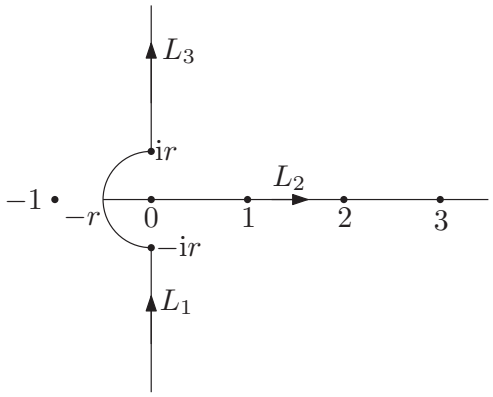

Figure 2.4: The fundamental contour for circular arc edges with $0 < r < 1$.

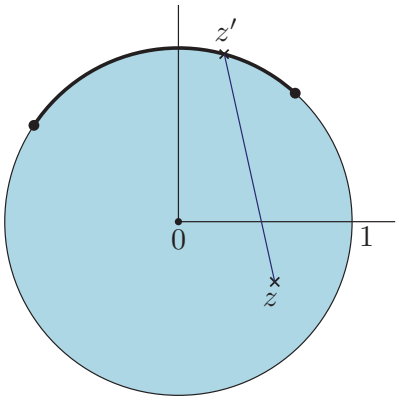

Figure 2.5: A point z' on boundary of the disc and point z in its interior.

For values $|z| < 1$ in D, we consider the integral

$$I \equiv \int_{L_1} \frac{1}{1 - e^{2\pi \mathrm{i} k}} z^k dk + \int_{L_2} z^k dk + \int_{L_3} \frac{e^{2\pi \mathrm{i} k}}{1 - e^{2\pi \mathrm{i} k}} z^k dk. \tag{2.17}$$

where it is integrated on the so called fundamental contour for circular arc edges, shown in Figure 2.4 which is the generalization of the fundamental contour $\mathcal{L}$ for straight line edges. We choose $0 < r < 1$. The contour L_1 is the union of the negative imaginary axis $(-\mathrm{i}\infty, -\mathrm{i}r]$ and the arc of the quarter circle $|k| = r$ in the third quadrant traversed in a clockwise sense; the contour L_2 is the real interval $[-r, \infty)$; the contour L_3 is the arc of the

quarter circle $|k| = r$ in the second quadrant traversed in a clockwise sense together with the portion of the positive imaginary axis $[\mathrm{i}r, \mathrm{i}\infty)$. All integrals in (2.17) are non-singular and all integrands are exponentially decaying as $|k| \to \infty$ uniformly for all $|z| < 1$. It can be shown that (Crowdy [18]), for $|z| < 1$,

$$I = \int_{L_1} \frac{1}{1 - e^{2\pi \mathrm{i}k}} z^k dk + \int_{L_2} z^k dk + \int_{L_3} \frac{e^{2\pi \mathrm{i}k}}{1 - e^{2\pi \mathrm{i}k}} z^k dk = \frac{1}{1 - z}. \tag{2.18}$$

To show that (2.18) holds, we observe that (Crowdy [18])

$$\begin{aligned} \int_{L_2} z^k dk &= \mathcal{P} \int_{L_2} \left[\frac{1 - e^{2\pi \mathrm{i}k}}{1 - e^{2\pi \mathrm{i}k}} \right] z^k dk \\ &= \mathcal{P} \int_{L_2} \left[\frac{1}{1 - e^{2\pi \mathrm{i}k}} \right] z^k dk - \mathcal{P} \int_{L_2} \left[\frac{e^{2\pi \mathrm{i}k}}{1 - e^{2\pi \mathrm{i}k}} \right] z^k dk \end{aligned} \tag{2.19}$$

where $\mathcal{P}$ is the principal value integral. For the contours L_- and L_+ illustrated in Figure 2.6, for some $0 < \epsilon < r$,

$$\begin{aligned} \int_{L_-} \left[\frac{z^k}{1 - e^{2\pi \mathrm{i}k}} \right] dk &= +\mathcal{P} \int_{L_2} \left[\frac{z^k}{1 - e^{2\pi \mathrm{i}k}} \right] dk + \sum_{n=0}^{\infty} \lim_{\epsilon \to 0} \int_{C_{n\epsilon}^-} \left[\frac{z^k}{1 - e^{2\pi \mathrm{i}k}} \right] dk, \\ \int_{L_+} \left[\frac{e^{2\pi \mathrm{i}k} z^k}{1 - e^{2\pi \mathrm{i}k}} \right] dk &= -\mathcal{P} \int_{L_2} \left[\frac{e^{2\pi \mathrm{i}k} z^k}{1 - e^{2\pi \mathrm{i}k}} \right] dk + \sum_{n=0}^{\infty} \lim_{\epsilon \to 0} \int_{C_{n\epsilon}^+} \left[\frac{e^{2\pi \mathrm{i}k} z^k}{1 - e^{2\pi \mathrm{i}k}} \right] dk. \end{aligned} \tag{2.20}$$

The contours L_- and L_+ consist of the union of the radius-ϵ semi-circles $\{C_{n\epsilon}^{\pm} | n \geq 0\}$ centred at $k = n$ (for $n \geq 0$) traversed anti-clockwise together with the portions of the real k-axis between them. Computation of the integrals around $\{C_{n\epsilon}^{\pm} | n \geq 0\}$ and substitution for the principal value integrals in (2.19) using (2.20) gives

$$I = \int_{\mathcal{L}_-} \left[\frac{1}{1 - e^{2\pi \mathrm{i}k}} \right] z^k dk + \sum_{n=0}^{\infty} z^n + \int_{\mathcal{L}_+} \left[\frac{e^{2\pi \mathrm{i}k}}{1 - e^{2\pi \mathrm{i}k}} \right] dk, \tag{2.21}$$

where $\mathcal{L}_- \equiv L_1 \cup L_-$ and $\mathcal{L}_+ \equiv L_+ \cup L_3$ are shown in Figure 2.7. Note that the integral around $\mathcal{L}_-$ vanishes because of the analyticity of the integrand in the fourth quadrant; similarly, the integral around $\mathcal{L}_+$ vanishes because of analyticity of the integrand in the

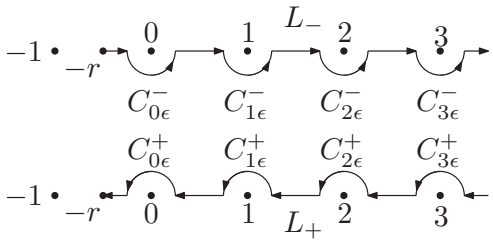

Figure 2.6: Contours L_- and L_+ in the spectral k-plane used to establish (2.18)

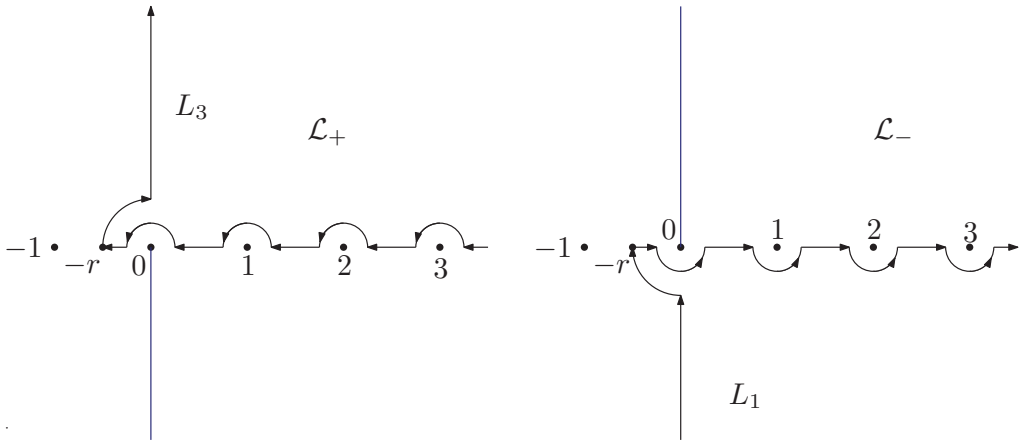

Figure 2.7: The contours $\mathcal{L}_+$ and $\mathcal{L}_-$

first quadrant. Hence, for $|z| < 1$, we have

$$I = \sum_{n=0}^{\infty} z^n = \frac{1}{1-z}, \tag{2.22}$$

which proves our result.

2.2.1 Transform pair for interior of unit disc

Let z' be a point on the unit circle and let $|z| < 1$ be a point in the interiot of the unit disc as illustrated in Figure 2.5. Then $|z/z'| < 1$ uniformly and it follows on letting $z \mapsto z/z'$

in (2.18) that

$$\frac{z'}{z'-z} = \int_{L_1} \frac{1}{1-e^{2\pi \mathrm{i}k}} \frac{z^k}{z'^k} dk + \int_{L_2} \frac{z^k}{z'^k} dk + \int_{L_3} \frac{e^{2\pi \mathrm{i}k}}{1-e^{2\pi \mathrm{i}k}} \frac{z^k}{z'^k} dk. \tag{2.23}$$

The Cauchy kernel has therefore therefore the following spectral representation:

$$\frac{1}{z'-z} = \int_{L_1} \frac{1}{1-e^{2\pi \mathrm{i}k}} \frac{z^k}{z'^{k+1}} dk + \int_{L_2} \frac{z^k}{z'^{k+1}} dk + \int_{L_3} \frac{e^{2\pi \mathrm{i}k}}{1-e^{2\pi \mathrm{i}k}} \frac{z^k}{z'^{k+1}} dk. \tag{2.24}$$

On substitution of (the uniformly valid) representation (2.24) in the Cauchy integral formula (2.2), we find that

$$f(z) = \frac{1}{2\pi \mathrm{i}} \oint_{|z'|=1} f(z') \left[\int_{L_1} \frac{1}{1-e^{2\pi \mathrm{i}k}} \frac{z^k}{z'^{k+1}} dk + \int_{L_2} \frac{z^k}{z'^{k+1}} dk + \int_{L_3} \frac{e^{2\pi \mathrm{i}k}}{1-e^{2\pi \mathrm{i}k}} \frac{z^k}{z'^{k+1}} dk \right] dz'. \tag{2.25}$$

Changing the order of integration, we find the following transform pair:

$$\begin{cases} f(z) = \dfrac{1}{2\pi \mathrm{i}} \left[\int_{L_1} \frac{\rho(k)}{1-e^{2\pi \mathrm{i}k}} z^k dk + \int_{L_2} \rho(k) z^k dk + \int_{L_3} \frac{\rho(k) e^{2\pi \mathrm{i}k}}{1-e^{2\pi \mathrm{i}k}} z^k dk \right], \\ \rho(k) = \oint_{|z'|=1} \frac{f(z')}{z'^{k+1}} dz', \end{cases} \tag{2.26}$$

The global relation is

$$\rho(k) = 0, \quad k \in -\mathbb{N} \tag{2.27}$$

since, for this discrete set of k-values, the integrand of the integral defining $\rho(k)$ is analytic in the unit disc.

2.2.2 Transform pair for exterior of unit disc

The transform pair for the exterior of the unit disc can be found similarly. For z' on the unit circle with $|z| > 1$ then $|z'/z| < 1$ uniformly and setting $z \mapsto z'/z$ in (2.18) gives

$$\frac{z}{z-z'} = \int_{L_1} \frac{1}{1-e^{2\pi \mathrm{i}k}} \frac{z'^k}{z^k} dk + \int_{L_2} \frac{z'^k}{z^k} dk + \int_{L_3} \frac{e^{2\pi \mathrm{i}k}}{1-e^{2\pi \mathrm{i}k}} \frac{z'^k}{z^k} dk. \tag{2.28}$$

We therefore have the following spectral representation for the Cauchy kernel:

$$\frac{1}{z-z'} = \int_{L_1} \frac{1}{1-e^{2\pi \mathrm{i}k}} \frac{z'^k}{z^{k+1}} dk + \int_{L_2} \frac{z'^k}{z^{k+1}} dk + \int_{L_3} \frac{e^{2\pi \mathrm{i}k}}{1-e^{2\pi \mathrm{i}k}} \frac{z'^k}{z^{k+1}} dk. \tag{2.29}$$

For $|z| > 1$ the Cauchy integral formula is given by

$$f(z) = -\frac{1}{2\pi \mathrm{i}} \oint_{|z'|=1} \frac{f(z')}{z'-z} dz'. \tag{2.30}$$

This is valid for an analytic function outside the unit disc that decays like $1/z$ as $z \to \infty$. Using (the uniformly valid) expression (2.29) in the Cauchy integral formula gives the following transform pair:

$$\begin{cases} f(z) = \dfrac{1}{2\pi \mathrm{i}} \left[\int_{L_1} \frac{\rho(k)}{1-e^{2\pi \mathrm{i}k}} \frac{dk}{z^{k+1}} + \int_{L_2} \rho(k) \frac{dk}{z^{k+1}} + \int_{L_3} \frac{\rho(k) e^{2\pi \mathrm{i}k}}{1-e^{2\pi \mathrm{i}k}} z \frac{dk}{z^{k+1}} \right], \\ \rho(k) = \oint_{|z'|=1} f(z') z'^k dz', \end{cases} \tag{2.31}$$

The global relation is now given by

$$\rho(k) = 0, \quad k \in -\mathbb{N} \tag{2.32}$$

since, for this discrete set of k-values, the integrand of the integral defining ρ_k is analytic outside the disc and is $\mathcal{O}(1/z^2)$ as $z \to \infty$.

2.2.3 Domains with both straight and circular edges

Of interest in this thesis is the analysis of boundary value problems in domains with both straight and circular edges. In Chapters 8-10, we shall be analyzing Stokes flow problems in such domains and present the associated transform pairs involving mixture of the results presented in this Chapter.

2.3 Summary

In this Chapter, following Crowdy [18, 19], we have presented a review of the Unified transform method, also known as the Fokas method, for Laplace's equation in polygonal

and circular domains. As we will see in the next Chapter, when solving a biharmonic boundary value problem it is necessary to find two unknown analytic functions; in all problems to be analyzed in this thesis, we will show how to find these two functions using the Unified transform method.

Chapter 3

Complex variable formulation of Stokes flows

In this chapter, we present a complex variable formulation of Stokes equations and then show how all physical quantities, flows of interest and fundamental singularities used to model fluid flows can be expressed using complex variables.

The Stokes equations are derived from the Navier-Stokes equations and they describe flows where the Reynolds number is very small, Re $\ll 1$, where Reynolds number is defined as the ratio of inertial forces to viscous forces. Therefore, these are flows in which inertial forces are negligible compared to viscous forces meaning that either the viscosity of the fluid is very high or velocity/length scales are very small.

3.1 Stokes equations in two dimensions

The two-dimensional Stokes equations are given by

$$\begin{aligned} \nabla p &= \eta \nabla^2 \mathbf{u}, \\ \nabla . \mathbf{u} &= 0, \end{aligned} \tag{3.1}$$

where $\mathbf{u} = (u, v)$ is the two-dimensional velocity field, p is the fluid pressure and η is the viscosity. Since the flow is incompressible and two-dimensional, we can introduce a

streamfunction ψ such that

$$u = \frac{\partial \psi}{\partial y}, \quad v = -\frac{\partial \psi}{\partial x}. \tag{3.2}$$

Taking the curl of the first equation in (3.1), we find that

$$\nabla \times \nabla p = \eta \nabla \times \nabla^2 \mathbf{u}. \tag{3.3}$$

Since the curl of a gradient field is equal to zero, we can write:

$$0 = \eta \nabla \times \nabla^2 \mathbf{u}. \tag{3.4}$$

Moreover, using the second equation in (3.1), (3.4) can be written as

$$0 = \eta \nabla^2 (\nabla \times \mathbf{u}). \tag{3.5}$$

Next, we define the fluid vorticity ω as the curl of the velocity field, which means that (3.5) can equivalently be written as

$$\nabla^2 \omega = 0, \qquad \omega \equiv \frac{\partial v}{\partial x} - \frac{\partial u}{\partial y}. \tag{3.6}$$

Using (3.2), we also have the relation:

$$\nabla^2 \psi = -\omega. \tag{3.7}$$

Combining (3.6) and (3.7), we find that the streamfunction satisfies the biharmonic equation

$$\nabla^4 \psi = 0. \tag{3.8}$$

We now present how to express the biharmonic operator using complex variables. Define the variable $z = x + \mathrm{i}y$ and its complex conjugate $\overline{z} = x - \mathrm{i}y$. Using these, we have

$$\frac{\partial}{\partial z} = \frac{1}{2}\left[\frac{\partial}{\partial x} - \mathrm{i}\frac{\partial}{\partial y}\right], \qquad \frac{\partial}{\partial \overline{z}} = \frac{1}{2}\left[\frac{\partial}{\partial x} + \mathrm{i}\frac{\partial}{\partial y}\right], \tag{3.9}$$

which implies that the harmonic and biharmonic operators can be expressed as

$$\nabla^2 = 4\frac{\partial^2}{\partial z \partial \overline{z}}, \qquad \nabla^4 = 16\frac{\partial^4}{\partial z^2 \partial \overline{z}^2}. \tag{3.10}$$

Therefore, (3.8) can be written in terms of complex variables as

$$\frac{\partial^4 \psi}{\partial z^2 \partial \overline{z}^2} = 0. \tag{3.11}$$

On integration of (3.11), we find that its general solution can be written as

$$\psi = \text{Im}[\overline{z} f(z) + g(z)], \tag{3.12}$$

where $f(z)$ and $g(z)$ are analytic functions of the complex variable $z = x + \mathrm{i}y$ and are known as the Goursat functions (Langlois [69]). It is clear, then, that to solve a Stokes flow problem in two dimensions, it is sufficient to determine these two analytic functions; this is usually done by making use of the boundary conditions. In this thesis, we will show that these two analytic functions can be found using the Unified transform method. It should be noted at this point that expression (3.12) also appears in plane elasticity with ψ in that case being the Airy stress function (Muskhelishvili [86]).

In the following subsections, we show that all physical quantities of interest can be expressed in terms of the Goursat functions $f(z)$ and $g(z)$.

3.1.1 Velocity

We employ the notation $\mapsto$ to indicate a change to the complex form of some vector quantity, i.e.,

$$\mathbf{a} = \begin{pmatrix} a_1 \\ a_2 \end{pmatrix} \mapsto a_1 + \mathrm{i}a_2. \tag{3.13}$$

With this convention, using (3.2) we can write

$$\mathbf{u} \mapsto u + \mathrm{i}v = \frac{\partial \psi}{\partial y} - \mathrm{i}\frac{\partial \psi}{\partial x} = -\mathrm{i}\left[\frac{\partial \psi}{\partial x} + \mathrm{i}\frac{\partial \psi}{\partial y}\right] = -2\mathrm{i}\frac{\partial \psi}{\partial \overline{z}}, \tag{3.14}$$

where we have used (3.9). Next, using (3.12), we can write

$$\psi = \frac{[\overline{z}f(z) + g(z)] - [z\overline{f(z)} + \overline{g(z)}]}{2\mathrm{i}}, \tag{3.15}$$

or, equivalently:

$$2\mathrm{i}\psi = \overline{z}f(z) + g(z) - z\overline{f(z)} - \overline{g(z)}. \tag{3.16}$$

The final expression can be used in (3.14) to give

$$u + \mathrm{i}v = -f(z) + z\overline{f'(z)} + \overline{g'(z)}. \tag{3.17}$$

It it sometimes useful to deal with the complex conjugate velocity which can be expressed as

$$u - \mathrm{i}v = -\overline{f(z)} + \overline{z}f'(z) + g'(z). \tag{3.18}$$

For example, the *no-slip* boundary condition which we shall refer to throughout this thesis can be expressed as

$$-\overline{f(z)} + \overline{z}f'(z) + g'(z) = 0. \tag{3.19}$$

3.1.2 Pressure and vorticity

The first equation in (3.1) can be written in complex form as

$$\nabla p = \eta\nabla^2\mathbf{u} \mapsto 2\frac{\partial}{\partial\overline{z}}p = 4\eta\frac{\partial^2}{\partial z\partial\overline{z}}(u + \mathrm{i}v). \tag{3.20}$$

On integration with respect to $\overline{z}$, we find that

$$\frac{p}{\eta} = 2\frac{\partial}{\partial z}(u + \mathrm{i}v) + F(z), \tag{3.21}$$

where $F(z)$ is an unknown analytic function. Using (3.17), this can be written as

$$\frac{p}{\eta} = 2(-f'(z) + \overline{f'(z)}) + F(z). \tag{3.22}$$

But since pressure p is a real quantity, we must pick the analytic function $F(z) = 4f'(z)$;

we therefore have

$$\frac{p}{\eta} = 2(f'(z) + \overline{f'(z)}) = 4\text{Re}[f'(z)]. \tag{3.23}$$

Next, expression (3.7) can be expressed in complex form as

$$\omega = -4\frac{\partial^2 \psi}{\partial z \partial \overline{z}}, \tag{3.24}$$

which, on substitution of (3.15), can be written as

$$\begin{aligned} \omega &= -4\frac{\partial^2}{\partial z \partial \overline{z}}\left[\frac{1}{2\text{i}}\left(\overline{z}f(z) + g(z) - z\overline{f(z)} - \overline{g(z)}\right)\right] \\ &= -4\left(\frac{f'(z) - \overline{f'(z)}}{2\text{i}}\right) \\ &= -4\text{Im}[f'(z)]. \end{aligned} \tag{3.25}$$

Expressions (3.23) and (3.25) can be written together as:

$$\frac{p}{\eta} - \text{i}\omega = 4f'(z). \tag{3.26}$$

3.1.3 Fluid stress

The fluid stress on a surface is given by

$$-pn_i + 2\eta e_{ij} n_j, \tag{3.27}$$

where n_i denotes the components of the unit normal vector to some closed curve in the fluid and e_{ij} is the usual fluid rate-of-strain tensor, see definition (3.31) below.

The complex form of the unit tangent vector $\mathbf{t}$ on some closed curve is

$$\mathbf{t} = \begin{pmatrix} t_1 \\ t_2 \end{pmatrix} \mapsto t_1 + \text{i}t_2 = \frac{dz}{ds}, \tag{3.28}$$

where s is arclength around the boundary and $ds^2 = dx^2 + dy^2 = dz\overline{dz}$. Therefore, the

complex form of the unit outward normal $\mathbf{n}$ is

$$\mathbf{n} = \begin{pmatrix} n_1 \\ n_2 \end{pmatrix} \mapsto n_1 + \mathrm{i}n_2 = -\mathrm{i}\frac{dz}{ds}, \tag{3.29}$$

where we have rotated the unit tangent vector $\mathbf{t}$ by $-\pi/2$. This rotation corresponds to multiplication by $(-\mathrm{i})$ if expressed in complex variable form. Using (3.23) and (3.29), we can write the complex form of $-pn_i$ as

$$-pn_i \mapsto 2\mathrm{i}\eta \left(f'(z) + \overline{f'(z)} \right) \frac{dz}{ds}. \tag{3.30}$$

Next, the term $2\eta e_{ij} n_j$ includes the rate-of-strain tensor e_{ij} and, hence, we need to express this in complex form. We define the fluid rate-of-strain tensor to be

$$e_{ij} = \frac{1}{2}\left(\frac{\partial u_i}{\partial x_j} + \frac{\partial u_j}{\partial x_i} \right) \tag{3.31}$$

where $u_1 \equiv u$, $u_2 \equiv v$, $x_1 \equiv x$ and $x_2 \equiv y$, and consider

$$\frac{\partial}{\partial \overline{z}}(u + \mathrm{i}v) = \frac{1}{2}\left(\frac{\partial}{\partial x} + \mathrm{i}\frac{\partial}{\partial y} \right)(u + \mathrm{i}v) = \frac{1}{2}\left[\frac{\partial u}{\partial x} - \frac{\partial v}{\partial y} + \mathrm{i}\left(\frac{\partial u}{\partial y} + \frac{\partial v}{\partial x} \right) \right]. \tag{3.32}$$

On use of the second equation in (3.1), this becomes

$$\frac{\partial}{\partial \overline{z}}(u + \mathrm{i}v) = z\overline{f''(z)} + \overline{g''(z)} = e_{11} + \mathrm{i}e_{12}. \tag{3.33}$$

The second term in (3.27) is

$$2\eta e_{ij} n_j = 2\eta \begin{pmatrix} e_{11}n_1 + e_{12}n_2 \\ e_{21}n_1 + e_{22}n_2 \end{pmatrix} = 2\eta \begin{pmatrix} e_{11}n_1 + e_{12}n_2 \\ e_{12}n_1 - e_{11}n_2, \end{pmatrix} \tag{3.34}$$

where we have used that $e_{22} = -e_{11}$ and $e_{21} = e_{12}$. We also have that

$$(e_{11} + \mathrm{i}e_{12})(n_1 - \mathrm{i}n_2) = e_{11}n_1 + e_{12}n_2 + \mathrm{i}(e_{12}n_1 - e_{11}n_2). \tag{3.35}$$

which means that

$$2\eta e_{ij}n_j \mapsto 2\mathrm{i}\eta(e_{11}+\mathrm{i}e_{12})\frac{d\overline{z}}{ds} = 2\mathrm{i}\eta\left(z\overline{f''(z)}+\overline{g''(z)}\right)\frac{d\overline{z}}{ds}. \tag{3.36}$$

Therefore, the complex form of the fluid stress on a surface is given by

$$-pn_i + 2\eta e_{ij}n_j \mapsto 2\mathrm{i}\eta\left(f'(z)+\overline{f'(z)}\right)\frac{dz}{ds} + 2\mathrm{i}\eta\left(z\overline{f''(z)}+\overline{g''(z)}\right)\frac{d\overline{z}}{ds}. \tag{3.37}$$

To express this in a concise form, we introduce

$$H(z,\overline{z}) \equiv f(z) + z\overline{f'(z)} + \overline{g'(z)}. \tag{3.38}$$

It can be seen that

$$\frac{\partial H}{\partial z} = f'(z) + \overline{f'(z)}, \qquad \frac{\partial H}{\partial \overline{z}} = z\overline{f''(z)} + \overline{g''(z)}, \tag{3.39}$$

which can be used in (3.37) to give:

$$-pn_i + 2\eta e_{ij}n_j \mapsto 2\mathrm{i}\eta\frac{dH}{ds}. \tag{3.40}$$

3.1.4 Force

The integral of the fluid stress around the boundary of a body is known as the Stokes drag. Any net Stokes drag on a body must be balanced by an external force on the body. The total Stokes drag on a body D with boundary ∂D is given by

$$\mathbf{F} = \oint_{\partial D}(-pn_i + 2\eta e_{ij}n_j)ds \mapsto 2\mathrm{i}\eta\oint_{\partial D}\frac{dH}{ds}ds = 2\mathrm{i}\eta[H]_{\partial D}, \tag{3.41}$$

where the square brackets denote the change in H on traversing ∂D. Thus logarithmic singularities of the Goursat functions inside the body are associated with non-zero net external forces on the it. Also, the force is zero if $f(z)$ and $g'(z)$ are both single-valued functions.

3.1.5 Torque

The torque on a body centred at z_d is defined as the integral $(\mathbf{x} - \mathbf{x_d}) \wedge \mathbf{F}$ around its boundary, where $\mathbf{F}$ is the hydrodynamic force on the body at position $\mathbf{x} - \mathbf{x_d}$. Since the cross product of two vectors $\mathbf{a}$ and $\mathbf{b}$ is $\mathrm{Im}[\overline{a}b]$ (where a and b denotes the complex forms of the corresponding vectors), the torque can be written in complex form as

$$T = \mathrm{Im}\left[2\eta \mathrm{i} \oint_{\partial D} (\overline{z} - \overline{z}_d)\frac{dH}{ds}ds\right], \tag{3.42}$$

where ∂D denotes the boundary of the body.

3.1.6 Remark

There is an additive degree of freedom in the definition of the Goursat functions, since redefining these to be

$$f(z) \mapsto f(z) + c, \qquad g'(z) \mapsto g'(z) + \overline{c}, \tag{3.43}$$

or/and:

$$f(z) \mapsto f(z) + \frac{p_\infty z}{4\eta}, \tag{3.44}$$

for some constant c and pressure p_∞, all the physical quantities remain unchanged. As we will see in the following chapters, (3.43)-(3.44) are useful to ensure that various conditions appearing in the analysis of sub-problems are compatible.

3.2 Goursat functions representations for flows of interest

In this section, we show how some flows of interest, namely a pressure-driven flow, shear flow and stagnation point flow, can be modeled and described using the Goursat functions $f(z)$ and $g(z)$. These will be useful in the next chapters, as we will be analysing some of these flows in more complex geometries.

3.2.1 Pressure-driven flow in a channel

Consider a pressure-driven flow in a channel defined by $-\infty < x < \infty$, $0 < y < h$, where the streamfunction is of the form

$$\psi = -Uy^2\left(\frac{h}{4} - \frac{y}{6}\right), \tag{3.45}$$

where U is a real constant related to the pressure drop between the channel ends and h is the channel height. A schematic of the configuration is illustrated in Figure 3.1.

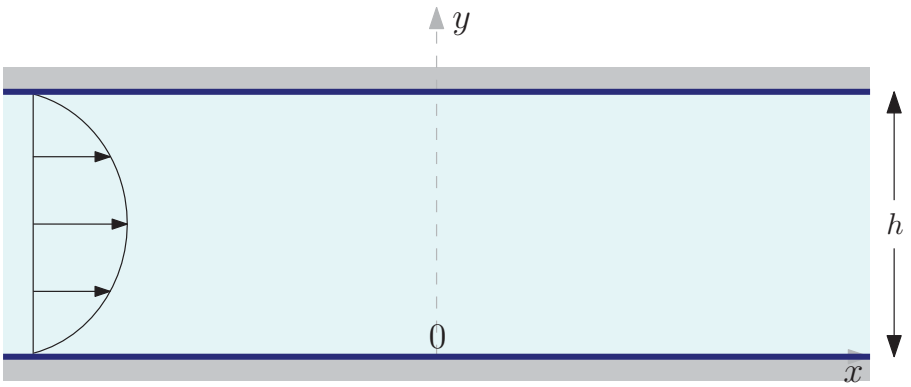

Figure 3.1: Pressure-driven flow

Using (3.2), the velocity components u, v can be computed:

$$u = \frac{Uy(y-h)}{2}, \qquad v = 0. \tag{3.46}$$

Then, the complex velocity can be written as

$$\begin{aligned} u + \mathrm{i}v = \frac{Uy(y-h)}{2} &= -\frac{Uz^2}{8} + \frac{Uz\overline{z}}{4} - \frac{U\overline{z}^2}{8} + \frac{\mathrm{i}Uhz}{4} - \frac{\mathrm{i}Uh\overline{z}}{4} \\ &= -f(z) + z\overline{f'(z)} + \overline{g'(z)}, \end{aligned} \tag{3.47}$$

where we have used that $y = (z - \overline{z})/2\mathrm{i}$. From this, we choose:

$$f(z) = \frac{Uz}{8}\left[z - \mathrm{i}h\right], \qquad g'(z) = \frac{Uz}{4}\left[\mathrm{i}h - \frac{z}{2}\right], \tag{3.48}$$

These are the Goursat functions related to a pressure-driven flow in the channel geometry $-\infty < x < \infty$, $0 < y < h$. Clearly, since this is a pressure-driven flow, we can redefine

$$f(z) \mapsto f(z) + \frac{p_\infty z}{4\eta}, \tag{3.49}$$

where p_∞ is an additive pressure, without affecting any of the physical quantities (as discussed previously).

3.2.2 Shear flow

Now, consider a uniform shear flow above a wall (Figure 3.2) of the form

$$\psi = Uy^2, \tag{3.50}$$

where U is a real constant which determines the strength of the flow.

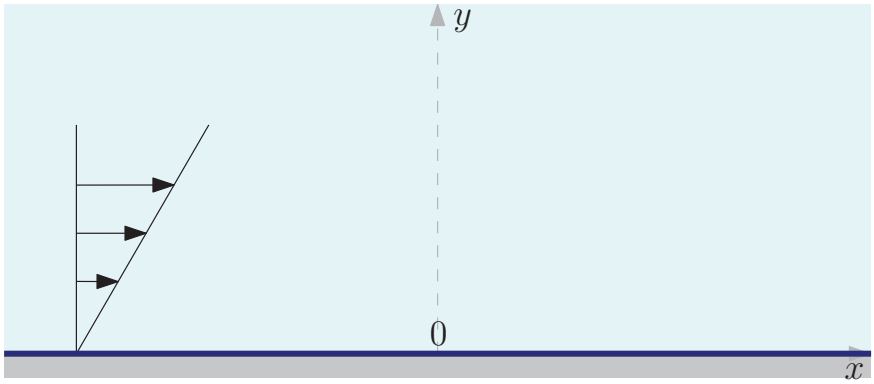

Figure 3.2: Shear flow

Using (3.2), the velocity components u, v can be computed:

$$u = 2Uy, \qquad v = 0. \tag{3.51}$$

The complex velocity can be written as

$$\begin{aligned} u + \mathrm{i}v = 2Uy &= -\mathrm{i}U(z - \overline{z}), \\ &= -f(z) + z\overline{f'(z)} + \overline{g'(z)}, \end{aligned} \tag{3.52}$$

where we have used that $y = (z - \overline{z})/2\mathrm{i}$. From this, we deduce that we must have

$$f(z) = \frac{\mathrm{i}Uz}{2}, \qquad g'(z) = -\mathrm{i}Uz. \tag{3.53}$$

3.2.3 Stagnation point flow

Consider a stagnation point flow of the form

$$\psi = Uxy^2, \tag{3.54}$$

where U is a real constant which determines the strength of the flow. A schematic is shown in Figure 3.3.

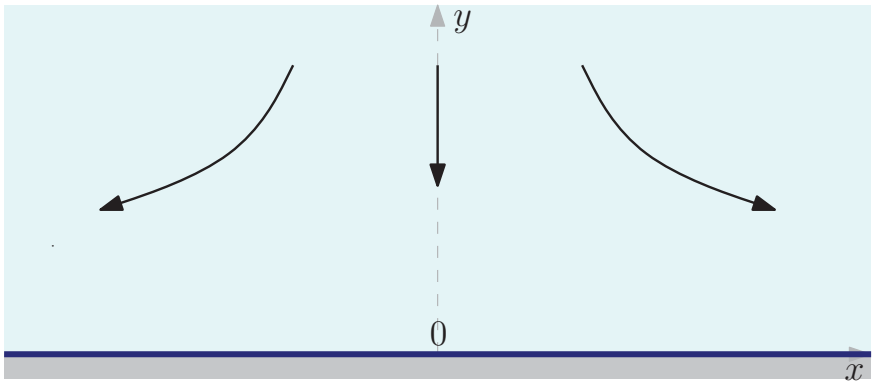

Figure 3.3: Stagnation point flow

Using (3.2), the velocity components u, v can be computed:

$$u = 2Uxy, \qquad v = -Uy^2. \tag{3.55}$$

The complex velocity can be written as

$$u + \mathrm{i}v = 2Uxy - \mathrm{i}Uy^2 = -\frac{\mathrm{i}Uz^2}{4} - \frac{\mathrm{i}Uz\overline{z}}{2} + \frac{3\mathrm{i}U\overline{z}^2}{4} \\ = -f(z) + z\overline{f'(z)} + \overline{g'(z)}, \tag{3.56}$$

In this case, we deduce that we must have:

$$f(z) = \frac{\mathrm{i}Uz^2}{4}, \qquad g'(z) = -\frac{3\mathrm{i}Uz^2}{4}. \tag{3.57}$$

3.3 Fundamental singularities of Stokes flows

In two-dimensional Stokes flows, in order to model various flows, such as bubbles, deforming bodies, microswimmers' dynamics, a distribution of point singularities can be used to describe the fluid flow. The fundamental singularities in Stokes flows are Stokeslet, stresslet, source (or sink), rotlet, irrotational dipole, irrotational quadrupole etc. (Blake [8], Crowdy & Or [23], Pozrikidis [89]). Figure 3.4 shows some of these singularities and their local streamlines.

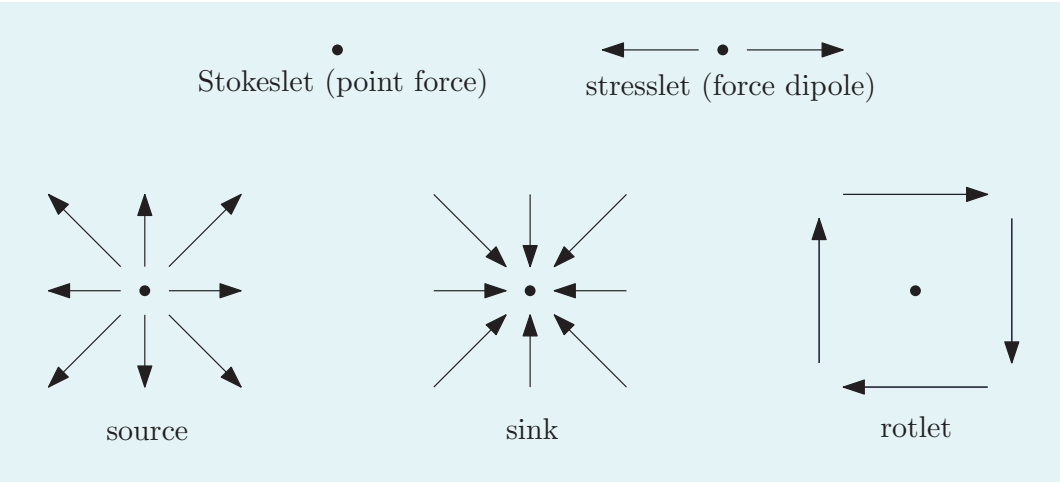

Figure 3.4: A collection of some Stokes flow singularities and their local streamlines.

In this section, we present how the fundamental singularities in Stokes flows appear as singularities of functions $f(z)$ and $g(z)$. Although $f(z)$ and $g(z)$ are supposed to be analytic

in the fluid region, they are allowed to have isolated singularities to model flows of interest.

3.3.1 Stokeslet (point force)

Consider a concentrated force (point force) whose magnitude and angle are represented by $\mu \in \mathbb{C}$ applied at a given point z_0. The resulting flow is called a Stokeslet at z_0 and requires that $f(z)$ and $g'(z)$ have the local expansions

$$f(z) = \mu \log(z - z_0), \quad g'(z) = -\overline{\mu} \log(z - z_0) - \frac{\mu \overline{z_0}}{z - z_0}. \tag{3.58}$$

Note that the singularities in $g'(z)$ were chosen according to those in $f(z)$ in order to ensure that the velocity field is both single-valued and logarithmically singular at z_0 (Crowdy & Or [23]).

3.3.2 Force dipole (stresslet)

Now, the form for $f(z)$ and $g'(z)$ given by

$$f(z) = \frac{\mu}{z - z_0}, \quad g'(z) = \frac{\mu \overline{z_0}}{(z - z_0)^2}. \tag{3.59}$$

corresponds to a point stresslet of strength $\mu \in \mathbb{C}$ at z_0. In this case, $g'(z)$ was imposed by the choice of $f(z)$ in order to ensure that the velocity field is singular like $1/|z - z_0|$ (rather than $1/|z - z_0|^2$).

3.3.3 Force quadrupole

Next, the choice for $f(z)$ and $g'(z)$:

$$f(z) = \frac{\mu}{(z - z_0)^2}, \quad g'(z) = \frac{2\mu \overline{z_0}}{(z - z_0)^3} \tag{3.60}$$

corresponds to a force quadrupole of strength $\mu \in \mathbb{C}$ at z_0. In this case, $g'(z)$ was imposed by the choice of $f(z)$ in order to ensure that the velocity field is singular like $1/|z - z_0|^2$.

3.3.4 Source/sink

Note that $g(z)$ can additionally have its own singularities, independently of those imposed by the choice of $f(z)$. If the function $g(z)$ has the following form:

$$g(z) = c\log(z - z_0) \tag{3.61}$$

and $c \in \mathbb{R}$, we have a source (or sink) at z_0.

3.3.5 Rotlet (rotational torque)

If the function $g(z)$ has the following form:

$$g(z) = c\log(z - z_0) \tag{3.62}$$

and $c \in i\mathbb{R}$, we have a rotlet at z_0, which corresponds to a rotational torque applied at the point z_0.

3.3.6 Source dipole

A simple pole of $g(z)$ is a source dipole singularity.

3.3.7 Source quadrupole

A double pole of $g(z)$ is a source quadrupole and so on.

Chapter 4

Stokes flows in the half-plane

4.1 Introduction

In this chapter, we illustrate how the transform method for polygonal domains can be used to solve boundary value problems in the half-plane. Specifically, we show how to solve the problem of a point singularity above a no-slip wall and above a wall with mixed boundary conditions.

The first problem to be considered is that of a point singularity in the upper half-plane satisfying a no-slip boundary condition along the real axis. Blake [8] presented, among others, the solution or the "image system" for various Stokes singularities in the half-plane due to the presence of the no-slip boundary. Crowdy & Or [23] used a complex variable formulation to solve for point singularities above a no-slip wall and proposed a simple singularity description for a point swimmer in the same geometry. Their model was able to capture qualitative agreement with experiments and was later used in various more complicated geometries (Davis & Crowdy [26, 27]). Motivated by these studies, we show how to rederive the "image system" solution for a point singularity above a no-slip wall using the transform method for polygonal domains. In addition, our solution to this problem serves as a model example for the standard steps to be followed when solving boundary value problems using the transform method.

Although there has been a lot of interest in solving Stokes flow problems in bounded by no-slip boundaries geometries, much more attention has recently been paid to the study of Stokes flow problems in geometries involving mixed boundary conditions. The analysis of such problems is of particular interest, since these can be used to model physical problems arising in the study of superhydrophobic surfaces and microfluidics. We mention the classical work by Philip [88] who motivated by porous media flows, studied various flow problems with mixed no-slip and no-shear stress boundary conditions and found analytical solutions using conformal mapping techniques. Lauga & Stone [72] studied Stokes flow problems with mixed boundary conditions to model superhydrophobic surfaces and investigate their frictional properties.

Other problems with mixed boundary conditions are the so called die-swell problems, concerning the emergence of a fluid jet from a confined channel geometry (or a circular tube for the three-dimensional case) into the atmosphere; these have received a great interest in the last decades owing to their direct relation with applications such as the polymer processing, the manufacture process of optical fibers (Ebendorff-Heidepriem & Monro [36]), etc.. It is known that, unlike high-Reynolds-number fluid flows, at low-Reynolds number a jet expands rather than contracts when exiting a no-slip region. Early investigations of these problems include the work of Richardson [92] within a two-dimensional model and the studies of Trogdon & Joseph [108, 109] for a three-dimensional round jet. Richardson [92] considered a two-dimensional pressure-driven fluid flow confined between two parallel stick-slip (i.e. no-slip and no-stress) boundaries which transforms to a uniform flow downstream in response to no-stress boundary conditions and obtained analytical solutions using the Wiener-Hopf method.

Our aim in later chapters is to present a systematic way to solve Stokes flow problems in complex geometries involving mixed boundary conditions. Therefore, as a first step towards understanding how to solve them using the transform method, we consider (as a second problem to be analyzed in this chapter) the following: the problem domain is the upper half-plane and the real axis is composed of mixed boundary conditions: no-slip along the negative real axis and no-shear stress along the positive one. According to Philip [88],

the no-shear stress boundary condition on a surface is defined "as the requirement that the shearing stress tangential to the surface and the component of flow velocity normal to the surface both vanish on it". Similarly to the no-slip boundary condition, we show that the no-shear boundary condition can also be expressed in terms of the Goursat functions. Then, we solve this problem using the transform method for polygonal domains and Riemann-Hilbert problem techniques along the real axis (Ablowitz & Fokas [1]). Interestingly, this problem allows us to investigate how these methods can be combined to solve mixed boundary value problems. Our solution is checked against an exact solution found using conformal mapping techniques.

4.2 A point stresslet above a no-slip boundary

4.2.1 Problem formulation

Consider the fluid domain to be the upper half-plane $-\infty < x < \infty$, $y > 0$ bounded by a no-slip wall along the real axis. Using complex variables $z = x + \mathrm{i}y$, the upper half-plane can be expressed as $\mathrm{Im}[z] > 0$ and the real axis as $\mathrm{Im}[z] = 0$ (or $\overline{z} = z$). A point stresslet of strength $\mu \in \mathbb{C}$ is placed at point z_0 above the wall, as shown in Figure 4.1. The aim is to compute the 'image system' due to the presence of the boundary and therefore determine the resulting flow everywhere in the fluid region.

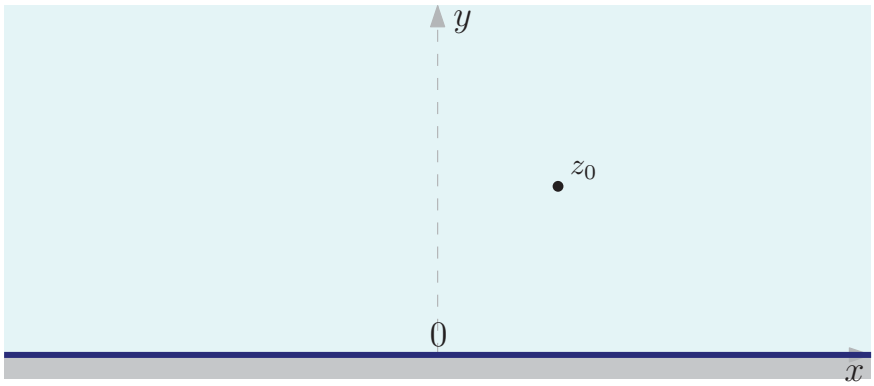

Figure 4.1: Problem configuration: a point stresslet at point z_0 above a wall.

The Goursat functions are represented by

$$\begin{cases} f(z) = f_s(z) + \hat{f}(z), \\ g'(z) = g'_s(z) + \hat{g}'(z), \end{cases} \tag{4.1}$$

where $f_s(z)$, $g'_s(z)$ are related to the point stresslet of strength $\mu \in \mathbb{C}$ at point z_0:

$$\begin{cases} f_s(z) = \dfrac{\mu}{z - z_0}, \\ \\ g'_s(z) = \dfrac{\mu \overline{z_0}}{(z - z_0)^2}, \end{cases} \tag{4.2}$$

and $\hat{f}(z)$, $\hat{g}'(z)$ are unknown analytic functions in the fluid region vanishing in the far-field. From now on, we shall refer to functions $f_s(z)$, $g'_s(z)$ as the forcing functions and to $\hat{f}(z)$, $\hat{g}'(z)$ as the (unknown) correction functions.

The no-slip boundary condition on the real axis ($\overline{z} = z$) can be expressed as

$$-\overline{f(z)} + z f'(z) + g'(z) = 0. \tag{4.3}$$

It is clear that, in general, the forcing functions $f_s(z)$, $g'_s(z)$ will not satisfy the given boundary conditions, in this case (4.3). But correction functions are included in (4.1); these will ensure that $f(z)$ and $g'(z)$ satisfy the boundary conditions. In the following subsections, we show how the correction functions $\hat{f}(z)$, $\hat{g}'(z)$ can be found after analyzing (4.3) using either a transform approach or a 'method of images' approach.

4.2.2 Transform approach

Function representation: We represent $\hat{f}(z)$ by

$$\hat{f}(z) = \frac{1}{2\pi} \int_0^\infty \rho_1(k) e^{\mathrm{i}kz} dk, \tag{4.4}$$

where the spectral function $\rho_1(k)$ is defined by

$$\rho_1(k) = \int_{-\infty}^{\infty} \hat{f}(z) e^{-\mathrm{i}kz} dz. \tag{4.5}$$

Similarly, we can write

$$\hat{g}'(z) = \frac{1}{2\pi} \int_{0}^{\infty} \hat{\rho}_1(k) e^{\mathrm{i}kz} dk, \tag{4.6}$$

where the spectral function $\hat{\rho}_1(k)$ is defined by

$$\hat{\rho}_1(k) = \int_{-\infty}^{\infty} \hat{g}'(z) e^{-\mathrm{i}kz} dz. \tag{4.7}$$

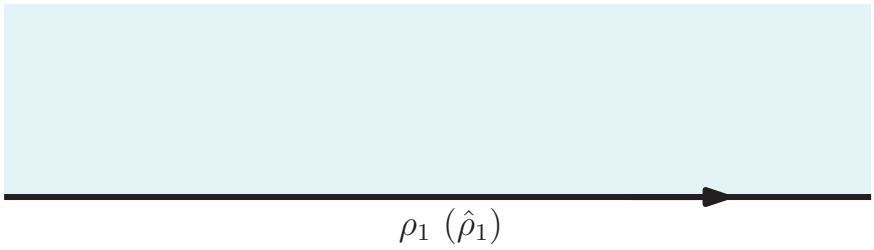

Figure 4.2: Schematic of the spectral functions along the real axis.

Global relations: Since the fluid domain is the upper half-plane, the global relations are given by

$$\begin{aligned} \rho_1(k) &= 0, \qquad \text{for } k < 0, \\ \hat{\rho}_1(k) &= 0, \qquad \text{for } k < 0. \end{aligned} \tag{4.8}$$

Boundary condition: Substitution of (4.1) into (4.3) gives

$$-\overline{\hat{f}(z)} + z\hat{f}'(z) + \hat{g}'(z) = \overline{f_s(z)} - z f_s'(z) - g_s'(z), \tag{4.9}$$

where the right-hand side of this equation involves known quantities.

Preliminary observations: The Schwarz conjugate function of an analytic function $f(z)$

is defined by

$$\overline{f}(z) \equiv \overline{f(\overline{z})} \tag{4.10}$$

and it is an analytic function. Taking the Schwarz conjugate of $\rho_1(k)$ we find that

$$\overline{\rho_1}(k) = \int_{-\infty}^{\infty} \overline{\hat{f}(z)} e^{\mathrm{i}kz} dz. \tag{4.11}$$

If we let $k \mapsto -k$ we find

$$\overline{\rho_1}(-k) = \int_{-\infty}^{\infty} \overline{\hat{f}(z)} e^{-\mathrm{i}kz} dz. \tag{4.12}$$

In addition, it can be shown that, after integration by parts, we find

$$\int_{-\infty}^{\infty} z\hat{f}'(z) e^{-\mathrm{i}kz} dz = -\frac{\partial[k\rho_1(k)]}{\partial k}. \tag{4.13}$$

Expressions (4.12)-(4.13) will be used in the spectral analysis which follows.

Spectral analysis: In this section, we will obtain more information about the spectral functions by making use of the boundary condition.

We multiply (4.9) by $e^{-\mathrm{i}kz}$ and integrate along the real axis:

$$-\int_{-\infty}^{\infty} \overline{\hat{f}(z)} e^{-\mathrm{i}kz} dz + \int_{-\infty}^{\infty} z\hat{f}'(z) e^{-\mathrm{i}kz} dz + \int_{-\infty}^{\infty} \hat{g}'(z) e^{-\mathrm{i}kz} dz = R(k), \tag{4.14}$$

where

$$R(k) \equiv \int_{-\infty}^{\infty} [\overline{f_s(z)} - z f_s'(z) - g_s'(z)] e^{-\mathrm{i}kz} dz. \tag{4.15}$$

Using (4.12)-(4.13), this can be expressed in terms of the spectral functions as

$$-\overline{\rho_1}(-k) - \frac{\partial[k\rho_1(k)]}{\partial k} + \hat{\rho}_1(k) = R(k). \tag{4.16}$$

Using the global relations (4.8), expression (4.16) can be simplified to

$$\overline{\rho_1}(-k) = -R(k), \qquad \text{for } k < 0, \tag{4.17}$$

or, taking Schwarz conjugate and letting $k \mapsto -k$,

$$\rho_1(k) = -\overline{R}(-k), \qquad \text{for } k > 0. \tag{4.18}$$

Expression $R(k)$ (and therefore $\overline{R}(-k)$) can be computed using residue calculus; we find that

$$\rho_1(k) = 2\pi \mathrm{i}\overline{\mu} e^{-\mathrm{i}k\overline{z_0}} + 2\pi\overline{\mu}(\overline{z_0} - z_0)ke^{-\mathrm{i}k\overline{z_0}}. \tag{4.19}$$

This is finally substituted into (4.4) to give

$$\begin{aligned} \hat{f}(z) &= \frac{1}{2\pi}\int_0^\infty \rho_1(k)e^{\mathrm{i}kz}dk \\ &= \mathrm{i}\overline{\mu}\int_0^\infty e^{\mathrm{i}k(z_0-\overline{z_0})}dk + \overline{\mu}(\overline{z_0} - z_0)\int_0^\infty ke^{\mathrm{i}k(z_0-\overline{z_0})}dk \\ &= -\frac{\overline{\mu}}{z-\overline{z_0}} + \frac{\overline{\mu}(z_0-\overline{z_0})}{(z-\overline{z_0})^2}, \end{aligned} \tag{4.20}$$

where we have used that

$$\int_0^\infty e^{\mathrm{i}k(z-\overline{z_0})}dk = -\frac{1}{\mathrm{i}(z-\overline{z_0})}, \qquad \int_0^\infty ke^{\mathrm{i}k(z-\overline{z_0})}dk = -\frac{1}{(z-\overline{z_0})^2}. \tag{4.21}$$

The correction function $\hat{g}'(z)$ can be computed from (4.9):

$$\hat{g}'(z) = \frac{2\overline{\mu}z_0 - 3\overline{\mu z_0}}{(z-\overline{z_0})^2} + \frac{2\overline{\mu z_0}(z_0-\overline{z_0})}{(z-\overline{z_0})^3}. \tag{4.22}$$

Note that although (4.9) is only valid on the real axis, it is also valid off the real axis by analytic continuation, which means that (4.22) is valid everywhere in the fluid region. Alternatively, the correction function $\hat{g}'(z)$ can be computed using the spectral relation (4.16) to find $\hat{\rho}_1(k)$ which can be then substituted in (4.6).

Summary: The Goursat functions related to a point stresslet of strength $\mu \in \mathbb{C}$ at point z_0

above a no-slip boundary are therefore given by

$$\begin{cases} f(z) = f_s(z) + \hat{f}(z) = \dfrac{\mu}{z - z_0} - \dfrac{\overline{\mu}}{z - \overline{z_0}} + \dfrac{\overline{\mu}(z_0 - \overline{z_0})}{(z - \overline{z_0})^2}, \\ \\ g'(z) = g'_s(z) + \hat{g}'(z) = \dfrac{\mu\overline{z_0}}{(z - z_0)^2} + \dfrac{2\overline{\mu}z_0 - 3\overline{\mu z_0}}{(z - \overline{z_0})^2} + \dfrac{2\overline{\mu z_0}(z_0 - \overline{z_0})}{(z - \overline{z_0})^3}. \end{cases} \tag{4.23}$$

4.2.3 Method of images

Crowdy & Or [23] presented a complex variable approach to solve for a point singularity above a no-slip wall; their analysis was akin to the classical method of images. In this section, we follow their work to retrieve their solution for a point stresslet. For a point stresslet of strength $\mu \in \mathbb{C}$ at z_0, we know that function $f(z)$ must have the form

$$f(z) = \frac{\mu}{z - z_0} + \text{locally analytic function.} \tag{4.24}$$

Since the point singularity is near (above) a wall, we expect that image singularities will appear in the solution. It is natural to try:

$$f(z) = \frac{\mu}{z - z_0} + \frac{\delta}{z - \overline{z_0}} + \frac{\lambda}{(z - \overline{z_0})^2}, \tag{4.25}$$

where we have included a first and second order image singularities at $\overline{z_0}$ for some constants δ and λ to be found. Note that higher order image singularities can be added, but as we will see these are not needed in the solution. Next, solving for $g'(z)$ in the boundary condition (4.3), we find that

$$g'(z) = \overline{f}(z) - zf'(z), \tag{4.26}$$

where we have used that, on $\overline{z} = z$,

$$\overline{f(z)} = \overline{f}(z). \tag{4.27}$$

On use of (4.25) in (4.26), $\hat{g}'(z)$ is found to be

$$g'(z) = \frac{\mu + \overline{\delta}}{z - z_0} + \frac{\overline{\lambda} + \mu z_0}{(z - z_0)^2} + \frac{\overline{\mu} + \delta}{z - \overline{z_0}} + \frac{\delta \overline{z_0} + 2\lambda}{(z - \overline{z_0})^2} + \frac{2\lambda \overline{z_0}}{(z - \overline{z_0})^3}. \tag{4.28}$$

But we know that $g'(z)$ must have the form

$$g'(z) = \frac{\mu \overline{z_0}}{(z - z_0)^2} + \text{locally analytic function}, \tag{4.29}$$

which implies that we must choose

$$\delta = -\overline{\mu}, \qquad \lambda = \overline{\mu}(z_0 - \overline{z_0}) \tag{4.30}$$

to obtain the required singularity. With this choice, we find

$$\begin{cases} f(z) = \dfrac{\mu}{z - z_0} - \dfrac{\overline{\mu}}{z - \overline{z_0}} + \dfrac{\overline{\mu}(z_0 - \overline{z_0})}{(z - \overline{z_0})^2}, \\ \\ g'(z) = \dfrac{\mu \overline{z_0}}{(z - z_0)^2} + \dfrac{2\overline{\mu} z_0 - 3\overline{\mu z_0}}{(z - \overline{z_0})^2} + \dfrac{2\overline{\mu z_0}(z_0 - \overline{z_0})}{(z - \overline{z_0})^3}, \end{cases} \tag{4.31}$$

which is identical to (4.23) found using the transform approach.

4.3 A point stresslet above a boundary with mixed boundary conditions

4.3.1 Problem formulation

Consider the fluid region to be again the upper half-plane $-\infty < x < \infty$, $y > 0$ (Figure 4.3), but now the boundary $x \in \mathbb{R}$, $y = 0$ consists of mixed boundary conditions; it is no-slip for $x < 0$ and no-stress for $x > 0$. A point stresslet of strength $\mu \in \mathbb{C}$ is placed at point z_0 in the fluid region.

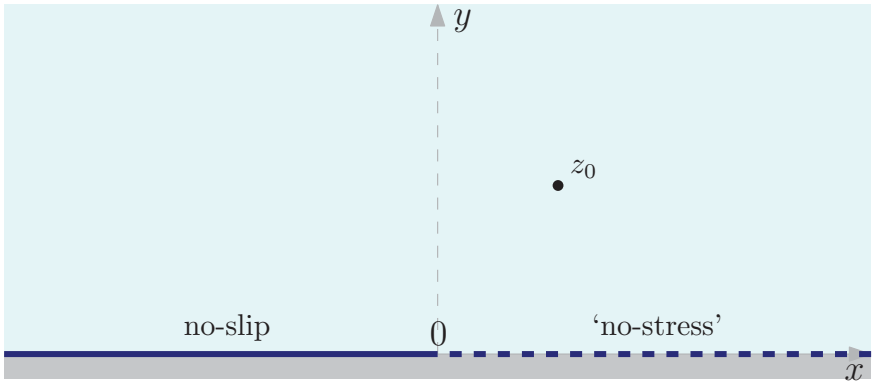

Figure 4.3: Problem configuration: a point stresslet at z_0 near a boundary with mixed boundary conditions.

The Goursat functions are, again, represented by

$$\begin{cases} f(z) = f_s(z) + \hat{f}(z), \\ g'(z) = g'_s(z) + \hat{g}'(z), \end{cases} \tag{4.32}$$

where $f_s(z)$, $g'_s(z)$ are related to the point stresslet:

$$\begin{cases} f_s(z) = \dfrac{\mu}{z - z_0}, \\ \\ g'_s(z) = \dfrac{\mu \overline{z_0}}{(z - z_0)^2}, \end{cases} \tag{4.33}$$

and $\hat{f}(z)$, $\hat{g}'(z)$ are unknown analytic functions in the fluid region vanishing in the far-field.

For $x < 0$, $y = 0$, the no-slip condition can be written as:

$$-\overline{f(z)} + z f'(z) + g'(z) = 0. \tag{4.34}$$

For $x > 0$, $y = 0$, the no-stress condition can be written as:

$$\overline{f(z)} + z f'(z) + g'(z) = 0, \tag{4.35}$$

which is equivalent to $H(z) = 0$; this, in turn, is equivalent to insisting that both tangential stress and normal velocity components on the boundary are equal to zero (Philip [88]). We observe that boundary conditions (4.34) and (4.35) look very similar, with only difference being the sign of the first term. This opposite sign implies that there is an associated square-root singularity at point $z = 0$ where the boundary conditions change type. This is crucial, since as we will see in the following subsections this singularity behaviour at the origin should be incorporated in the solution scheme.

The aim is again to determine the resulting fluid flow everywhere in the upper half-plane which has the required local behaviour near z_0 and which satisfies the given boundary conditions. To solve this problem, we decompose it into two sub-problems which can be solved separately using different techniques and whose superposition produces the problem of interest described above. This is, of course, possible due to the linearity of Stokes equations. The reason for decomposing into two sub-problems rather than solving the full problem directly is because we are then able to reduce, at each sub-problem, the number of unknown functions to one and this simplifies the analysis.

4.3.2 Problem I

Suppose that functions $f(z)$ and $g'(z)$ are such that

$$\begin{cases} f(z) = f_s(z) + \hat{f}(z), \\ g(z) = -zf(z), \end{cases} \tag{4.36}$$

where $\hat{f}(z)$ is analytic in the fluid region and decaying in the far-field and

$$f_s(z) = \frac{\mu}{z - z_0}. \tag{4.37}$$

Riemann-Hilbert approach (I):

Boundary conditions: For $x < 0$, we have no-slip condition on the boundary given by (4.34). Since $g'(z) = -zf'(z) - f(z)$, on substitution of (4.36) we find that

$$\hat{f}(z) + \overline{\hat{f}}(z) = -f_s(z) - \overline{f_s}(z), \tag{4.38}$$

where the terms on the right hand side of (4.38) are known functions.

For $x > 0$, we have 'no-stress' condition given by (4.35). On substitution of (4.36), we find that

$$\hat{f}(z) - \overline{\hat{f}}(z) = -f_s(z) + \overline{f_s}(z). \tag{4.39}$$

Analysis of the boundary conditions: We know that at point $z = 0$, where the boundary conditions change from no-slip to no-stress, there is an associated square-root singularity (Philip [88]). In this section, we will show how to incorporate this singularity structure in our solution scheme and then obtain the solution. It should be noted that, in general, it is not always possible to parametrise other singularity structures analytically.

Define the function

$$X(z) = \frac{1}{\sqrt{z}}, \tag{4.40}$$

which is a multivalued function; without loss of generality we take a branch cut on the negative real axis. Then

$$\begin{cases} X^+(z) + X^-(z) = 0, & \text{for } x < 0. \\ X^+(z) - X^-(z) = 0, & \text{for } x > 0. \end{cases} \tag{4.41}$$

where $X^+(z)$ and $X^-(z)$ are the limiting values of $X(z)$ as z approaches the real axis from the upper and lower half-plane respectively.

Next, we multiply (4.38) and (4.39) by $X^+(z)$ to obtain

$$\begin{cases} X^+(z)\hat{f}(z) + X^+(z)\overline{\hat{f}}(z) = -\dfrac{\mu X^+(z)}{z-z_0} - \dfrac{\overline{\mu} X^+(z)}{z-\overline{z_0}}, & \text{for } x<0. \\ \\ X^+(z)\hat{f}(z) - X^+(z)\overline{\hat{f}}(z) = -\dfrac{\mu X^+(z)}{z-z_0} + \dfrac{\overline{\mu} X^+(z)}{z-\overline{z_0}}, & \text{for } x>0. \end{cases} \tag{4.42}$$

Using (4.41), we can write:

$$X^+(z)\hat{f}(z) - X^-(z)\overline{\hat{f}}(z) = \begin{cases} -\dfrac{\mu X^+(z)}{z-z_0} - \dfrac{\overline{\mu} X^+(z)}{z-\overline{z_0}}, & \text{for } x<0. \\ \\ -\dfrac{\mu X^+(z)}{z-z_0} + \dfrac{\overline{\mu} X^+(z)}{z-\overline{z_0}}, & \text{for } x>0. \end{cases} \tag{4.43}$$

Let $r(z) = X(z)\hat{f}(z)$, such that

$$\begin{cases} r(z) \equiv r^+(z) = X^+(z)\hat{f}(z), & \text{for } z \text{ in the upper half-plane.} \\ r(z) \equiv r^-(z) = X^-(z)\overline{\hat{f}}(z), & \text{for } z \text{ in the lower half-plane.} \end{cases} \tag{4.44}$$

Expressions (4.43) can be then written as

$$r^+(z) - r^-(z) = \phi(z), \tag{4.45}$$

where

$$\phi(z) = \begin{cases} -\dfrac{\mu X^+(z)}{z-z_0} - \dfrac{\overline{\mu} X^+(z)}{z-\overline{z_0}}, & \text{for } x<0. \\ \\ -\dfrac{\mu X^+(z)}{z-z_0} + \dfrac{\overline{\mu} X^+(z)}{z-\overline{z_0}}, & \text{for } x>0. \end{cases} \tag{4.46}$$

This is a Riemann-Hilbert problem on the real axis. It can be solved in closed form (Ablowitz & Fokas [1]) using the fact that $\hat{f}(z)$ is analytic in the upper half-plane (fluid region) and hence $\overline{\hat{f}}(z)$ is analytic in the lower half-plane. Using the Cauchy integral for-

mula, we find

$$r(z) = X(z)\hat{f}(z) = \frac{1}{2\pi \mathrm{i}} \int_{-\infty}^{0} \left(-\frac{\mu}{\sqrt{z'}(z'-z_0)} - \frac{\overline{\mu}}{\sqrt{z'}(z'-\overline{z_0})} \right) \frac{dz'}{z'-z} + \frac{1}{2\pi \mathrm{i}} \int_{0}^{\infty} \left(-\frac{\mu}{\sqrt{z'}(z'-z_0)} + \frac{\overline{\mu}}{\sqrt{z'}(z'-\overline{z_0})} \right) \frac{dz'}{z'-z}. \tag{4.47}$$

Using residue calculus, we find that

$$\begin{aligned} \int_{-\infty}^{\infty} \frac{\mu}{\sqrt{z'}(z'-z_0)(z'-z)} dz' &= \frac{2\pi \mathrm{i}\mu}{z-z_0} \left(\frac{1}{\sqrt{z}} - \frac{1}{\sqrt{z_0}} \right), \\ \int_{-\infty}^{0} \frac{\overline{\mu}}{\sqrt{z'}(z'-\overline{z_0})(z'-z)} dz' &= \frac{\pi \mathrm{i}\overline{\mu}}{z-\overline{z_0}} \left(\frac{1}{\sqrt{z}} - \frac{1}{\sqrt{\overline{z_0}}} \right), \\ \int_{0}^{\infty} \frac{\overline{\mu}}{\sqrt{z'}(z'-\overline{z_0})(z'-z)} dz' &= \frac{\pi \mathrm{i}\overline{\mu}}{z-\overline{z_0}} \left(\frac{1}{\sqrt{z}} + \frac{1}{\sqrt{\overline{z_0}}} \right). \end{aligned} \tag{4.48}$$

Substitution of (4.48) into (4.47) and solving for $\hat{f}(z)$ gives

$$\hat{f}(z) = \frac{\mu}{z-z_0} \left(\frac{\sqrt{z}}{\sqrt{z_0}} - 1 \right) + \frac{\overline{\mu}}{z-\overline{z_0}} \frac{\sqrt{z}}{\sqrt{\overline{z_0}}}. \tag{4.49}$$

Summary: The solution is given by

$$\begin{cases} f(z) = \dfrac{\mu}{z-z_0} \dfrac{\sqrt{z}}{\sqrt{z_0}} + \dfrac{\overline{\mu}}{z-\overline{z_0}} \dfrac{\sqrt{z}}{\sqrt{\overline{z_0}}}, \\ \\ g(z) = -zf(z), \end{cases} \tag{4.50}$$

which is found upon substitution of (4.49) into (4.36).

Conformal mapping (I):

We now present a different method for solving problem I which is based on conformal mappings. Note that, as already mentioned, although Stokes equations are not conformally invariant, analytical progress can be made in some cases. As we show in this subsection, a closed-form solution can be found in this problem.

Consider the composed conformal mapping (Crowdy [16]):

$$z = z(\zeta) = \chi(\eta(\zeta)), \tag{4.51}$$

where

$$\eta(\zeta) = \frac{(\zeta - \alpha)(\zeta - 1/\alpha)}{(\zeta - \overline{\alpha})(\zeta - 1/\overline{\alpha})}, \quad \alpha = \mathrm{i}r, \quad 0 < r < 1, \tag{4.52}$$

and

$$\chi(\eta) = e^{-\mathrm{i}\beta}\left(\frac{\eta - c}{\eta - \overline{c}}\right), \quad c = e^{\mathrm{i}\beta}, \quad 0 < \beta < \pi. \tag{4.53}$$

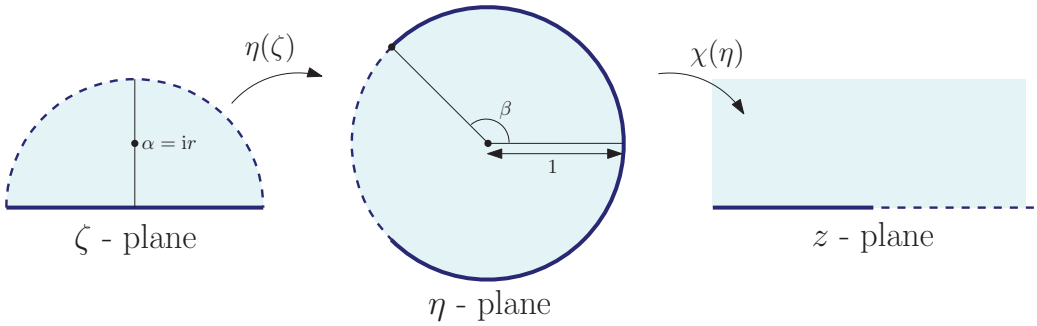

Figure 4.4: Conformal mapping from the upper unit ζ-disc (left) to the unit η-disc (centre) and finally to the fluid region in the upper half-plane (right). The correspondence of the boundaries is illustrated by the solid and dashed lines.

The conformal mapping (5.47) (Fig. 4.4) takes the parametric ζ-plane and transplants it on the physical z-plane. More specifically, the first mapping (5.48) transplants the upper unit semi-disc in a parametric ζ-plane to a unit disc in another parametric η-plane. The point $\zeta = \alpha$ maps to $\eta = 0$, the real interval $\zeta \in [-1, 1]$ maps to the arc of the unit η circle with $\arg[\eta] \in [-\beta, \beta]$, and the upper half semicircle $|\zeta| = 1$, $\mathrm{Im}[\zeta] \geq 0$ maps to the arc of the

unit η circle with $\arg[\eta] \in [\beta, 2\pi - \beta]$. The point $\eta = \overline{c} = e^{-i\beta}$ for $0 < \beta < \pi$ is the image of $\zeta = -1$ so that $\overline{c} = e^{-i\beta} = \eta(-1)$, from which it can be deduced that

$$r = \tan\left(\frac{\pi}{4} - \frac{\beta}{4}\right). \tag{4.54}$$

Next, the second mapping given by (4.53) transplants the unit η disc to the fluid region (z-plane) above the planar boundary. The arc given by $\arg[\eta] \in [-\beta, \beta]$ is mapped to the negative real axis while the arc given by $\arg[\eta] \in [\beta, 2\pi - \beta]$ is mapped to the positive one.

Next, we define the composed functions

$$F(\zeta) \equiv f(z(\zeta)), \quad G(\zeta) \equiv g'(z(\zeta)). \tag{4.55}$$

which will be fully determined using the boundary conditions and the expressions for $f(z)$ and $g'(z)$ associated with a point stresslet.

Mathematical formulation: The no-slip condition on $z = x < 0$ is given by (4.34) which upon substitution of $g(z) = -zf(z)$ becomes

$$f(z) + \overline{f(z)} = 0. \tag{4.56}$$

Since the no-slip boundary $z = x < 0$ corresponds to the real interval $\zeta \in [-1, 1]$ in the ζ-plane, (4.56) is equivalent to

$$\overline{F}(\zeta) = -F(\zeta). \tag{4.57}$$

In a similar way, the 'no-stress' condition on $z = x > 0$ is given by (4.35) which upon substitution of $g(z) = -zf(z)$ becomes

$$f(z) - \overline{f(z)} = 0. \tag{4.58}$$

Since the 'no-stress' boundary $z = x > 0$ corresponds to the upper half semicircle $|\zeta| = 1$

in the ζ-plane, (4.58) is equivalent to

$$\overline{F}(1/\zeta) = F(\zeta). \tag{4.59}$$

Requiring $F(\zeta)$ to have the local behaviour of (4.36) and satisfying the conditions (4.57) and (4.59), we can write down its general form

$$F(\zeta) = \frac{A}{\zeta - \zeta_0} - \frac{\overline{A}}{\zeta - \overline{\zeta_0}} - \frac{A}{1/\zeta - \zeta_0} + \frac{\overline{A}}{1/\zeta - \overline{\zeta_0}}, \tag{4.60}$$

where A is a constant to be determined. Using partial fractions and equating coefficients such that $F(\zeta)$ has the local behaviour of (4.36), we find that

$$A = \frac{\mu}{z'(\zeta_0)}. \tag{4.61}$$

Function $G(\zeta)$ can be found upon substitution of (4.60) into one of the boundary conditions.

Comparison of the two methods:

The solutions found using the two methods have been compared numerically and were found to be identical. Note that, although we have closed-form expressions for the Goursat functions in both cases, the conformal mapping approach gives expressions for these functions in terms of variable ζ. Therefore, we can also check the two methods by expressing both solutions in terms of ζ using the conformal mapping $z(\zeta)$.

4.3.3 Problem II

Now, suppose that

$$\begin{cases} f(z) = \hat{f}(z), \\ g'(z) = g'_s(z) + \hat{g}'(z), \end{cases} \tag{4.62}$$

where $\hat{f}(z)$ and $\hat{g}'(z)$ are analytic functions which decay in the far-field and

$$g_s'(z) = \frac{\mu(\overline{z_0} - z_0)}{(z - z_0)^2}. \tag{4.63}$$

The choice of these functions was led by the requirement that superposition of the two problems (I & II) produces (4.32).

Transform approach (II):

Boundary conditions: Again, for $x < 0$, we have no-slip condition (4.34). On substitution of (4.62), we find that

$$-\overline{\hat{f}(z)} + z\hat{f}'(z) + \hat{g}'(z) = -g_s'(z). \tag{4.64}$$

For $x > 0$, we have 'no-stress' condition on the boundary (4.35). On substitution of (4.62), we find that

$$\overline{\hat{f}(z)} + z\hat{f}'(z) + \hat{g}'(z) = -g_s'(z). \tag{4.65}$$

Function representation: Function $\hat{f}(z)$, which is analytic in the region above the planar boundary and decaying in the far-field, will be represented by

$$\hat{f}(z) = \frac{1}{2\pi}\int_0^\infty \rho_1(k)e^{\mathrm{i}kz}dk, \tag{4.66}$$

with $\rho_1(k)$ defined by

$$\rho_1(k) = \int_{-\infty}^{\infty} \hat{f}(z)e^{-\mathrm{i}kz}dz = \sigma_1(k) + \sigma_2(k), \tag{4.67}$$

where

$$\sigma_1(k) = \int_{-\infty}^{0} \hat{f}(z)e^{-\mathrm{i}kz}dz, \qquad \sigma_2(k) = \int_0^\infty \hat{f}(z)e^{-\mathrm{i}kz}dz. \tag{4.68}$$

Similarly, we write:

$$\hat{g}'(z) = \frac{1}{2\pi}\int_0^\infty \hat{\rho}_1(k)e^{\mathrm{i}kz}dk, \tag{4.69}$$

with $\hat{\rho}_1(k)$ defined by

$$\hat{\rho}_1(k) = \int_{-\infty}^{\infty} \hat{g}'(z) e^{-\mathrm{i}kz} dz = \hat{\sigma}_1(k) + \hat{\sigma}_2(k), \tag{4.70}$$

where

$$\hat{\sigma}_1(k) = \int_{-\infty}^{0} \hat{g}'(z) e^{-\mathrm{i}kz} dz, \qquad \hat{\sigma}_2(k) = \int_{0}^{\infty} \hat{g}'(z) e^{-\mathrm{i}kz} dz. \tag{4.71}$$

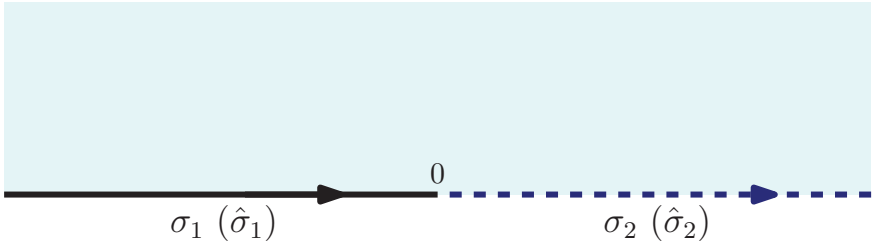

Figure 4.5: Schematic of the spectral functions along the real axis.

Global relations: The spectral functions satisfy

$$\begin{aligned} \rho_1(k) &= \sigma_1(k) + \sigma_2(k) = 0, \qquad \text{for } k < 0, \\ \hat{\rho}_1(k) &= \hat{\sigma}_1(k) + \hat{\sigma}_2(k) = 0, \qquad \text{for } k < 0. \end{aligned} \tag{4.72}$$

Preliminary observations: Taking the Schwarz conjugate of $\sigma_1(k)$ we find that

$$\overline{\sigma_1}(k) = \int_{-\infty}^{0} \overline{\hat{f}(z)} e^{\mathrm{i}kz} dz. \tag{4.73}$$

If we let $k \mapsto -k$ we find

$$\overline{\sigma_1}(-k) = \int_{-\infty}^{0} \overline{\hat{f}(z)} e^{-\mathrm{i}kz} dz. \tag{4.74}$$

Similarly, taking the Schwarz conjugate of $\sigma_2(k)$ and mapping $k \to -k$, we find

$$\overline{\sigma_2}(-k) = \int_{0}^{\infty} \overline{\hat{f}(z)} e^{-\mathrm{i}kz} dz. \tag{4.75}$$

In addition, it can be shown that, after integration by parts,

$$\int_{-\infty}^{0} z\hat{f}'(z)e^{-\mathrm{i}kz}dz = -\frac{\partial[k\sigma_1(k)]}{\partial k}, \qquad \int_{0}^{\infty} z\hat{f}'(z)e^{-\mathrm{i}kz}dz = -\frac{\partial[k\sigma_2(k)]}{\partial k}. \tag{4.76}$$

The expressions above will be needed in the spectral analysis which follows.

Spectral analysis: In this section, we will obtain more information about the spectral functions by making use of the boundary conditions.

We multiply the boundary condition (4.64) by $e^{-\mathrm{i}kz}$ and integrate along the negative real axis:

$$-\int_{-\infty}^{0} \overline{\hat{f}(z)}e^{-\mathrm{i}kz}dz + \int_{-\infty}^{0} z\hat{f}'(z)e^{-\mathrm{i}kz}dz + \int_{-\infty}^{0} \hat{g}'(z)e^{-\mathrm{i}kz}dz = R_1(k), \tag{4.77}$$

where

$$R_1(k) \equiv -\int_{-\infty}^{0} g_s'(z)e^{-\mathrm{i}kz}dz. \tag{4.78}$$

The function $R_1(k)$ is known. On use of (4.74) and the first expression in (4.76), this can be written as

$$-\overline{\sigma_1}(-k) - \frac{\partial[k\sigma_1(k)]}{\partial k} + \hat{\sigma}_1(k) = R_1(k). \tag{4.79}$$

Next, we multiply the second boundary condition (4.65) by $e^{-\mathrm{i}kz}$ and integrate along the positive real axis we find

$$\int_{0}^{\infty} \overline{\hat{f}(z)}e^{-\mathrm{i}kz}dz + \int_{0}^{\infty} z\hat{f}'(z)e^{-\mathrm{i}kz}dz + \int_{0}^{\infty} \hat{g}'(z)e^{-\mathrm{i}kz}dz = R_2(k), \tag{4.80}$$

where

$$R_2(k) \equiv -\int_{0}^{\infty} g_s'(z)e^{-\mathrm{i}kz}dz. \tag{4.81}$$

Simlarly, on use of (4.75) and the second expression in (4.76), (4.80) can be written as

$$\overline{\sigma_2}(-k) - \frac{\partial[k\sigma_2(k)]}{\partial k} + \hat{\sigma}_2(k) = R_2(k). \tag{4.82}$$

Analysis of derived relations: Adding (4.79) and (4.82), we obtain

$$-\overline{\sigma_1}(-k)+\overline{\sigma_2}(-k)-\frac{\partial[k(\sigma_1(k)+\sigma_2(k))]}{\partial k}+\hat{\sigma}_1(k)+\hat{\sigma}_2(k)=S(k), \tag{4.83}$$

where

$$S(k)\equiv R_1(k)+R_2(k)=-\int_{-\infty}^{\infty} g_s'(z)e^{-\mathrm{i}kz}dz. \tag{4.84}$$

Using the global relations (4.72), we obtain

$$-\overline{\sigma_1}(-k)+\overline{\sigma_2}(-k)=S(k), \qquad \text{for } k<0. \tag{4.85}$$

Taking a complex conjugate and letting $k\mapsto -k$, we find

$$-\sigma_1(k)+\sigma_2(k)=\overline{S}(-k), \qquad \text{for } k>0. \tag{4.86}$$

Hence we have two equations for $\sigma_1(k)$ and $\sigma_2(k)$ given by (4.72) and (4.86) which are defined on the negative and positive real axis respectively. Note that, for $z=x\in\mathbb{R}$,

$$|e^{-\mathrm{i}kz}|=|e^{-\mathrm{i}(k_r+\mathrm{i}k_i)x}|=e^{k_i x}, \tag{4.87}$$

and therefore $\sigma_1(k)$ is upper analytic (since it is integrated over $x<0$), while $\sigma_2(k)$ is lower analytic (since it is integrated over $x>0$).

Riemann-Hilbert problem on the real axis: We have found that

$$\begin{cases} \sigma_1(k)-\sigma_2(k)=-\overline{S}(-k), & \text{for } k>0. \\ \sigma_1(k)+\sigma_2(k)=0, & \text{for } k<0. \end{cases} \tag{4.88}$$

Note that $\sigma_1(k)$ is analytic in the upper half-plane, while $\sigma_2(k)$ is analytic in the lower half-plane. Next, let

$$X(k)=\sqrt{k} \tag{4.89}$$

and, without loss of generality, introduce a branch cut on the negative real axis. Using that

$$\begin{cases} X^+(k) + X^-(k) = 0, & \text{for } k < 0. \\ X^+(k) - X^-(k) = 0, & \text{for } k > 0. \end{cases} \tag{4.90}$$

we multiply (4.88) by $X^+(k)$ to obtain

$$X^+(k)\sigma_1(k) - X^-(k)\sigma_2(k) = \phi(k) = \begin{cases} -X^+(k)\overline{S}(-k), & \text{for } k > 0. \\ 0, & \text{for } k < 0. \end{cases} \tag{4.91}$$

This is again a Riemann-Hilbert problem on the real axis, where $X^+(k)\sigma_1(k)$ is analytic in the upper half-plane and $X^-(k)\sigma_2(k)$ is analytic in the lower half-plane. Using the Plemelj formulae (since the sum of $\sigma_1(k)$ and $\sigma_2(k)$ is the unknown) [1], we find that

$$X^+(k)\sigma_1(k) + X^-(k)\sigma_2(k) = \frac{1}{\pi \mathrm{i}} \int_{-\infty}^{\infty} \frac{\phi(k')}{k' - k} dk', \quad \text{for } k \in \mathbb{R}. \tag{4.92}$$

Recall that, for $k > 0$, $X^+(k) = X^-(k)$. Therefore dividing by $X^+(k)$ gives

$$\rho_1(k) = \sigma_1(k) + \sigma_2(k) = \frac{1}{\pi \mathrm{i}} \frac{1}{X^+(k)} \int_{-\infty}^{\infty} \frac{\phi(k')}{k' - k} dk', \quad \text{for } k > 0. \tag{4.93}$$

Note that $\overline{S}(-k')$ can be computed explicitly using residue calculus;

$$\overline{S}(-k') = 2\pi\overline{\mu}k'(z_0 - \overline{z_0})e^{-\mathrm{i}k'\overline{z_0}}, \quad \text{for } k' > 0. \tag{4.94}$$

which is finally substituted in (4.93) to give

$$\rho_1(k) = \frac{2\mathrm{i}\overline{\mu}(z_0 - \overline{z_0})}{\sqrt{k}} \int_0^{\infty} \frac{(k')^{\frac{3}{2}} e^{-\mathrm{i}k'\overline{z_0}}}{k' - k} dk', \quad \text{for } k > 0, \tag{4.95}$$

and hence $\hat{f}(z)$ is found using

$$\hat{f}(z) = \frac{1}{2\pi} \int_0^{\infty} \rho_1(k) e^{\mathrm{i}kz} dk. \tag{4.96}$$

The spectral function $\hat{\rho}_1(k)$ can be computed from (4.83) and therefore $\hat{g}'(z)$ can be com-

puted.

Conformal mapping (II):

Consider the composed conformal mapping given by (5.47)-(4.53) and define the composed functions

$$F(\zeta) \equiv f(z(\zeta)), \quad G(\zeta) = g'(z(\zeta)). \tag{4.97}$$

Mathematical formulation: The no-slip condition on $z = x < 0$ (which corresponds to $\zeta \in [-1, 1]$ in the ζ-plane) implies that

$$G(\zeta) = \overline{F}(\zeta) - \overline{z}(\zeta)\frac{F'(\zeta)}{z'(\zeta)}, \tag{4.98}$$

while the no-stress condition on $z = x > 0$ (which corresponds to the upper half semicircle $|\zeta| = 1$ in the ζ-plane) gives

$$G(\zeta) = -\overline{F}(1/\zeta) - \overline{z}(1/\zeta)\frac{F'(\zeta)}{z'(\zeta)}. \tag{4.99}$$

Analytic continuation off the boundaries and use of the fact that $\overline{z}(\zeta) = \overline{z}(1/\zeta)$ implies the following condition,

$$F(\zeta) = -F(1/\zeta). \tag{4.100}$$

Requiring $G(\zeta)$ to have the local behavior of (4.62), we can write down the general form of function $F(\zeta)$ satisfying (4.100); this is given by

$$F(\zeta) = \frac{A}{\zeta - \overline{\zeta_0}} - \frac{A}{1/\zeta - \overline{\zeta_0}} + \frac{B}{(\zeta - \overline{\zeta_0})^2} - \frac{B}{(1/\zeta - \overline{\zeta_0})^2}, \tag{4.101}$$

where A and B are constants to be determined. Using partial fractions and equating coefficients such that $G(\zeta)$ has the local behavior of (4.62), we find that

$$B = \frac{\overline{\mu}(z_0 - \overline{z_0})}{\overline{\hat{\alpha}}^2}, \quad \text{where } \hat{\alpha} = z'(\zeta_0), \tag{4.102}$$

$$A = -\overline{\hat{\beta}}B, \quad \text{where } \hat{\beta} = \frac{z''(\zeta_0)}{z'(\zeta_0)}. \tag{4.103}$$

Function $G(\zeta)$ can be computed using either (4.98) or (4.99).

Comparison of the two approaches:

The solutions found using the two methods have been compared numerically. We have found that our solution (4.95)-(4.96) given in 'closed form' (as infinite integrals) converges to the exact conformal mapping solution. It should be noted that expression (4.95) involves computation of a Cauchy principal value integral which means that special care should be taken when numerically integrating (4.96).

4.3.4 Conformal mapping (full problem)

For completeness, we present a conformal mapping approach to solve the full problem (4.32)-(4.35). We have also used this solution to check that superposition of problems I and II produces the solution to the problem of interest.

Consider the composed conformal mapping given by (5.47)-(4.53) and define the composed functions

$$F(\zeta) \equiv f(z(\zeta)), \quad G(\zeta) = g'(z(\zeta)). \tag{4.104}$$

The no-slip condition on $z = x < 0$ implies that, on $\overline{\zeta} = \zeta$,

$$0 = -\overline{F}(\zeta) + \overline{z}(\zeta)\frac{F'(\zeta)}{z'(\zeta)} + G(\zeta), \tag{4.105}$$

while the no-stress condition on $z = x > 0$ implies that, on $|\zeta| = 1$ (upper semicircle),

$$0 = \overline{F}(1/\zeta) + \overline{z}(1/\zeta)\frac{F'(\zeta)}{z'(\zeta)} + G(\zeta). \tag{4.106}$$

Adding (4.105) and (4.106) (analytic continuation off the boundary) and using the fact that

$$\overline{z}(\zeta) = \overline{z}(1/\zeta), \tag{4.107}$$

which can be demonstrated from (5.47)-(4.53), it can be deduced that

$$F(\zeta) = -F(1/\zeta). \tag{4.108}$$

Also (4.105) can be rearranged to

$$\overline{F}(\zeta) = \overline{z}(\zeta)\frac{F'(\zeta)}{z'(\zeta)} + G(\zeta). \tag{4.109}$$

Simple observations reveal that both terms on the right-hand side of (4.109) have a second-order pole at ζ_0 ($z_0 = z(\zeta_0)$) and as a result $F(\zeta)$ has a second-order pole at $\overline{\zeta_0}$.

Requiring $F(\zeta)$ to have the local behaviour of (4.32)-(4.33) and satisfying the conditions deduced above, we can write down its general form

$$F(\zeta) = \frac{A}{\zeta - \zeta_0} - \frac{A}{1/\zeta - \zeta_0} + \frac{B}{(\zeta - \overline{\zeta_0})^2} - \frac{B}{(1/\zeta - \overline{\zeta_0})^2} + \frac{C}{\zeta - \overline{\zeta_0}} - \frac{C}{1/\zeta - \overline{\zeta_0}}, \tag{4.110}$$

where A, B and C are constants to be determined. The function $G(\zeta)$ can be computed using (4.105)

$$G(\zeta) = \overline{F}(\zeta) - h(\zeta)F'(\zeta), \quad \text{where } h(\zeta) = \frac{\overline{z}(\zeta)}{z'(\zeta)} \tag{4.111}$$

Using partial fractions and equating coefficients such that $F(\zeta)$ and $G(\zeta)$ have the local behaviour of (4.33), we find that

$$A = \frac{\mu}{z'(\zeta_0)}, \tag{4.112}$$

$$B = \frac{\overline{\mu} z_0}{\overline{\hat{\alpha}}^2} - \overline{Ah(\zeta_0)}, \quad \text{where } \hat{\alpha} = z'(\zeta_0), \tag{4.113}$$

$$C = -\overline{\hat{\beta}}\left[B + \overline{Ah(\zeta_0)}\right] - \overline{Ah'(\zeta_0)}, \quad \text{where } \hat{\beta} = \frac{z''(\zeta_0)}{z'(\zeta_0)}. \tag{4.114}$$

4.4 Summary

In this chapter, we have shown how to solve boundary value problems in the half-plane using the transform method for polygonal domains. The two problems considered were

that of a point singularity above a no-slip wall and above a wall with mixed boundary conditions. In the first problem, we have shown that the transform method can be used to retrieve the exact solution which can be found using the classical method of images. The second problem was analyzed using the transform method and Riemann-Hilbert problem techniques along the real axis. Notably, we have shown how these two methods can be combined to solve this mixed boundary value problem. All solutions found using the transform method were checked against other techniques (method of images, conformal mapping).

Chapter 5

Shear flow past a periodic array of semi-infinite plates

5.1 Introduction

In this chapter, we present our transform approach for polygonal domains for solving two mixed-type boundary value problems which were previously solved using the Wiener-Hopf technique. The model problems involve shear flow past a periodic array of semi-infinite flat plates: if the shear flow is longitudinal, the boundary value problem is for a harmonic field; if the shear flow is transverse a biharmonic field is relevant. Luchini *et al.* [78] were the first to use Wiener-Hopf techniques to solve both problems in 1991 in the physical context of shear flow over riblets; ten years later Jeong [54], who was motivated by porous media flows, solved the same boundary value problem also using the Wiener-Hopf method but with some technical differences in his approach.

The four main steps of our approach to problems of Wiener-Hopf type are as follows:

(a) **Domain splitting:** for a problem domain involving boundary conditions of mixed type, find a convenient "splitting" of the problem domain (domain decomposition) into distinct boundary value sub-problems and solve each using the unified transform method;

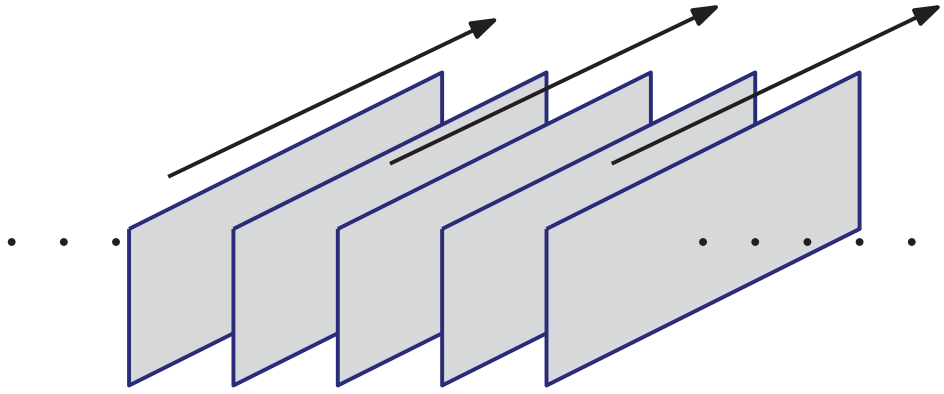

Figure 5.1: Shear flow past a periodic array of semi-infinite flat plates in the longitudinal direction: the boundary value problem to be solved is for a harmonic field. This problem was solved by Luchini *et al.* [78] and Jeong [54].

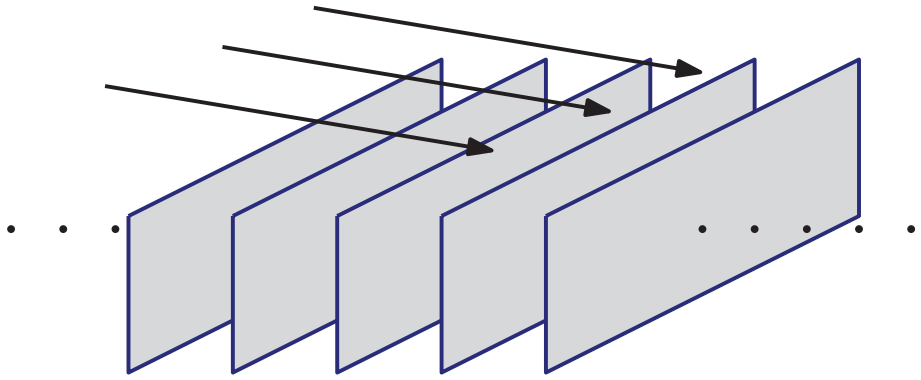

Figure 5.2: Shear flow past a periodic array of semi-infinite flat plates in the transverse direction: the boundary value problem to be solved is for a biharmonic field. This problem was solved by Luchini *et al.* [78] and Jeong [54].

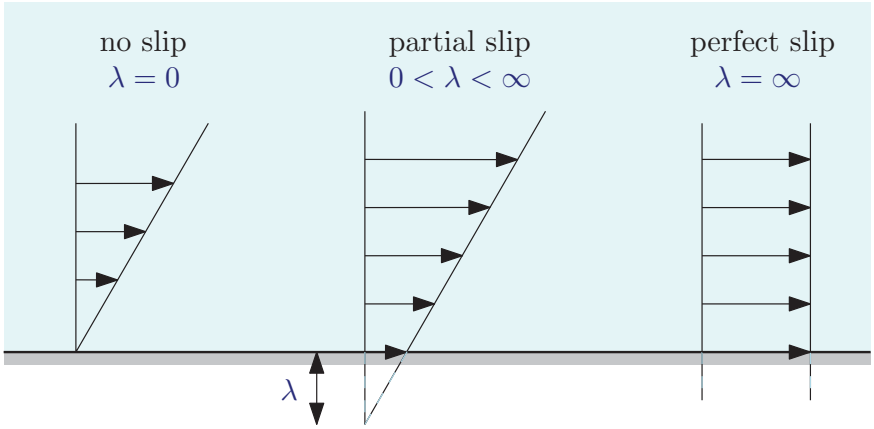

Figure 5.3: Interpretation of the slip length λ: the fictitious distance below the surface where the no-slip boundary condition would be satisfied.

(b) **Boundary conditions:** couple the resulting sub-problems by employing the same spectral parameter for each and by imposing appropriate continuity conditions on any common edges;

(c) **Spectral analysis:** analyse the spectral relations arising from the boundary conditions, together with the global relations, to identify special points in the spectral plane whereby information on a reduced set of unknown spectral functions can be determined;

(d) **Solution scheme and function representation:** identify the precise nature of the singularities occurring at boundary points where the boundary conditions change type and represent unknown boundary data in terms of specially tailored variables that incorporate those edge singularities. Solve for a reduced set of spectral functions, with the rest following by back-substitution into the spectral relations.

5.2 The slip length λ

In both longitudinal and transverse flow problems, there is an associated slip length λ (which is different for these flow directions). The slip length λ is a characteristic quantity in problems with mixed boundary conditions in low-Reynolds-number flows (applications

to microfluidics and superhydrophobic surfaces). For a shear flow, λ can be interpreted as the fictitious distance below the surface where the no-slip boundary condition would be satisfied (Lauga, Brenner & Stone [70]), as shown in Figure 5.3.

5.3 Longitudinal flow problem

Consider a steady longitudinal shear flow past an array of semi-infinite walls where the velocity $\mathbf{u}$ in Cartesian coordinates (x, y, z) has the form

$$\mathbf{u} = (0, 0, w(x, y)). \tag{5.1}$$

The walls are half-planes parallel to the flow direction occupying the region $-\infty < x < 0$ for $y = h/2+nh$ where $n \in \mathbb{Z}$ and $h > 0$. Since the geometry is periodic in the y-direction, it is enough to analyze the problem in the domain $-\infty < x < \infty, -h/2 < y < h/2$ as shown in Figure 6.1.

Assuming no pressure gradient drives the flow then velocity $w(x, y)$ satisfies Laplace's equation

$$\nabla^2 w(x, y) = 0 \tag{5.2}$$

in the flow domain. As $x \to +\infty$, the flow tends to a shear flow of the form

$$(u, v, w) \to (0, 0, Ux + \lambda), \tag{5.3}$$

where U is the shear rate and λ has an interpretation as the longitudinal slip length. While U is externally specifiable the value of λ is determined by the solution. On the other hand, as $x \to -\infty$,

$$w(x, y) \to 0. \tag{5.4}$$

Next, we introduce a complex potential function $q(z)$ given by

$$q(z) = w(x, y) + \mathrm{i}\chi(x, y), \tag{5.5}$$

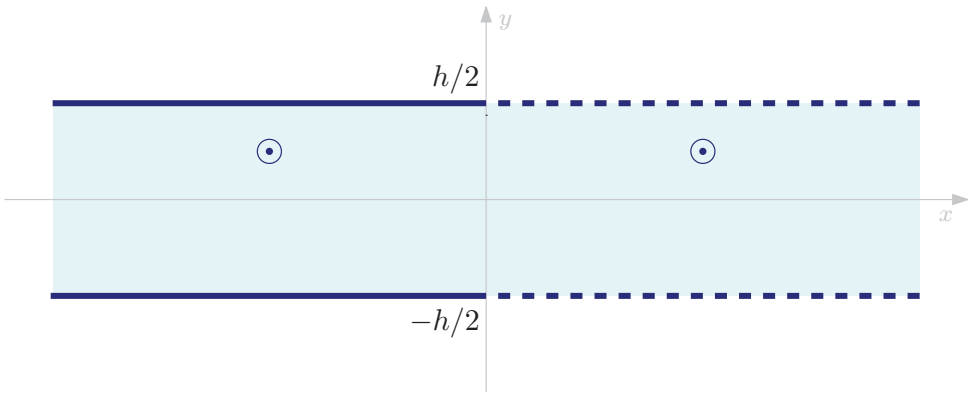

Figure 5.4: Schematic of a single period of the longitudinal problem of shear flow past an array of semi-infinite flat plates (extending indefinitely into $y \to \pm\infty$). The no-slip walls of this period window are defined for $x < 0$ and $y = \pm h/2$. The velocity $w(x, y)$, which is into the page (direction is denoted by the two circles), tends to a uniform shear as $x \to +\infty$ and vanishes as $x \to -\infty$.

with $\chi(x, y)$ being the harmonic conjugate to $w(x, y)$. It is clear that finding the complex potential and then taking its real part will give us the velocity in the fluid region.

Flow symmetry: The flow is symmetric with respect to $y = 0$ and this implies that the complex potential and its Schwarz conjugate satisfy the condition

$$\overline{q}(z) = q(z). \tag{5.6}$$

5.3.1 Domain splitting: left and right semi-strips

Since the configuration consists of mixed boundary conditions in a channel geometry, it is natural to split the domain into left and right semi-strips separated by the common edge $x = 0, y \in [-h/2, h/2]$. Figure 5.5 shows a schematic of the domain splitting.

Left semi-strip: In the left semi-strip we define the complex potential to be given by

$$q(z) = q_L(z), \tag{5.7}$$

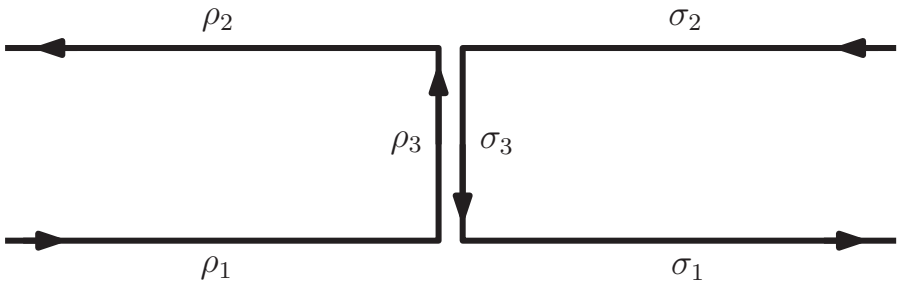

Figure 5.5: Domain splitting into two semi-strips and related spectral functions. (the common edge at $x = 0$ is shown separately for each sub-problem).

where $q_L(z)$ is analytic in the left semi-strip and vanishes as $x \to -\infty$.

Following Fokas & Kapaev [43] and Fokas [38], the analytic function $q_L(z)$ can be represented by

$$q_L(z) = \frac{1}{2\pi}\left[\int_0^{\infty} \rho_1(k)e^{\mathrm{i}kz}dk + \int_0^{-\infty} \rho_2(k)e^{\mathrm{i}kz}dk + \int_0^{-\mathrm{i}\infty} \rho_3(k)e^{\mathrm{i}kz}dk\right], \tag{5.8}$$

where the spectral functions $\rho_1(k)$, $\rho_2(k)$ and $\rho_3(k)$ are defined by

$$\begin{aligned}
\rho_1(k) &= \int_{-\infty-\mathrm{i}h/2}^{-\mathrm{i}h/2} q_L(z)e^{-\mathrm{i}kz}dz, \\
\rho_2(k) &= \int_{\mathrm{i}h/2}^{-\infty+\mathrm{i}h/2} q_L(z)e^{-\mathrm{i}kz}dz, \\
\rho_3(k) &= \int_{-\mathrm{i}h/2}^{\mathrm{i}h/2} q_L(z)e^{-\mathrm{i}kz}dz
\end{aligned} \tag{5.9}$$

and are illustrated in Figure 5.5.

The global relation (Fokas & Kapaev [43], Fokas [38]) for the left semi-strip is given by

$$\rho_1(k) + \rho_2(k) + \rho_3(k) = 0, \quad \mathrm{Im}k \geq 0. \tag{5.10}$$

Right semi-strip: In the right semi-strip the complex potential is defined to be

$$q(z) = q_s(z) + q_R(z), \tag{5.11}$$

where $q_s(z)$ is the forcing function related to the longitudinal shear flow

$$q_s(z) = Uz + \lambda, \tag{5.12}$$

and $q_R(z)$ is analytic in the right semi-strip and vanishes as $x \to +\infty$.

Similarly, the analytic function $q_R(z)$ can be represented by

$$q_R(z) = \frac{1}{2\pi}\left[\int_0^{\infty} \sigma_1(k)e^{\mathrm{i}kz}dk + \int_0^{-\infty} \sigma_2(k)e^{\mathrm{i}kz}dk + \int_0^{\mathrm{i}\infty} \sigma_3(k)e^{\mathrm{i}kz}dk\right], \tag{5.13}$$

where $\sigma_1(k)$, $\sigma_2(k)$ and $\sigma_3(k)$ are defined by

$$\begin{aligned}
\sigma_1(k) &= \int_{-\mathrm{i}h/2}^{\infty-\mathrm{i}h/2} q_R(z)e^{-\mathrm{i}kz}dz, \\
\sigma_2(k) &= \int_{\infty+\mathrm{i}h/2}^{\mathrm{i}h/2} q_R(z)e^{-\mathrm{i}kz}dz, \\
\sigma_3(k) &= \int_{\mathrm{i}h/2}^{-\mathrm{i}h/2} q_R(z)e^{-\mathrm{i}kz}dz.
\end{aligned} \tag{5.14}$$

The global relation for the right semi-strip is given by

$$\sigma_1(k) + \sigma_2(k) + \sigma_3(k) = 0, \quad \mathrm{Im}k \leq 0. \tag{5.15}$$

5.3.2 Boundary conditions

Left semi-strip: For $x < 0$, we have no-slip conditions on the two boundaries:

$$w = \mathrm{Re}[q(z)] = 0, \qquad \text{on } \overline{z} = z + \mathrm{i}h \text{ and } \overline{z} = z - \mathrm{i}h. \tag{5.16}$$

On use of the symmetry condition (5.6), this can be written as

$$q(z) = -q(\overline{z}). \tag{5.17}$$

On substitution of (5.7), we find that, on $\overline{z} = z + \mathrm{i}h$,

$$q_L(z) = -q_L(z + \mathrm{i}h). \tag{5.18}$$

Right semi-strip: For $x > 0$, the symmetry of the flow implies the condition

$$\frac{\partial \chi}{\partial x} = 0, \qquad \text{on } \overline{z} = z + \mathrm{i}h \text{ and } \overline{z} = z - \mathrm{i}h. \tag{5.19}$$

The Cauchy-Riemann equations imply that $\partial w/\partial y = 0$ and, therefore, we can write

$$\mathrm{Im}[q'(z)] = 0, \qquad \text{on } \overline{z} = z + \mathrm{i}h \text{ and } \overline{z} = z - \mathrm{i}h. \tag{5.20}$$

On use of the symmetry condition (5.6), this can be written as

$$q'(z) = q'(\overline{z}). \tag{5.21}$$

On substitution of (5.11) we find that, on $\overline{z} = z + \mathrm{i}h$,

$$q'_R(z) = q'_R(z + \mathrm{i}h). \tag{5.22}$$

5.3.3 Spectral analysis

We now show how to deduce more information about the spectral functions using the boundary conditions.

Left semi-strip: We multiply the boundary condition (5.18) by $e^{-\mathrm{i}kz}$ and integrate along the lower boundary ($x < 0$):

$$\int_{-\infty - \mathrm{i}h/2}^{-\mathrm{i}h/2} q_L(z) e^{-\mathrm{i}kz} dz = -\int_{-\infty - \mathrm{i}h/2}^{-\mathrm{i}h/2} q_L(z + \mathrm{i}h) e^{-\mathrm{i}kz} dz. \tag{5.23}$$

This can be written in terms of the spectral functions as

$$\rho_1(k) = e^{-kh}\rho_2(k), \tag{5.24}$$

or,

$$\rho_2(k) = e^{kh}\rho_1(k). \tag{5.25}$$

Substitution of this into the global relation (5.10) gives

$$[1 + e^{kh}]\rho_1(k) + \rho_3(k) = 0, \quad \text{Im}k \geq 0. \tag{5.26}$$

Right semi-strip: We multiply (5.22) by $e^{-\mathrm{i}kz}$ and integrate along the lower boundary ($x > 0$) to find

$$\int_{-\mathrm{i}h/2}^{\infty-\mathrm{i}h/2} q_R'(z)e^{-\mathrm{i}kz}dz = \int_{-\mathrm{i}h/2}^{\infty-\mathrm{i}h/2} q_R'(z+\mathrm{i}h)e^{-\mathrm{i}kz}dz. \tag{5.27}$$

On integration by parts,

$$\mathrm{i}k\sigma_1(k) = -\mathrm{i}ke^{-kh}\sigma_2(k) - [q_R(+) - q_R(-)]e^{-kh/2}, \tag{5.28}$$

where $q_R(+) \equiv q_R(\mathrm{i}h/2)$ and $q_R(-) \equiv q_R(-\mathrm{i}h/2)$. From this relation we immediately deduce that we must have

$$q_R(+) = q_R(-), \tag{5.29}$$

otherwise the spectral function $\sigma_1(k)$ will have a singularity at $k = 0$. Therefore

$$\sigma_1(k) = -e^{-kh}\sigma_2(k). \tag{5.30}$$

Substitution into the global relation (5.15) gives

$$[1 - e^{kh}]\sigma_1(k) + \sigma_3(k) = 0, \quad \text{Im}k \leq 0. \tag{5.31}$$

Continuity conditions: Additional relations between the spectral functions arise from the requirement of continuity of the global solution across the common edge at $x = 0$.

The complex potentials are continuous at $x = 0$ and this implies the condition

$$\rho_3(k) + \sigma_3(k) = R(k), \quad k \in \mathbb{C}, \tag{5.32}$$

where

$$R(k) = \int_{-\mathrm{i}h/2}^{\mathrm{i}h/2} q_s(z) e^{-\mathrm{i}kz} dz = -\frac{Uh}{k} \cosh\left(\frac{kh}{2}\right) + \left[\frac{2\mathrm{i}\lambda}{k} + \frac{2U}{k^2}\right] \sinh\left(\frac{kh}{2}\right). \tag{5.33}$$

In addition, the no-slip condition on the two walls for $x < 0$ implies that the solution of the right semi-strip problem must satisfy this condition at points $z = \pm \mathrm{i}h/2$, i.e.

$$\mathrm{Re}[q(z)] = \mathrm{Re}[q_s(z) + q_R(z)] = 0. \tag{5.34}$$

On substitution of (5.11) we find that

$$\lambda = -\frac{1}{2}\left[q_R(+) + \overline{q_R(+)}\right]. \tag{5.35}$$

Using the symmetry condition (5.6) and (5.29), this can be written as

$$\lambda = -\frac{1}{2}\left[q_R(+) + q_R(-)\right] = -q_R(+). \tag{5.36}$$

5.3.4 Solution scheme and function representation

From equation (5.26) and the fact that $\rho_1(k)$ is analytic in the upper half plane we deduce that $\rho_3(k)$ must vanish at solutions of $1 + e^{kh} = 0$ in the upper half k-plane, that is, at points in the set

$$\Sigma_1 \equiv \left\{ k_m = \frac{\mathrm{i}m\pi}{h} \middle| m = 2p + 1, p = 0, 1, 2, \ldots \right\}. \tag{5.37}$$

But (5.32) then implies that

$$\sigma_3(k) = R(k), \quad k \in \Sigma_1. \tag{5.38}$$

Similarly, (5.31) and the fact that $\sigma_1(k)$ is a lower analytic function together imply that

$\sigma_3(k)$ must satisfy

$$\sigma_3(k) = 0, \quad k \in \Sigma_2, \tag{5.39}$$

where

$$\Sigma_2 \equiv \left\{ k_m = \frac{\mathrm{i}m\pi}{h} \middle| m = -2p, p = 0, 1, 2, \dots \right\}. \tag{5.40}$$

The conditions on the spectral function $\sigma_3(k)$ at discrete points in the k-plane are illustrated in Figure 5.6 and these clearly have different forms in the upper and lower half spectral k-plane; these conditions are enough to determine $\sigma_3(k)$. It is precisely this asymmetry between the conditions on $\sigma_3(k)$ in the upper and lower-half spectral k-plane that reflects the need, using the traditional Wiener-Hopf approach, to factorize the associated kernel functions arising there. Our approach obviates the need for any such factorization and the inherent spectral asymmetry in the problem now manifests itself differently. Once $\sigma_3(k)$ has been determined the other unknown spectral functions follow by back substitution into the various spectral relations just derived.

We now show how to find $\sigma_3(k)$ by a highly accurate numerical scheme that properly accounts for known singularities of the solution at the corners of the semi-strip. It is easy to show by a local analysis that, at a transition point between a boundary condition of Dirichlet type (left semi-strip) to one of Neumann type (right semi-strip), a harmonic function exhibits a branch point singularity of order 1/2 (a square root) (Driscoll & Trefethen [35]).

At $z = \pm \mathrm{i}h/2$ we know that the problem admits square-root singularities; this suggests use of a specially tailored basis which will implicitly take them into account. A convenient option is to define the new complex variable ζ via the relation

$$z(\zeta) = \frac{h}{4}\left(\zeta - \frac{1}{\zeta}\right), \tag{5.41}$$

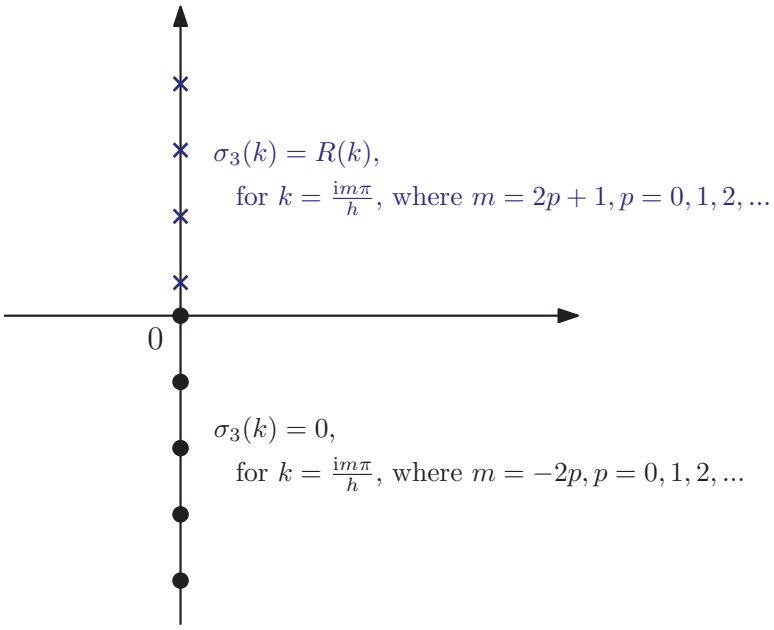

Figure 5.6: Schematic illustrating the conditions on $\sigma_3(k)$ from different sectors of the complex k-plane.

for ζ on the semi-circle $\zeta = e^{\mathrm{i}\theta}, \theta \in [\pi/2, 3\pi/2]$ and to write

$$q_R(z(\zeta)) = \sum_{n=-\infty}^{\infty} a_n \zeta^n, \tag{5.42}$$

to represent $q_R(z)$ on the common boundary for some set of coefficients $\{a_n\}$ to be found. This approach is especially suited to this problem because the inverse function $\zeta = \zeta(z)$ has precisely the same square root singularities at $z = \pm \mathrm{i}h/2$ as required of the solution, i.e., with $h = 2$,

$$\zeta = z - \sqrt{z^2 + 1}, \tag{5.43}$$

which clearly has square root singularities at the semi-strip corner points $z = \pm \mathrm{i}h/2 = \pm \mathrm{i}$. It follows that

$$\sigma_3(k) = \sum_{n=-\infty}^{\infty} a_n \left[\frac{\mathrm{i}h}{2} \int_{\pi/2}^{3\pi/2} (e^{\mathrm{i}n\theta + \frac{kh}{2}\sin\theta}) \cos\theta d\theta \right]. \tag{5.44}$$

The expression in square brackets in (5.44) can be written in terms of Bessel functions

N	slip length λ
8	**0.441271**2602353
9	**0.441271**2107070
10	**0.4412712**021809
11	**0.4412712**006539
12	**0.4412712003**716
13	**0.4412712003**181
14	**0.4412712003**078
15	**0.4412712003**058
16	**0.4412712003053**

Table 5.1: Evaluation of the longitudinal slip length λ for $h = 2$ and $U = 1$ for different values of the truncation parameter N of the sum (5.42).

using well-known integral representations thereof [5]. It is also noted that in other studies of boundary value problems by the same unified transform method, previous authors have proposed alternative representations of unknown boundary data in terms of Fourier [98], Chebyshev [100], and Legendre [46] expansions. We emphasize that our own choice (5.41) is motivated by the specific demands of the problem, i.e., the known form of the corner singularities.

The sum (5.42) is truncated to include only terms $n = -N, ..., N$ for suitable N and an overdetermined linear system for the $2N + 1$ unknown coefficients $\{a_n\}$ and slip length λ is solved by a least-squares method. This linear system comprises (5.36) together with (5.38) and (5.39) evaluated at sufficiently many points in Σ_1 and Σ_2 closest to the real k axis (typically we used twice as many equations as the number of unknowns).

5.3.5 Comparison with Jeong [54] and Luchini *et al.* [78]

On solving the linear system for $U = 1$, $h = 2$ we show in Table 5.1 the rapid convergence to the theoretical value

$$\lambda = \frac{\log 4}{\pi} = 0.4412712003053 \tag{5.45}$$

given by Jeong [54]. The fact that adding just a few more coefficients can give an order of magnitude improvement in accuracy is indicative of a spectrally accurate method.

5.3.6 Conformal geometric approach

It turns out to be possible to bypass Wiener-Hopf and transform methods altogether and solve this particular problem by means of a construction based on conformal slit mappings ([13, 15, 17, 16]). The solution is

$$q(z) = \frac{2U}{\pi} \log \left[\sqrt{1 + e^{\pi z}} + e^{\pi z/2} \right], \tag{5.46}$$

where we have taken $h = 2$ (note that the square root branch points at $z = \pm \mathrm{i}$ are clearly seen in this explicit form of the solution). To confirm that the results in Table 5.1 for λ properly reflect convergence of the method we have also used (5.46) to check other features of the transform solution. Jeong [54] also derived (5.46) by summing an infinite series generated by his Wiener-Hopf method.

Consider the composed conformal mapping given by

$$z = z(\zeta) = P(\chi(\eta(\zeta))), \tag{5.47}$$

where

$$\begin{aligned} \eta(\zeta) &= \frac{1}{2}\left(\frac{1}{\zeta} + \zeta\right) = \frac{1+\zeta^2}{2\zeta}, \\ \chi(\eta) &= \frac{2}{\eta - 1}, \\ P(\chi) &= \frac{h}{2\pi} \log \chi = \frac{h}{2\pi} \log \left[\frac{4\zeta}{(1-\zeta)^2} \right]. \end{aligned} \tag{5.48}$$

The conformal mapping (5.47) (Figure 5.7) takes the parametric ζ plane and transplants it on the physical z plane. More specifically, the first mapping in (5.48) takes the unit ζ disc to the whole complex plane in the η plane: the unit ζ circle and $[-1, 1]$ of ζ plane are mapped to the real line in the η plane. A second mapping transplants the unbounded η plane to the unbounded χ plane, where the slits on real axis of η plane are rearranged on the real axis of χ plane. Finally, the mapping $P(\chi)$ takes the unbounded χ plane to our fluid region in z plane.

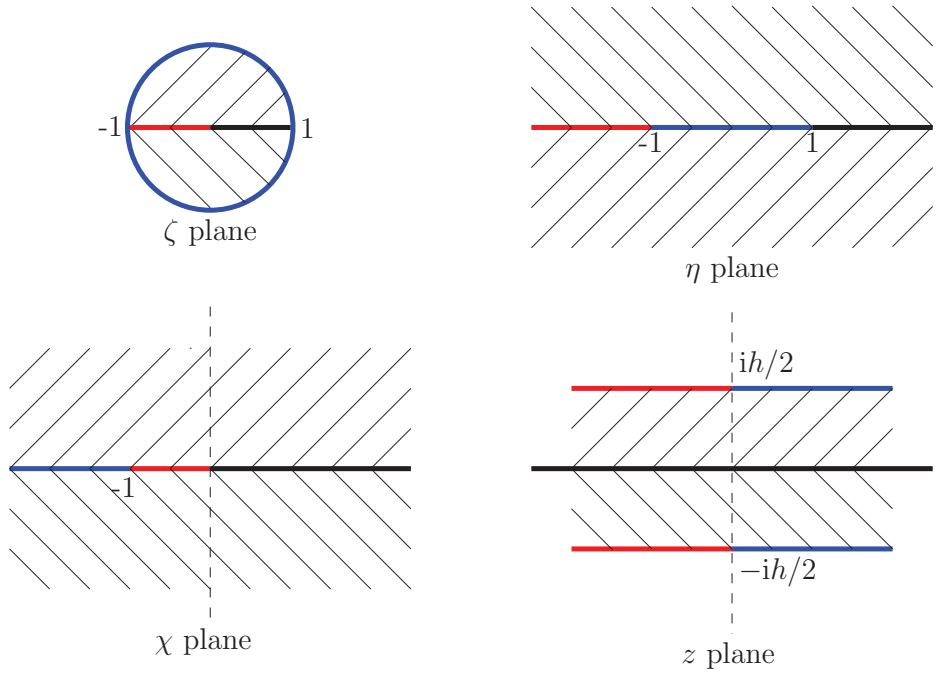

Figure 5.7: The sequence of conformal mappings (5.48).

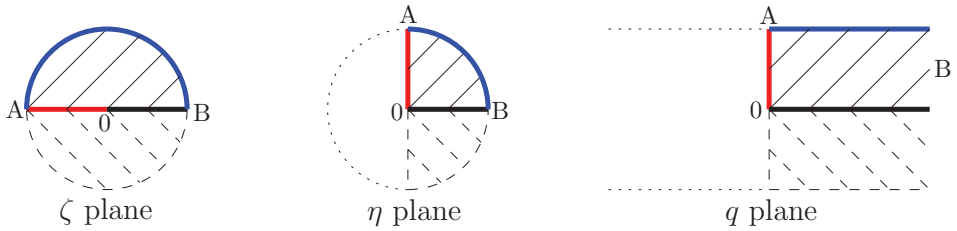

Figure 5.8: The sequence of conformal mappings (5.49)–(5.50).

Now define a second sequence of conformal mappings shown in Figure 5.8 by

$$\zeta \mapsto \eta = \sqrt{\zeta} \tag{5.49}$$

and

$$\eta \mapsto q = \frac{Uh}{\pi} \log\left[\frac{1+\eta}{1-\eta}\right] = \frac{Uh}{\pi} \log\left[\frac{(1+\sqrt{\zeta})^2}{1-\zeta}\right]. \tag{5.50}$$

It can be shown that (5.50) satifies the required boundary conditions (5.16) and (5.20). With

$$z = \frac{h}{2\pi} \log\left[\frac{4\zeta}{(1-\zeta)^2}\right], \tag{5.51}$$

we can deduce that

$$\sqrt{\zeta} = -e^{-\pi z/h} + \sqrt{e^{-2\pi z/h}+1}, \tag{5.52}$$

where a branch of the inverse is chosen so that $\zeta = 0$ corresponds to $z \to -\infty$.
Substitution into (5.50) gives

$$q(z) = \frac{Uh}{\pi} \log\left[\sqrt{1+e^{2\pi z/h}} + e^{\pi z/h}\right]. \tag{5.53}$$

On setting $h = 2$ and $U = a$, we find

$$q(z) = \frac{2a}{\pi} \log\left[\sqrt{1+e^{\pi z}} + e^{\pi z/2}\right], \tag{5.54}$$

which is identical to the solution reported by Jeong [54] once we let $z \mapsto -z + \mathrm{i}$.

5.4 Transverse flow problem

We now consider the transverse flow problem in which the flow now takes place in the (x, y)-plane and is independent of the perpendicular direction. The velocity field has the form

$$(u, v) = \left(\frac{\partial \psi}{\partial y}, -\frac{\partial \psi}{\partial x}\right), \tag{5.55}$$

where ψ is the streamfunction describing shear flow past an array of semi-infinite plates occupying $-\infty < x < 0, y = h/2 + nh$ for $n \in \mathbb{Z}$ and $h > 0$. By the periodicity in the

y-direction it is enough to consider the domain $-\infty < x < \infty, -h/2 < y < h/2$ shown in Figure 5.9. We have

$$(u, v) = (0, Ux + \lambda), \quad \text{as } x \to \infty, \tag{5.56}$$

with shear rate U and slip length λ. As $x \to -\infty$ the flow is taken to vanish. It is important to note that, as in the previous problem, the nature of the boundary conditions on $y = \pm h/2$ changes type at $x = 0$: for $x < 0$ the boundary conditions are those of no-slip; for $x > 0$ we must impose that $p = u = 0$ where p is the fluid pressure [54]. It is known [13, 15, 17, 16] that, at any boundary point z_c where the boundary condition changes from a no-slip condition to a no-shear condition there are square root singularities where $f(z)$ and $g'(z)$ have the local behaviour

$$\begin{aligned} f(z) &= f_0 + f_{1/2}(z - z_c)^{1/2} + f_1(z - z_c) + f_{3/2}(z - z_c)^{3/2} + \dots, \\ g(z) &= g_0 + g_{1/2}(z - z_c)^{1/2} + g_1(z - z_c) + g_{3/2}(z - z_c)^{3/2} + \dots, \end{aligned} \tag{5.57}$$

where $\{f_0, f_{1/2}, \dots, g_0, g_{1/2}, \dots\}$ are some coefficients.

The resulting flow is antisymmetric about $y = 0$; this implies that the Goursat functions satisfy the following conditions:

$$\begin{cases} \overline{f}(z) = -f(z), \\ \overline{g}'(z) = -g'(z). \end{cases} \tag{5.58}$$

5.4.1 Domain splitting: left and right semi-strips

Left semi-strip: The Goursat functions are given by

$$\begin{cases} f(z) = \mu + f_L(z), \\ g'(z) = \overline{\mu} + g'_L(z), \end{cases} \tag{5.59}$$

for some constant μ and where $f_L(z)$, $g'_L(z)$ are analytic in the fluid region and vanish as $x \to -\infty$. The antisymmetry condition together with the fact that $f_L(z)$ and $g'_L(z)$ vanish

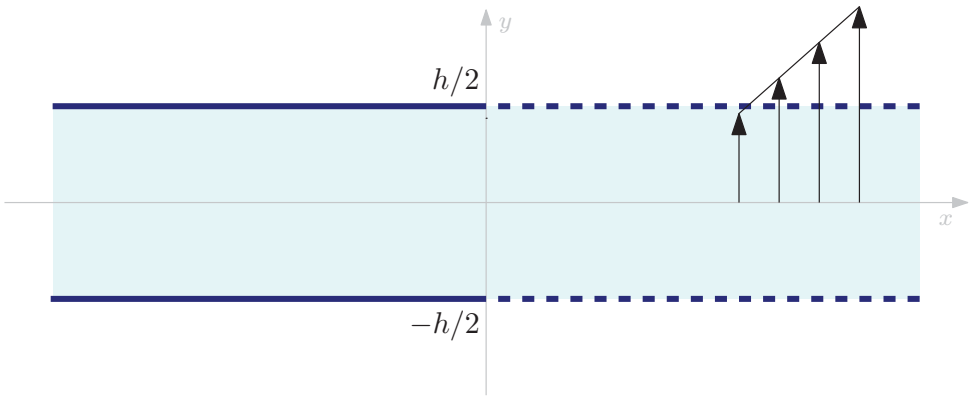

Figure 5.9: Schematic of a single period of the transverse shear flow problem past an array of semi-infinite plates.

at $x \to -\infty$ implies that

$$\overline{\mu} = -\mu. \tag{5.60}$$

The function $f_L(z)$ can be represented by

$$f_L(z) = \frac{1}{2\pi}\left[\int_0^{\infty} \rho_1(k)e^{\mathrm{i}kz}dk + \int_0^{-\infty} \rho_2(k)e^{\mathrm{i}kz}dk + \int_0^{-\mathrm{i}\infty} \rho_3(k)e^{\mathrm{i}kz}dk\right], \tag{5.61}$$

where the spectral functions $\rho_1(k)$, $\rho_2(k)$ and $\rho_3(k)$ are defined by

$$\begin{aligned}
\rho_1(k) &= \int_{-\infty-\mathrm{i}h/2}^{-\mathrm{i}h/2} f_L(z)e^{-\mathrm{i}kz}dz, \\
\rho_2(k) &= \int_{\mathrm{i}h/2}^{-\infty+\mathrm{i}h/2} f_L(z)e^{-\mathrm{i}kz}dz, \\
\rho_3(k) &= \int_{-\mathrm{i}h/2}^{\mathrm{i}h/2} f_L(z)e^{-\mathrm{i}kz}dz.
\end{aligned} \tag{5.62}$$

Similarly, we can write

$$g_L'(z) = \frac{1}{2\pi}\left[\int_0^{\infty} \hat{\rho}_1(k)e^{\mathrm{i}kz}dk + \int_0^{-\infty} \hat{\rho}_2(k)e^{\mathrm{i}kz}dk + \int_0^{-\mathrm{i}\infty} \hat{\rho}_3(k)e^{\mathrm{i}kz}dk\right], \tag{5.63}$$

where

$$\begin{aligned}\hat{\rho}_1(k) &= \int_{-\infty-\mathrm{i}h/2}^{-\mathrm{i}h/2} g_L'(z)e^{-\mathrm{i}kz}dz,\\ \hat{\rho}_2(k) &= \int_{\mathrm{i}h/2}^{-\infty+\mathrm{i}h/2} g_L'(z)e^{-\mathrm{i}kz}dz,\\ \hat{\rho}_3(k) &= \int_{-\mathrm{i}h/2}^{\mathrm{i}h/2} g_L'(z)e^{-\mathrm{i}kz}dz.\end{aligned} \tag{5.64}$$

The global relations for the left semi-strip satisfy

$$\begin{aligned}&\rho_1(k)+\rho_2(k)+\rho_3(k)=0, \quad \mathrm{Im}k\geq 0,\\ &\hat{\rho}_1(k)+\hat{\rho}_2(k)+\hat{\rho}_3(k)=0, \quad \mathrm{Im}k\geq 0.\end{aligned} \tag{5.65}$$

Right semi-strip: The Goursat functions are given by

$$\begin{cases} f(z)=f_s(z)+f_R(z),\\ g'(z)=g_s'(z)+g_R'(z),\end{cases} \tag{5.66}$$

where $f_R(z)$, $g_R'(z)$ are analytic in the fluid region and vanishing as $x\to+\infty$ while, in order to satisfy the far-field condition (5.56), we take

$$\begin{cases} f_s(z)=-\dfrac{\mathrm{i}Uz}{4},\\[2ex] g_s'(z)=-\dfrac{\mathrm{i}Uz}{2}-\mathrm{i}\lambda.\end{cases} \tag{5.67}$$

As before, the shear rate U is externally specified but we expect μ and λ to be determined by the solution.

Representations analogous to (5.61) and (5.63), albeit with different spectral functions as indicated in Figure 5.10, can be written for $f_R(z)$ and $g_R'(z)$ with spectral functions $\sigma_j(k)$, $\hat{\sigma}_j(k)$, $j=1,2,3$ as illustrated in Figure 5.10. The global relations associated with the

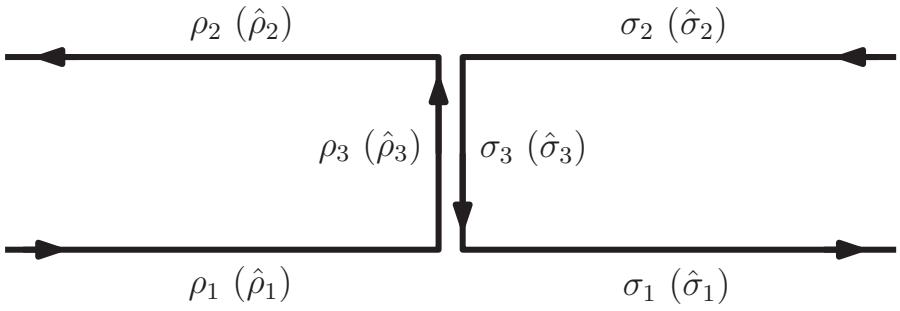

Figure 5.10: The two semi-strips and assignation of the associated spectral functions. In this problem each edge has two associated spectral functions.

right semi-strip satisfy

$$\begin{aligned} \sigma_1(k) + \sigma_2(k) + \sigma_3(k) = 0, \quad \text{Im}k \leq 0, \\ \hat{\sigma}_1(k) + \hat{\sigma}_2(k) + \hat{\sigma}_3(k) = 0, \quad \text{Im}k \leq 0. \end{aligned} \tag{5.68}$$

5.4.2 Boundary conditions

Left semi-strip: For $x < 0$ we have no-slip conditions on the two boundaries:

$$-\overline{f(z)} + \overline{z}f'(z) + g'(z) = 0, \qquad \text{on } \overline{z} = z + \mathrm{i}h \text{ and } \overline{z} = z - \mathrm{i}h. \tag{5.69}$$

On substitution of (5.59), we find that, on $\overline{z} = z + \mathrm{i}h$,

$$-\overline{f_L(z)} + (z + \mathrm{i}h)f_L'(z) + g_L'(z) = 0, \tag{5.70}$$

which, using (5.58), can be written as

$$f_L(z + \mathrm{i}h) + (z + \mathrm{i}h)f_L'(z) + g_L'(z) = 0. \tag{5.71}$$

Similarly, we find that, on $\overline{z} = z - \mathrm{i}h$,

$$f_L(z - \mathrm{i}h) + (z - \mathrm{i}h)f_L'(z) + g_L'(z) = 0. \tag{5.72}$$

Right semi-strip: For $x > 0$ we have

$$p = 0 \ \text{ and } \ u = 0, \qquad \text{on } \ \overline{z} = z + \mathrm{i}h \ \text{ and } \ \overline{z} = z - \mathrm{i}h. \tag{5.73}$$

The first condition in (5.73) can be expressed as

$$\mathrm{Re}[f'(z)] = 0. \tag{5.74}$$

On substitution of (5.66), we find

$$\mathrm{Re}[f_s'(z) + f_R'(z)] = 0. \tag{5.75}$$

Using the fact that $\mathrm{Re}[f_s'(z)] = 0$, we have

$$\mathrm{Re}[f_R'(z)] = 0. \tag{5.76}$$

On use of (5.58), we find that, on $\overline{z} = z + \mathrm{i}h$,

$$f_R'(z) = -\overline{f_R'(z)} = -\overline{f_R'}(z + \mathrm{i}h) = f_R'(z + \mathrm{i}h). \tag{5.77}$$

The second condition in (5.73) can be expressed as

$$\mathrm{Re}[u - \mathrm{i}v] = \mathrm{Re}[-\overline{f(z)} + \overline{z}f'(z) + g'(z)] = 0. \tag{5.78}$$

On substitution of (5.66) and use of (5.77), we find that, on $\overline{z} = z + \mathrm{i}h$,

$$g_R'(z) - g_R'(z + \mathrm{i}h) = f_R(z) - f_R(z + \mathrm{i}h) - \mathrm{i}hf_R'(z). \tag{5.79}$$

5.4.3 Spectral analysis

Preliminary observations: Note that

$$\int_{-\infty-\mathrm{i}h/2}^{-\mathrm{i}h/2} f_L(z+\mathrm{i}h)e^{-\mathrm{i}kz}dz = e^{-kh}\int_{-\infty+\mathrm{i}h/2}^{\mathrm{i}h/2} f_L(z)e^{-\mathrm{i}kz}dz$$
$$= -e^{-kh}\rho_2(k) \tag{5.80}$$

and

$$\int_{\mathrm{i}h/2}^{-\infty+\mathrm{i}h/2} f_L(z-\mathrm{i}h)e^{-\mathrm{i}kz}dz = e^{kh}\int_{-\mathrm{i}h/2}^{-\infty-\mathrm{i}h/2} f_L(z)e^{-\mathrm{i}kz}dz$$
$$= -e^{kh}\rho_1(k). \tag{5.81}$$

In addition, integration by parts gives

$$\int_{-\infty-\mathrm{i}h/2}^{-\mathrm{i}h/2} (z+\mathrm{i}h)f_L'(z)e^{-\mathrm{i}kz}dz = -\frac{\partial[k\rho_1(k)]}{\partial k} - kh\rho_1(k) + \frac{\mathrm{i}h}{2}f_L(-)e^{-kh/2} \tag{5.82}$$

and

$$\int_{\mathrm{i}h/2}^{-\infty+\mathrm{i}h/2} (z-\mathrm{i}h)f_L'(z)e^{-\mathrm{i}kz}dz = -\frac{\partial[k\rho_2(k)]}{\partial k} + kh\rho_2(k) + \frac{\mathrm{i}h}{2}f_L(+)e^{kh/2}, \tag{5.83}$$

where, henceforth, we employ the shorthand notation $f_L(+) \equiv f_L(\mathrm{i}h/2)$ and $f_L(-) \equiv f_L(-\mathrm{i}h/2)$. Expressions (5.82)–(5.83) will appear in the transform of the boundary conditions on the no-slip boundaries.

Left semi-strip: We multiply the boundary condition (5.71) by $e^{-\mathrm{i}kz}$ and integrate along the lower no-slip boundary:

$$\int_{-\infty-\mathrm{i}h/2}^{-\mathrm{i}h/2} [f_L(z+\mathrm{i}h)e^{-\mathrm{i}kz} + (z+\mathrm{i}h)f_L'(z)e^{-\mathrm{i}kz} + g_L'(z)e^{-\mathrm{i}kz}]dz = 0. \tag{5.84}$$

On use of (5.80) and (5.82), this can be written as

$$-e^{-kh}\rho_2(k)-\frac{\partial[k\rho_1(k)]}{\partial k}-kh\rho_1(k)+\frac{\mathrm{i}hf_L(-)}{2}e^{-kh/2}+\hat{\rho}_1(k)=0. \tag{5.85}$$

We multiply (5.72) by $e^{-\mathrm{i}kz}$ and integrate over the upper no-slip boundary

$$\int_{\mathrm{i}h/2}^{-\infty+\mathrm{i}h/2}[f_L(z-\mathrm{i}h)e^{-\mathrm{i}kz}+(z-\mathrm{i}h)f_L'(z)e^{-\mathrm{i}kz}+g_L'(z)e^{-\mathrm{i}kz}]dz=0. \tag{5.86}$$

On use of (5.81) and (5.83), we find

$$-e^{kh}\rho_1(k)-\frac{\partial[k\rho_2(k)]}{\partial k}+kh\rho_2(k)+\frac{\mathrm{i}hf_L(+)}{2}e^{kh/2}+\hat{\rho}_2(k)=0. \tag{5.87}$$

Addition of (5.85) and (5.87) gives

$$\begin{aligned}-e^{kh}\rho_1(k)-e^{-kh}\rho_2(k)-\frac{\partial[k(\rho_1(k)+\rho_2(k))]}{\partial k}-kh\rho_1(k)+kh\rho_2(k)\\ +\frac{\mathrm{i}h}{2}[f_L(+)e^{kh/2}+f_L(-)e^{-kh/2}]+\hat{\rho}_1(k)+\hat{\rho}_2(k)=0.\end{aligned} \tag{5.88}$$

On use of the global relations (5.65), this can be written as

$$\begin{aligned}2[\sinh(kh)+kh]\rho_1(k)=(e^{-kh}-kh)\rho_3(k)+\frac{\partial[k\rho_3(k)]}{\partial k}-\hat{\rho}_3(k)\\ +\frac{\mathrm{i}h}{2}[f_L(+)e^{kh/2}+f_L(-)e^{-kh/2}],\quad \mathrm{Im}k\geq 0.\end{aligned} \tag{5.89}$$

Right semi-strip: In the right semi-strip we multiply (5.77) by $e^{-\mathrm{i}kz}$ and integrate along the lower boundary:

$$\int_{-\mathrm{i}h/2}^{\infty-\mathrm{i}h/2}f_R'(z)e^{-\mathrm{i}kz}dz=\int_{-\mathrm{i}h/2}^{\infty-\mathrm{i}h/2}f_R'(z+\mathrm{i}h)e^{-\mathrm{i}kz}dz. \tag{5.90}$$

Integration by parts gives

$$\mathrm{i}k\sigma_1(k)=-\mathrm{i}ke^{-kh}\sigma_2(k)-[f_R(+)-f_R(-)]e^{-kh/2}. \tag{5.91}$$

From this relation we deduce that we must have

$$f_R(+) = f_R(-) \tag{5.92}$$

and therefore we have

$$\sigma_1(k) = -e^{-kh}\sigma_2(k). \tag{5.93}$$

Equation (5.93) relates $\sigma_1(k)$ and $\sigma_2(k)$. On substitution of (5.93) into the global relation (5.68), we find

$$[1 - e^{kh}]\sigma_1(k) = -\sigma_3(k), \quad \text{Im}k \leq 0. \tag{5.94}$$

Similarly, we can obtain a relation between the spectral functions $\hat{\sigma}_1(k)$ and $\hat{\sigma}_2(k)$. Substitution of (5.79) into the expression for $\hat{\sigma}_1(k)$ gives

$$\hat{\sigma}_1(k) + e^{-kh}\hat{\sigma}_2(k) = \mathrm{i}hf_R(-)e^{-kh/2} + kh\sigma_1(k), \tag{5.95}$$

so that

$$\hat{\sigma}_2(k) = -\hat{\sigma}_1(k)e^{kh} + kh\sigma_1(k)e^{kh} + \mathrm{i}hf_R(-)e^{kh/2}. \tag{5.96}$$

On use of (5.68) and (5.94), we find

$$\hat{\sigma}_1(k)[1 - e^{kh}] = -\hat{\sigma}_3(k) + \frac{khe^{kh}}{1 - e^{kh}}\sigma_3(k) - \mathrm{i}hf_R(-)e^{kh/2}, \quad \text{Im}k \leq 0. \tag{5.97}$$

Continuity conditions: We must impose continuity of velocity, pressure and vorticity across the common edge. This is equivalent to insisting that $f(z)$ and $g'(z)$ are continuous at $x = 0$. The spectral form of these conditions can be written as

$$\begin{aligned} \rho_3(k) + \sigma_3(k) &= R(k), \quad \text{for } k \in \mathbb{C}, \\ \hat{\rho}_3(k) + \hat{\sigma}_3(k) &= \hat{R}(k), \quad \text{for } k \in \mathbb{C}, \end{aligned} \tag{5.98}$$

where

$$R(k) = \int_{-\mathrm{i}h/2}^{\mathrm{i}h/2} [f_s(z) - \mu]\, e^{-\mathrm{i}kz} dz = \frac{\mathrm{i}Uh}{4k} \cosh\left(\frac{kh}{2}\right) - \left[\frac{2\mathrm{i}\mu}{k} + \frac{\mathrm{i}U}{2k^2}\right] \sinh\left(\frac{kh}{2}\right) \tag{5.99}$$

and

$$\hat{R}(k) = \int_{-\mathrm{i}h/2}^{\mathrm{i}h/2} [g_s'(z) - \overline{\mu}]\, e^{-\mathrm{i}kz} dz = \frac{\mathrm{i}Uh}{2k} \cosh\left(\frac{kh}{2}\right) + \left[\frac{2(\lambda + \mathrm{i}\mu)}{k} - \frac{\mathrm{i}U}{k^2}\right] \sinh\left(\frac{kh}{2}\right). \tag{5.100}$$

In addition, we insist that functions $f(z)$ for left and right semi-strip problems are compatible at the corner points $z = \pm \mathrm{i}h/2$: this can be written as

$$\mu + f_L(+) = \frac{Uh}{8} + f_R(+), \qquad \mu + f_L(-) = -\frac{Uh}{8} + f_R(-). \tag{5.101}$$

Finally, the no-slip condition on the two walls for $x < 0$ implies that the solution of the right semi-strip problem must satisfy this condition at points $z = \pm \mathrm{i}h/2$, i.e.,

$$-\overline{f(z)} + \overline{z} f'(z) + g'(z) = 0 \tag{5.102}$$

for $f(z)$ and $g'(z)$ of the right semi-strip problem. On substitution of (5.58) and (5.66), we find that

$$f_R(-) - \frac{\mathrm{i}h}{2} f_R'(+) + g_R'(+) = \mathrm{i}\lambda. \tag{5.103}$$

5.4.4 Solution scheme and function representation

Substitution of (5.98) and (5.101) into (5.89) gives

$$2[\sinh(kh) + kh]\rho_1(k) = W(k), \tag{5.104}$$

where

$$W(k) = -(e^{-kh} - kh + 1)\sigma_3(k) - k\sigma_3'(k) + \mathrm{i}hf_R(-)\cosh\left(\frac{kh}{2}\right) + \hat{\sigma}_3(k) + (e^{-kh} - kh + 1)R(k) + kR'(k) - \hat{R}(k) - \mathrm{i}\mu h\cosh\left(\frac{kh}{2}\right) + \frac{\mathrm{i}Uh^2}{8}\sinh\left(\frac{kh}{2}\right). \tag{5.105}$$

The right hand side of (5.105) contains only known functions, the two unknown spectral functions $\sigma_3(k)$, $\hat{\sigma}_3(k)$ and unknown constants μ, λ. But $\rho_1(k)$ is upper analytic which implies that

$$W(k) = 0, \quad k \in \Sigma_3, \tag{5.106}$$

where Σ_3 denotes the set of zeros of $\sinh(kh) + kh = 0$ in the upper half-plane. This gives one set of conditions to be satisfied by the unknown $\sigma_3(k)$ and $\hat{\sigma}_3(k)$.

We now take advantage of the fact that $\sigma_1(k)$ and $\hat{\sigma}_1(k)$ are analytic in the lower half-plane to obtain additional conditions on $\sigma_3(k)$ and $\hat{\sigma}_3(k)$. Equation (5.94) implies

$$\sigma_3(k) = 0, \quad k \in \Sigma_2, \tag{5.107}$$

where Σ_2 is the same set defined in (5.40). Similarly, equation (5.97) gives

$$-\hat{\sigma}_3(k) + \frac{khe^{kh}}{1 - e^{kh}}\sigma_3(k) - \mathrm{i}hf_R(-)e^{kh/2} = 0, \quad k \in \Sigma_2, \tag{5.108}$$

or,

$$\hat{\sigma}_3(k) + k\sigma_3'(k) + \mathrm{i}hf_R(-)e^{kh/2} = 0, \quad k \in \Sigma_2, \tag{5.109}$$

where we have performed a Taylor expansion of the second term on the left hand side of (5.108).

Figure 5.11 shows a schematic of the points in the spectral k-plane where information on $\sigma_3(k)$ and $\hat{\sigma}_3(k)$ is available. Note that the single condition (5.106) holds at the left-right symmetric set of points Σ_3 in the upper half plane while two conditions (5.107) and (5.108)

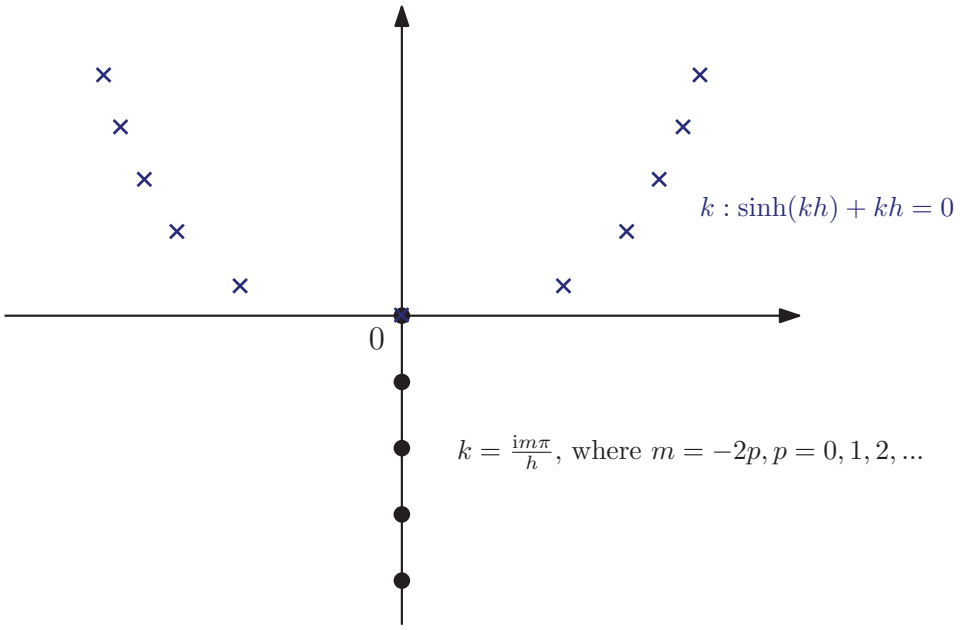

Figure 5.11: Schematic of the points in the spectral k-plane at which information on the spectral functions is available.

hold at the points in Σ_2. Again, this up-down asymmetric distribution of information in the spectral plane underlies the need for a kernel decomposition in the usual Wiener-Hopf method.

The known square-root form of the singularities in the Goursat functions at $z = \pm \mathrm{i}h/2$ means that we should again use the variable ζ defined by (5.41) together with the representations

$$f_R(z(\zeta)) = \sum_{n=-\infty}^{\infty} c_n \zeta^n, \qquad g_R(z(\zeta)) = \sum_{n=-\infty}^{\infty} d_n \zeta^n \tag{5.110}$$

for values of z on the slit $[-\mathrm{i}h/2, \mathrm{i}h/2]$. It can be shown that,

$$\begin{aligned} \sigma_3(k) &= \sum_{n=-\infty}^{\infty} c_n \left[\frac{\mathrm{i}h}{2} \int_{\pi/2}^{3\pi/2} (e^{\mathrm{i}n\theta + \frac{kh}{2}\sin\theta}) \cos\theta d\theta \right], \\ \hat{\sigma}_3(k) &= \sum_{n=-\infty}^{\infty} d_n \left[\mathrm{i}n \int_{\pi/2}^{3\pi/2} (e^{\mathrm{i}n\theta + \frac{kh}{2}\sin\theta}) d\theta \right]. \end{aligned} \tag{5.111}$$

By truncating the expansions (5.110) for $f_R(z)$ and $g'_R(z)$ as before, we formed an overdetermined linear system for the unknown coefficients $\{c_n\}$, $\{d_n\}$ and the parameters μ and λ. It is noted that two conditions associated with equation (5.103) are included in the linear system; the known square-root singularity of $f(z)$ and $g(z)$ at point $z = \mathrm{i}h/2$ implies that the second and third terms in the left hand side of (5.103) are unbounded and therefore one condition (independent of λ) forces cancellation of these singularities while a balancing of the regular terms gives an equation containing λ. Other equations in the linear system are found by evaluating (5.106), (5.107) and (5.109) at as many points in the sets Σ_2 and Σ_3 as needed. Once coefficients $\{c_n\}$, $\{d_n\}$ and parameters μ and λ are determined, all spectral functions follow by back substitution into the various spectral relations.

5.4.5 Comparison with solution of Jeong [54]

Jeong [54] derived the following formula for λ:

$$\lambda = \mathrm{i}\frac{K'_+(0)}{K_+(0)}, \tag{5.112}$$

where the kernel function $K_+(\zeta)$ is defined as

$$K_+(\zeta) \equiv \prod_{n=1}^{\infty}\left[\frac{(1+\zeta/\zeta_n)(1-\zeta/\overline{\zeta_n})}{(1+\zeta/(n\pi\mathrm{i}))^2}\right] \tag{5.113}$$

and where ζ_n are the roots of $\zeta + \sinh\zeta\cosh\zeta = 0$ with positive real and imaginary parts. Table 5.2 records the values for λ computed from (5.112) by truncating the infinite product (5.113) to M terms. Clearly the convergence of the scheme is impracticably slow if high accuracy is required. On the other hand, Table 5.3 shows that only a moderate number of coefficients are required to achieve many digits of accuracy using the new approach expounded herein. It should be pointed out that the set Σ_3 coincides with the eigenvalue set associated with the so-called Papkovich-Fadle eigenfunctions in a semi-strip. While our formulation does not involve consideration of these functions we anticipated that finding the solution to our linear system might be problematic owing to well-known ill-conditioning associated with these eigenfunctions [107]. However, as seen in Table 5.3, no such difficulties were

M	slip length λ
10^2	**0.17**55868669
10^3	**0.17**69731985
10^4	**0.1771**156720
10^5	**0.1771**299844

Table 5.2: Convergence of slip length λ, for $h = 2$ and $U = 1$, computed using (5.112) and by truncating the infinite product (5.113) to M terms. This formula is generated by the Wiener-Hopf method of [54].

N	slip length λ
8	**0.1771**308458
9	**0.177131**4127
10	**0.1771315**397
11	**0.1771315**677
12	**0.177131575**39
13	**0.1771315753**
14	**0.1771315757**
15	**0.1771315758**
16	**0.1771315758**

Table 5.3: Convergence of slip length λ, for $h = 2$ and $U = 1$, as computed by truncating the sums (5.110) in the new transform approach.

encountered using a least-squares approach.

5.5 Summary

We presented a transform approach for solving two mixed-type boundary value problems previously solved by Luchini *et al.* [78] and Jeong [54] using Wiener-Hopf techniques. These involved shear flow past a periodic array of semi-infinite flat plates in longitudinal (harmonic field) and transverse (biharmonic field) flow directions.

The idea of our transform approach (in both longitudinal and transverse flow problems) was, firstly, to split the domain into sub-polygons (semi-strips) and solve each sub-problem separately using the Fokas method for polygonal domains. Then we analyzed the boundary conditions by performing spectral analysis and imposing continuity conditions across the

common edge. The analysis of spectral relations provided conditions at distinct points in the spectral k-plane satisfied by a reduced set of spectral functions (those related to the edge of finite length). These conditions were sufficient to determine the unknown boundary data. Importantly, we used an appropriate function representation for the unknown boundary data on the edge of finite length which accounted for the square-root singularities associated with points where boundary conditions changed type. A linear system was solved for the unknown coefficients of the series expansion(s) and slip length λ. Once this was solved, all the spectral functions followed by back-substitution into the spectral relations.

Our transform approach reduced the spectral problem to simple linear systems that was solved to high accuracy with strategic choices of basis representations that take account of any corner singularities inherent in the problem. Our choice of representation of unknown boundary data in terms of the Joukowski-type conformal slit mapping (5.41) was tailored to the known form of the corner singularities in our examples; with this choice of basis functions, we have seen that small systems can give spectral convergence. In a similar vein, Smitheman *et al.* [100] have introduced a so-called spectral collocation method in which a spectral analysis of the boundary conditions and use of the global relations gives rise to a set of equations to determine the unknown boundary data. Their numerical experiments suggest that the method inherits the order of convergence of the basis used to expand the unknown functions, namely, exponential for a polynomial basis such as Chebyshev, and algebraic for a Fourier basis. On the other hand Fornberg & Flyer [46] have presented an alternative numerical approach based on Legendre expansions of the unknown boundary data on polygonal boundary segments. When the corner points are free of singularities the method gives exponential accuracy, but that fails when corner singularities are present. In the latter case, the authors show that including leading order singular terms of known type improves accuracy. A crucial distinction between the work of Smitheman *et al.* [100] and Fornberg & Flyer [46] is that the former workers derive equations for the unknown spectral data by inspecting the spectral relations to find special points in the spectral plane where information on a reduced set of spectral functions can be found (as we have done here); the latter authors, on the other hand, evaluate the global relations – which relate all unknown

spectral functions – at a set of points in the spectral plane chosen to provide good numerical conditioning.

Fokas [38] and Fokas & Spence [45] have discussed general connections between the unified transform method and Wiener-Hopf techniques. In this chapter, we have shown how Wiener-Hopf problems for harmonic and biharmonic fields can be solved using the transform method. The advantage of our approach was that we were able to avoid the challenging part of kernel factorization associated to the Wiener-Hopf method and propose a systematic method for solving problems with mixed boundary conditions. A collection of other Stokes flow problems in polygonal domains, including matrix and three-part Wiener-Hopf problems and a brief discussion of how the transform method for polygonal domains can be used to solve them will be presented in Chapter 7.

Chapter 6

Periodic array of point singularities in a channel

6.1 Introduction

A number of studies have been devoted to finding solutions to Stokes flow problems in singly/doubly/triply-periodic domains in two/three dimensions, owing to their many applications in various fields of fluid dynamics. Hasimoto [50] studied problems for the fundamental singularities of the Stokes equations in two/three -dimensional periodic arrays and proposed various techniques to improve the convergence of the associated Fourier series [51]. Pozrikidis in his monograph [89] developed boundary integral methods and singularity methods to solve problems in general geometries, including periodic domains. Also, Pozrikidis [90] proposed efficient summation methods to solve problems in periodic structures.

In this chapter, we present our transform approach to solve for a periodic array of point stresslets in a two-dimensional channel geometry. We then compare our approach to an alternative method based on conformal mapping (Crowdy [private communication]). The main purpose is to show that the transform method for polygonal domains can be used to solve problems with periodic boundary conditions, as well as to illustrate how periodicity conditions can be utilized to reduce the number of unknown spectral functions and therefore

provide solutions to these problems. Results obtained are compared to Crowdy's [private communication] alternative method.

6.2 Problem formulation

In this section, we solve the problem of a periodic array of point singularities in a channel geometry using the transform method for polygonal domains. As we see, since the geometry is periodic it is sufficient to analyze the problem in a single period window. In the previous chapter, we have analyzed problems in semi-strip geometries; we now show how the transform method can be used to solve problems in bounded rectangular domains.

Consider a two-dimensional channel $-\infty < x < \infty$, $0 \leq y \leq h$ and a periodic array of point stresslets (with period l) placed at points $z = z_0 + nl$, $n \in \mathbb{Z}$, with $0 < \text{Re}[z_0] < l$. Figure 6.1 shows a schematic of the configuration. The aim is to determine the resulting fluid flow due to these point singularities. It should be noted that the following analysis can be very easily adapted to other Stokes flow singularities, namely Stokeslets, quadrupoles etc. (presented in Chapter 3); we have chosen to consider point stresslets, since these have applications in modelling of microswimmers in low-Reynolds-number flows.

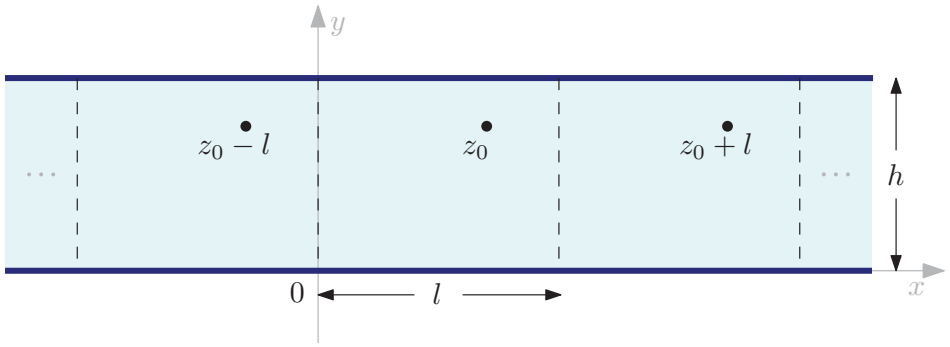

Figure 6.1: Schematic of the configuration: A periodic array of point stresslets placed at points $z = z_0 + nl$, $n \in \mathbb{Z}$ in a two-dimensional channel $-\infty < x < \infty$, $0 \leq y \leq h$.

Given the periodic structure of the configuration, it is sufficient to consider a single periodic window; for simplicity, we will analyze the problem in $0 \leq x \leq l$, $0 \leq y \leq h$ (Figure 6.2).

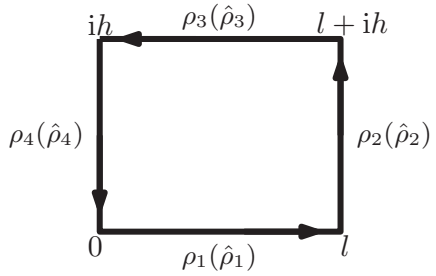

Figure 6.2: The period window $0 \leq x \leq l$, $0 \leq y \leq h$ and associated spectral functions.

6.3 Goursat functions and transform representation

The Goursat functions can be represented by

$$\begin{cases} f(z) = f_s(z) + \hat{f}(z), \\ g'(z) = g'_s(z) + \hat{g}'(z), \end{cases} \tag{6.1}$$

where $f_s(z)$, $g'_s(z)$ are the forcing functions related to a point stresslet of strength $\mu \in \mathbb{C}$ at point z_0:

$$\begin{cases} f_s(z) = \dfrac{\mu}{z - z_0}, \\ \\ g'_s(z) = \dfrac{\mu \overline{z_0}}{(z - z_0)^2} \end{cases} \tag{6.2}$$

and $\hat{f}(z)$, $\hat{g}'(z)$ are the correction functions to be found. As already mentioned, the correction functions are analytic and single-valued in the fluid region. We note that (6.2) can alternatively be replaced by trigonometric meromorphic functions which have the same local behaviour (Crowdy & Davis [20]).

We can write the following integral representation for $\hat{f}(z)$:

$$\hat{f}(z) = \frac{1}{2\pi} \left[\int_0^{\infty} \rho_1(k) e^{\mathrm{i}kz} dk + \int_0^{-\mathrm{i}\infty} \rho_2(k) e^{\mathrm{i}kz} dk + \int_0^{-\infty} \rho_3(k) e^{\mathrm{i}kz} dk + \int_0^{\mathrm{i}\infty} \rho_4(k) e^{\mathrm{i}kz} dk \right], \tag{6.3}$$

where $\rho_j(k)$, $j = 1, 2, 3, 4$ are the spectral functions defined by

$$\begin{aligned}
\rho_1(k) &= \int_0^l \hat{f}(z)e^{-\mathrm{i}kz}dz, \\
\rho_2(k) &= \int_l^{l+\mathrm{i}h} \hat{f}(z)e^{-\mathrm{i}kz}dz, \\
\rho_3(k) &= \int_{l+\mathrm{i}h}^{\mathrm{i}h} \hat{f}(z)e^{-\mathrm{i}kz}dz, \\
\rho_4(k) &= \int_{\mathrm{i}h}^{0} \hat{f}(z)e^{-\mathrm{i}kz}dz.
\end{aligned} \tag{6.4}$$

Similarly, we can write an integral representation for $\hat{g}'(z)$:

$$\hat{g}'(z) = \frac{1}{2\pi}\left[\int_0^{\infty} \hat{\rho}_1(k)e^{\mathrm{i}kz}dk + \int_0^{-\mathrm{i}\infty} \hat{\rho}_2(k)e^{\mathrm{i}kz}dk + \int_0^{-\infty} \hat{\rho}_3(k)e^{\mathrm{i}kz}dk + \int_0^{\mathrm{i}\infty} \hat{\rho}_4(k)e^{\mathrm{i}kz}dk\right], \tag{6.5}$$

where $\hat{\rho}_j(k)$, $j = 1, 2, 3, 4$ are defined by

$$\begin{aligned}
\hat{\rho}_1(k) &= \int_0^l \hat{g}'(z)e^{-\mathrm{i}kz}dz, \\
\hat{\rho}_2(k) &= \int_l^{l+\mathrm{i}h} \hat{g}'(z)e^{-\mathrm{i}kz}dz, \\
\hat{\rho}_3(k) &= \int_{l+\mathrm{i}h}^{\mathrm{i}h} \hat{g}'(z)e^{-\mathrm{i}kz}dz, \\
\hat{\rho}_4(k) &= \int_{\mathrm{i}h}^{0} \hat{g}'(z)e^{-\mathrm{i}kz}dz.
\end{aligned} \tag{6.6}$$

Spectral functions (A.6) and (6.6) are illustrated in Figure 6.2.

Global relations: Since the period window is a bounded polygon, the global relations are valid for all $k \in \mathbb{C}$ and they are given by

$$\begin{aligned}
&\rho_1(k) + \rho_2(k) + \rho_3(k) + \rho_4(k) = 0, \qquad k \in \mathbb{C}, \\
&\hat{\rho}_1(k) + \hat{\rho}_2(k) + \hat{\rho}_3(k) + \hat{\rho}_4(k) = 0, \qquad k \in \mathbb{C}.
\end{aligned} \tag{6.7}$$

6.4 Boundary conditions

The channel walls are no-slip boundaries and therefore on substitution of (6.1) into (3.19), we find that, on the lower boundary $\overline{z} = z$,

$$-\overline{\hat{f}(z)} + z\hat{f}'(z) + \hat{g}'(z) = \overline{f_s(z)} - zf_s'(z) - g_s'(z). \tag{6.8}$$

Similarly, on the upper boundary $\overline{z} = z - 2\mathrm{i}h$,

$$-\overline{\hat{f}(z)} + (z - 2\mathrm{i}h)\hat{f}'(z) + \hat{g}'(z) = \overline{f_s(z)} - (z - 2\mathrm{i}h)f_s'(z) - g_s'(z). \tag{6.9}$$

The periodicity of the configuration implies that velocity, pressure and vorticity must be l-periodic. Without loss of generality, we assume that fluid is of unit viscosity which implies that pressure and vorticity can be expressed in terms of the Goursat functions as

$$p - \mathrm{i}\omega = 4f'(z). \tag{6.10}$$

Therefore, since p and ω are l-periodic, we must require

$$f'(z) = f'(z + l), \tag{6.11}$$

or, on integration with respect to z,

$$f(z) + c = f(z + l), \tag{6.12}$$

where c is a complex constant. Substitution of (6.1) into (6.12) gives

$$\hat{f}(z) - \hat{f}(z + l) + c = -f_s(z) + f_s(z + l). \tag{6.13}$$

In addition, the l-periodicity of velocity can be expressed as

$$-\overline{f(z)} + \overline{z}f'(z) + g'(z) = -\overline{f(z + l)} + (\overline{z} + l)f'(z + l) + g'(z + l), \tag{6.14}$$

which on use of (6.11)-(6.12) simplifies to

$$-lf'(z)+g'(z)-g'(z+l)+\overline{c}=0. \tag{6.15}$$

On substitution of (6.1) we obtain

$$-l\hat{f}'(z)+\hat{g}'(z)-\hat{g}'(z+l)+\overline{c}=lf_s'(z)-g_s'(z)+g_s'(z+l). \tag{6.16}$$

Note that periodicity conditions (6.11) and (6.14) are valid in the entire fluid domain. However, as we will see in the next section, these will only be used to relate the unknown spectral functions on the vertical 'boundaries' of the period window.

6.5 Spectral analysis

The boundary and periodicity conditions allow us to deduce more information about the spectral functions.

We multiply (6.8) by $e^{-\mathrm{i}kz}$ and integrate along the lower boundary:

$$-\int_0^l \overline{\hat{f}(z)}e^{-\mathrm{i}kz}dz+\int_0^l z\hat{f}'(z)e^{-\mathrm{i}kz}dz+\int_0^l \hat{g}'(z)e^{-\mathrm{i}kz}dz=R_1(k), \tag{6.17}$$

where

$$R_1(k)\equiv\int_0^l [\overline{f_s(z)}-zf_s'(z)-g_s'(z)]e^{-\mathrm{i}kz}dz. \tag{6.18}$$

Expression (6.17) can be written in terms of the spectral functions as

$$-\overline{\rho_1}(-k)-\frac{\partial[k\rho_1(k)]}{\partial k}+\hat{\rho}_1(k)+l\hat{f}(l)e^{-\mathrm{i}kl}=R_1(k). \tag{6.19}$$

Similarly, we multiply (6.9) by $e^{-\mathrm{i}kz}$ and integrate along the upper boundary:

$$-\int_{l+\mathrm{i}h}^{\mathrm{i}h}\overline{\hat{f}(z)}e^{-\mathrm{i}kz}dz+\int_{l+\mathrm{i}h}^{\mathrm{i}h}(z-2\mathrm{i}h)\hat{f}'(z)e^{-\mathrm{i}kz}dz+\int_{l+\mathrm{i}h}^{\mathrm{i}h}\hat{g}'(z)e^{-\mathrm{i}kz}dz=R_3(k), \quad (6.20)$$

where

$$R_3(k)\equiv\int_{l+\mathrm{i}h}^{\mathrm{i}h}[\overline{f_s(z)}-(z-2\mathrm{i}h)f_s'(z)-g_s'(z)]e^{-\mathrm{i}kz}dz. \quad (6.21)$$

Expression (6.20) can be written in terms of the spectral functions as

$$-e^{2kh}\overline{\rho_3}(-k)-\frac{\partial[k\rho_3(k)]}{\partial k}+2kh\rho_3(k)+\hat{\rho}_3(k)-\mathrm{i}h\hat{f}(\mathrm{i}h)e^{kh}-(l-\mathrm{i}h)\hat{f}(l+\mathrm{i}h)e^{-\mathrm{i}k(l+\mathrm{i}h)}=R_3(k). \quad (6.22)$$

To obtain relations between the spectral functions $\rho_2(k)$, $\rho_4(k)$ (and $\hat{\rho}_2(k)$, $\hat{\rho}_4(k)$), we use the periodicity conditions (6.13) and (6.16):

We multiply (6.13) by $e^{-\mathrm{i}kz}$ and integrate along 'boundary' $z=\mathrm{i}y$, $0\le y\le h$:

$$\int_{\mathrm{i}h}^{0}\hat{f}(z)e^{-\mathrm{i}kz}dz-\int_{\mathrm{i}h}^{0}\hat{f}(z+l)e^{-\mathrm{i}kz}dz+c\int_{\mathrm{i}h}^{0}e^{-\mathrm{i}kz}dz=R_2(k), \quad (6.23)$$

where

$$R_2(k)\equiv\int_{\mathrm{i}h}^{0}[-f_s(z)+f_s(z+l)]e^{-\mathrm{i}kz}dz. \quad (6.24)$$

This can be written in terms of the spectral functions as

$$\rho_4(k)+e^{\mathrm{i}kl}\rho_2(k)+c\,q(k)=R_2(k), \quad (6.25)$$

with

$$q(k)\equiv\int_{\mathrm{i}h}^{0}e^{-\mathrm{i}kz}dz=\begin{cases}\dfrac{\mathrm{i}(1-e^{kh})}{k}, & \text{if } k\neq 0,\\ -\mathrm{i}h, & \text{if } k=0.\end{cases} \quad (6.26)$$

We multiply (6.16) by $e^{-\mathrm{i}kz}$ and integrate, again, along 'boundary' $z = \mathrm{i}y$, $0 \le y \le h$:

$$-l\int_{\mathrm{i}h}^{0}\hat{f}'(z)e^{-\mathrm{i}kz}dz + \int_{\mathrm{i}h}^{0}\hat{g}'(z)e^{-\mathrm{i}kz}dz - \int_{\mathrm{i}h}^{0}\hat{g}'(z+l)e^{-\mathrm{i}kz}dz + \overline{c}\,q(k) = R_4(k), \quad (6.27)$$

where

$$R_4(k) \equiv \int_{\mathrm{i}h}^{0}[lf_s'(z) - g_s'(z) + g_s'(z+l)]e^{-\mathrm{i}kz}dz. \quad (6.28)$$

Expression (6.27) can be written in terms of the spectral functions as

$$-\mathrm{i}kl\rho_4(k) + \hat{\rho}_4(k) + e^{\mathrm{i}kl}\hat{\rho}_2(k) - l\hat{f}(0) + l\hat{f}(\mathrm{i}h)e^{kh} + \overline{c}\,q(k) = R_4(k). \quad (6.29)$$

6.6 Solution scheme

Addition of (6.19) and (6.22) and use of the global relations (A.16) gives

$$(e^{2kh}-1)\overline{\rho_1}(-k) - 2kh\rho_1(k) = W(k), \quad (6.30)$$

where

$$\begin{aligned} W(k) =& 2kh[\rho_2(k)+\rho_4(k)] - \left[\frac{\partial[k\rho_2(k)]}{\partial k} + \frac{\partial[k\rho_4(k)]}{\partial k}\right] - e^{2kh}[\overline{\rho_2}(-k) + \overline{\rho_4}(-k)] \\ & - l\hat{f}(l)e^{-\mathrm{i}kl} + \mathrm{i}h\hat{f}(\mathrm{i}h)e^{kh} + (l-\mathrm{i}h)\hat{f}(l+\mathrm{i}h)e^{-\mathrm{i}k(l+\mathrm{i}h)} + [\hat{\rho}_2(k)+\hat{\rho}_4(k)] \\ & + R_1(k) + R_3(k). \end{aligned} \quad (6.31)$$

On use of (6.13), (6.25) and (6.29), spectral functions $\{\rho_2(k), \hat{\rho}_2(k)\}$ and corner values $\hat{f}(l)$, $\hat{f}(l+\mathrm{i}h)$ can be eliminated from $W(k)$ to give an expression for $W(k)$ in terms of $\{\rho_4(k), \hat{\rho}_4(k)\}$, corner values $\hat{f}(0)$, $\hat{f}(\mathrm{i}h)$, parameter c and known quantities only.

Taking Schwarz conjugate and letting $k \mapsto -k$ in (6.30), we find

$$(e^{-2kh}-1)\rho_1(k) + 2kh\overline{\rho_1}(-k)\rho_1(k) = \overline{W}(-k). \quad (6.32)$$

Elimination of $\overline{\rho_1}(-k)$ from (6.30) and (6.32) gives:

$$\rho_1(k) = \frac{2khW(k) - (e^{2kh} - 1)\overline{W}(-k)}{\Delta(k)}, \tag{6.33}$$

where

$$\Delta(k) \equiv 4[\sinh^2(kh) - k^2h^2]. \tag{6.34}$$

But spectral function $\rho_1(k)$ is analytic everywhere in the complex k-plane (since its integrand is over an edge of finite length) which means that its numerator in (6.33) must vanish at zeros of $\Delta(k)$ in the k-plane, i.e. we must require

$$X(k) \equiv 2khW(k) - (e^{2kh} - 1)\overline{W}(-k) = 0, \tag{6.35}$$

for points in the set

$$\Sigma_1 \equiv \{k \in \mathbb{C} | \Delta(k) = 0\}. \tag{6.36}$$

The set of points Σ_1 coincides with the eigenvalue set associated with the so-called Papkovich-Fadle eigenfunctions in a semi-strip (Joseph [64, 65]). Figure 6.3 shows a schematic of the points in the spectral k-plane where information on $\rho_4(k)$ and $\hat{\rho}_4(k)$ is available. In addition, using Taylor expansions, it can be shown that

$$\Delta(k) = 4[\sinh^2(kh) - k^2h^2] = \mathcal{O}(k^4), \quad \text{as } k \to 0, \tag{6.37}$$

which implies that $X(k)$ must also satisfy

$$X(0) = X'(0) = X''(0) = X'''(0) = 0. \tag{6.38}$$

Conditions (6.35) and (6.38) are enough to determine $\{\rho_4(k), \hat{\rho}_4(k)\}$, corner values $\hat{f}(0)$, $\hat{f}(\mathrm{i}h)$ and complex parameter c.

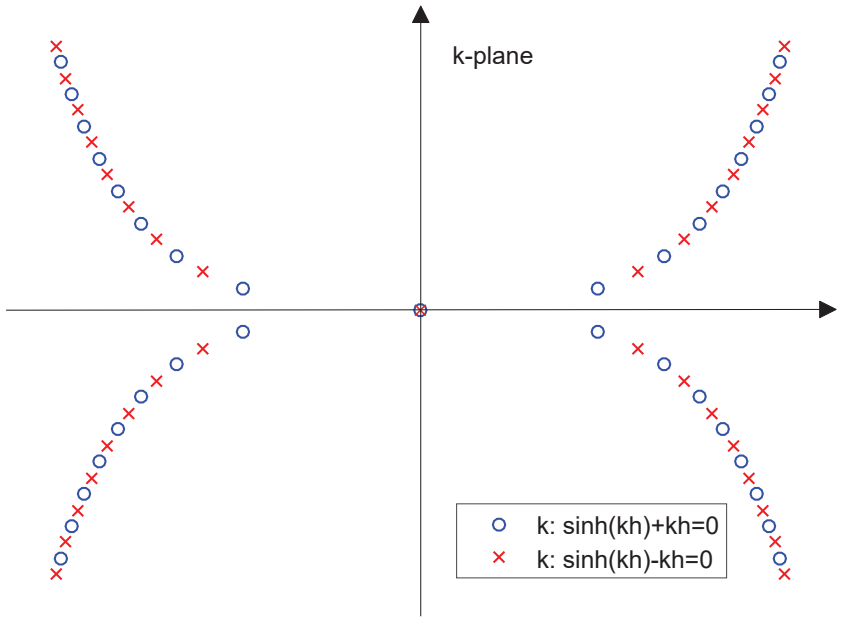

Figure 6.3: Schematic of the points in the spectral k-plane at which information on the spectral functions is available. These points coincide with the eigenvalue set associated with the so-called Papkovich-Fadle eigenfunctions in a semi-strip.

6.6.1 Function representations

The correction functions $\hat{f}(z)$ and $\hat{g}'(z)$ on the 'boundary' $z = \mathrm{i}y$, $0 \leq y \leq h$ are represented using Fourier type series expansions:

$$\hat{f}(z) = \frac{1}{h} \sum_{m=-\infty}^{\infty} a_m e^{m\pi z/h}, \qquad \hat{g}(z) = \frac{1}{h} \sum_{m=-\infty}^{\infty} b_m e^{m\pi z/h}, \tag{6.39}$$

where $\{a_m, b_m \in \mathbb{C} | m \in \mathbb{Z}\}$ are to be found. We note that these function representations can be replaced by different basis expansions, such as Chebyshev, but since there are not any associated singularities at the endpoints of the boundary, a Fourier type basis seems a

natural choice. Using (6.39), we can write

$$\rho_4(k) = \sum_{m=-\infty}^{\infty} a_m[T(k,m)], \qquad \hat{\rho}_4(k) = \sum_{m=-\infty}^{\infty} b_m[U(k,m)], \tag{6.40}$$

where

$$T(k,m) \equiv \frac{1}{h}\int_{\mathrm{i}h}^{0} e^{(m\pi/h - \mathrm{i}k)z}dz = \begin{cases} \dfrac{1-e^{\mathrm{i}m\pi+kh}}{m\pi - \mathrm{i}kh}, & k \neq \dfrac{m\pi}{\mathrm{i}h}, \\ -\mathrm{i}, & k = \dfrac{m\pi}{\mathrm{i}h}. \end{cases} \tag{6.41}$$

and

$$U(k,m) = \left(\frac{m\pi}{h}\right) T(k,m). \tag{6.42}$$

6.6.2 Formulation of a linear system

The sums in (6.39) are truncated to include only terms $m = -M, ..., M$ for suitable M and we formulate a linear system for the unknown coefficients $\{a_m\}$, $\{b_m\}$ and parameter c (and their complex conjugates). The linear system comprises conditions (6.35) evaluated at as many points in the set Σ_1 as needed, together with conditions (6.38). Note that, since (6.38) must be added in the linear system, this implies that we must analytically compute expressions for $X(k)$ and its derivatives (up to third order) and then evaluate them at $k = 0$. To avoid this (since this involves a considerable amount of algebra), we observe that, if we insist

$$\oint_{|k|=r} \frac{X(k)}{k^s}dk = 0, \quad \text{for } s = 1, 2, 3, 4, \tag{6.43}$$

for sufficiently small $r \in \mathbb{R}$ so that $|k| = r$ does not enclose any roots of $\Delta(k)$ other than $k = 0$, then we obtain equivalent conditions to (6.38). The advantage is that (6.43) can be computed numerically for small r.

Once coefficients $\{a_m\}$, $\{b_m\}$ are found, spectral functions $\{\rho_4(k), \hat{\rho}_4(k)\}$ can be computed. The remaining spectral functions can be found by back substitution into various relations and therefore the correction functions $\hat{f}(z)$ and $\hat{g}'(z)$ can be computed. The cor-

rection functions are then substituted into (6.1) to find $f(z)$ and $g'(z)$.

6.7 Comparison to an alternative method

Our solution was compared with a solution obtained using an alternative method based on conformal mappings (Crowdy [private communication]) and results were the same to within an accuracy of $\mathcal{O}(10^{-8})$.

6.8 Summary

In this chapter, we analyzed the problem of a periodic array of point stresslets in a two-dimensional channel geometry using our transform approach for polygonal domains. Our aim was to show that the transform method for polygonal domains can be used to solve problems with periodic boundary conditions, as well as to illustrate how periodicity conditions can be utilized to reduce the number of unknown spectral functions.

The idea of our transform approach was again to obtain conditions at some special points in the spectral k-plane satisfied by a reduced number of spectral functions. These conditions were found by performing spectral analysis of the boundary and periodicity conditions and analyzing the obtained relations between spectral functions. By exploiting the analyticity of one of the spectral functions ($\rho_1(k)$) in the entire k-plane, we obtained conditions on the spectral functions associated to one of the vertical 'boundaries' of the period window. Using series expansions to represent the unknown boundary data on that edge, we showed that the set of conditions obtained was sufficient to determine the solution.

Our results were compared to an alternative method based on conformal mappings (Crowdy [private communication]) and we obtained an agreement to within an accuracy of $\mathcal{O}(10^{-8})$. The transform approach produces accurate results with only few truncation terms. In addition, it should be noted that the transform method can be very easily adapted to other point singularities with minor differences (only functions $R_j(k), j = 1, 2, 3, 4$ will be different). Remarkably, our approach can be generalized to finding the solution due to periodic ar-

ray of Stokeslets in a two-dimensional channel which is known that the evaluation of the associated Green's function using classical boundary integral methods has numerical difficulties and slow convergence [50, 51, 89, 90].

Finally, we mention that our transform approach can also be used to solve problems in doubly-periodic domains where there are two periods l and h in the x and y directions respectively. A schematic of a doubly-periodic array of point singularities is shown in Figure 6.4. Hasimoto [50] studied problems for the fundamental singularities of the Stokes equations in two and three-dimensional periodic arrays and proposed various techniques to improve the convergence of the associated Fourier series. Pozrikidis [89] presented solutions in such geometries using boundary integral methods and proposed efficient summation methods to solve them. It is an interesting application to solve problems in doubly-periodic domains using the transform method and, furthermore, to investigate the convergence of the resulting schemes. To illustrate how the transform method can be used to solve problems in doubly-periodic domains, we present a problem in such geometry in Appendix A. The problem analyzed concerns the Weierstrass $\mathcal{P}$- function (Abramowitz & Stegun[5]) and the aim is to find a spectral representation for it. Although it is not a biharmonic boundary value problem, it is instructive to see how the doubly-periodicity nature of the problem provides conditions between the spectral functions which can be used to solve the problem. It is expected that similar ideas can be used to find spectral representations for doubly-periodic arrays of the fundamental Stokes flow singularities.

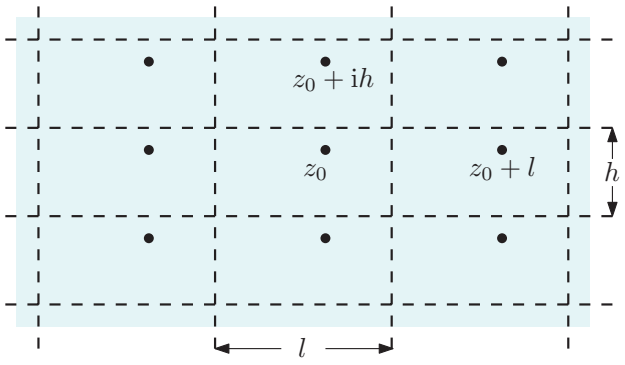

Figure 6.4: A doubly-periodic array of point singularities placed at points $z = z_0 + nl + \mathrm{i}mh$, $n, m \in \mathbb{Z}$.

Chapter 7

Applications in polygonal domains

7.1 Introduction

In Chapters 5 and 6, we analyzed problems in semi-strip and rectangular domains (Figure 7.1). In this chapter, we discuss how Stokes flow problems in more complex channel geometries can be solved by decomposing the problem domain into semi-strips and rectangles.

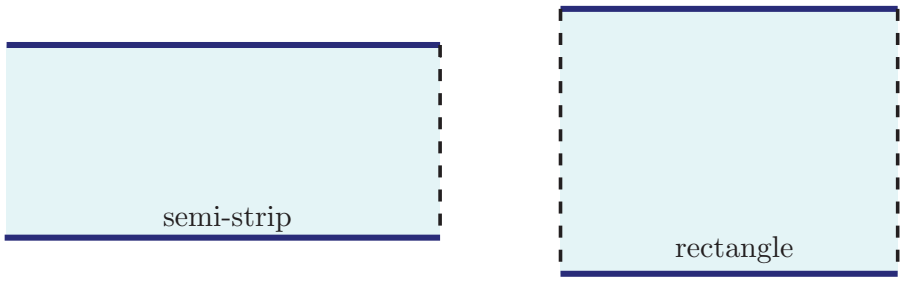

Figure 7.1: Problems presented in Chapters 5 and 6 were solved by decomposing the problem domain into semi-strip and rectangular domains.

The ideas to solve these problems are similar to those used to solve Scalar Wiener-Hopf problems (Chapter 5). For completeness, we present the four main steps again (with an addition in step (a)):

(a) **Domain splitting:** for a problem domain involving boundary conditions of mixed type, find a convenient "splitting" of the problem domain (domain decomposition)

into distinct boundary value sub-problems. Preferably, sub-domains have the same type of boundary conditions on at least two opposite sides and any symmetry of the resulting flow should be taken into consideration when splitting the domain. Once the problem domain is decomposed into semi-strip and rectangular domains, solve each sub-problem using the transform method for polygonal domains;

(b) **Boundary conditions:** couple the resulting sub-problems by employing the same spectral parameter for each and by imposing appropriate continuity conditions on any common edges;

(c) **Spectral analysis:** analyse the spectral relations arising from the boundary conditions, together with the global relations, to identify special points in the spectral plane whereby information on a reduced set of unknown spectral functions can be determined;

(d) **Solution scheme and function representation:** identify the precise nature of the singularities occurring at boundary points where the boundary conditions change type and represent unknown boundary data in terms of specially tailored variables that incorporate those edge singularities. Solve for a reduced set of spectral functions, with the rest following by back-substitution into the spectral relations.

Following steps (a)-(d), we will discuss how problems in more complex channel geometries can be solved using the transform method. The problems presented have appeared in the literature and have been solved using different techniques: scalar (Jeong [55]) and matrix Wiener-Hopf (Abrahams, Davis & Llewellyn Smith [4]) problems, three-part Wiener-Hopf problem (Setchi *et al*. [97]) and biorthogonal expansions of Papkovich-Fadle eigenfunctions (Kim & Chung [67]). Our aim is to illustrate that the transform method for polygonal domains can be used to solve these problems following the main steps presented above. Although analytical solutions using our transform approach are not presented in detail in this chapter, we outline the key ideas to solve them; similar ideas have already been presented to solve problems in Chapters 5-6.

7.2 Flow in a 'partitioned' channel (or symmetric channel divider)

Jeong [55] considered a Stokes flow in a 'partitioned' channel composed of two infinite walls and a semi-infinite one located midway between the infinite walls. The flow was allowed to 'turn around' the semi-infinite wall driven by a pressure gradient. A schematic is shown in Figure 7.2. This author obtained an exact solution for the streamfunction using the Wiener-Hopf technique (scalar case) and, then, investigated among others the formation of Moffatt eddies in the channel for different flux rates. Owing to the linearity of Stokes equations, general flows were solved by superposing symmetric and antisymmetric flows.

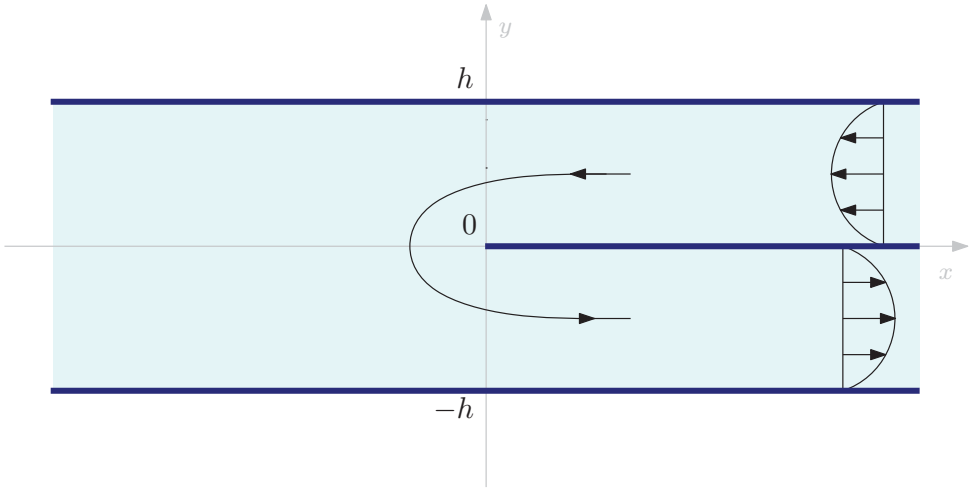

Figure 7.2: Stokes flow in a symmetric channel divider driven by pressure gradient. This problem was solved by Jeong [55] using the Wiener-Hopf technique (scalar case).

Assuming (without loss of generality) that the flow is either symmetric or antisymmetric, if we wish to solve this problem using our transform approach, it is sufficient to analyze the problem in domains I and II as illustrated in Figure 7.3. The resulting flow in domain I is either symmetric or antisymmetric and this should be used to eliminate the complex conjugate expressions of the Goursat functions appearing in the boundary conditions (this idea was used in Chapter 5). In domain II, the flow does not possess any symmetry. The spectral analysis in each sub-domain will give conditions on the spectral functions

associated to the vertical edges of semi-strips I and II at points in the spectral k-plane:

$$\begin{aligned} \Sigma_I &= \{k \in \mathbb{C}^+ | \sinh(2kh) \pm 2kh = 0\}, \\ \Sigma_{II} &= \{k \in \mathbb{C}^- | \sinh^2(kh) - k^2h^2 = 0\}, \end{aligned} \tag{7.1}$$

where $\mathbb{C}^+$ and $\mathbb{C}^-$ denote the upper and lower half-planes respectively and the $\pm$ in Σ_I is found according to the symmetry of the flow. Using the symmety and continuity conditions, all conditions can be written in terms of the spectral functions associated to the vertical edge of semi-strip II. The next step is to use appropriate basis expansions to represent the unknown boundary data on that edge taking into account that now the Goursat functions $f(z)$ and $g'(z)$ have square-roots singularities only at one end, instead of at both ends (Chapter 5). Solving for these expansions, all other spectral functions will follow from back substitution into relations found in the spectral analysis part.

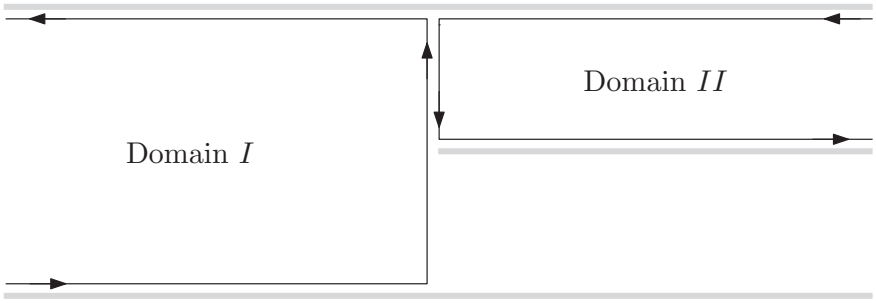

Figure 7.3: Domain decomposition for Jeong's [55] problem.

7.3 Flow in an asymmetric channel divider

Abrahams, Davis & Llewellyn Smith [4] considered a flow in the asymmetric channel divider shown in Figure 7.4. The flow was driven by the motion of the upper and lower boundaries with prescribed velocities U_1 and U_2 respectively. These authors solved this problem using the Wiener-Hopf technique (matrix case) and use of Padé approximants.

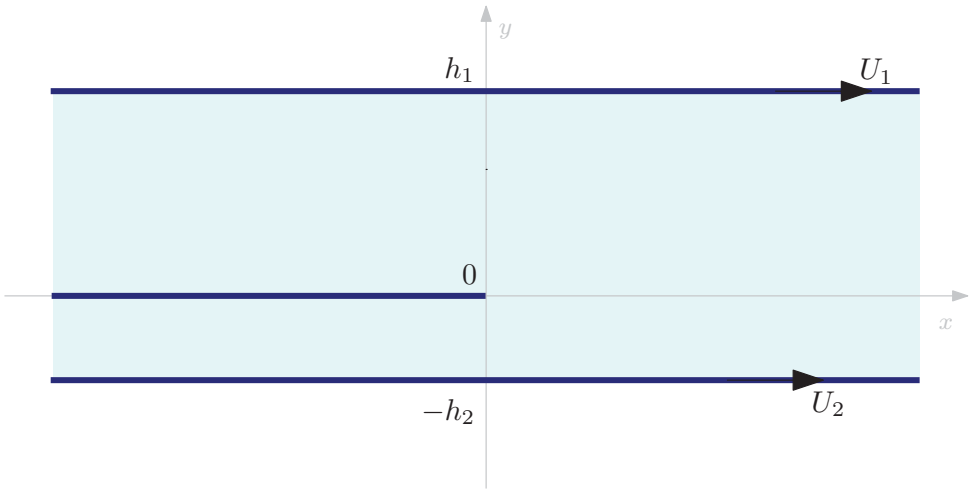

Figure 7.4: Stokes flow in an asymmetric channel divider driven by the motion of the upper and lower boundaries with prescribed velocities U_1 and U_2 respectively. This problem was solved by Abrahams, Davis & Llewellyn Smith [4].

Our transform approach can be used to solve this problem; in order to do so, the fluid domain should be decomposed into the three sub-domains illustrated in Figure 7.5 and follow similar steps to obtain conditions on the spectral functions associated to the vertical edges at spectral k-points:

$$\begin{aligned}\Sigma_I &= \{k \in \mathbb{C}^+ | \sinh^2(kh_1) - k^2h_1^2 = 0\},\\ \Sigma_{II} &= \{k \in \mathbb{C}^+ | \sinh^2(kh_2) - k^2h_2^2 = 0\},\\ \Sigma_{III} &= \{k \in \mathbb{C}^- | \sinh^2(k(h_1+h_2)) - k^2(h_1+h_2)^2 = 0\}.\end{aligned} \tag{7.2}$$

Using the continuity conditions, the conditions on the spectral functions at k-points in the sets (7.2) can be written in terms of spectral functions associated to the vertical edges of semi-strips I and II only. Again, the unknown data can be presented by suitable basis expansions taking account of the singularity at point $z = 0$. For this problem, two sets of representations are needed: for the vertical edges of semi-strips I and II. It is therefore necessary to add compatibility conditions at points where they are both valid, in this case at point $z = 0$. Solving for these expansions, all other spectral functions will follow from back substitution into relations found in the spectral analysis part.

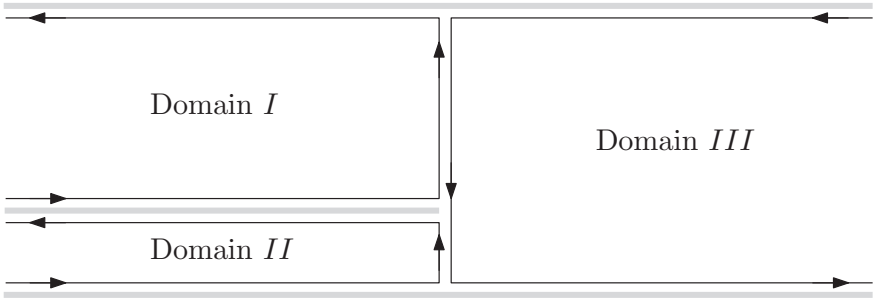

Figure 7.5: Domain decomposition for Abrahams, Davis & Llewellyn Smith's [4] problem.

7.4 Flow through a shunt between two channels

Setchi *et al*. [97] considered Stokes flows through a shunt between two channel for different inlet and outlet fluxes. They obtained analytical solution for the streamfunction by matching biorthogonal expansions of Papkovich-Fadle eigenfunctions in rectangular subregions. As they state, although the geometry suggested the use of Wiener-Hopf techniques similar to problems in the previous subsections, these authors preferred to analyze the problem using the method of Papkovich-Fadle eigenfunctions, since the additional boundaries would have complicated the analysis.

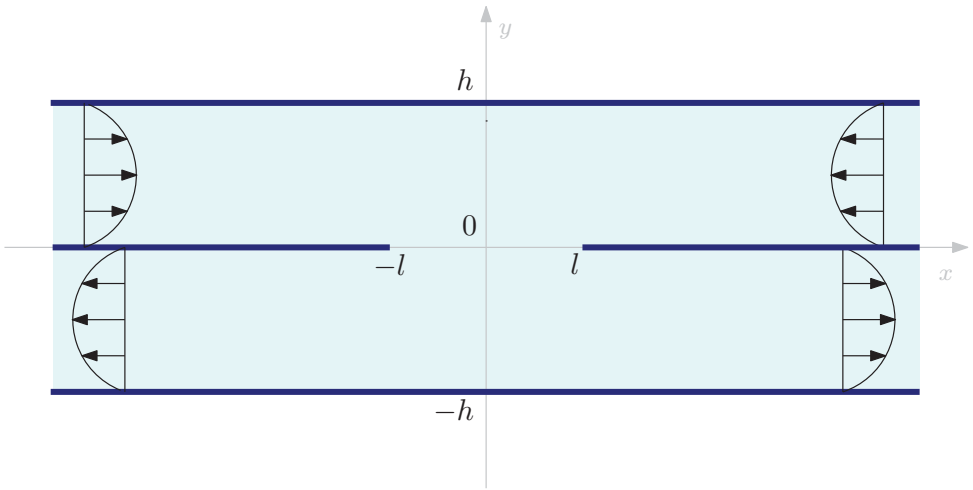

Figure 7.6: Stokes flow through a shunt between two channels; the flow is driven by pressure gradient. This problem was solved by Setchi *et al.* [97] for different inlet and outlet fluxes.

Our transform approach can again be used to solve this problem. If the resulting flow does not, in general, possess any symmetry, the problem domain should be decomposed into the five sub-domains illustrated in Figure 7.7 and steps (a)-(d) should be followed. If the problem admits symmetries with respect to, for example, the horizontal and vertical centrelines, then it is sufficient to analyze the problem in domains I and II as shown in Figure 7.7. The difference of this problem from previously presented problems is that the domains for the two sub-problems are a rectangle and a semi-strip: a bounded and an unbounded polygon respectively. But the main steps are the same and spectral analysis will give conditions on the spectral functions of the vertical edges at k-points in the sets:

$$\begin{aligned} \Sigma_I &= \{k \in \mathbb{C} | \sinh^2(2kh) - (2kh)^2 = 0\}, \\ \Sigma_{II} &= \{k \in \mathbb{C}^- | \sinh^2(kh) - k^2h^2 = 0\}. \end{aligned} \tag{7.3}$$

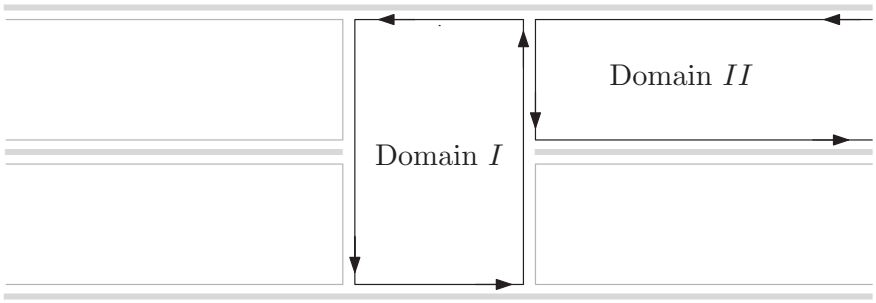

Figure 7.7: Domain decomposition for the one of the problems considered by Setchi *et al.* [97]: For a flow admitting symmetries with respect to $x = 0$ and $y = 0$, it is sufficient to analyze the problem in the two domains only.

7.5 Flow past a plate located midway in a channel

The final problem presented in this chapter was solved by Kim & Chung [67]. It concerns a pressure-driven flow in a channel with a plate located midway. These authors employed Wiener-Hopf techniques and specifically they analyzed this problem as a three-part Wiener-Hopf problem.

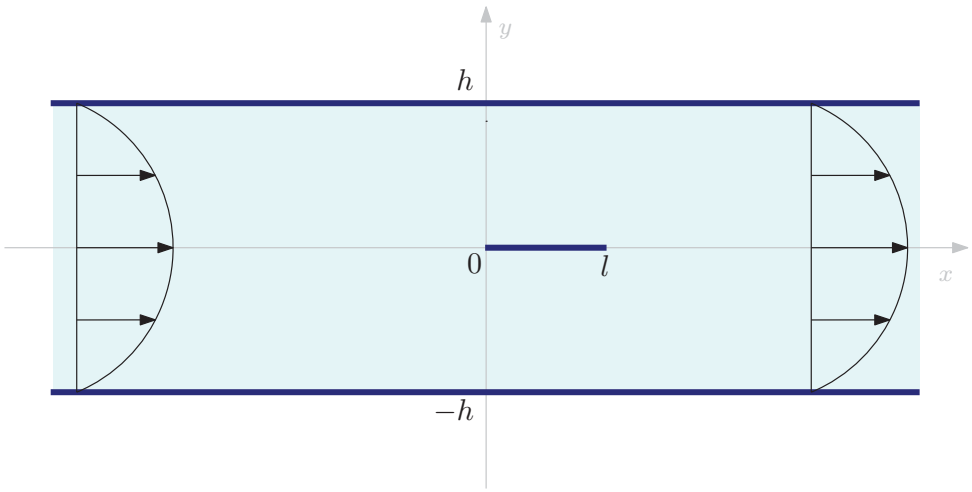

Figure 7.8: Pressure-driven flow past a plate located midway in a channel; this problem was solved by Kim & Chung [67] using a three-part Wiener-Hopf method.

The domain decomposition for solving this problem using our transform approach is shown in Figure 7.9 and obviously has many similarities with the problem presented in the previous subsection. Following the main steps again, we can solve this problem.

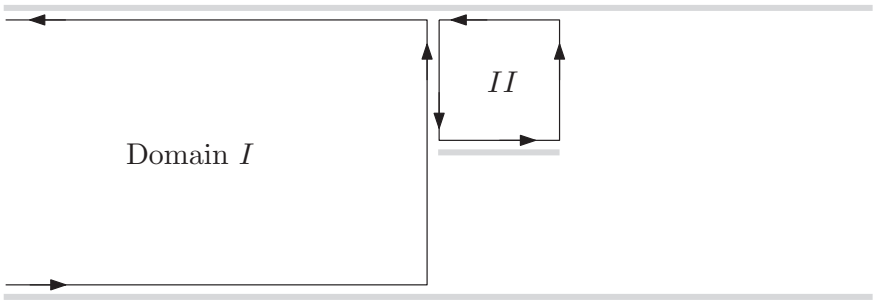

Figure 7.9: Domain decomposition for Kim & Chung's [67] problem.

Interestingly, the fluid domain in this case is a multiply-connected one and, as discussed above, the problem can be solved by splitting the domain into sub-regions. We note that our transform approach can be used to solve problems in more general multiply-connected polygonal domains with main idea being the decomposition of the exterior of any slits/rectangular 'holes' into a collection of convex polygons which can be analyzed using the unified transform method. This idea was introduced by Charalambopoulos, Dassios & Fokas [12] for solving Laplace's equation in the exterior of an equilateral triangle.

7.6 Summary

In this chapter, we presented a brief discussion on how to solve problems in more complex channel geometries using our transform approach by showing its implementation to a number of problems. The example problems presented in this chapter were previously solved using different techniques: scalar and matrix Wiener-Hopf problems, three-part Wiener-Hopf problem and biorthogonal expansions of Papkovich-Fadle eigenfunctions. We illustrated how these can be solved following the four basic steps (a)-(d). Our main purpose was to show that our transform approach can be adopted to analyze problems in complex simply- and multiply-connected polygonal domains.

Chapter 8

Stagnation point flow past a semicircular ridge

8.1 Introduction

In previous chapters, we have solved different problems in domains with boundaries consisting of straight line edges using the transform method for polygonal domains. In this chapter, we present a transform approach for a Stokes flow problem in a simply connected circular domain - whose boundary consists of a combination of straight and circular edges.

We have chosen to study a problem previously solved by Davis & O'Neill [30]. Davis & O'Neill [30] considered a stagnation point flow past a ridge or trough with the aim of understanding the separation of the flow near the point of intersection. They investigated the formation of Moffatt eddies [85] which are formed if the angle of intersection between the planar and ridge boundaries is less than 146°, as well as the separation of the flow for different angles of intersection. To solve this problem, these authors employed bipolar coordinates to map the fluid domain to a channel geometry and then used Fourier transform techniques.

In this chapter, we will first present Davis & O'Neill's [30] problem followed by a brief overview of their solution. We will then show how to solve the problem using our transform

approach for circular domains. The fluid domain in this case can be thought as the intersection of the upper half-plane and the exterior of unit disc and therefore ideas presented in Chapter 2 will be employed. Next, owing to the simplicity of the configuration, we will show how this problem can also be solved using ideas from conformal mapping theory and the transform method for polygonal domains. The idea in this second approach is to map the fluid domain to a semi-strip and then analyse the problem in this new geometry. We will then show a comparison of our results to Davis & O'Neill's solution [30]. Finally, we will present a variety of problems in similar geometries which are amenable to our transform approach for circular domains.

8.2 Problem formulation

Consider a stagnation point flow past a plane with a cylindrical ridge as shown in Figure 8.1. Davis & O'Neill [30] analysed this problem for a general angle of intersection, but we hereby assume a cylinder of unit radius which intersects the plane boundary at a corner of angle $\pi/2$.

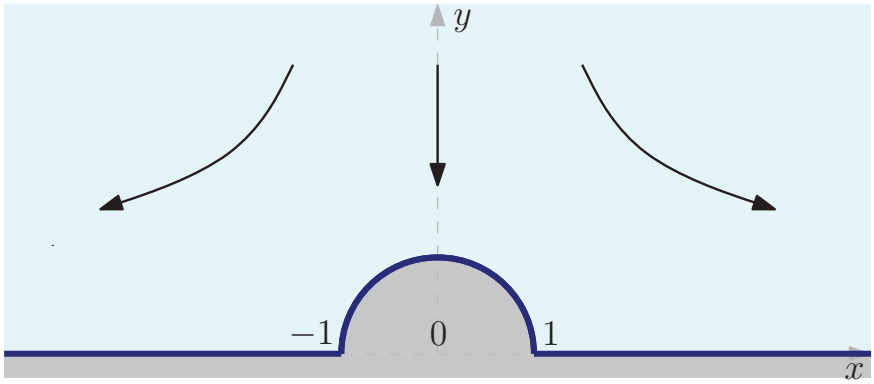

Figure 8.1: Schematic of the configuration. A stagnation point flow past a plane with a cylindrical ridge with angle of intersection between the two boundaries equal to $\pi/2$.

In the far-field, the stagnation point flow has associated velocity profile

$$(u, v) = (2axy, -ay^2), \tag{8.1}$$

where $a \in \mathbb{R}$ is a constant which determines the strength of the flow (Davis & O'Neill [30] chose $a = 1/2$). In the absence of the semicircular boundary, the flow is a stagnation point flow described by (8.1); however, the presence of the no-slip semicircular boundary alters the resulting fluid flow.

8.3 Davis & O'Neill's [30] solution

Davis & O'Neill [30] introduced bipolar coordinates ξ and η which are defined by

$$x = \frac{c \sinh \xi}{(\cosh \xi - \cos \eta)}, \qquad y = \frac{c \sin \eta}{(\cosh \xi - \cos \eta)}. \tag{8.2}$$

In terms of these coordinates, the plane and cylindrical parts of the boundary are given by $\eta = 0$ and $\eta = \eta_0$ respectively, the region of flow being defined by $0 < \eta < \eta_0 \leq 2\pi$, $-\infty < \xi < \infty$. Parameter η_0 is related to the angle of intersection between the plane and cylindrical boundaries and c is related to the points of intersection $x = \pm c$ of the circular arc with the planar boundary. Using Fourier transform techniques to analyse the boundary conditions, they found that the streamfunction (for $\xi > 0$ since the streamfunction is an odd function of ξ) is given by

$$\begin{aligned}\psi =& \frac{\pi c^3}{(\cosh \xi - \cos \eta)} \times \\ & \mathrm{Re}\Big[k_1 \sum_{n=1}^{\infty} \frac{t_n [\sin(t_n \eta) \sin(\eta_0 - \eta) - \sin(\eta) \sin(t_n(\eta_0 - \eta))]}{(\eta_0 \cos(t_n \eta_0 - \sin(\eta_0))} e^{-t_n \xi} \\ & - k_2 \sum_{n=1}^{\infty} \frac{T_n [\sin(T_n \eta) \sin(\eta_0 - \eta) + \sin(\eta) \sin(T_n(\eta_0 - \eta))]}{(\eta_0 \cos(T_n \eta_0 + \sin(\eta_0))} e^{-T_n \xi} \Big], \quad \text{for } \xi > 0,\end{aligned} \tag{8.3}$$

where t_n and T_n are respectively the roots of equations

$$\sin(t\eta_0) = t\sin(\eta_0), \tag{8.4}$$

$$\sin(t\eta_0) = -t\sin(\eta_0), \tag{8.5}$$

in the first quadrant of the complex t-plane. The constants k_i $(i = 1, 2)$ take the values 1/2 or 1 according (8.4) or (8.5) has real or complex roots. Using expression (8.3) for the streamfunction, all physical quantities of interest (velocity, pressure, vorticity etc.) can be computed. Expression (8.3) will be used later to compare/validate our results to Davis & O'Neill's solution [30].

8.4 Approach I: Transform method for circular domains

In this section, we show how the transform method for circular domains presented in Chapter 2 can be used to solve this problem.

8.4.1 Goursat functions and transform representation

The Goursat functions can be represented by

$$\begin{cases} f(z) = f_s(z) + \hat{f}(z), \\ g'(z) = g'_s(z) + \hat{g}'(z), \end{cases} \tag{8.6}$$

where $f_s(z)$, $g'_s(z)$ are the forcing functions related to the stagnation point flow and $\hat{f}(z)$, $\hat{g}'(z)$ are the correction functions to be found. It can be shown (Chapter 3) that the following forcing functions

$$\begin{cases} f_s(z) = \dfrac{\mathrm{i}az^2}{4}, \\ \\ g'_s(z) = -\dfrac{3\mathrm{i}az^2}{4} \end{cases} \tag{8.7}$$

satisfy the far-field conditions (8.1). In addition, the resulting flow admits symmetry with respect to $x = 0$ which implies that the Goursat functions satisfy the following conditions

$$\begin{cases} \overline{f}(z) = -f(-z), \\ \overline{g'}(z) = -g'(-z). \end{cases} \tag{8.8}$$

We will use the transform method for circular domains and therefore we firstly write integral representations for the unknown correction functions $\hat{f}(z)$ and $\hat{g}'(z)$ in terms of spectral functions. The fluid domain can be thought as the intersection of the upper half-plane and the exterior of the unit disc centred at the origin. Therefore, we can write the following integral representation for the analytic correction function $\hat{f}(z)$ (and similarly for $\hat{g}'(z)$):

$$\begin{aligned} \hat{f}(z) = \frac{1}{2\pi} \int_{\mathcal{L}} \rho_{11}(k) e^{\mathrm{i}kz} dk \\ - \frac{1}{2\pi \mathrm{i}} \left[\int_{L_1} \frac{\rho_{22}(k)}{1 - e^{2\pi \mathrm{i}k}} \frac{1}{z^{k+1}} dk + \int_{L_2} \rho_{22}(k) \frac{1}{z^{k+1}} dk + \int_{L_3} \frac{\rho_{22}(k) e^{2\pi \mathrm{i}k}}{1 - e^{2\pi \mathrm{i}k}} \frac{1}{z^{k+1}} dk \right], \end{aligned} \tag{8.9}$$

where $\mathcal{L} = [0, \infty)$ is the fundamental contour for straight line edges and $\{L_j | j = 1, 2, 3\}$ are the fundamental contours for circular edges. The two spectral functions are given by

$$\rho_{11}(k) = \int_L \hat{f}(z) e^{-\mathrm{i}kz} dz, \qquad \rho_{22}(k) = -\int_C \hat{f}(z) z^k dz. \tag{8.10}$$

with $L = [1, \infty) \cup (-\infty, -1]$ and $C = \{z : |z| = 1, \mathrm{Im}[z] > 0\}$ (contour C is transversed counterclockwise). The other elements of the spectral matrix are

$$\rho_{12}(k) = -\int_C \hat{f}(z) e^{-\mathrm{i}kz} dz, \qquad \rho_{21}(k) = \int_L \hat{f}(z) z^k dz. \tag{8.11}$$

The global relations are

$$\rho_{11}(k) + \rho_{12}(k) = 0, \quad k < 0 \tag{8.12}$$

and

$$\rho_{21}(k) + \rho_{22}(k) = 0, \quad k \in -\mathbb{N}. \tag{8.13}$$

The global relations (8.12)-(8.13) are equivalent statements of analyticity of $\hat{f}(z)$ in the

fluid domain.

Similar expressions to (8.9)-(8.13) can be written for the analytic correction function $\hat{g}'(z)$ (and $\hat{\rho}_{mn}(k)$, $m, n = 1, 2$). The analytic function $\hat{g}'(z)$ can be represented by

$$\hat{g}'(z) = \frac{1}{2\pi}\int_{\mathcal{L}} \hat{\rho}_{11}(k) e^{\mathrm{i}kz} dk \\ - \frac{1}{2\pi\mathrm{i}}\left[\int_{L_1} \frac{\hat{\rho}_{22}(k)}{1-e^{2\pi\mathrm{i}k}} \frac{1}{z^{k+1}} dk + \int_{L_2} \hat{\rho}_{22}(k) \frac{1}{z^{k+1}} dk + \int_{L_3} \frac{\hat{\rho}_{22}(k) e^{2\pi\mathrm{i}k}}{1-e^{2\pi\mathrm{i}k}} \frac{1}{z^{k+1}} dk\right], \tag{8.14}$$

with elements of the spectral matrix given by

$$\begin{aligned} \hat{\rho}_{11}(k) &= \int_L \hat{g}'(z) e^{-\mathrm{i}kz} dz, \qquad & \hat{\rho}_{12}(k) &= -\int_C \hat{g}'(z) e^{-\mathrm{i}kz} dz, \\ \hat{\rho}_{21}(k) &= \int_L \hat{g}'(z) z^k dz, & \hat{\rho}_{22}(k) &= -\int_C \hat{g}'(z) z^k dz. \end{aligned} \tag{8.15}$$

The global relations are

$$\hat{\rho}_{11}(k) + \hat{\rho}_{12}(k) = 0, \quad k < 0 \tag{8.16}$$

and

$$\hat{\rho}_{21}(k) + \hat{\rho}_{22}(k) = 0, \quad k \in -\mathbb{N}. \tag{8.17}$$

8.4.2 Boundary conditions

The no-slip boundary condition on boundary $L = [1, \infty) \cup (-\infty, -1]$, where $\overline{z} = z$ is given by (3.19). On substitution of (8.6) becomes

$$-\overline{\hat{f}(z)} + z\hat{f}'(z) + \hat{g}'(z) = \overline{f_s(z)} - z f_s'(z) - g_s'(z) = 0. \tag{8.18}$$

Note that the forcing functions for a stagnation point flow satisfy the no-slip boundary condition on $\overline{z} = z$ and therefore the right-hand side is equal to zero.

Similarly, on the semicircular boundary $C = \{z : |z| = 1, \mathrm{Im}[z] > 0\}$, where $\overline{z} = 1/z$,

(3.19) can be expressed as

$$-\overline{f(z)} + (1/z)f'(z) + g'(z) = 0. \tag{8.19}$$

Substitution of (8.6) into (8.19) gives

$$-\overline{\hat{f}(z)} + (1/z)\hat{f}'(z) + \hat{g}'(z) = \overline{f_s(z)} - (1/z)f_s'(z) - g_s'(z). \tag{8.20}$$

8.4.3 Spectral analysis

We multiply (8.18) by z^k and integrate along L:

$$-\int_L \overline{\hat{f}(z)}z^k dz + \int_L z\hat{f}'(z)z^k dz + \int_L \hat{g}'(z)z^k dz = R_{21}(k), \tag{8.21}$$

where

$$R_{21}(k) \equiv \int_L [\overline{f_s(z)} - zf_s'(z) - g_s'(z)]z^k dz = 0. \tag{8.22}$$

This can be written in terms of the spectral functions as

$$-\overline{\rho_{21}}(k) - (k+1)\rho_{21}(k) + \hat{\rho}_{21}(k) + (-1)^{k+1}\hat{f}(-1) - \hat{f}(1) = R_{21}(k) = 0. \tag{8.23}$$

Next, we multiply (8.20) by z^k and integrate along C (orientation is counterclockwise):

$$\int_C \overline{\hat{f}(z)}z^k dz - \int_C (1/z)\hat{f}'(z)z^k dz - \int_C \hat{g}'(z)z^k dz = R_{22}(k), \tag{8.24}$$

where

$$\begin{aligned} R_{22}(k) &\equiv -\int_C [\overline{f_s(z)} - (1/z)f_s'(z) - g_s'(z)]z^k dz \\ &= -\frac{2\mathrm{i}ak(1+e^{\mathrm{i}\pi k})}{(k+3)(k^2-1)}, \quad k \neq \pm 1, 3, \end{aligned} \tag{8.25}$$

and

$$R_{22}(-3) = \frac{3a\pi}{4}, \quad R_{22}(-1) = -\frac{a\pi}{2}, \quad R_{22}(1) = -\frac{a\pi}{4}. \tag{8.26}$$

Expression $R_{22}(k)$ was computed using residue calculus. Expression (8.24) can be written

in terms of the spectral functions as

$$\overline{\rho_{22}}(-k-2)-(k-1)\rho_{22}(k-2)+\hat{\rho}_{22}(k)+\hat{f}(1)-(-1)^{k-1}\hat{f}(-1)=R_{22}(k). \quad (8.27)$$

At this stage, we pause to make a remark. In this section, we have transformed our boundary conditions by performing a Mellin-type spectral analysis (our boundary conditions were multiplied by z^k) and integrating along the boundaries to obtain conditions between the spectral functions. A possible question would be why not perform a Fourier-type spectral analysis to analyse the boundary conditions. The answer is firstly that for simply connected circular domains performing a Fourier or a Mellin -type analysis is equivalent. Secondly, the reason for performing a Mellin-type analysis in this problem was only for convenience; for this particular geometry, as we will see in the next subsection, this gives relations between spectral functions which can be simplified using the global relation (8.13).

8.4.4 Solution scheme

From the spectral analysis we have found two expressions for the unknown spectral functions given by

$$-\overline{\rho_{21}}(k)-(k+1)\rho_{21}(k)+\hat{\rho}_{21}(k)+(-1)^{k+1}\hat{f}(-1)-\hat{f}(1)=R_{21}(k), \quad (8.28)$$

$$\overline{\rho_{22}}(-k-2)-(k-1)\rho_{22}(k-2)+\hat{\rho}_{22}(k)+\hat{f}(1)-(-1)^{k-1}\hat{f}(-1)=R_{22}(k), \quad (8.29)$$

to be analysed together with the global relations

$$\begin{aligned}\rho_{21}(k)+\rho_{22}(k)&=0, \quad k\in-\mathbb{N},\\ \hat{\rho}_{21}(k)+\hat{\rho}_{22}(k)&=0, \quad k\in-\mathbb{N}.\end{aligned} \quad (8.30)$$

Addition of (8.28)-(8.29) and use of the global relations (8.30) to eliminate the spectral functions $\rho_{21}(k), \hat{\rho}_{21}(k), \hat{\rho}_{22}(k)$ gives

$$(k+1)\rho_{22}(k)+\overline{\rho_{22}}(k)-(k-1)\rho_{22}(k-2)+\overline{\rho_{22}}(-k-2)=R(k), \quad \text{for } k\in-\mathbb{N}, \quad (8.31)$$

where

$$R(k) \equiv R_{21}(k) + R_{22}(k). \tag{8.32}$$

As we will see next, this (infinite) set of conditions is sufficient to determine the unknown spectral function $\rho_{22}(k)$.

Function representation

Conditions (8.31) contain only the spectral function $\rho_{22}(k)$ which is related to the semi-circular boundary C. The next step is to represent $\hat{f}(z)$ on this boundary using a suitable basis expansion. Note that, as already mentioned, Moffatt eddies will be former near the points of intersection between the planar and semicircular boundaries and therefore our basis expansion should be able to capture this complex behaviour. We propose the use of a Chebyshev basis to represent the unknown boundary data along the semicircular edge C; this boundary can be parametrized by

$$z(s) = e^{\mathrm{i}\pi(s+1)/2}, \quad \text{for } s \in [-1, 1], \tag{8.33}$$

with $z(-1) = 1$ and $z(1) = -1$. We write

$$\hat{f}(z(s)) = \sum_{m=0}^{\infty} a_m T_m(s), \tag{8.34}$$

for some set of coefficients $\{a_m\}$ to be found and where $T_m(s) = \cos(m\mathrm{acos}s)$, $s \in [-1, 1]$. Substitution of (8.34) into the expression for $\rho_{22}(k)$ gives

$$\rho_{22}(k) = \sum_{m=0}^{\infty} a_m T(k, m), \tag{8.35}$$

where

$$T(k, m) = -\frac{\mathrm{i}\pi}{2} \int_{-1}^{1} T_m(s) e^{\mathrm{i}\pi(k+1)(s+1)/2} ds. \tag{8.36}$$

The sum in (8.35) is truncated to include only terms $m = 0, ..., M$. Substitution of (8.35)

into (8.31) gives

$$\sum_{m=0}^{M} a_m \Big[(k+1)T(k,m) - (k-1)T(k-2,m)\Big] + \sum_{m=0}^{M} \overline{a_m}\Big[\overline{T}(k,m) + \overline{T}(-k-2,m)\Big] = R(k), \quad \text{for } k \in -\mathbb{N}. \tag{8.37}$$

The unknown coefficients $\{a_0, ..., a_M\}$ (and their complex conjugates) are computed by solving an overdetermined linear system for suitable number of $k \in -\mathbb{N}$. Once the coefficients $\{a_m\}$ are found, $\rho_{22}(k)$ can be computed using (8.35).

Finding the other spectral functions

As discussed previously, once the coefficients $\{a_m\}$ are found, $\rho_{22}(k)$ can be computed using (8.35). Then, expansion (8.34) is substituted in (8.20) to give an expression for $\hat{g}'(z)$ on the semicircular boundary. Substitution of this expression into $\hat{\rho}_{22}(k)$ will give us this spectral function. But the transform representations for $\hat{f}(z)$ and $\hat{g}'(z)$ given by (8.9) and (8.14) respectively also contain the spectral functions $\rho_{11}(k)$ and $\hat{\rho}_{11}(k)$ (integrated on $k > 0$). To find these, we proceed as follows:

We multiply (8.18) by $e^{-\mathrm{i}kz}$ and integrate along L:

$$-\int_L \overline{\hat{f}(z)} e^{-\mathrm{i}kz} dz + \int_L z\hat{f}'(z) e^{-\mathrm{i}kz} dz + \int_L \hat{g}'(z) e^{-\mathrm{i}kz} dz = 0. \tag{8.38}$$

The right-hand side is equal to zero, since the forcing functions $f_s(z)$ and $g_s'(z)$ satisfy the no-slip boundary condition on $\overline{z} = z$. This expression can be written in terms of the spectral functions as

$$-\overline{\rho_{11}}(-k) - \frac{\partial[k\rho_{11}(k)]}{\partial k} + \hat{\rho}_{11}(k) - \hat{f}(-1)e^{\mathrm{i}k} - \hat{f}(1)e^{-\mathrm{i}k} = 0. \tag{8.39}$$

Solving for $\overline{\rho_{11}}(-k)$ and using the global relations (8.12) and (8.16), this becomes

$$\overline{\rho_{11}}(-k) = \frac{\partial[k\rho_{12}(k)]}{\partial k} - \hat{\rho}_{12}(k) - \hat{f}(-1)e^{\mathrm{i}k} - \hat{f}(1)e^{-\mathrm{i}k}, \quad \text{for } k < 0. \tag{8.40}$$

If we take Schwarz conjugate and let $k \mapsto -k$, we find

$$\rho_{11}(k) = \frac{\partial[k\overline{\rho_{12}}(-k)]}{\partial k} - \overline{\hat{\rho}_{12}}(-k) - \overline{\hat{f}(-1)}e^{\mathrm{i}k} - \overline{\hat{f}(1)}e^{-\mathrm{i}k}, \quad \text{for } k > 0. \tag{8.41}$$

This gives an expression for the unknown spectral function $\rho_{11}(k)$ (for $k > 0$) in terms of quantities associated to the semicircular boundary; all these can be computed using the expressions for $\hat{f}(z)$ and $\hat{g}'(z)$ on this boundary found above.

Finally, to find $\hat{\rho}_{11}(k)$, we rearrange (8.39):

$$\hat{\rho}_{11}(k) = \overline{\rho_{11}}(-k) + \frac{\partial[k\rho_{11}(k)]}{\partial k} + \hat{f}(-1)e^{\mathrm{i}k} + \hat{f}(1)e^{-\mathrm{i}k}, \tag{8.42}$$

which, on use of the global relations, can be written as

$$\hat{\rho}_{11}(k) = -\overline{\rho_{12}}(-k) + \frac{\partial[k\rho_{11}(k)]}{\partial k} + \hat{f}(-1)e^{\mathrm{i}k} + \hat{f}(1)e^{-\mathrm{i}k}, \quad \text{for } k > 0. \tag{8.43}$$

Again, this is an expression for the unknown spectral function $\hat{\rho}_{11}(k)$ (for $k > 0$) in terms of quantities associated to the semicircular boundary (having used (8.41)).

In this section, we have shown that all spectral functions needed for the computation of the corrections functions $\hat{f}(z)$ and $\hat{g}'(z)$ can be expressed in terms of 'known' quantities. The forcing functions (8.7) together with the correction functions fully determine the Goursat functions $f(z)$ and $g'(z)$ which are enough to describe the resulting flow (as we have shown earlier, all the physical parameters of interest can be expressed in terms of these two functions).

8.5 Approach II: Transform method for polygons

We now present an alternative approach to the problem considered in the previous section. We show that, using a conformal mapping, the fluid domain can be mapped to a semi-strip geometry and then the tranform method for polygonal domains (consisting of straight line edges) can be used to solve the problem. It should be noted that, although the biharmonic equation is not conformally invariant (as discussed in Chapter 1), analytical progress can still be made in the new parametric plane.

8.5.1 Conformal mapping and function representation

Consider the conformal mapping given by

$$\eta = \eta(z) = \log z, \tag{8.44}$$

which maps the fluid region in the z-plane to the semi-strip geometry in the parametric η-plane (Figure 8.2). The inverse map is given by

$$z(\eta) = e^{\eta}. \tag{8.45}$$

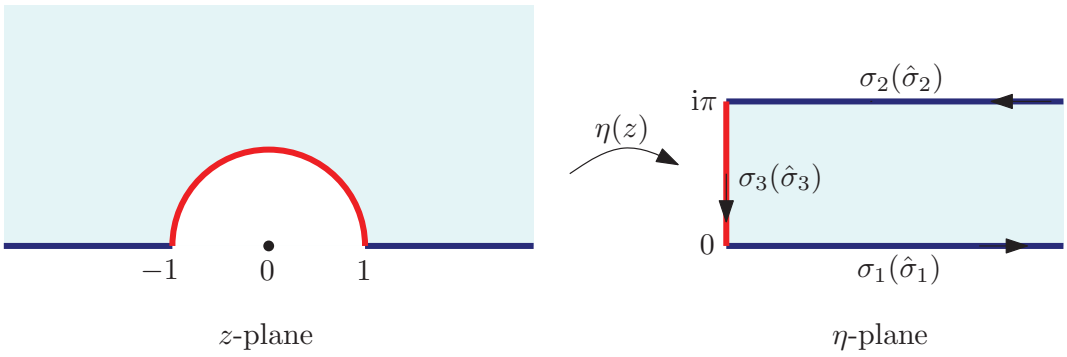

Figure 8.2: Conformal mapping from the physical z-plane to the parametric η-plane. Associated spectral functions are also illustrated (η-plane).

Next, introduce

$$F(\eta) = f(z(\eta)), \qquad G(\eta) = g'(z(\eta)), \tag{8.46}$$

and write

$$\begin{cases} F(\eta) = F_s(\eta) + \hat{F}(\eta), \\ G(\eta) = G_s(\eta) + \hat{G}(\eta), \end{cases} \tag{8.47}$$

where $F_s(\eta)$, $G_s(\eta)$ are the forcing functions related to the stagnation point flow and $\hat{F}(\eta)$, $\hat{G}(\eta)$ are the correction functions to be found using the transform method. It is necessary to express the forcing functions (8.7) in terms of variable η; using (8.45), we can write

$$\begin{cases} F_s(\eta) = \dfrac{\mathrm{i}ae^{2\eta}}{4}, \\ \\ G_s(\eta) = -\dfrac{3\mathrm{i}ae^{2\eta}}{4}. \end{cases} \tag{8.48}$$

The symmetry condition with respect to $x = 0$ in the physical plane corresponds to symmetry with respect to the semi-strip centre-line $\mathrm{Im}[\eta] = \pi/2$ in the η-plane. For η on the boundaries, this symmetry corresponds to

$$\begin{cases} \overline{F}(\eta) = -F(\eta + \mathrm{i}\pi), \\ \overline{G}(\eta) = -G(\eta + \mathrm{i}\pi). \end{cases} \tag{8.49}$$

The analytic correction function $\hat{F}(\eta)$ in the semi-strip geometry can be represented by

$$\hat{F}(\eta) = \frac{1}{2\pi}\left[\int_0^{\infty} \sigma_1(k)e^{\mathrm{i}k\eta}dk + \int_0^{-\infty} \sigma_2(k)e^{\mathrm{i}k\eta}dk + \int_0^{\mathrm{i}\infty} \sigma_3(k)e^{\mathrm{i}k\eta}dk\right], \tag{8.50}$$

where the spectral functions are given by

$$\begin{aligned} \sigma_1(k) &= \int_0^{\infty} \hat{F}(\eta)e^{-\mathrm{i}k\eta}d\eta, \\ \sigma_2(k) &= \int_{\infty+\mathrm{i}\pi}^{\mathrm{i}\pi} \hat{F}(\eta)e^{-\mathrm{i}k\eta}d\eta, \\ \sigma_3(k) &= \int_{\mathrm{i}\pi}^{0} \hat{F}(\eta)e^{-\mathrm{i}k\eta}d\eta. \end{aligned} \tag{8.51}$$

Similarly, we can write an integral representation for $\hat{G}(\eta)$:

$$\hat{G}(\eta) = \frac{1}{2\pi}\left[\int_0^{\infty} \hat{\sigma}_1(k)e^{\mathrm{i}k\eta}dk + \int_0^{-\infty} \hat{\sigma}_2(k)e^{\mathrm{i}k\eta}dk + \int_0^{\mathrm{i}\infty} \hat{\sigma}_3(k)e^{\mathrm{i}k\eta}dk\right], \tag{8.52}$$

where

$$\begin{aligned}
\hat{\sigma}_1(k) &= \int_0^{\infty} \hat{G}(\eta)e^{-\mathrm{i}k\eta}d\eta, \\
\hat{\sigma}_2(k) &= \int_{\infty+\mathrm{i}\pi}^{\mathrm{i}\pi} \hat{G}(\eta)e^{-\mathrm{i}k\eta}d\eta, \\
\hat{\sigma}_3(k) &= \int_{\mathrm{i}\pi}^{0} \hat{G}(\eta)e^{-\mathrm{i}k\eta}d\eta.
\end{aligned} \tag{8.53}$$

The global relations are given by

$$\begin{aligned}
&\sigma_1(k) + \sigma_2(k) + \sigma_3(k) = 0, \qquad \mathrm{Im}k \leq 0, \\
&\hat{\sigma}_1(k) + \hat{\sigma}_2(k) + \hat{\sigma}_3(k) = 0, \qquad \mathrm{Im}k \leq 0.
\end{aligned} \tag{8.54}$$

8.5.2 Boundary conditions

We will analyze the problem in the η-plane and we must therefore express our boundary conditions in terms of variable η. In order to do so, the chain rule will be useful:

$$\frac{d}{dz} = \frac{d\eta}{dz}\frac{d}{d\eta} = e^{-\eta}\frac{d}{d\eta}. \tag{8.55}$$

The no-slip boundary condition on $\overline{z} = z$ (corresponding to the horizontal boundaries $\overline{\eta} = \eta$ and $\overline{\eta} = \eta - 2\mathrm{i}\pi$ in the η-plane) can be expressed as

$$-\overline{F(\eta)} + F'(\eta) + G(\eta) = 0. \tag{8.56}$$

Substitution of (8.47) into (8.56) gives

$$-\overline{\hat{F}(\eta)} + \hat{F}'(\eta) + \hat{G}(\eta) = \overline{F_s(\eta)} - F_s'(\eta) - G_s(\eta) = 0. \tag{8.57}$$

The boundary condition on $\overline{z} = 1/z$ (corresponding to the vertical boundary $\overline{\eta} = -\eta$ in the

η-plane) can be expressed as

$$-\overline{F(\eta)} + e^{-2\eta}F'(\eta) + G(\eta) = 0. \tag{8.58}$$

Substitution of (8.47) into (8.58) gives

$$-\overline{\hat{F}(\eta)} + e^{-2\eta}\hat{F}'(\eta) + \hat{G}(\eta) = \overline{F_s(\eta)} - e^{-2\eta}F_s'(\eta) - G_s(\eta). \tag{8.59}$$

8.5.3 Spectral analysis

We multiply (8.57) by $e^{-\mathrm{i}k\eta}$ and integrate along the lower boundary:

$$-\int_0^\infty \overline{\hat{F}(\eta)}e^{-\mathrm{i}k\eta}d\eta + \int_0^\infty \hat{F}'(\eta)e^{-\mathrm{i}k\eta}d\eta + \int_0^\infty \hat{G}(\eta)e^{-\mathrm{i}k\eta}d\eta = S_1(k), \tag{8.60}$$

where

$$S_1(k) \equiv \int_0^\infty [\overline{F_s(\eta)} - F_s'(\eta) - G_s(\eta)]e^{-\mathrm{i}k\eta}d\eta = 0. \tag{8.61}$$

It can be shown that this can be written in terms of the spectral functions as

$$-\overline{\sigma_1}(-k) + \mathrm{i}k\sigma_1(k) + \hat{\sigma}_1(k) - \hat{F}(0) = S_1(k). \tag{8.62}$$

Similarly, we multiply (8.57) by $e^{-\mathrm{i}k\eta}$ and integrate along the upper boundary:

$$-\int_{\mathrm{i}\pi+\infty}^{\mathrm{i}\pi} \overline{\hat{F}(\eta)}e^{-\mathrm{i}k\eta}d\eta + \int_{\mathrm{i}\pi+\infty}^{\mathrm{i}\pi} \hat{F}'(\eta)e^{-\mathrm{i}k\eta}d\eta + \int_{\mathrm{i}\pi+\infty}^{\mathrm{i}\pi} \hat{G}(\eta)e^{-\mathrm{i}k\eta}d\eta = S_2(k), \tag{8.63}$$

where

$$S_2(k) \equiv \int_{\mathrm{i}\pi+\infty}^{\mathrm{i}\pi} [\overline{F_s(\eta)} - F_s'(\eta) - G_s(\eta)]e^{-\mathrm{i}k\eta}d\eta = 0. \tag{8.64}$$

This can be written in terms of the spectral functions as

$$-e^{2k\pi}\overline{\sigma_2}(-k) + \mathrm{i}k\sigma_2(k) + \hat{\sigma}_2(k) + \hat{F}(\mathrm{i}\pi)e^{k\pi} = S_2(k). \tag{8.65}$$

Finally, we multiply (8.59) by $e^{-\mathrm{i}k\eta}$ and integrate along the third edge of the semi-strip:

$$-\int_{\mathrm{i}\pi}^{0}\overline{\hat{F}(\eta)}e^{-\mathrm{i}k\eta}d\eta+\int_{\mathrm{i}\pi}^{0}e^{-2\eta}\hat{F}'(\eta)e^{-\mathrm{i}k\eta}d\eta+\int_{\mathrm{i}\pi}^{0}\hat{G}(\eta)e^{-\mathrm{i}k\eta}d\eta=S_3(k), \tag{8.66}$$

where

$$\begin{aligned}S_3(k)&\equiv\int_{\mathrm{i}\pi}^{0}\left[\overline{F_s(\eta)}-e^{-2\eta}F_s'(\eta)-G_s(\eta)\right]e^{-\mathrm{i}k\eta}d\eta\\&=\frac{2a(1-e^{k\pi})(\mathrm{i}k+1)}{k(k^2+4)},\quad k\neq 0,\pm 2\mathrm{i},\end{aligned} \tag{8.67}$$

and

$$S_3(0)=-\frac{a\pi}{2},\quad S_3(-2\mathrm{i})=\frac{3a\pi}{4},\quad S_3(2\mathrm{i})=-\frac{a\pi}{4}. \tag{8.68}$$

It can be shown that this can be written in terms of the spectral functions as

$$\overline{\sigma_3}(k)+\mathrm{i}(k-2\mathrm{i})\sigma_3(k-2\mathrm{i})+\hat{\sigma}_3(k)+\hat{F}(0)-\hat{F}(\mathrm{i}\pi)e^{k\pi}=S_3(k). \tag{8.69}$$

8.5.4 Solution scheme

From the spectral analysis we have found three expressions for the unknown spectral functions given by

$$-\overline{\sigma_1}(-k)+\mathrm{i}k\sigma_1(k)+\hat{\sigma}_1(k)-\hat{F}(0)=S_1(k), \tag{8.70}$$

$$-e^{2k\pi}\overline{\sigma_2}(-k)+\mathrm{i}k\sigma_2(k)+\hat{\sigma}_2(k)+\hat{F}(\mathrm{i}\pi)e^{k\pi}=S_2(k), \tag{8.71}$$

$$\overline{\sigma_3}(k)+\mathrm{i}(k-2\mathrm{i})\sigma_3(k-2\mathrm{i})+\hat{\sigma}_3(k)+\hat{F}(0)-\hat{F}(\mathrm{i}\pi)e^{k\pi}=S_3(k), \tag{8.72}$$

to be analyzed together with the global relations

$$\begin{aligned}\sigma_1(k)+\sigma_2(k)+\sigma_3(k)&=0,\qquad \mathrm{Im}k\leq 0,\\\hat{\sigma}_1(k)+\hat{\sigma}_2(k)+\hat{\sigma}_3(k)&=0,\qquad \mathrm{Im}k\leq 0.\end{aligned} \tag{8.73}$$

Addition of (8.70)-(8.72) and use of the global relations (8.73) gives (after rearrangement):

$$(1-e^{2k\pi})\overline{\sigma_1}(-k)=e^{2k\pi}\overline{\sigma_3}(-k)-\mathrm{i}k\sigma_3(k)+\overline{\sigma_3}(k)+\mathrm{i}(k-2\mathrm{i})\sigma_3(k-2\mathrm{i})-S(k), \tag{8.74}$$

where

$$S(k) \equiv S_1(k) + S_2(k) + S_3(k). \tag{8.75}$$

But $\overline{\sigma_1}(-k)$ is analytic in the lower half-plane which implies that the right-hand side of (8.74) must vanish at solutions of $1 - e^{2k\pi} = 0$ in the lower half k-plane, that is, at points in the set

$$\Sigma_1 \equiv \left\{ k_p = -\mathrm{i}p \middle| p = 0, 1, 2, \dots \right\}. \tag{8.76}$$

We must therefore have

$$\overline{\sigma_3}(-k) - \mathrm{i}k\sigma_3(k) + \overline{\sigma_3}(k) + \mathrm{i}(k - 2\mathrm{i})\sigma_3(k - 2\mathrm{i}) = S(k), \quad \text{for } k \in \Sigma_1. \tag{8.77}$$

It is interesting to note the similarities between (8.31) and (8.77) found using the two approaches. As we will see next, the (infinite) set of conditions (8.77) is sufficient to determine the unknown spectral function $\sigma_3(k)$.

Function representation

The next step is to represent $\hat{F}(\eta)$ on $\eta = \mathrm{i}\eta_y$, $\eta_y \in [0, \pi]$ using a Chebyshev basis expansion. The boundary $\eta = \mathrm{i}\eta_y$, $\eta_y \in [0, \pi]$ can be parametrized by

$$\eta(s) = \frac{\mathrm{i}\pi}{2}(1 - s), \quad \text{for } s \in [-1, 1], \tag{8.78}$$

with $\eta(-1) = \mathrm{i}\pi$ and $\eta(1) = 0$. We write

$$\hat{F}(\eta(s)) = \sum_{m=0}^{\infty} b_m T_m(s), \tag{8.79}$$

for some set of coefficients $\{b_m\}$ to be found and where $T_m(s) = \cos(m\mathrm{acos}s)$, $s \in [-1, 1]$. Substitution of (8.79) into the expression for $\sigma_3(k)$ gives

$$\sigma_3(k) = \sum_{m=0}^{\infty} b_m T(k, m), \tag{8.80}$$

where

$$T(k,m) = -\frac{\mathrm{i}\pi}{2}\int_{-1}^{1} T_m(s)e^{k\pi(1-s)/2}ds. \tag{8.81}$$

The sum in (8.80) is truncated to include only terms $m = 0, ..., M$. Substitution of (8.80) into (8.77) gives

$$\sum_{m=0}^{M} b_m\Big[-\mathrm{i}kT(k,m) + \mathrm{i}(k-2\mathrm{i})T(k-2\mathrm{i},m)\Big] + \sum_{m=0}^{M}\overline{b_m}\Big[\overline{T}(k,m) + \overline{T}(-k,m)\Big] = S(k), \quad \text{for } k \in \Sigma_1. \tag{8.82}$$

The unknown coefficients $\{b_0, ..., b_M\}$ (and their complex conjugates) are computed by solving an overdetermined linear system for suitable number of $k \in \Sigma_1$. Once the coefficients $\{b_m\}$ are found, $\sigma_3(k)$ can be computed using (8.80). Once $\sigma_3(k)$ is found, all the other spectral functions can be found by back substitution into various relations.

8.6 Results and comparison to Davis & O'Neill's solution [30]

Davis & O'Neill [30] found an expression for the streamfunction ψ given by (8.3); using this, all physical quantities of interest can be computed. For example, recall that vorticity can be expressed in terms of the streamfunction as

$$\omega = -\nabla^2\psi \tag{8.83}$$

(Chapter 3). Since their solution is found in terms of bipolar coordinates ξ and η, it is necessary to express the Laplacian operator in terms of (ξ, η). It is straightforward to show that

$$\nabla^2\psi = \frac{(\cosh\xi - \cos\eta)^2}{c^2}\left(\frac{\partial^2\psi}{\partial\eta^2} + \frac{\partial^2\psi}{\partial\xi^2}\right). \tag{8.84}$$

Using (8.84), we can compute the vorticity in the fluid region. In a similar manner, all other physical quantities of interest can be found by expressing them in terms of (ξ, η).

To compare our results to Davis & O'Neills' [30], we use that the angle of intersection is

$\eta_0 = \pi/2$ and the semicircular boundary intersects the planar boundary at points $x = \pm 1$ hence $c = 1$. Also, we choose $k_1 = k_2 = 1$, since for $\eta_0 = \pi/2$ both (8.4)-(8.5) have complex roots. Our results were checked against Davis & O'Neills' [30] and were foung to be the same to within an accuracy of $\mathcal{O}(10^{-3})$ of each other (with truncation parameter $M = 12$). Also, as we increased the truncation parameters, the solutions were converging to each other.

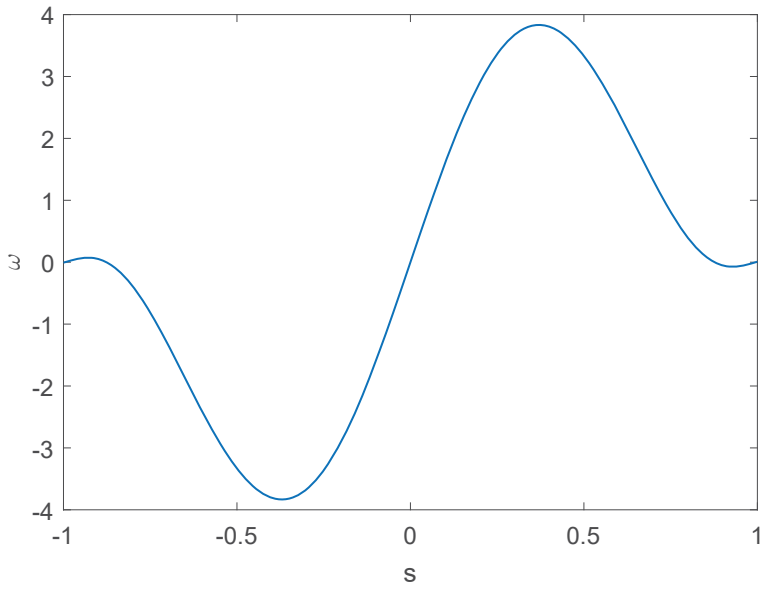

Figure 8.3: Vorticity ω along the circular boundary in terms of parametrization variable s defined in (8.33) computed using our transform approach (I/II).

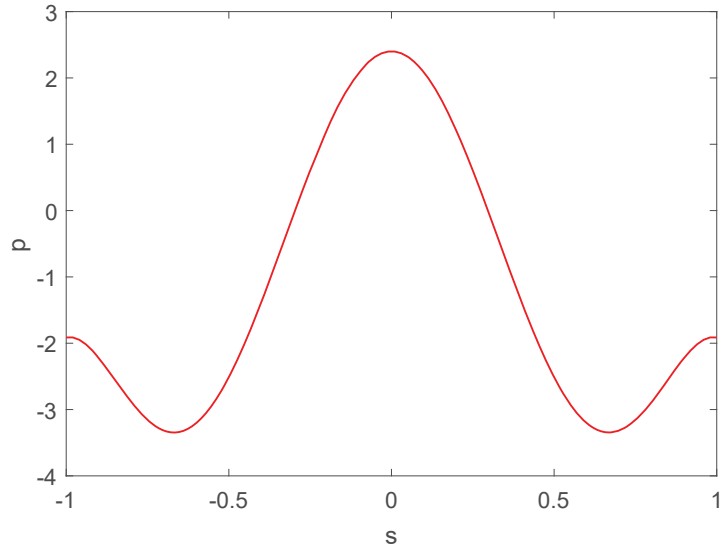

Figure 8.4: Pressure p along the circular boundary in terms of parametrization variable of s defined in (8.33)computed using our transform approach (I/II).

8.7 Summary

We have presented new transform approaches for solving a Stokes flow problem in a simply connected circular domain. The problem considered was that of a stagnation point flow past a semicircular ridge with angle of intersection between the plane and circular boundaries taken to be $\pi/2$. This problem was previously solved by Davis & O'Neill [30] for a general angle of intersection, using bipolar coordinates and Fourier transform techniques. Our transform approaches were based on the transform method for circular domains (I) and combination of ideas from conformal mapping theory together with the transform method for polygonal domains (II).

In the first approach, by first noticing that the fluid region can be thought as the intersection of the upper half-plane and the exterior of unit disc, we used the transform method for circular domains presented in Chapter 2. The spectral analysis allowed us to derive an infinite set of conditions satisfied by the (Mellin-type) spectral function associated to the cylindrical boundary. The unknown boundary data was then represented using an appropri-

ate basis expansion which allowed us to form and solve an overdetermined linear system for the unknown coefficients. Finally, we showed that all spectral functions and, therefore, correction functions $\hat{f}(z)$, $\hat{g}'(z)$ were expressed in terms of 'known' quantities.

Next, owing to the simplicity of the configuration, we showed that ideas from conformal mapping theory and the transform method for polygonal domains can also be used to solve this problem. The idea was to map the fluid domain to a semi-strip and then analyse the problem in this new geometry. The spectral analysis gave again an infinite set of conditions on the spectral function associated to the edge of finite length and these conditions were sufficient to determine it. However, in this case, the unknown boundary data was represented on a straight edge rather than a semicircular arc (of approach I).

Both approaches were checked against Davis & O'Neill's solution [30] and results were found to be in good agreement. In both methods, Chebyshev-like basis expansions were used to represent the unknown boundary data, but different series representations can also be used. Although not presented here, we have checked if using different expansions, such as a Fourier series, can improve the accuracy but we have concluded that the Chebyshev-like basis expansions give better accuracy against the solution of Davis & O'Neill [30].

Although in this chapter we have analysed the particular problem of a stagnation point flow past a semicircular ridge of angle of intersection $\pi/2$, it should be noted that a significant advantage of this new transform approach is that it can be adapted to model other interesting problems in the same or similar geometries. To name a few:

Modelling other flows of interest: Other flows can be analysed in the same geometry by only changing the forcing functions $f_s(z)$, $g_s'(z)$ to satify the given far-field conditions. For example, we can solve for a shear flow by choosing the correct form for the forcing functions.

Dynamics of a point swimmer near this geometry: Crowdy & Or [23] proposed a singularity description of a non-self-propelling microswimmer in order to investigate wall ef-

fects. This consisted of a point stresslet with a superposed source quadrupole at swimmer's position. They wrote

$$\begin{cases} f(z) = f_{stresslet}(z) + \epsilon^2 f_{quadrupole}(z), \\ g'(z) = g'_{stresslet}(z) + \epsilon^2 g'_{quadrupole}(z), \end{cases} \tag{8.85}$$

where parameter ϵ measured the strength of the source quadrupole relative to the stresslet.

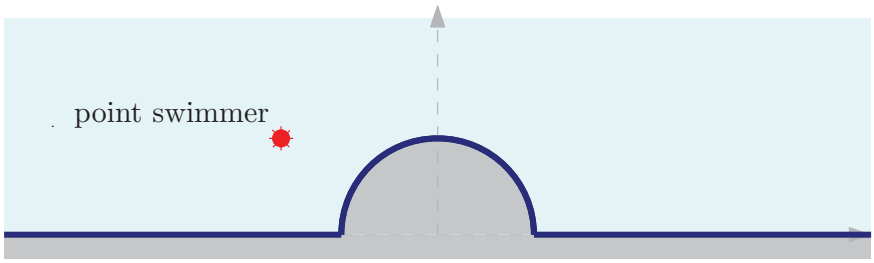

Figure 8.5: Schematic of the configuration. A point swimmer near a semicircular ridge of unit radius.

Therefore, by changing the forcing functions $f_s(z)$, $g'_s(z)$ in our transform approaches, we can solve for a point stresslet and then for a source quadrupole. The resulting Goursat functions can then be substituted in (8.85). Following Crowdy & Or [23], to find the evolution equations governing the point swimmer dynamics, we compute the first few coefficients of the Taylor expansion of the analytic parts of the Goursat functions at the singularity position z_0. For a point stresslet, we write

$$\begin{cases} f_{stresslet}(z) = \dfrac{\mu}{z - z_0} + f_{0s} + f_{1s}(z - z_0) + ... \\ \\ g'_{stresslet}(z) = \dfrac{\mu \overline{z_0}}{(z - z_0)^2} + g_{0s} + g_{1s}(z - z_0) + ... \end{cases} \tag{8.86}$$

and, similarly, for a point quadrupole we have

$$\begin{cases} f_{quadrupole}(z) = f_{0q} + f_{1q}(z - z_0) + ... \\ \\ g'_{quadrupole}(z) = \dfrac{2\mu}{(z - z_0)^3} + g_{0q} + g_{1q}(z - z_0) + ... \end{cases} \tag{8.87}$$

Following Crowdy & Or [23], the evolution of the swimmer is given by the solution of the system

$$\begin{cases} \dfrac{dz_0}{dt} = -f_{0s} + z_0\overline{f_{1s}} + \overline{g_{0s}} + \epsilon^2\big[- f_{0q} + z_0\overline{f_{1q}} + \overline{g_{0q}}\big], \\ \\ \dfrac{d\theta}{dt} = -2\text{Im}[f_{1s}] - \epsilon^2\text{Im}[f_{1q}]. \end{cases} \tag{8.88}$$

Flows past a trough: Davis & O'Neill [30] also presented the problem of a stagnation point flow past a trough where the angle of intersection between the plane and cylindrical boundaries was greater than π. A schematic is illustrated in Figure 8.6.

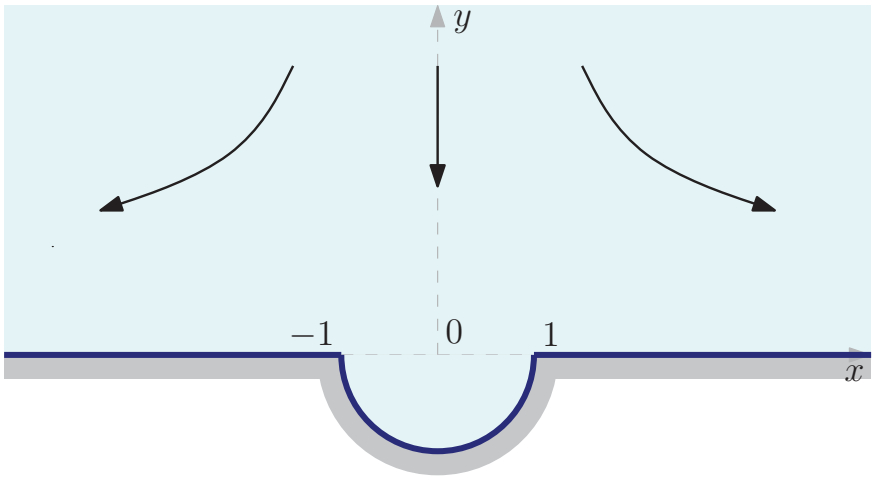

Figure 8.6: A stagnation point flow past a plane with a cylindrical trough. The angle of intersection θ between the plane and cylindrical boundaries is $\theta > \pi$ (here $\theta = 3\pi/2$). This problem was solved by Davis & O'Neill [30] for a general angle of intersection.

This problem can also be solved using the transform methods presented in this chapter. First, we recall that the transform method for circular domains works for domains which can be formed from the intersection of half-planes and exterior or interior of unit discs. However, the configuration illustrated in Figure 8.7 can not be directly formed from these two fundamental objects. To solve this problem, it is therefore necessary to split the fluid domain into two sub-domains as illustrated in Figure 8.7. In each of these sub-domains, a different transform representation can be written. Domain 1 is the upper half-plane exte-

rior to the semi-disc and Domain 2 is the interior of the semi-disc. The idea is then (similar to problems of Wiener-Hopf type presented in Chapter 5) to solve each sub-problem separately and then couple the two sub-problems by imposing continuity conditions along common boundaries. This procedure provides, again, an infinite set of conditions which are sufficient to determine the unknown spectral functions.

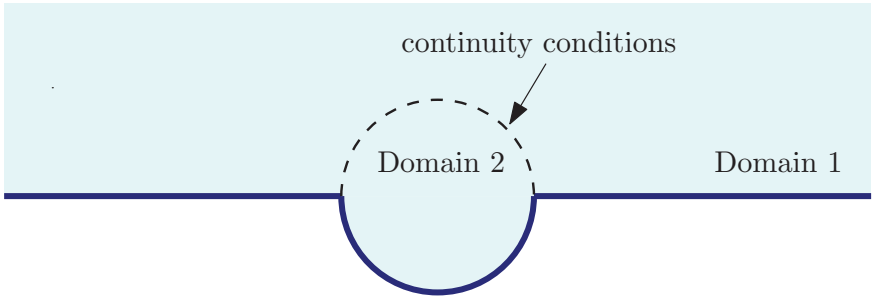

Figure 8.7: Domain splitting for analysis using the transform method for circular domains.

On the other hand, this problem can be easily solved using our transform approach II (conformal mapping theory and the transform method for polygonal domains). The difference from the analysis presented previously in this chapter will only be that the semi-strip will be shifted in the vertical direction in the η-plane. However, it is straightforward to adapt the spectral analysis and solve this problem.

General angle of intersection: Although in this chapter we have analysed the particular case of configuration where the angle of intersection between the plane and cylindrical boundaries was $\theta = \pi/2$, it is an interesting extension to consider a general angle of intersection. In the latter case, the unknown boundary data must be represented on a general circular arc rather than a semicircular boundary.

Bubble matresses: Davis & Lauga [28] considered a shear flow past a two-dimensional array of bubbles and calculated analytically the effective slip length of the surface as a function of the bubble geometry in the dilute limit ($c/l \ll 1$). A schematic is shown in Figure 8.8. The boundary conditions for this problem are no-slip on the rigid plane on either side of the bubble and perfect slip (no-shear) on the bubble surface. A possible

application of the transform method would be, firstly, to rederive this problem, as well as solve it in the non-dilute limit. In the non-dilute limit, the periodicity of the configuration implies that it will be sufficient to analyse the problem in a single period window e.g. $-l < x < l$, $0 < y < \infty$ and periodicity conditions must be imposed at the ends of the period window (similar to problem presented in Chapter 6).

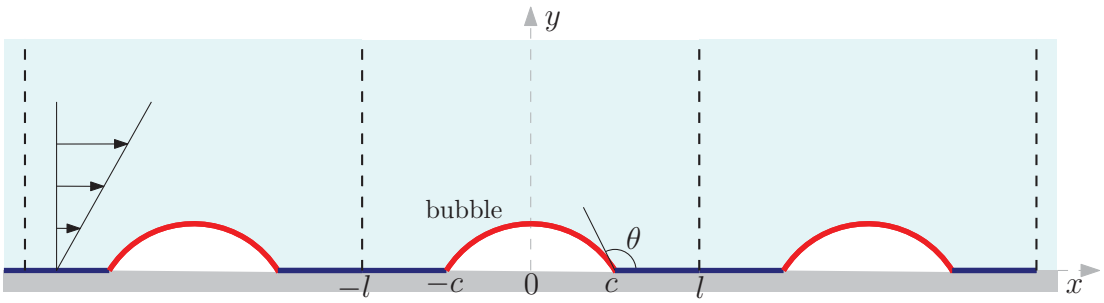

Figure 8.8: Shear flow past a periodic array of bubbles. This problem was solved by Davis & Lauga [28] in the dilute limit $c/l \ll 1$.

Plane elasticity problems: The monograph by Muskhelishvili [86] provides a detailed account of mathematical techniques to solve elasticity problems. In plane elasticity, the associated Airy stress function ψ satisfies the biharmonic equation and it is, therefore, an interesting application to use the transform method to solve these problems. Previous work on using the unified transform method for solving elasticity problems was presented by Crowdy & Fokas [21] who solved problems in a semi-strip geometry. Extending this work, the transform method for circular domains can be employed to solve various other problems (some of these are listed below).

It is remarkable, that several elasticity problems in a similar configuration to the Davis & O'Neill [30] geometry have been solved. Maunsell [80] and Isibasi [52] solved the problem of a notched plate under tension when the notch was of semicircular shape in the real plane; the configuration was the same with the problem presented in this chapter. Yeung [116] reformulated and solved the same problem using complex variable techniques. Ling [75] and Weinel [114] (Figure 8.9) extended previous work to circular notch for a general angle of intersection between the planar and circular boundaries using bipolar coordinates and

infinite integrals.

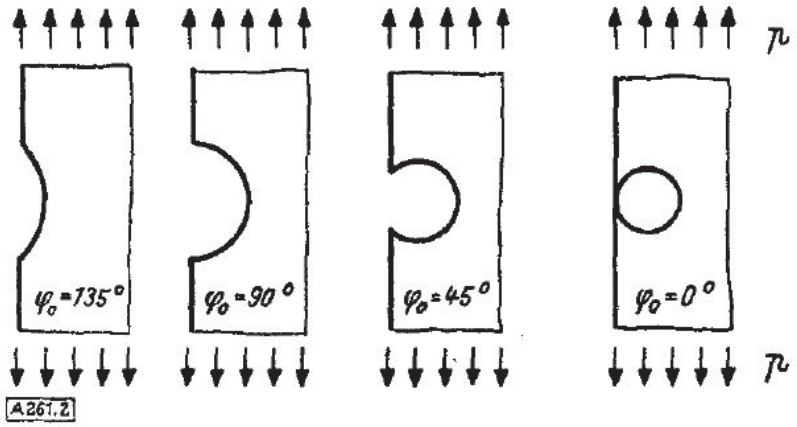

Figure 8.9: Weinel [114] considered a notched plate under tension for a general angle of intrsection between the planar and circular boundaries. (Figure reproduced from [114]).

There have been several other investigations in similar geometries. To name a few, we mention the work of Ling [76] who considered an infinite strip under tension containing two semicircular notches placed symmetrically on the opposite edges. Atsumi [7] used Mausell's method [80] to obtain the stresses in a plate under tension containing a periodic row of semicircular nodges. A schematic from this work is shown in Figure 8.10. In another study, Atsumi [6] analysed the stress problem for a strip with periodic row of semicircular nodges (Figure 8.11).

It is expected that all problems presented in this section can be analysed and solved using the transform method for circular (simply-connected) domains.

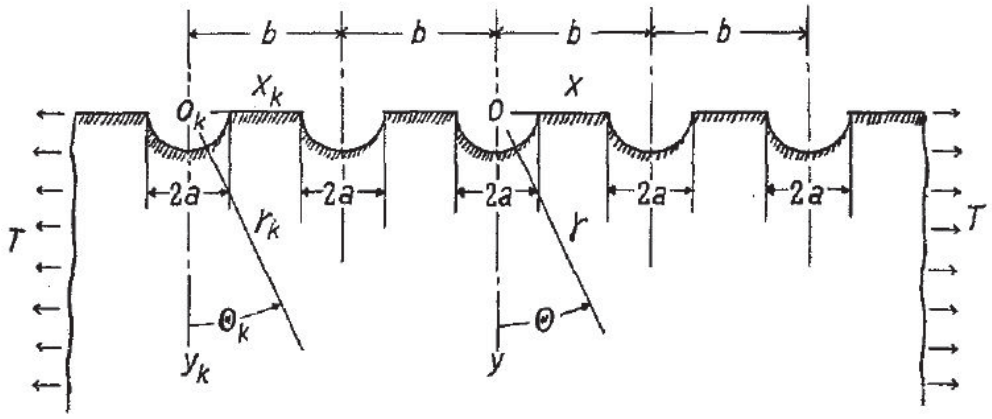

Figure 8.10: Problem configuration considered by Atsumi [7]. This author determined the stresses in a plate under tension containing a periodic row of semicircular nodges. (Figure reproduced from [7]).

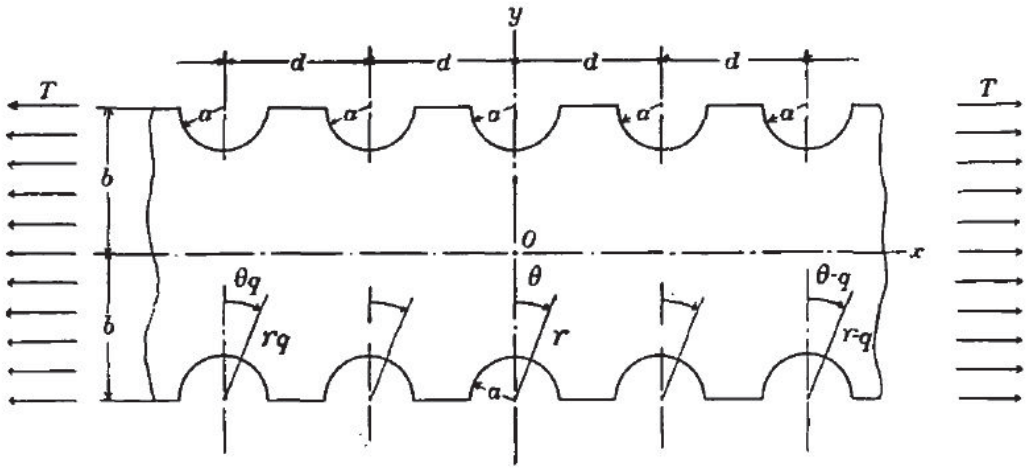

Figure 8.11: In another study, Atsumi [6] analyzed the problem of determining the stresses in an infinite strip under tension containing an infinite row of semicircular notches. (Figure reproduced from [6]).

Chapter 9

A translating and rotating cylinder near a wall

9.1 Introduction

In this chapter, we present our transform approach for solving a Stokes flow problem in a multiply connected circular domain, particularly in a doubly connected one. The problem considered concerns a translating and rotating cylinder near a wall and our aim is to compute the forces and torques acting on the cylinder for given translational/angular velocities. Since Stokes equations are linear, forces and torques are linearly related to translational and angular velocities and this relation can be expressed through a tensor which is known as the mobility or resistance matrix (Lauga & Powers [71]).

The problem of a translating and rotating cylinder near a wall is a classical problem in two-dimensional slow viscous flows and importantly it is one of few problems which admits an exact solution. This problem was originally solved by Jeffrey & Onishi [53] who employed bipolar coordinates to solve for the resulting flow and to compute forces and torque acting on the cylinder. More recently, Crowdy [14] rederived Jeffrey & Onishi's [53] solution using complex variable techniques and then combined it with the reciprocal theorem (Stone & Samuel [104]) to compute the dynamics of a circular swimmer above a wall. Remarkably, the reciprocal theorem was used to find the linear and angular velocity of a force-free

and torque-free circular swimmer with an imposed velocity profile on its surface, without solving for the entire flow field.

In the following sections, we present our transform appoach to solve this problem and show that all elements of the mobility matrix can be computed. We also show a comparison of our results to Jeffrey & Onishi's [53] exact solution.

9.2 Problem formulation

Consider a circular cylinder of unit radius centred at $z_0 = \mathrm{i}y_0$, with $y_0 > 1$, above a wall along the real axis in a z-plane (Figure 9.1). The cylinder is translating with complex speed $U = U_x + \mathrm{i}U_y, (U_x, U_y \in \mathbb{R})$ and rotating with angular velocity Ω and experiencing a non-zero net force $F = F_x + \mathrm{i}F_y, (F_x, F_y \in \mathbb{R})$ and torque T.

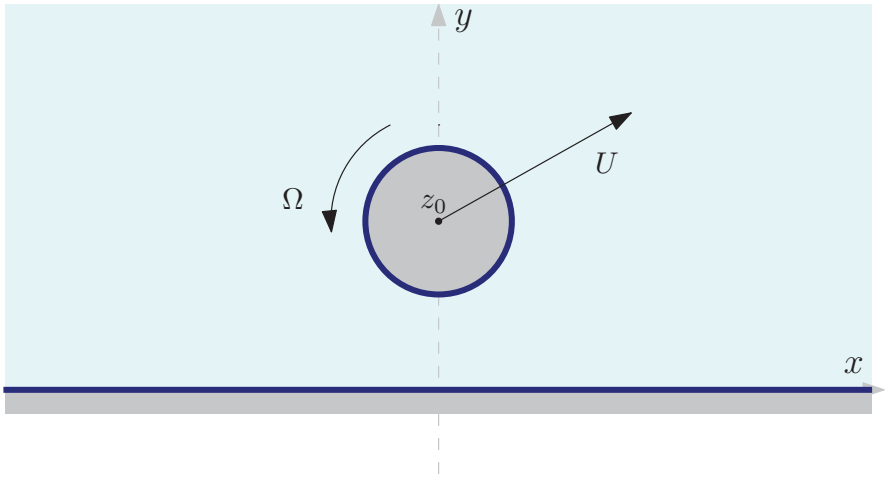

Figure 9.1: Schematic of the configuration: a translating and rotating cylinder of unit radius centred at $z_0 = \mathrm{i}y_0$, with $y_0 > 1$, above a straight wall.

The relation between $\{U, \Omega\}$ and $\{F, T\}$ acting on the cylinder can be expressed through

the mobility matrix $\mathbf{A}$:

$$\begin{bmatrix} U \\ V \\ \Omega \end{bmatrix} = \mathbf{A} \begin{bmatrix} F_x \\ F_y \\ T \end{bmatrix}, \qquad \text{where} \qquad \mathbf{A} = \begin{bmatrix} a_{11} & 0 & 0 \\ 0 & a_{22} & 0 \\ 0 & 0 & a_{33} \end{bmatrix}, \tag{9.1}$$

with $a_{jj} \in \mathbb{R}, j = 1, 2, 3$. In general, $\mathbf{A}$ is a 3×3 full-element tensor, but for this particular problem it has a diagonal form (Jeffrey & Onishi [53], Crowdy [14]). Equivalently, (9.1) can be written as

$$\begin{bmatrix} F_x \\ F_y \\ T \end{bmatrix} = \mathbf{B} \begin{bmatrix} U \\ V \\ \Omega \end{bmatrix}, \tag{9.2}$$

where $\mathbf{B} = \mathbf{A}^{-\mathbf{1}}$ is called the resistance matrix (Lauga & Powers [71]).

9.3 Jeffrey & Onishi's [53] solution

Jeffrey & Onishi [53] using bipolar coordinates, they found explicit expressions for the forces and torque in terms of linear and angular velocities. They found that:

- if the cylinder translates parallel to the wall with velocity $\overline{U} = U$, then the force on it is given by

$$F = F_x = -\frac{4\pi\eta U}{\log\left(y_0/r + \sqrt{(y_0/r)^2 - 1}\right)}, \tag{9.3}$$

  where r is the cylinder radius.

- if the cylinder translates parallel to the wall with velocity $\overline{U} = -U$, then the force on it is given by

$$F = \mathrm{i}F_y = -\frac{4\pi\eta U}{\log((d+a)/r) - (a/d)}. \tag{9.4}$$

- if the cylinder is in pure rotation with angular velocity Ω, then the torque acting on it is given by

$$T = -\frac{4\pi\eta\Omega y_0 r^2}{(y_0^2 - r^2)^{1/2}}, \tag{9.5}$$

  where $a^2 = y_0^2 - r^2$.

Using (9.3)-(9.5), all the elements of the mobility matrix $\mathbf{A}$ given by (9.1) can be found. These expressions will be used later to compare/validate our results to Jeffrey & Onishi's [53] solution.

9.4 Goursat functions and transform representation

The Goursat functions are represented by

$$\begin{cases} f(z) = f_s(z) + \hat{f}(z), \\ g'(z) = g'_s(z) + \hat{g}'(z), \end{cases} \tag{9.6}$$

where $f_s(z)$, $g'_s(z)$ are defined by

$$\begin{cases} f_s(z) = \lambda \log\left(\dfrac{z - z_0}{z + z_0}\right), \\ \\ g'_s(z) = -\overline{\lambda} \log\left(\dfrac{z - z_0}{z + z_0}\right), \end{cases} \tag{9.7}$$

where $\lambda \in \mathbb{C}$ is an unknown constant which will be found as part of the solution and $\hat{f}(z)$, $\hat{g}'(z)$ are the correction functions to be found using the transform method. The above form of $f_s(z)$ and $\hat{g}'_s(z)$ has be chosen for the following reasons: First, the logarithmic singularities at z_0 were included to ensure that there is a non-zero contribution in function $H(z)$, defined by (3.37), as traversing the cylinder $|z - z_0| = 1$ and therefore a force. The coefficients of the logarithmic terms were forced to have the above form by requiring that velocity is single-valued. Finally, the appropriate image singularities at $\overline{z_0} = -z_0$ have been included to facilitate the computation of integral expressions appearing in the analysis; with this choice, it can be shown that the velocity decays at infinity.

In this problem, the fluid domain can be thought as the intersection of the upper half-plane and the exterior of the unit disc centred at z_0. Therefore, we can write the following integral

representation for $\hat{f}(z)$:

$$\begin{aligned}\hat{f}(z) = \frac{1}{2\pi}\int_{\mathcal{L}} \rho_{11}(k) e^{\mathrm{i}kz} dk \\ -\frac{1}{2\pi\mathrm{i}}\Big[\int_{L_1} \frac{\rho_{22}(k)}{1-e^{2\pi\mathrm{i}k}} \frac{1}{(z-z_0)^{k+1}} dk + \int_{L_2} \rho_{22}(k) \frac{1}{(z-z_0)^{k+1}} dk \\ + \int_{L_3} \frac{\rho_{22}(k) e^{2\pi\mathrm{i}k}}{1-e^{2\pi\mathrm{i}k}} \frac{1}{(z-z_0)^{k+1}} dk\Big],\end{aligned} \tag{9.8}$$

where $\mathcal{L} = [0, \infty)$ and $\{L_j | j = 1, 2, 3\}$ are the fundamental contours for circular edges. The two spectral functions are given by

$$\rho_{11}(k) = \int_{-\infty}^{\infty} \hat{f}(z) e^{-\mathrm{i}kz} dz, \qquad \rho_{22}(k) = -\oint_{|z-z_0|=1} \hat{f}(z)(z-z_0)^k dz. \tag{9.9}$$

The other elements of the spectral matrix are given by

$$\rho_{12}(k) = -\oint_{|z-z_0|=1} \hat{f}(z) e^{-\mathrm{i}kz} dz, \qquad \rho_{21}(k) = \int_{-\infty}^{\infty} \hat{f}(z)(z-z_0)^k dz. \tag{9.10}$$

The global relations are

$$\rho_{11}(k) + \rho_{12}(k) = 0, \quad k < 0 \tag{9.11}$$

and

$$\rho_{21}(k) + \rho_{22}(k) = 0, \quad k \in -\mathbb{N}. \tag{9.12}$$

Similarly, we can write an integral representation for $\hat{g}'(z)$:

$$\begin{aligned}\hat{g}'(z) = \frac{1}{2\pi}\int_{\mathcal{L}} \hat{\rho}_{11}(k) e^{\mathrm{i}kz} dk \\ -\frac{1}{2\pi\mathrm{i}}\Big[\int_{L_1} \frac{\hat{\rho}_{22}(k)}{1-e^{2\pi\mathrm{i}k}} \frac{1}{(z-z_0)^{k+1}} dk + \int_{L_2} \hat{\rho}_{22}(k) \frac{1}{(z-z_0)^{k+1}} dk \\ + \int_{L_3} \frac{\hat{\rho}_{22}(k) e^{2\pi\mathrm{i}k}}{1-e^{2\pi\mathrm{i}k}} \frac{1}{(z-z_0)^{k+1}} dk\Big],\end{aligned} \tag{9.13}$$

where the two spectral functions are given by

$$\hat{\rho}_{11}(k) = \int_{-\infty}^{\infty} \hat{g}'(z) e^{-\mathrm{i}kz} dz, \qquad \hat{\rho}_{22}(k) = -\oint_{|z-z_0|=1} \hat{g}'(z)(z-z_0)^k dz. \tag{9.14}$$

The other elements of the spectral matrix are given by

$$\hat{\rho}_{12}(k) = -\oint_{|z-z_0|=1} \hat{g}'(z) e^{-\mathrm{i}kz} dz, \qquad \hat{\rho}_{21}(k) = \int_{-\infty}^{\infty} \hat{g}'(z)(z-z_0)^k dz. \tag{9.15}$$

Finally, the global relations are given by

$$\hat{\rho}_{11}(k) + \hat{\rho}_{12}(k) = 0, \quad k < 0 \tag{9.16}$$

and

$$\hat{\rho}_{21}(k) + \hat{\rho}_{22}(k) = 0, \quad k \in -\mathbb{N}. \tag{9.17}$$

9.5 Boundary conditions

The no-slip boundary condition on $\overline{z} = z$ is given by (3.19), which on substitution of (9.6) becomes

$$-\overline{\hat{f}(z)} + z\hat{f}'(z) + \hat{g}'(z) = \overline{f_s(z)} - z f_s'(z) - g_s'(z). \tag{9.18}$$

The boundary condition on the cylinder can be written as

$$-\overline{f(z)} + \left(\overline{z_0} + \frac{1}{z-z_0}\right) f'(z) + g'(z) = \overline{U} - \mathrm{i}\Omega \frac{1}{z-z_0}. \tag{9.19}$$

Substitution of (9.6) and solving for $\hat{g}'(z)$ gives

$$\begin{aligned} \hat{g}'(z) = {} & \overline{\hat{f}(z)} - \left(\overline{z_0} + \frac{1}{z-z_0}\right) \hat{f}'(z) \\ & + \overline{f_s(z)} - \left(\overline{z_0} + \frac{1}{z-z_0}\right) f_s'(z) - g_s'(z) + \overline{U} - \mathrm{i}\Omega \frac{1}{z-z_0}. \end{aligned} \tag{9.20}$$

9.6 Spectral analysis

9.6.1 Fourier transform

We multiply (9.18) by $e^{-\mathrm{i}kz}$ and integrate along the lower boundary:

$$-\int_{-\infty}^{\infty}\overline{\hat{f}(z)}e^{-\mathrm{i}kz}dz+\int_{-\infty}^{\infty}z\hat{f}'(z)e^{-\mathrm{i}kz}dz+\int_{-\infty}^{\infty}\hat{g}'(z)e^{-\mathrm{i}kz}dz=R(k), \tag{9.21}$$

where

$$R(k)\equiv\int_{-\infty}^{\infty}[\overline{f_s(z)}-zf_s'(z)-g_s'(z)]e^{-\mathrm{i}kz}dz. \tag{9.22}$$

Using residue calculus, we can compute $R(k)$:

$$R(k)=\lambda\begin{cases}2\pi\mathrm{i}z_0e^{\mathrm{i}kz_0}, & k>0,\\ 0, & k=0,\\ -2\pi\mathrm{i}z_0e^{-\mathrm{i}kz_0}, & k<0.\end{cases} \tag{9.23}$$

Expression (9.21) can be written in terms of the spectral functions as

$$-\overline{\rho_{11}}(-k)-\frac{\partial[k\rho_{11}(k)]}{\partial k}+\hat{\rho}_{11}(k)=R(k), \tag{9.24}$$

which can equivalently be written as

$$\rho_{11}(-k)=-\frac{\partial[k\overline{\rho_{11}}(k)]}{\partial k}+\overline{\hat{\rho}_{11}}(k)-\overline{R}(k), \tag{9.25}$$

or

$$\rho_{11}(k)=-\frac{\partial[k\overline{\rho_{11}}(-k)]}{\partial k}+\overline{\hat{\rho}_{11}}(-k)-\overline{R}(-k). \tag{9.26}$$

On use of the global relation (9.11), we can write

$$\rho_{11}(k)=\frac{\partial[k\overline{\rho_{12}}(-k)]}{\partial k}-\overline{\hat{\rho}_{12}}(-k)-\overline{R}(-k),\quad \text{for } k>0. \tag{9.27}$$

Next, we observe that

$$\rho_{11}(k) = \int_{-\infty}^{\infty} \hat{f}(x) e^{-\mathrm{i}kx} dx = \frac{\partial[k\overline{\rho_{12}}(-k)]}{\partial k} - \overline{\hat{\rho}_{12}}(-k) - \overline{R}(-k), \quad \text{for } k > 0, \tag{9.28}$$

which means that taking the inverse Fourier transform for the upper half-plane (Crowdy [19]), we can write

$$\hat{f}(x) = \frac{1}{2\pi} \int_0^{\infty} \left[\frac{\partial[k\overline{\rho_{12}}(-k)]}{\partial k} - \overline{\hat{\rho}_{12}}(-k) - \overline{R}(-k) \right] e^{\mathrm{i}kx} dk, \quad \text{for } x \in \mathbb{R}. \tag{9.29}$$

This gives a relation between the unknown function $\hat{f}(x)$ on the lower boundary in terms of spectral functions associated to the cylindrical boundary. Note that, using (9.29) in (9.18), the correction function $\hat{g}'(z)$ on the lower boundary can be also expressed in terms of spectral functions associated to the cylinder.

9.6.2 Mellin-type transforms

Function $\hat{f}(z)$: The second global relation (9.12):

$$\rho_{21}(k) + \rho_{22}(k) = 0, \quad k \in -\mathbb{N}, \tag{9.30}$$

can be written as

$$\int_{-\infty}^{\infty} \hat{f}(z)(z - z_0)^{-n} dz - \oint_{|z-z_0|=1} \hat{f}(z)(z - z_0)^{-n} dz = 0, \quad n \in \mathbb{N}. \tag{9.31}$$

Using expression (9.29) for $\hat{f}(z)$ on the lower boundary, this becomes

$$\oint_{|z-z_0|=1} \hat{f}(z)(z - z_0)^{-n} dz = \int_0^{\infty} I(k, n) \left[\frac{\partial[k\overline{\rho_{12}}(-k)]}{\partial k} - \overline{\hat{\rho}_{12}}(-k) - \overline{R}(-k) \right] dk, \tag{9.32}$$

for $n \in \mathbb{N}$, where we have defined

$$I(k, n) \equiv \frac{1}{2\pi} \int_{-\infty}^{\infty} \frac{e^{\mathrm{i}kx}}{(x - z_0)^n} dx. \tag{9.33}$$

It can be shown that, for $n = 1$,

$$I(k,1) \equiv \frac{1}{2\pi}\int_{-\infty}^{\infty} \frac{e^{\mathrm{i}kx}}{(x-z_0)^n}dx = \begin{cases} \mathrm{i}e^{\mathrm{i}kz_0}, & k > 0, \\ \mathrm{i}/2, & k = 0, \\ 0, & k < 0, \end{cases} \tag{9.34}$$

and, for $n \geq 2$,

$$I(k,n) \equiv \frac{1}{2\pi}\int_{-\infty}^{\infty} \frac{e^{\mathrm{i}kx}}{(x-z_0)^n}dx = \begin{cases} \dfrac{\mathrm{i}^n k^{n-1} e^{\mathrm{i}kz_0}}{(n-1)!}, & k \geq 0, \\ \\ 0, & k < 0. \end{cases} \tag{9.35}$$

Function $\hat{g}'(z)$: Next, the second global relation for $\hat{g}'(z)$:

$$\hat{\rho}_{21}(k) + \hat{\rho}_{22}(k) = 0, \quad k \in -\mathbb{N}, \tag{9.36}$$

can be equivalently expressed as

$$\oint_{|z-z_0|=1} \hat{g}'(z)(z-z_0)^{-n}dz = \int_{-\infty}^{\infty} \hat{g}'(z)(z-z_0)^{-n}dz, \quad n \in \mathbb{N}. \tag{9.37}$$

But for $\hat{g}'(z)$ on the lower boundary, we can use the boundary condition (9.18) and the (inverse Fourier transform) representation for $\hat{f}(z)$ found previously to express $\hat{g}'(z)$ in terms of quantities integrated on the cylindrical boundary. It can be shown that

$$\oint_{|z-z_0|=1} \hat{g}'(z)(z-z_0)^{-n}dz = (n-1)\rho_{22}(-n) + nz_0\rho_{22}(-n-1) + B(n), \quad n \in \mathbb{N}, \tag{9.38}$$

with

$$B(n) \equiv \int_{-\infty}^{\infty} [\overline{f_s(z)} - zf_s'(z) - g_s'(z)](z-z_0)^{-n}dz. \tag{9.39}$$

where we have used the global relation (9.12).

9.7 Solution scheme

From the spectral analysis part presented in the previous section, we have found two sets of conditions given by (9.32) and (9.38) which are both valid for $n \in \mathbb{N}$. In this section, we show how on use of these conditions and a Laurent series expansion for $\hat{f}(z)$ on the cylindrical boundary, a linear system for the unknown coefficients (of the Laurent expansion) and parameter λ can be formulated. The solution of this linear system gives the unknown boundary data on the cylinder and this is sufficient to compute the mobility matrix (as we will see in a subsequent section). However, in general, the solution in the fluid domain is required; in this case, once the unknown data on the cylinder is found, all the spectral functions can be computed by back substitution in various relations.

9.7.1 Function representation

To represent $\hat{f}(z)$ on the cylinder $|z - z_0| = 1$, we use a Laurent series expansion:

$$\hat{f}(z) = \sum_{m=-\infty}^{\infty} a_m (z - z_0)^m, \tag{9.40}$$

where the coefficients $\{a_m | m \in \mathbb{Z}\}$ are to be found. Using (9.40), we have

$$\rho_{12}(k) = -\oint_{|z-z_0|=1} \hat{f}(z) e^{-\mathrm{i}kz} dz = \sum_{m=-\infty}^{\infty} a_m [T(k, m)], \tag{9.41}$$

where

$$T(k, m) \equiv -\oint_{|z-z_0|=1} (z - z_0)^m e^{-\mathrm{i}kz} dz = \begin{cases} 0, & m \geq 0, \\ -\dfrac{2\pi\mathrm{i}(-\mathrm{i}k)^{-m-1} e^{-\mathrm{i}kz_0}}{(-m-1)!}, & m < 0. \end{cases} \tag{9.42}$$

In addition,

$$\begin{aligned}\hat{\rho}_{12}(k) &= -\oint_{|z-z_0|=1} \hat{g}'(z)e^{-\mathrm{i}kz}dz, \\ &= -\oint_{|z-z_0|=1} \left[\overline{\hat{f}(z)} - \left(\overline{z_0} + \frac{1}{z-z_0}\right)\hat{f}'(z)\right] e^{-\mathrm{i}kz}dz + S(k),\end{aligned} \tag{9.43}$$

where we have used the boundary condition (9.20) and

$$\begin{aligned}S(k) &\equiv -\oint_{|z-z_0|=1} \left[\overline{f_s(z)} - \left(\overline{z_0} + \frac{1}{z-z_0}\right) f_s'(z) - g_s'(z) + \overline{U} - \mathrm{i}\Omega\frac{1}{z-z_0}\right] e^{-\mathrm{i}kz}dz, \\ &= -2\pi\Omega e^{-\mathrm{i}kz_0} - \oint_{|z-z_0|=1} \left[\overline{f_s(z)} - \left(\overline{z_0} + \frac{1}{z-z_0}\right) f_s'(z) - g_s'(z)\right] e^{-\mathrm{i}kz}dz.\end{aligned} \tag{9.44}$$

On substitution of (9.40) into (9.43), we find that $\hat{\rho}_{12}(k)$ can be written as

$$\hat{\rho}_{12}(k) = \sum_{m=-\infty}^{\infty} a_m[Y(k,m)] + \sum_{m=-\infty}^{\infty} \overline{a_m}[V(k,m)] + S(k), \tag{9.45}$$

with

$$Y(k,m) = mz_0\, T(k,m-1) - mT(k,m-2), \tag{9.46}$$

$$V(k,m) = T(k,-m). \tag{9.47}$$

9.7.2 Formulation of the linear system

Using the function representation for $\hat{f}(z)$ and expressions $\rho_{12}(k)$ and $\hat{\rho}_{12}(k)$ defined by (9.41) and (9.45) respectively, conditions (9.32) and (9.38) can be expressed in terms of the unknown coefficients a_m, parameter λ and known quantities.

Conditions (9.32)**:** These can be written as

$$a_{n-1} = \sum_{m=-\infty}^{\infty} a_m P_{nm} + \sum_{m=-\infty}^{\infty} \overline{a_m} Q_{nm} + L_n, \quad n = 1, 2, ..., \tag{9.48}$$

where

$$P_{nm} = -\frac{1}{2\pi \mathrm{i}} \int_0^\infty I(k,n)\overline{V}(-k,m)dk, \tag{9.49}$$

$$Q_{nm} = \frac{1}{2\pi \mathrm{i}} \int_0^\infty I(k,n) \left[\overline{T}(-k,m) + k\frac{\partial \overline{T}(-k,m)}{\partial k} - \overline{Y}(-k,m)\right] dk, \tag{9.50}$$

$$L_n = -\frac{1}{2\pi \mathrm{i}} \int_0^\infty I(k,n) \left[\overline{S}(-k) + \overline{R}(-k)\right] dk. \tag{9.51}$$

Note that terms $\{L_n | n = 1, 2, ...\}$ contain the unknown complex parameter λ. Conditions (9.48) together with their complex conjugates are added to the linear system.

Conditions (9.38)**:** Similarly, these can be expressed as:

$$(n-1)a_{n-1} + 2nz_0 a_n - (n+1)a_{n+1} + \overline{a_{-n+1}} = \frac{1}{2\pi \mathrm{i}} \left[B(n) - A(n)\right], \quad n = 1, 2, ..., \tag{9.52}$$

where

$$A(n) \equiv \oint_{|z-z_0|=1} \left[\overline{f_s(z)} - \left(\overline{z_0} + \frac{1}{z - z_0}\right) f_s'(z) - g_s'(z) + \overline{U} - \mathrm{i}\Omega \frac{1}{z - z_0}\right] (z - z_0)^{-n} dz, \tag{9.53}$$

Conditions (9.52) together with their complex conjugates are added to the linear system.

The linear system consisting of (9.48) and (9.52) (and their complex conjugates) is solved for coefficients $\{a_m | m = -M, ...M\}$ (for suitable truncation parameter M) and the complex parameter λ and their complex conjugates. It is found that the coefficient matrix is well-conditioned and as we see in the next section, we get good agreement with the exact solution (Jeffrey & Onishi [53], Crowdy [14]).

9.8 Computation of the mobility matrix

Once $\{a_m | m \in \mathbb{Z}\}$ and λ are computed, we can calculate all elements of the mobility matrix, i.e. forces and torque acting on the cylinder for given translational/angular velocities. To determine these, we consider the following cylinder motions: (a) motion parallel to the wall, i.e. $\overline{U} = U$, $\Omega = 0$, (b) motion away from the wall, i.e. $\overline{U} = -U$, $\Omega = 0$ and (c) pure rotation, i.e. $U = 0$, $\Omega \neq 0$. The mobility matrix for this problem is diagonal (Jeffrey & Onishi [53]) which means that for case (a) we expect a horizontal force acting on the cylinder and no torque, for (b) a vertical force and no torque and finally for (c) a torque and no force.

The force F on the cylinder is given by

$$F = [2\eta \mathrm{i} H(z)]_{|z-z_0|=1} = [2\eta \mathrm{i}(2\lambda \log(z - z_0)]_{|z-z_0|=1} = -8\pi\eta\lambda, \tag{9.54}$$

where η is the viscosity and square brackets with subscript denote the change in the quantity they contain as a single circuit $|z - z_0| = 1$ is traversed. Expression $H(z)$ is defined by (3.37). We note that if the cylinder is in pure rotation, the solution of the linear system gives λ equal to zero which means that, as expected, there is no force exerted on the cylinder.

The torque T on the cylinder is given by

$$T = 2\eta \,\mathrm{Re}\left[2\pi \mathrm{i} z_0 \lambda + \oint_{|z-z_0|=1} (z - z_0) g''(z) dz\right] \tag{9.55}$$

where Re$[.]$ denotes the real part of the expression in square brackets. Derivation of this formula is given in the Appendix B. Using (9.20) and (9.40) in (B.6), we find that

$$T = 4\eta\pi\Big[\mathrm{Re}[\mathrm{i} z_0 \lambda] - \Omega - 2\mathrm{Im}[a_1]\Big], \tag{9.56}$$

in terms of parameter λ, angular velocity Ω and coefficient a_1. If the cylinder is moving parallel or perpendicular to the wall, expression (9.56) is found to be equal to zero. If the

cylinder is in pure rotation, parameter λ is equal to zero and (9.56) simplifies to

$$T = -4\eta\pi\Big[\Omega + 2\text{Im}[a_1]\Big]. \tag{9.57}$$

Interestingly, knowing that the mobility matrix for this problem is diagonal, the form of (9.57) suggests that coefficient a_1 has an inherent linear relation with angular velocity Ω through the linear system.

9.9 Comparison to Jeffrey & Onishi's [53] solution

Figures 9.2-9.4 show comparison of horizontal force F_x, vertical force F_y and torque T for cases (a)-(c) respectively as computed using our transform approach and exact solution by Jeffrey & Onishi [53] (and Crowdy [14]). The results were found to be the same to within an accuracy of $\mathcal{O}(10^{-3} - 10^{-4})$. As noted, as cylinder approaches the planar no-slip wall, more terms are required in the sum (9.40). Also, many integral expressions appearing in our analysis are computed numerically: the results presented here are for moderate truncation parameters, e.g. $dk = 0.01$, $\infty = 10$; increasing these parameters improves the accuracy, but on the other hand the solution scheme becomes slower.

9.10 Summary

We have presented a transform approach for solving a Stokes flow problem in a doubly connected circular domain. The problem considered was that of a translating and rotating cylinder near a wall. This problem was previously solved exactly by Jeffrey & Onishi [53] using bipolar coordinates and, more recently, rederived by Crowdy [14] using complex variable techniques. The idea of our transform approach was to consider the fluid region as being the intersection of the upper half-plane and the exterior of unit disc, write an appropriate integral representations for the unknown correction functions $\hat{f}(z)$, $\hat{g}'(z)$ and proceed to spectral analysis to determine the unknown boundary data and spectral functions. Our method was checked against Jeffrey & Onishi's [53] solution (Crowdy [14]) and results were found to be in good agreement.

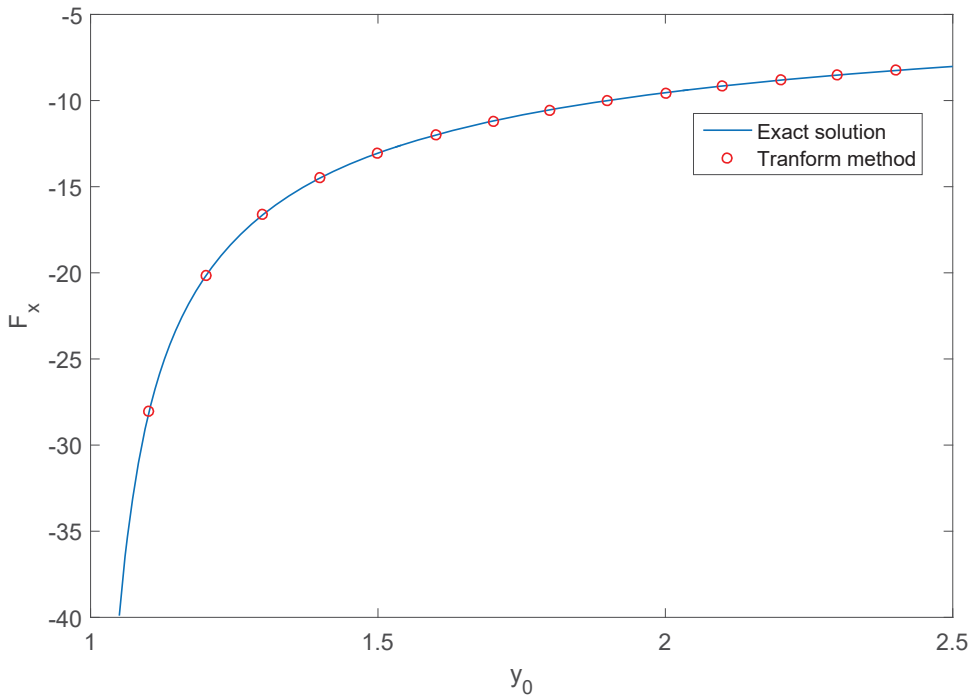

Figure 9.2: Comparison between our transform approach and the exact solution by Jeffrey & Onishi [53]: (a) computation of the force $F = F_x$ when cylinder is moving parallel to the wall (for $U = 1$) as a function of the distance from the wall y_0.

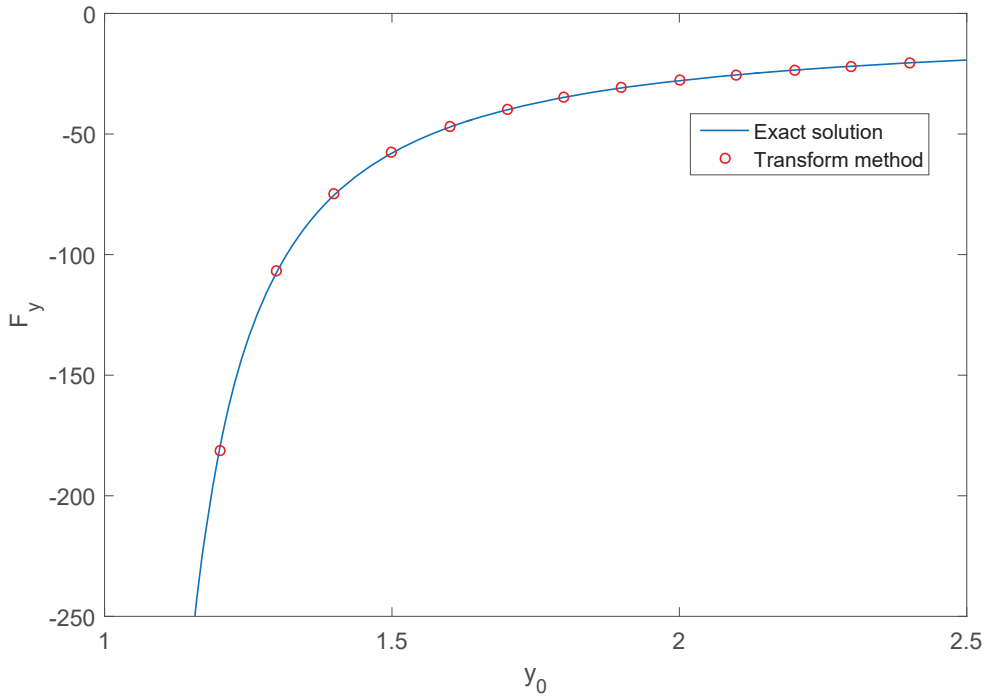

Figure 9.3: Comparison between our transform approach and the exact solution by Jeffrey & Onishi [53]: (b) computation of the force $F = \mathrm{i}F_y$ when the cylinder is moving away from the wall (for $U = \mathrm{i}$) as a function of the distance from the wall y_0.

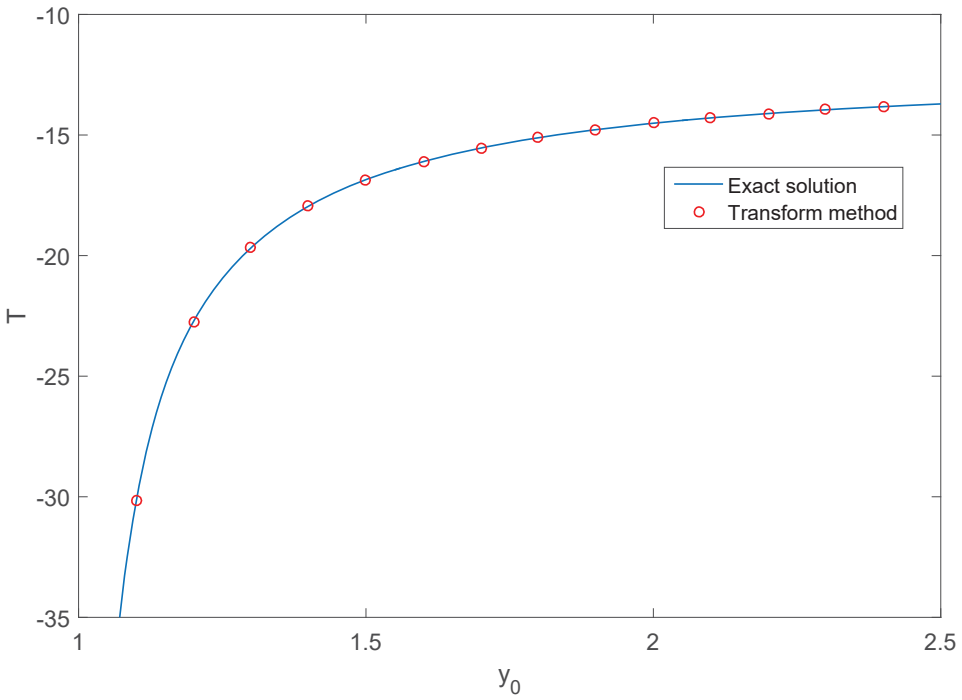

Figure 9.4: Comparison between our transform approach and the exact solution by Jeffrey & Onishi [53]: (c) computation of the torque T when the cylinder is in pure rotation (for $\Omega = 1$) as a function of the distance from the wall y_0.

Our transform approach can also be used to solve other Stokes flow problems in the same geometry. We mention the work by Davis & O'Neill [29] who solved the problem of a shear flow past a cylinder above a wall. Davis & O'Neill [29] used bipolar coordinates to map the fluid region to a channel geometry and then employ Fourier transform techniques. They investigated the separation from the boundaries as a function of cylinder's distance from the wall, as well as the formation of Moffatt eddies [85]. In addition, Samson [95] presented an accurate method based on conformal mapping theory and numerical methods to solve problems in doubly connected regions, including Davis & O'Neill's [29]. Since Davis & O'Neill's [29] geometry is the same to the problem analysed in this chapter, our transform method can also be used to solve this problem; the only difference would be the definition of forcing functions $f_s(z)$, $g'_s(z)$ (any symmetry of the resulting flow can be exploited to obtain additional relations between the spectral functions which can further simplify spectral analysis).

Chapter 10

A translating and rotating cylinder in a channel

10.1 Introduction

In this Chapter, we shall be considering the problem of a translating and rotating cylinder in a channel geometry and again the aim is to compute the mobility matrix, i.e. the tensor relating forces and torques and translational/angular velocities.

Jeong & Yoon [63] and Jeong & Jang [58] have recently analyzed Stokes flow problems for a cylinder in a channel geometry. Jeong & Yoon [63] have considered the problem of a translating cylinder along the centreline of the channel subject to a background pressure-driven flow using Papkovich-Fadle eigenfunction expansion and a least square method. Jeong & Jang [58] have solved the problem of a translating and rotating cylinder not necessarily placed along the centreline subject to a background pressure-driven flow using the same techniques as Jeong & Yoon [63].

In this chapter, we follow Jeong & Jang [58] and restrict our interest to the case where there is no background flow.

10.2 Problem formulation

Consider a circular cylinder of unit radius centred at $z_0 = \mathrm{i}y_0$, $1 < y_0 < h - 1$ in a channel $-\infty < x < \infty$, $0 < y < h$ (Figure 10.1). Similarly to the problem considered in the previous Chapter, the cylinder is translating with complex speed U and rotating with angular velocity Ω and experiencing a non-zero net force $F = F_x + \mathrm{i}F_y$, $(F_x, F_y \in \mathbb{R})$ and torque T. The aim is again to compute the mobility matrix for the cylinder, i.e. a tensor relating $\{U, \Omega\}$ and $\{F, T\}$.

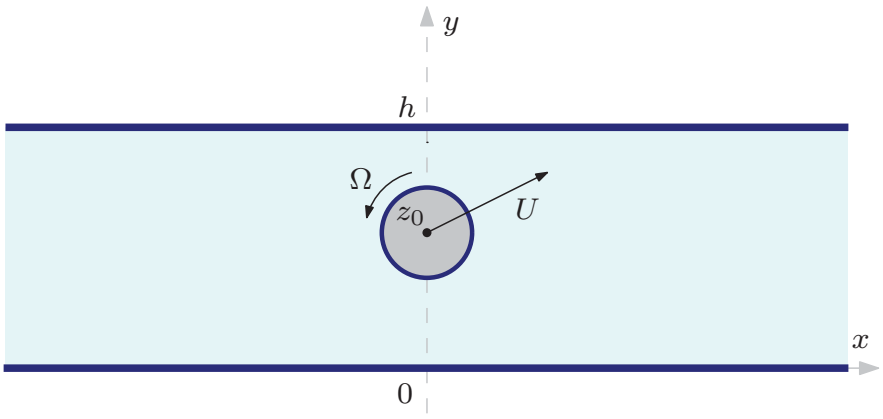

Figure 10.1: Schematic of the configuration: a translating and rotating cylinder of unit radius centred at z_0 in a channel geometry.

10.3 Goursat functions and transform representation

The Goursat functions are respresented by

$$\begin{cases} f(z) = f_s(z) + \hat{f}(z), \\ g'(z) = g'_s(z) + \hat{g}'(z), \end{cases} \tag{10.1}$$

where $f_s(z)$, $g'_s(z)$ are defined by

$$\begin{cases} f_s(z) = \lambda \log\left[\tanh\left(\dfrac{\pi}{2h}(z - z_0)\right)\right], \\ \\ g'_s(z) = -\overline{\lambda} \log\left[\tanh\left(\dfrac{\pi}{2h}(z - z_0)\right)\right], \end{cases} \tag{10.2}$$

where $\lambda \in \mathbb{C}$ is an unknown constant which will be found as part of the solution and $\hat{f}(z)$, $\hat{g}'(z)$ are the correction functions to be found. Note that $f_s(z)$, $g'_s(z)$ are $2h\mathrm{i}$-periodic and this will be useful later.

In this problem, the fluid domain can be thought as the intersection of two half-planes (upper and shifted lower) and the exterior of the unit disc centred at z_0. Therefore, we can write the following integral representation for $\hat{f}(z)$:

$$\begin{aligned}\hat{f}(z) = &\frac{1}{2\pi}\int_{\mathcal{L}_1}\rho_{11}(k)e^{\mathrm{i}kz}dk \\ &-\frac{1}{2\pi\mathrm{i}}\left[\int_{L_1}\frac{\rho_{22}(k)}{1-e^{2\pi\mathrm{i}k}}\frac{1}{(z-z_0)^{k+1}}dk+\int_{L_2}\frac{\rho_{22}(k)}{(z-z_0)^{k+1}}dk+\int_{L_3}\frac{\rho_{22}(k)e^{2\pi\mathrm{i}k}}{1-e^{2\pi\mathrm{i}k}}\frac{1}{(z-z_0)^{k+1}}dk\right] \\ &+\frac{1}{2\pi}\int_{\mathcal{L}_2}\rho_{33}(k)e^{\mathrm{i}kz}dk,\end{aligned} \tag{10.3}$$

where $\mathcal{L}_1 = [0,\infty)$ and $\mathcal{L}_2 = [0,-\infty)$ and $\{L_j | j = 1,2,3\}$ are the fundamental contours for circular edges. The three spectral functions are given by

$$\rho_{11}(k) = \int_{-\infty}^{\infty}\hat{f}(z)e^{-\mathrm{i}kz}dz, \qquad \rho_{22}(k) = -\oint_{|z-z_0|=1}\hat{f}(z)(z-z_0)^k dz \tag{10.4}$$

and

$$\rho_{33}(k) = \int_{\infty+\mathrm{i}h}^{-\infty+\mathrm{i}h}\hat{f}(z)e^{-\mathrm{i}kz}dz. \tag{10.5}$$

The remaining elements of the matrix of spectral functions are given by

$$\rho_{21}(k) = \int_{-\infty}^{\infty}\hat{f}(z)(z-z_0)^k dz, \qquad \rho_{23}(k) = \int_{\infty+\mathrm{i}h}^{-\infty+\mathrm{i}h}\hat{f}(z)(z-z_0)^k dz, \tag{10.6}$$

$$\rho_{12}(k) = \rho_{32}(k) = -\oint_{|z-z_0|=1}\hat{f}(z)e^{-\mathrm{i}kz}dz \tag{10.7}$$

and $\rho_{31}(k) = \rho_{11}(k)$ and $\rho_{13}(k) = \rho_{33}(k)$.

The global relations are

$$\begin{aligned} \rho_{11}(k) + \rho_{12}(k) + \rho_{13}(k) = 0, \quad k \in \mathbb{R}, \\ \rho_{31}(k) + \rho_{32}(k) + \rho_{33}(k) = 0, \quad k \in \mathbb{R}, \end{aligned} \tag{10.8}$$

which are equivalent, and

$$\rho_{21}(k) + \rho_{22}(k) + \rho_{23}(k) = 0, \quad k \in -\mathbb{N}. \tag{10.9}$$

Similar expressions to (10.3)-(10.9) can be written for $\hat{g}'(z)$ (and $\hat{\rho}_{mn}(k)$, $m, n = 1, 2, 3$). We write

$$\begin{aligned} \hat{g}'(z) = \frac{1}{2\pi} \int_{\mathcal{L}_1} \hat{\rho}_{11}(k) e^{\mathrm{i}kz} dk \\ - \frac{1}{2\pi \mathrm{i}} \left[\int_{L_1} \frac{\hat{\rho}_{22}(k)}{1 - e^{2\pi \mathrm{i}k}} \frac{1}{(z - z_0)^{k+1}} dk + \int_{L_2} \frac{\hat{\rho}_{22}(k)}{(z - z_0)^{k+1}} dk + \int_{L_3} \frac{\hat{\rho}_{22}(k) e^{2\pi \mathrm{i}k}}{1 - e^{2\pi \mathrm{i}k}} \frac{1}{(z - z_0)^{k+1}} dk \right] \\ + \frac{1}{2\pi} \int_{\mathcal{L}_2} \hat{\rho}_{33}(k) e^{\mathrm{i}kz} dk, \end{aligned} \tag{10.10}$$

where the three spectral functions are given by

$$\hat{\rho}_{11}(k) = \int_{-\infty}^{\infty} \hat{g}'(z) e^{-\mathrm{i}kz} dz, \qquad \hat{\rho}_{22}(k) = - \oint_{|z - z_0| = 1} \hat{g}'(z) (z - z_0)^k dz \tag{10.11}$$

and

$$\hat{\rho}_{33}(k) = \int_{\infty + \mathrm{i}h}^{-\infty + \mathrm{i}h} \hat{g}'(z) e^{-\mathrm{i}kz} dz. \tag{10.12}$$

The remaining elements of the matrix of spectral functions are given by

$$\hat{\rho}_{21}(k) = \int_{-\infty}^{\infty} \hat{g}'(z) (z - z_0)^k dz, \qquad \hat{\rho}_{23}(k) = \int_{\infty + \mathrm{i}h}^{-\infty + \mathrm{i}h} \hat{g}'(z) (z - z_0)^k dz, \tag{10.13}$$

$$\hat{\rho}_{12}(k) = \hat{\rho}_{32}(k) = - \oint_{|z - z_0| = 1} \hat{g}'(z) e^{-\mathrm{i}kz} dz \tag{10.14}$$

and $\hat{\rho}_{31}(k) = \hat{\rho}_{11}(k)$ and $\hat{\rho}_{13}(k) = \hat{\rho}_{33}(k)$.

The global relations are

$$\begin{aligned} \hat{\rho}_{11}(k) + \hat{\rho}_{12}(k) + \hat{\rho}_{13}(k) = 0, \quad k \in \mathbb{R}, \\ \hat{\rho}_{31}(k) + \hat{\rho}_{32}(k) + \hat{\rho}_{33}(k) = 0, \quad k \in \mathbb{R}, \end{aligned} \tag{10.15}$$

which are equivalent, and

$$\hat{\rho}_{21}(k) + \hat{\rho}_{22}(k) + \hat{\rho}_{23}(k) = 0, \quad k \in -\mathbb{N}. \tag{10.16}$$

10.4 Boundary conditions

The no-slip boundary condition on $\overline{z} = z$ (lower channel wall) is given by (3.19). Substitution of (10.1) gives

$$-\overline{\hat{f}(z)} + z\hat{f}'(z) + \hat{g}'(z) = \overline{f_s(z)} - zf_s'(z) - g_s'(z). \tag{10.17}$$

Similarly, the no-slip boundary condition on $\overline{z} = z - 2\mathrm{i}h$ (upper channel wall) can be written as

$$-\overline{\hat{f}(z)} + (z - 2\mathrm{i}h)\hat{f}'(z) + \hat{g}'(z) = \overline{f_s(z)} - (z - 2\mathrm{i}h)f_s'(z) - g_s'(z). \tag{10.18}$$

Finally, the boundary condition on $|z - z_0| = 1$ can be written as

$$-\overline{f(z)} + \left(\overline{z_0} + \frac{1}{z - z_0}\right) f'(z) + g'(z) = \overline{U} - \mathrm{i}\Omega\frac{1}{z - z_0}. \tag{10.19}$$

Substitution of (10.1) and solving for $\hat{g}'(z)$ gives

$$\begin{aligned} \hat{g}'(z) = \overline{\hat{f}(z)} - \left(\overline{z_0} + \frac{1}{z - z_0}\right) \hat{f}'(z) \\ + \overline{f_s(z)} - \left(\overline{z_0} + \frac{1}{z - z_0}\right) f_s'(z) - g_s'(z) + \overline{U} - \mathrm{i}\Omega\frac{1}{z - z_0}. \end{aligned} \tag{10.20}$$

10.5 Spectral analysis

10.5.1 Fourier transforms

We multiply (10.17) by $e^{-\mathrm{i}kz}$ and integrate along the lower boundary:

$$-\int_{-\infty}^{\infty}\overline{\hat{f}(z)}e^{-\mathrm{i}kz}dz+\int_{-\infty}^{\infty}z\hat{f}'(z)e^{-\mathrm{i}kz}dz+\int_{-\infty}^{\infty}\hat{g}'(z)e^{-\mathrm{i}kz}dz=R_1(k), \tag{10.21}$$

where

$$R_1(k)\equiv\int_{-\infty}^{\infty}[\overline{f_s(z)}-zf_s'(z)-g_s'(z)]e^{-\mathrm{i}kz}dz. \tag{10.22}$$

This can be written in terms of the spectral functions as

$$-\overline{\rho_{11}}(-k)-\frac{\partial[k\rho_{11}(k)]}{\partial k}+\hat{\rho}_{11}(k)=R_1(k). \tag{10.23}$$

Similarly if we multiply (10.18) by $e^{-\mathrm{i}kz}$ and integrate along the upper boundary we find

$$-e^{2kh}\overline{\rho_{13}}(-k)-\frac{\partial[k\rho_{13}(k)]}{\partial k}+2kh\rho_{13}(k)+\hat{\rho}_{13}(k)=R_3(k), \tag{10.24}$$

where

$$R_3(k)\equiv\int_{\infty+\mathrm{i}h}^{-\infty+\mathrm{i}h}[\overline{f_s(z)}-(z-2\mathrm{i}h)f_s'(z)-g_s'(z)]e^{-\mathrm{i}kz}dz. \tag{10.25}$$

Addition of (10.23) and (10.24) and use of the first global relation (10.8) gives (after some algebra):

$$\rho_{11}(k)=\frac{2khW(k)-(e^{2kh}-1)\overline{W}(-k)}{\Delta(k)},\qquad\text{for } k\in\mathbb{R}, \tag{10.26}$$

where

$$W(k)=-e^{2kh}\overline{\rho_{12}}(-k)-\frac{\partial[k\rho_{12}(k)]}{\partial k}+2kh\rho_{12}(k)+\hat{\rho}_{12}(k)+R(k), \tag{10.27}$$

with

$$R(k)=R_1(k)+R_3(k) \tag{10.28}$$

and

$$\Delta(k) \equiv 4(\sinh^2(hk) - h^2k^2). \tag{10.29}$$

But

$$\rho_{11}(k) = \int_{-\infty}^{\infty} \hat{f}(z)e^{-\mathrm{i}kz}dz \tag{10.30}$$

and therefore taking inverse Fourier transform, we find

$$\hat{f}(z) = \frac{1}{2\pi}\int_{-\infty}^{\infty} \rho_{11}(k)e^{\mathrm{i}kz}dk = \frac{1}{2\pi}\int_{-\infty}^{\infty} \left[\frac{2khW(k) - (e^{2kh}-1)\overline{W}(-k)}{\Delta(k)}\right] e^{\mathrm{i}kz}dk, \tag{10.31}$$

for $z = x \in \mathbb{R}$. This expression gives a relation between the unknown function $\hat{f}(z)$ on the lower channel wall in terms of quantities on the cylinder. Note that, using (10.31) in (10.17), the correction function $\hat{g}'(z)$ on the lower channel wall can be also expressed in terms of spectral functions associated to the cylinder. But, near $k = 0$,

$$\Delta(k) \sim \mathcal{O}(k^4) \tag{10.32}$$

which means that, if we define

$$L(k) \equiv 2khW(k) - (e^{2kh}-1)\overline{W}(-k), \tag{10.33}$$

then we must require

$$L(0) = L'(0) = L''(0) = L'''(0) = 0 \tag{10.34}$$

in order to remove the singularity at $k = 0$ of the integrand in (10.31).

A similar expression to (10.31) can be written for $\hat{f}(z)$ on the upper channel wall. In fact, using the first global relation in (10.8), we can write

$$\rho_{13}(k) = \int_{\infty+\mathrm{i}h}^{-\infty+\mathrm{i}h} \hat{f}(z)e^{-\mathrm{i}kz}dz = -\rho_{11}(k) - \rho_{12}(k), \qquad \text{for } k \in \mathbb{R}. \tag{10.35}$$

Again, taking inverse Fourier transform, we find

$$\hat{f}(z) = \frac{1}{2\pi}\int_{-\infty}^{\infty} \left[\rho_{11}(k) + \rho_{12}(k)\right] e^{\mathrm{i}kz} dk, \tag{10.36}$$

for $z = x + \mathrm{i}h$, $x \in \mathbb{R}$. Using (10.26), this expression gives a relation between the unknown function $\hat{f}(z)$ on the upper channel wall in terms of quantities on the cylinder. Similarly, using (10.36) in (10.18), the correction function $\hat{g}'(z)$ on the lower channel wall can be expressed in terms of spectral functions associated to the cylinder.

10.5.2 Mellin-type transforms

Function $\hat{f}(z)$: The second global relation given by (10.9):

$$\rho_{21}(k) + \rho_{22}(k) + \rho_{23}(k) = 0, \quad k \in -\mathbb{N}, \tag{10.37}$$

can be written as

$$\int_{-\infty}^{\infty} \hat{f}(z)(z-z_0)^{-n} dz + \int_{\infty+\mathrm{i}h}^{-\infty+\mathrm{i}h} \hat{f}(z)(z-z_0)^{-n} dz - \oint_{|z-z_0|=1} \hat{f}(z)(z-z_0)^{-n} dz = 0, \quad n \in \mathbb{N}. \tag{10.38}$$

Substitution of (10.31) and (10.36) on their respective integrals gives

$$\begin{aligned}\oint_{|z-z_0|=1} \hat{f}(z)(z-z_0)^{-n} dz = &\int_{-\infty}^{\infty} \left[\frac{1}{2\pi}\int_{-\infty}^{\infty} \rho_{11}(k) e^{\mathrm{i}kz} dk\right] (z-z_0)^{-n} dz \\ &+ \int_{\infty+\mathrm{i}h}^{-\infty+\mathrm{i}h} \left[\frac{1}{2\pi}\int_{-\infty}^{\infty} \left[\rho_{11}(k) + \rho_{12}(k)\right] e^{\mathrm{i}kz} dk\right] (z-z_0)^{-n} dz,\end{aligned} \tag{10.39}$$

which, after changing the order of integration, can be written as

$$\oint_{|z-z_0|=1} \hat{f}(z)(z-z_0)^{-n} dz = \int_{-\infty}^{\infty} \rho_{11}(k) I_1(k,n) dk + \int_{-\infty}^{\infty} \left[\rho_{11}(k) + \rho_{12}(k)\right] I_2(k,n) dk, \tag{10.40}$$

for $n \in \mathbb{N}$, where we have defined

$$I_1(k,n) \equiv \frac{1}{2\pi}\int_{-\infty}^{\infty} \frac{e^{\mathrm{i}kz}}{(z-z_0)^n}dz, \qquad I_2(k,n) \equiv \frac{1}{2\pi}\int_{\infty+\mathrm{i}h}^{-\infty+\mathrm{i}h} \frac{e^{\mathrm{i}kz}}{(z-z_0)^n}dz. \tag{10.41}$$

Using residue calculus, it can be shown that, for $n = 1$,

$$I_1(k,1) = \frac{1}{2\pi}\int_{-\infty}^{\infty} \frac{e^{\mathrm{i}kz}}{(z-z_0)}dz = \begin{cases} \mathrm{i}e^{\mathrm{i}kz_0}, & k > 0, \\ \mathrm{i}/2, & k = 0, \\ 0, & k < 0, \end{cases} \tag{10.42}$$

and, for $n \geq 2$,

$$I_1(k,n) = \frac{1}{2\pi}\int_{-\infty}^{\infty} \frac{e^{\mathrm{i}kz}}{(z-z_0)^n}dz = \begin{cases} \dfrac{\mathrm{i}^n k^{n-1} e^{\mathrm{i}kz_0}}{(n-1)!}, & k \geq 0, \\ 0, & k < 0. \end{cases} \tag{10.43}$$

Similarly, for $n = 1$, we have

$$I_2(k,1) = \frac{1}{2\pi}\int_{\infty+\mathrm{i}h}^{-\infty+\mathrm{i}h} \frac{e^{\mathrm{i}kz}}{(z-z_0)}dz = \begin{cases} 0, & k > 0, \\ \mathrm{i}/2, & k = 0, \\ \mathrm{i}e^{\mathrm{i}kz_0}, & k < 0, \end{cases} \tag{10.44}$$

and, for $n \geq 2$,

$$I_2(k,n) = \frac{1}{2\pi}\int_{\infty+\mathrm{i}h}^{-\infty+\mathrm{i}h} \frac{e^{\mathrm{i}kz}}{(z-z_0)^n}dz = \begin{cases} 0, & k \geq 0, \\ \dfrac{\mathrm{i}^n k^{n-1} e^{\mathrm{i}kz_0}}{(n-1)!}, & k < 0. \end{cases} \tag{10.45}$$

Function $\hat{g}'(z)$: The second global relation for $\hat{g}'(z)$ (similar to (10.9)):

$$\hat{\rho}_{21}(k) + \hat{\rho}_{22}(k) + \hat{\rho}_{23}(k) = 0, \quad k \in -\mathbb{N}, \tag{10.46}$$

which can be equivalently expressed as

$$\oint_{|z-z_0|=1} \hat{g}'(z)(z-z_0)^{-n}dz = \int_{-\infty}^{\infty} \hat{g}'(z)(z-z_0)^{-n}dz + \int_{\infty+\mathrm{i}h}^{-\infty+\mathrm{i}h} \hat{g}'(z)(z-z_0)^{-n}dz, \quad n \in \mathbb{N}. \tag{10.47}$$

But for $\hat{g}'(z)$ on the channel boundaries, we can use the boundary conditions (10.17) and (10.18) and the (inverse Fourier transform) representations for $\hat{f}(z)$ found previously to express $\hat{g}'(z)$ in terms of quantities integrated on the cylindrical boundary. It can be shown that

$$\begin{aligned}\oint_{|z-z_0|=1} \hat{g}'(z)(z-z_0)^{-n}dz = &\int_{-\infty}^{\infty} \overline{\rho_{11}}(k)I_1(-k,n)dk + \int_{-\infty}^{\infty} [\overline{\rho_{11}}(k) + \overline{\rho_{12}}(k)]e^{-2kh}I_2(-k,n)dk \\ &+ 2\mathrm{i}nh\int_{-\infty}^{\infty} [\rho_{11}(k) + \rho_{12}(k)]I_2(k,n+1)dk \\ &+ (n-1)\rho_{22}(-n) + nz_0\rho_{22}(-n-1) + B(n) + C(n), \quad n \in \mathbb{N},\end{aligned} \tag{10.48}$$

with

$$\begin{aligned}B(n) &\equiv \int_{-\infty}^{\infty} [\overline{f_s(z)} - zf_s'(z) - g_s'(z)](z-z_0)^{-n}dz, \\ C(n) &\equiv \int_{\infty+\mathrm{i}h}^{-\infty+\mathrm{i}h} [\overline{f_s(z)} - (z-2\mathrm{i}h)f_s'(z) - g_s'(z)](z-z_0)^{-n}dz,\end{aligned} \tag{10.49}$$

where we have used the global relation (10.9).

10.6 Solution scheme

From the spectral analysis of the previous section, we have found conditions (10.40) and (10.48) which are both valid for $n \in \mathbb{N}$. In this section, we show how using these conditions

and a Laurent series expansion for $\hat{f}(z)$ on the cylindrical boundary, one can formulate a linear system for the unknown coefficients and parameter λ. The solution of this linear system gives the unknown boundary data on the cylinder and this is sufficient to compute the mobility matrix (as we will see in a subsequent section). However, in general, the solution in the fluid domain is required; in this case, once the unknown data on the cylinder is found, all the spectral functions can be computed by back-substitution in various relations.

10.6.1 Function representation

We use a Laurent series expansion to represent $\hat{f}(z)$ on $|z - z_0| = 1$:

$$\hat{f}(z) = \sum_{m=-\infty}^{\infty} a_m (z - z_0)^m, \tag{10.50}$$

where the coefficients $\{a_m | m \in \mathbb{Z}\}$ are to be found. Using (10.50), it can be shown that

$$\begin{aligned} \rho_{12}(k) &= \sum_{m=-\infty}^{\infty} a_m [T(k,m)], \\ \hat{\rho}_{12}(k) &= \sum_{m=-\infty}^{\infty} a_m [Y(k,m)] + \sum_{m=-\infty}^{\infty} \overline{a_m} [V(k,m)] + S(k), \end{aligned} \tag{10.51}$$

with

$$Y(k,m) = m z_0 \, T(k, m-1) - m T(k, m-2), \tag{10.52}$$

$$V(k,m) = T(k,-m). \tag{10.53}$$

Expressions $T(k,m)$, $Y(k,m)$ and $V(k,m)$ are given by (9.42), (9.46) and (9.47).

10.6.2 Formulation of the linear system

Conditions (10.40)**:** Using the function representation presented in the previous subsection and $\rho_{12}(k)$ and $\hat{\rho}_{12}(k)$ written as infinite series, these conditions can be expressed as

$$a_{n-1} = \sum_{m=-\infty}^{\infty} a_m A_{nm} + \sum_{m=-\infty}^{\infty} \overline{a_m} B_{nm} + C_n, \quad n = 1, 2, ..., \tag{10.54}$$

where

$$\begin{aligned} A_{nm} = & \frac{1}{2\pi \mathrm{i}} \int_{-\infty}^{\infty} P(k,m) I_1(k,n) dk \\ & + \frac{1}{2\pi \mathrm{i}} \int_{-\infty}^{\infty} [P(k,m) + T(k,m)] I_2(k,n) dk, \end{aligned} \tag{10.55}$$

$$B_{nm} = \frac{1}{2\pi \mathrm{i}} \int_{-\infty}^{\infty} Q(k,m)[I_1(k,n) + I_2(k,n)] dk, \tag{10.56}$$

$$C_n = \frac{1}{2\pi \mathrm{i}} \int_{-\infty}^{\infty} N(k)[I_1(k,n) + I_2(k,n)] dk, \tag{10.57}$$

with

$$P(k,m) = \frac{2khw_1(k,m) - (e^{2kh} - 1)\overline{w_2}(-k,m)}{\Delta(k)},$$

$$Q(k,m) = \frac{2khw_2(k,m) - (e^{2kh} - 1)\overline{w_1}(-k,m)}{\Delta(k)}, \tag{10.58}$$

$$N(k) = \frac{2khw_3(k) - (e^{2kh} - 1)\overline{w_3}(-k)}{\Delta(k)},$$

and

$$w_1(k,m) = -\frac{\partial[kT(k,m)]}{\partial k} + 2khT(k,m) + Y(k,m),$$

$$w_2(k,m) = -e^{2kh}\overline{T}(-k,m) + V(k,m), \tag{10.59}$$

$$w_3(k) = S(k) + R(k).$$

Note that terms $\{C_n | n = 1, 2, ...\}$ contain the unknown complex parameter λ. Conditions (10.54) together with their complex conjugates are added to the linear system.

Conditions (10.48)**:** Similarly, these can be expressed as:

$$(n-1)a_{n-1}+2nz_0a_n-(n+1)a_{n+1}+\overline{a_{-n+1}} = \sum_{m=-\infty}^{\infty} a_m A'_{nm}+ \sum_{m=-\infty}^{\infty} \overline{a_m} B'_{nm}+C'_n, \tag{10.60}$$

for $n = 1, 2, ...$, and where

$$\begin{aligned} A'_{nm} = &\frac{1}{2\pi \mathrm{i}} \int_{-\infty}^{\infty} \overline{Q}(-k,m)[I_1(k,n) + e^{2kh} I_2(k,n)]dk \\ &+ \frac{nh}{\pi} \int_{-\infty}^{\infty} [P(k,m) + T(k,m)] I_2(k,n+1)dk, \end{aligned} \tag{10.61}$$

$$\begin{aligned} B'_{nm} = &\frac{1}{2\pi \mathrm{i}} \int_{-\infty}^{\infty} \overline{P}(-k,m) I_1(k,n)dk \\ &+ \frac{1}{2\pi \mathrm{i}} \int_{-\infty}^{\infty} [\overline{P}(-k,m) + \overline{T}(-k,m)] e^{2kh} I_2(k,n)dk \\ &+ \frac{nh}{\pi} \int_{-\infty}^{\infty} Q(k,m) I_2(k,n+1)dk, \end{aligned} \tag{10.62}$$

$$\begin{aligned} C_n' = &\frac{1}{2\pi \mathrm{i}} \int_{-\infty}^{\infty} \overline{N}(-k)[I_1(k,n) + e^{2kh} I_2(k,n)]dk \\ &+ \frac{nh}{\pi} \int_{-\infty}^{\infty} N(k) I_2(k, n+1) dk \\ &+ \frac{1}{2\pi \mathrm{i}} [B(n) + C(n) - A(n)], \end{aligned} \tag{10.63}$$

with

$$A(n) \equiv \oint_{|z-z_0|} \left[\overline{f_s(z)} - \left(\overline{z_0} + \frac{1}{z - z_0} \right) f_s'(z) - g_s'(z) + \overline{U} - \mathrm{i}\Omega \frac{1}{z - z_0} \right] (z - z_0)^{-n} dz, \tag{10.64}$$

Conditions (10.60) together with their complex conjugates are added to the linear system.

Conditions at $k = 0$: We must require

$$L(0) = L'(0) = L''(0) = L'''(0) = 0, \tag{10.65}$$

with $L(k)$ given by

$$L(k) \equiv 2khW(k) - (e^{2kh} - 1)\overline{W}(-k). \tag{10.66}$$

Note, however, that these would require computation of the first few terms in the Taylor expansion of $L(k)$ which is a complicated expression. To avoid this, the following equivalent conditions which can be computed numerically are added to the linear system:

$$\oint_{|k|=\epsilon} \frac{L(k)}{k^s} dk = 0, \quad \text{for } s = 1, 2, 3, 4, \tag{10.67}$$

where ϵ is a small constant.

The linear system consisting of (10.54) and (10.60) together with (10.67) and their complex conjugates is solved for $\{a_m | m \in \mathbb{Z}\}$ and the complex parameter λ (and their complex conjugates).

10.7 Computation of the mobility matrix

Once $\{a_m | m \in \mathbb{Z}\}$ and λ are computed, we can calculate all elements of the mobility matrix, i.e. forces and torque acting on the cylinder for given translational/angular velocities. The formulae for computing the forces and torque on the cylinder are the same to those found in the previous Chapter; they are given by

$$F = -8\pi\eta\lambda, \qquad T = 2\eta \,\mathrm{Re}\left[2\pi \mathrm{i} z_0 \lambda + \oint_{|z-z_0|=1} (z - z_0) g''(z) dz\right]. \tag{10.68}$$

To determine the mobility matrix, we consider, as previously, the following cylinder motions: (a) motion parallel to the channel wall, i.e. $\overline{U} = U$, $\Omega = 0$, (b) motion to/away from the channel walls, i.e. $\overline{U} = -U$, $\Omega = 0$ and (c) pure rotation, i.e. $U = 0$, $\Omega \neq 0$. Our results show agreement to the results obtained by Jeong & Jang [58] for these three different cylinder motions. In addition, if the cylinder is placed near the lower channel wall and the upper boundary is located at a large distance h away from the lower boundary, then the mobility matrix converges to Jeffrey & Onishi's [53] results for a translating and rotating cylinder above a wall.

10.8 Summary

We have presented a transform approach for solving a Stokes flow problem in a doubly connected circular domain. The problem considered was that of a translating and rotating cylinder in a channel. This problem was previously solved by Jeong & Jang [58] using Papkovich-Fadle eigenfunction expansion and a least square method. The idea of our transform approach was to consider the fluid region as being the intersection of two half-planes and the exterior of unit disc, write an appropriate integral representations for the unknown correction functions $\hat{f}(z)$, $\hat{g}'(z)$ and proceed to spectral analysis to determine the unknown boundary data and spectral functions. Our results were checked to Jeong & Jang's [58] and Jeffrey & Onishi's [53] (for large h) solutions.

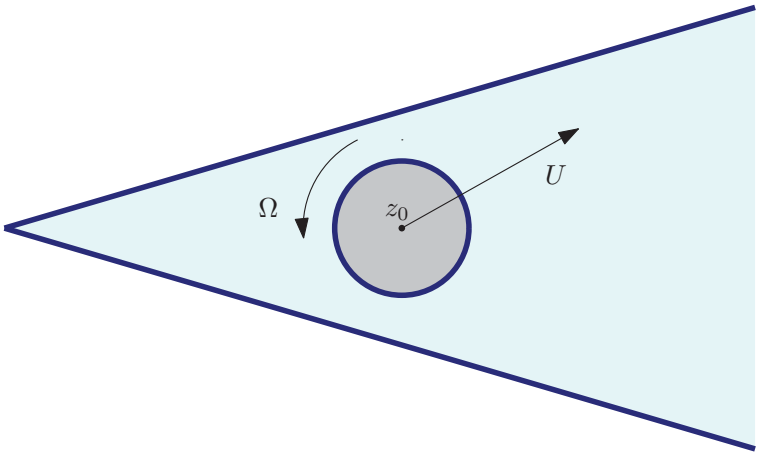

Figure 10.2: A translating and rotating cylinder centred at z_0 in a wedge geometry.

An interesting further application of our transform approach would be to consider a translating and rotating cylinder in a wedge, as illustrated in Figure 10.2 and analyze the problem using Mellin tranforms. We mention the work by Kim [66] who considered a cylinder located and translating along the centre-line of the wedge and computed the drag and the velocity field of the cylinder using an approximation technique.

Chapter 11

Conclusion

In this thesis we have presented a transform approach for solving biharmonic boundary value problems and shown its implementation in various Stokes flow problems in polygonal and circular domains. Specifically, we analyzed problems in simply- and multiply-connected circular domains previously solved using other techniques and presented a systematic approach to solve them. It should be noted that similar ideas can be used to solve problems in plane elasticity, since the associate stress field also satisfies the biharmonic equation. Our approach was based on the Unified transform method (Fokas [38, 39]). Fokas & Kapaev [42, 43] presented a transform method for solving Laplace's equation in polygonal domains. Recently, Crowdy [18] has presented an alternative derivation of the associated transform pairs for Laplace's equation in polygonal domains and has extended the method to circular domains. Our analysis in this thesis follows the latter work.

We firstly showed how to use our transform approach to solve boundary value problems in the half-plane; we showed how to solve the problem of a point singularity above a no-slip wall and above a wall with mixed boundary conditions. In the first case, we were able to retrieve the exact solution which can be found using a method of images approach. In the second case, we analyzed the problem in the half-plane subject to mixed boundary conditions along the real axis: no-slip along the negative real axis and no-shear stress along the positive one and solved this problem using the transform method for polygonal domains and Riemann-Hilbert problem techniques along the real axis.

In Chapter 5, we solved two mixed-type boundary value problems which were previously solved using the Wiener-Hopf technique by Luchini *et al.* [78] and Jeong [54]. The model problems involved a shear flow past a periodic array of semi-infinite flat plates: if the shear flow was longitudinal, the boundary value problem was for a harmonic field; if the shear flow was transverse a biharmonic field was relevant. The idea of our transform approach for these Wiener-Hopf problems was, firstly, to split the domain into sub-polygons (semi-strips) and solve each sub-problem separately using the transform method for polygonal domains. Then we analyzed the boundary conditions by performing spectral analysis and imposing continuity conditions across the common edge. The analysis of spectral relations provided conditions at distinct points in the spectral k-plane satisfied by a reduced set of spectral functions (those related to the edge of finite length). These conditions were sufficient to determine the unknown boundary data. Importantly, we used an appropriate function representation for the unknown boundary data on the edge of finite length which accounted for the square-root singularities associated with points where boundary conditions changed type. A linear system was solved for the unknown coefficients of the series expansion(s) and slip length λ. Once this was solved, all the spectral functions followed by back-substitution into the spectral relations.

Next, we analyzed the problem of a periodic array of point stresslets in a two-dimensional channel geometry. The key idea of our transform approach was again to obtain conditions at some special points in the spectral k-plane satisfied by a reduced number of spectral functions. These conditions were found by performing spectral analysis of the boundary and periodicity conditions and analyzing the obtained relations between spectral functions. By exploiting the analyticity of the spectral functions, we obtained conditions on the spectral functions associated to one of the vertical 'boundaries' of the period window. Using series expansions to represent the unknown boundary data on that edge, we showed that the set of conditions obtained was sufficient to determine the solution.

In Chapter 7, we discussed how Stokes flow problems in more complex channel geometries can be solved by decomposing the problem domain into semi-strips and rectangles, simi-

lar to problems presented in Chapter 5 and 6. In summary, the main steps to be followed when solving problems in polygonal domains are: (a) domain splitting into subproblems which can be analysed using the transform method for polygonal domains, (b) analysis of the boundary and continuity conditions, (c) spectral analysis to obtain information on a reduced set of spectral functions and (d) solution scheme and function representation to form linear systems which can be easily solved numerically.

In Chapters 8-10, we analyzed problems in circular domains; whose boundaries consisted of a combination of straight and circular edges, First, we solved a problem previously analyzed by Davis & O'Neill [30]. This concerned a stagnation point flow past a semicircular ridge. The idea of our transform approach was to consider the fluid region as being the intersection of the upper half-plane and the exterior of the unit disc centred at the origin, write an appropriate integral representations for the unknown correction functions $\hat{f}(z)$, $\hat{g}'(z)$ and proceed to spectral analysis to determine the unknown boundary data and spectral functions. Our method was checked against Davis & O'Neill's [30] solution.

Next, we solved the problem of a translating and rotating cylinder near a wall, previously solved by Jeffrey & Onishi [53]. The idea of our transform approach was to consider the fluid region as being the intersection of the upper half-plane and the exterior of unit disc, write an appropriate integral representations for the unknown correction functions $\hat{f}(z)$, $\hat{g}'(z)$ and proceed to spectral analysis to determine the unknown boundary data and spectral functions. Our method was checked against Jeffrey & Onishi's [53] solution (Crowdy [14]) and results were found to be in good agreement. Finally, we considered the problem of a translating and rotating cylinder in a channel geometry. Following similar steps as previously, we obtained the unknown boundary data and checked our results to Jeong & Jang's [58] and Jeffrey & Onishi's [53] solutions.

An important step of our transform approach was the numerical part and the choice of the basis expansion to represent unknown boundary data along edges of finite length. Other studies where numerical methods were used to solve problems using the Unified transform method include the study by Smitheman *et al.* [100] who introduced a spectral collocation

method in which a spectral analysis of the boundary conditions and use of the global relations gives a linear system to determine the unknown boundary data. They found that the efficacy of their numerical scheme was related to the basis choice (Fourier, Chebyshev etc.) used to represent the unknown boundary data. Fornberg & Flyer [46] presented an alternative numerical approach based on Legendre expansions of the unknown boundary data on polygonal boundary segments. More recently, Hashemzadeh, Fokas & Smitheman [49] proposed a numerical technique for linear elliptic partial differential equations in bounded polygonal domains and gave formulae for best choosing the collocation k-points for which to evaluate the global relations.

In this thesis, we have used different basis expansions to represent unknown boundary data: Chebyshev-like expansions (Chapter 5), Fourier (Chapter 6), Chebyshev (Chapter 8) and Laurent series expansions (Chapters 9-10). We conclude by proposing an empirical rule for choosing the basis expansion when solving a biharmonic boundary value problem; if the unknown boundary data is a periodic function or if the Goursat functions are singularity-free at the endpoints, then Fourier type basis should be chosen (Chapter 6). If there is a known singularity structure at the endpoints which can be parametrized as done in Chapter 5, then a Chebyshev-like expansion should be used. If the unknown boundary data must be represented along circular boundaries, then Laurent series expansions should be used. Finally, if the singularity structure at the endpoints is complex (e.g. formation of Moffatt eddies near corners [85]), then a Chebyshev basis expansion should be used.

The aim of this thesis was to present a general and systematic approach for solving biharmonic boundary value problems in polygonal and circular domains. The main steps of our transform approach were: domain splitting (if required) and transform representation in each domain, analysis of the boundary conditions, spectral analysis and solution scheme and function representation. A number of Stokes flow and plane elasticity problems which can be solved using our transform method (following the main steps stated above) have been presented at the end of each chapter.

Appendix A

Spectral representation of the Weierstrass $\mathcal{P}$-function

In this appendix, we present our transform approach for polygonal domains to solve a problem in a doubly-period domain. The problem considered concerns the Weierstrass $\mathcal{P}$-function (Abramowitz & Stegun [5]). Our aim is to show that our transform approach can also be used to solve problems in doubly-periodic domains, as well as to see how the doubly-periodicity nature of the problem provides conditions between the spectral functions which can be used to solve the problem.

Although the problem presented in this appendix is not a biharmonic boundary value problem, it is expected that similar ideas can be used to solve doubly-periodic biharmonic boundary value problems - for example, to find spectral representations for doubly-periodic arrays of Stokes flow singularities.

A.1 The Weierstrass $\mathcal{P}$-function

The Weierstrass $\mathcal{P}$-function (Abramowitz & Stegun [5]) is a doubly-periodic and meromorphic function with second-order poles at points $z = z_0 + nl + \mathrm{i}mh$, $n, m \in \mathbb{Z}$ with $l, h > 0$, where z_0 is in the interior of the period rectangle shown in Figure A.1. If we denote it by

$f(z)$, then we can write

$$f(z) = \frac{1}{(z - z_0)^2} + \hat{f}(z), \tag{A.1}$$

where $\hat{f}(z)$ is analytic in the period rectangle and which must ensure that $f(z)$ has the following properties

$$f(z + l) = f(z), \qquad f(z + \mathrm{i}h) = f(z). \tag{A.2}$$

In the following subsections, we will show that the analytic correction function $\hat{f}(z)$ can be found using our transform approach for polygonal domains.

A.2 Problem formulation and solution

Consider a period rectangle $x \in [0, l]$ and $y \in [0, h]$ as shown in Figure A.1.

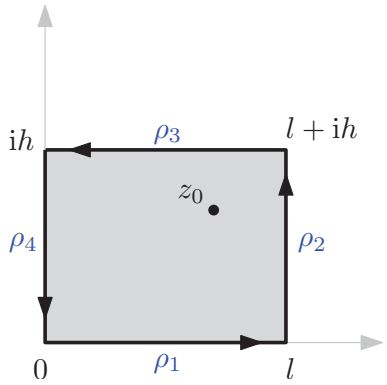

Figure A.1: Schematic of a period window and associated spectral functions.

Let

$$f(z) = \frac{1}{(z - z_0)^2} + \hat{f}(z), \tag{A.3}$$

where $\hat{f}(z)$ is to be determined so that $f(z)$ is a doubly periodic function with periods l and h:

$$f(z + l) = f(z), \qquad f(z + \mathrm{i}h) = f(z). \tag{A.4}$$

We only expect to determine $\hat{f}(z)$ up to an arbitrary constant since it is clear that any con-

stant can be added to $\hat{f}(z)$ and (A.4) will still hold.

Transform representation: We can write the following integral representation for $\hat{f}(z)$:

$$\hat{f}(z) = \frac{1}{2\pi}\left[\int_0^{\infty} \rho_1(k)e^{\mathrm{i}kz}dk + \int_0^{-\mathrm{i}\infty} \rho_2(k)e^{\mathrm{i}kz}dk + \int_0^{-\infty} \rho_3(k)e^{\mathrm{i}kz}dk + \int_0^{\mathrm{i}\infty} \rho_4(k)e^{\mathrm{i}kz}dk\right], \tag{A.5}$$

where $\rho_j(k)$, $j = 1, 2, 3, 4$ are the spectral functions defined by

$$\begin{aligned}
\rho_1(k) &= \int_0^{l} \hat{f}(z)e^{-\mathrm{i}kz}dz, \\
\rho_2(k) &= \int_l^{l+\mathrm{i}h} \hat{f}(z)e^{-\mathrm{i}kz}dz, \\
\rho_3(k) &= \int_{l+\mathrm{i}h}^{\mathrm{i}h} \hat{f}(z)e^{-\mathrm{i}kz}dz, \\
\rho_4(k) &= \int_{\mathrm{i}h}^{0} \hat{f}(z)e^{-\mathrm{i}kz}dz.
\end{aligned} \tag{A.6}$$

Spectral analysis: We integrate the x-periodicity condition along $-L_4$ we find

$$\int_0^{\mathrm{i}h} e^{-\mathrm{i}kz} f(z+l)dz = \int_0^{\mathrm{i}h} e^{-\mathrm{i}kz} f(z)dz \tag{A.7}$$

which can be rewritten as

$$\int_0^{\mathrm{i}h} e^{-\mathrm{i}kz}\left[\frac{1}{(z+l-z_0)^2} - \frac{1}{(z-z_0)^2}\right]dz = \int_0^{\mathrm{i}h} e^{-\mathrm{i}kz}[\hat{f}(z) - \hat{f}(z+l)]dz. \tag{A.8}$$

But

$$\int_0^{\mathrm{i}h} e^{-\mathrm{i}kz}\hat{f}(z+l)dz = \int_l^{l+\mathrm{i}h} e^{-\mathrm{i}k(u-l)}\hat{f}(u)du = e^{\mathrm{i}kl}\rho_2(k), \tag{A.9}$$

where we have made the substitution $u = z + l$. Therefore defining

$$R_1(k) \equiv \int_0^{\mathrm{i}h} e^{-\mathrm{i}kz}\left[\frac{1}{(z+l-z_0)^2} - \frac{1}{(z-z_0)^2}\right]dz, \tag{A.10}$$

then (A.8) is

$$-\rho_4(k) - e^{\mathrm{i}kl}\rho_2(k) = R_1(k). \tag{A.11}$$

Similarly if we integrate the y-periodicity condition along L_1 we find

$$\int_0^l e^{-\mathrm{i}kz}[\hat{f}(z+\mathrm{i}h)-\hat{f}(z)]dz = R_2(k), \tag{A.12}$$

where

$$R_2(k) \equiv \int_0^l e^{-\mathrm{i}kz}\left[\frac{1}{(z-z_0)^2}-\frac{1}{(z+\mathrm{i}h-z_0)^2}\right]dz. \tag{A.13}$$

But

$$\int_0^l e^{-\mathrm{i}kz}\hat{f}(z+\mathrm{i}h)dz = \int_{\mathrm{i}h}^{l+\mathrm{i}h} e^{-\mathrm{i}k(u-\mathrm{i}h)}\hat{f}(u)du = -e^{-kh}\rho_3(k), \tag{A.14}$$

where we have made the substitution $u = z + \mathrm{i}h$. Hence

$$-\rho_1(k) - e^{-kh}\rho_3(k) = R_2(k). \tag{A.15}$$

Global relation:

$$\rho_1(k)+\rho_2(k)+\rho_3(k)+\rho_4(k) = 0, \qquad k \in \mathbb{C}. \tag{A.16}$$

Solution scheme: Relations (A.11) and (A.15) imply that

$$\rho_4(k) = -R_1(k) - e^{\mathrm{i}kl}\rho_2(k), \qquad \rho_3(k) = -R_2(k)e^{kh} - \rho_1(k)e^{kh}, \tag{A.17}$$

and on substitution of these relations into (A.16) we find

$$\rho_1(k)[1-e^{kh}] + \rho_2(k)[1-e^{\mathrm{i}kl}] = R_1(k) + R_2(k)e^{kh}. \tag{A.18}$$

Now let $\{k_n\}$ denote all the non-zero solutions of

$$1 - e^{\mathrm{i}kl} = 0, \tag{A.19}$$

namely,

$$k_n = \frac{2n\pi}{l}, \qquad n \in \mathbb{Z}/\{0\}. \tag{A.20}$$

Then, from (A.18), we find

$$\rho_1(k_n) = G_n, \tag{A.21}$$

where

$$G_n \equiv \frac{R_1(k_n) + R_2(k_n)e^{k_n h}}{1 - e^{k_n h}}. \tag{A.22}$$

However

$$\rho_1(k_n) = \int_0^l \hat{f}(z)e^{-\mathrm{i}k_n z}dz = \int_0^l \hat{f}(z)e^{-\mathrm{i}2\pi nz/l}dz, \tag{A.23}$$

implying

$$\int_0^l \hat{f}(z)e^{-2n\pi\mathrm{i}z/l}dz = G_n, \qquad n \in \mathbb{Z}/\{0\}. \tag{A.24}$$

We write

$$\hat{f}(z) = \alpha z + \frac{1}{l}\sum_{m\neq 0} C_m e^{2m\pi\mathrm{i}z/l} + a_0. \tag{A.25}$$

Here a_0 is some undetermined constant which we can, without loss of generality, take to be zero.

Note: In general, the correction function $\hat{f}(z)$ can be defined as

$$\hat{f}(z) = g(z) + \frac{1}{l}\sum_{m\neq 0} C_m e^{2m\pi\mathrm{i}z/l}, \tag{A.26}$$

where $g(z)$ is an analytic function (e.g. $g(z) = \alpha e^z$) to model the 'jump' of the forcing term in $f(z)$ between points $z = 0$ and $z = l$.

Substitution of (A.25) into (A.24) gives

$$\int_0^l \left[\frac{1}{l}\sum_{m\neq 0} C_m e^{2m\pi\mathrm{i}z/l}\right] e^{-2n\pi\mathrm{i}z/l}dz + \alpha\int_0^l ze^{-2n\pi\mathrm{i}z/l}dz = G_n. \tag{A.27}$$

Using the orthogonality properties

$$\int_0^l e^{2\pi \mathrm{i}(m-n)z/l} dz = \begin{cases} l & \text{if } m = n, \\ 0 & \text{otherwise.} \end{cases} \tag{A.28}$$

expression (A.27) can be written as

$$C_n = G_n - \alpha H_n, \qquad n \in \mathbb{Z}/\{0\}, \tag{A.29}$$

where

$$H_n \equiv \int_0^l z e^{-2n\pi \mathrm{i}z/l} dz = \frac{\mathrm{i}l^2}{2n\pi}. \tag{A.30}$$

In addition, constant α can be found explicitly using the x-periodicity of $f(z)$; using that $f(0) = f(l)$, we find

$$\alpha = \frac{1}{l}\left[\frac{1}{z_0^2} - \frac{1}{(l-z_0)^2}\right]. \tag{A.31}$$

Therefore, coefficients $\{C_n, n \in \mathbb{Z}/\{0\}\}$ defined by (A.29) are expressed in terms of known quantities.

It follows that $\rho_1(k)$ is now known:

$$\begin{aligned} \rho_1(k) &= \int_0^l \left[\frac{1}{l}\sum_{m\neq 0} C_m e^{2m\pi \mathrm{i}z/l}\right] e^{-\mathrm{i}kz} dz + \alpha \int_0^l z e^{-\mathrm{i}kz} dz, \\ &= \sum_{m\neq 0} \mathrm{i}C_m \left[\frac{1-e^{-\mathrm{i}kl}}{2m\pi - kl}\right] + \alpha\left[\frac{\mathrm{i}l}{k}e^{-\mathrm{i}kl} + \frac{1}{k^2}(e^{-\mathrm{i}kl} - 1)\right]. \end{aligned} \tag{A.32}$$

With $\rho_1(k)$ determined, $\rho_2(k)$ follows from (A.18) while $\rho_3(k)$ and $\rho_4(k)$ follow from (A.17). Hence $\hat{f}(z)$ can be computed using (A.5) and therefore $f(z)$ can be found.

A.3 Alternative solution

We now present an alternative derivation which is based on analytic function theory; this will provide a check of our transform approach solution.

Consider the conformal mapping

$$z(\zeta) = -\frac{\mathrm{i}l}{2\pi}\log\zeta, \tag{A.33}$$

which transplants the annulus $\rho < |\zeta| < 1$ with $\rho = e^{-2\pi h/l}$ in a parametric ζ-plane to a period rectangle in the physical z-plane occupying the region

$$0 \le x \le l, \qquad 0 \le y \le h, \tag{A.34}$$

as illustrated in Figure A.2.

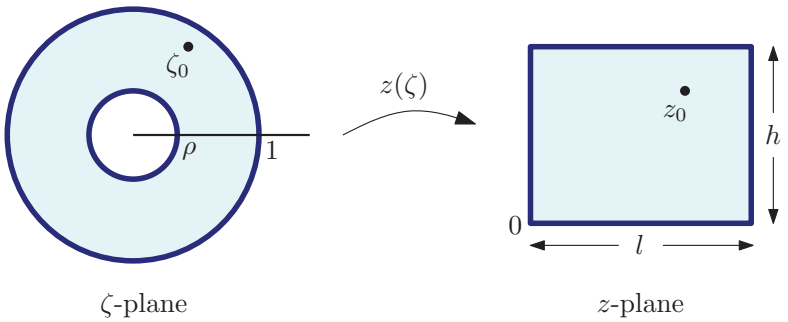

Figure A.2: Conformal mapping from the annulus $\rho < |\zeta| < 1$ in ζ-plane to the period rectangle in the physical z-plane occupying the region $0 \le x \le l$, $0 \le y \le h$.

Our aim is to find analytical expression for the Weierstrass $\mathcal{P}$-function in terms of variable ζ using analytic function theory. If required to re-express the solution in terms of z, then we can use the inverse mapping of (A.33) which is given by

$$\zeta = e^{2\pi \mathrm{i}z/l}. \tag{A.35}$$

Next, we write

$$F(\zeta) \equiv f(z(\zeta)), \tag{A.36}$$

to represent the Weierstrass $\mathcal{P}$-function which is a doubly-periodic, meromorphic function with second-order poles at points $z = z_0 + nl + \mathrm{i}mh$, $n, m \in \mathbb{Z}$ with $l, h > 0$, where z_0 is in the interior of the period rectangle shown in Figure A.2. Next, we write $z_0 = z(\zeta_0)$ and using the inverse mapping, we have

$$\zeta_0 = e^{2\pi \mathrm{i} z_0/l}. \tag{A.37}$$

Next, we introduce the Schottky-Klein prime function associated with the annulus $\rho < |\zeta| < 1$ (a detailed review of associated analytic function theory is given in Crowdy [**?**]):

$$P(\zeta, \rho) \equiv (1 - \zeta) \prod_{n=1}^{\infty} (1 - \rho^n \zeta)(1 - \rho^n/\zeta), \tag{A.38}$$

which is a convergent infinite product expansion. It can be seen from this representation that, $P(\zeta, \rho)$ has simple zeros at $\zeta = \rho^n$, $n \in \mathbb{Z}$. We also define

$$K(\zeta, \rho) = \frac{\zeta P_\zeta(\zeta, \rho)}{P(\zeta, \rho)}, \tag{A.39}$$

which is related to the logarithmic derivative of $P(\zeta, \rho)$ and function $L(\zeta, \rho)$:

$$L(\zeta, \rho) = \zeta K_\zeta(\zeta, \rho). \tag{A.40}$$

As we will see, function $L(\zeta, \rho)$ will be used to construct the representation for the Weierstrass $\mathcal{P}$-function. It can be shown that, as $\zeta \to \zeta_0$,

$$L(\zeta/\zeta_0, \rho) \sim -\frac{\zeta_0^2}{(\zeta - \zeta_0)^2} - \frac{\zeta_0}{\zeta - \zeta_0}. \tag{A.41}$$

As a function of z, $L(\zeta/\zeta_0, \rho)$ has a double-order pole at z_0. Using Taylor expansions, we can write

$$z - z_0 = -\frac{\mathrm{i}l}{2\pi\zeta_0}(\zeta - \zeta_0) + ..., \quad \text{as } \zeta \to \zeta_0, \tag{A.42}$$

which can be used in (A.41) to give

$$L(\zeta/\zeta_0,\rho) \sim -\zeta_0^2 \left[-\frac{\mathrm{i}l}{2\pi\zeta_0}\right]^2 \frac{1}{(z-z_0)^2}, \quad \text{as } z \to z_0. \tag{A.43}$$

Finally, using (A.43), we can write

$$F(\zeta) = \left(\frac{2\pi}{l}\right)^2 L(\zeta/\zeta_0,\rho) + c, \tag{A.44}$$

for some additive constant c. This is an alternative (and rapidly convergent) representation of the Weierstrass $\mathcal{P}$-function.

A.4 Comparison of the two methods

We have numerically checked the solutions found using the two methods (transform approach and function theory) and results were the same to within an accuracy of $\mathcal{O}(10^{-5})$ of each other for moderate truncation parameters (e.g. in our transform approach, we take $dk = 0.01$, $\infty = 10$). Our transform approach solution converged to the rapidly convergent function theoretic solution (A.44) as we increased the integration steps and other parameters when numerically evaluating the solution (A.5).

A.5 Summary

In this appendix, we presented a spectral representation of the Weierstrass $\mathcal{P}$-function using our transform approach for polygonal domains.We showed that our transform approach can also be used to solve problems in doubly-periodic domains. Our results were checked against an alternative (and rapidly convergent) representation of the Weierstrass $\mathcal{P}$-function found using analytic function theory. Results were found to be in good agreement. It is expected that similar ideas can be used to solve doubly-periodic biharmonic boundary value problems.

Appendix B

Calculation of the torque on a cylinder

In this appendix, we present a derivation of the expression for the torque on a cylinder given by (9.56). The torque on a cylinder centred at z_0 with boundary ∂D is given by

$$T = \text{Im}\left[2\eta\text{i}\oint_{\partial D}(\overline{z}-\overline{z_0})\frac{dH}{ds}ds\right] = \text{Im}\left[2\eta\text{i}\oint_{\partial D}(\overline{z}-\overline{z_0})dH\right], \tag{B.1}$$

where $H \equiv H(z)$ is given by (3.38) (definition was presented in Chapter 3). On integration by parts, this can be written as

$$\begin{aligned} T &= \text{Im}\left[2\eta\text{i}H(\overline{z}-\overline{z_0})\right]_{\partial D} - \text{Im}\left[2\eta\text{i}\oint_{\partial D}Hd\overline{z}\right] \\ &= \eta\left[H(\overline{z}-\overline{z_0})+\overline{H}(z-z_0)\right]_{\partial D} - \text{Im}\left[2\eta\text{i}\oint_{\partial D}Hd\overline{z}\right], \end{aligned} \tag{B.2}$$

where the square brackets denote the change in the quantity they contain on traversing ∂D. Using that

$$H(z,\overline{z}) \equiv f(z) + z\overline{f'(z)} + \overline{g'(z)}, \tag{B.3}$$

we find, after some algebra, that expression (B.2) can be simplified to

$$T = 2\eta\,\text{Re}\left[\oint_{\partial D}(z-z_0)g''(z)dz\right] - \eta\left[\oint_{\partial D}\overline{z_0}df + z_0d\overline{f}\right]. \tag{B.4}$$

For the translating and rotating cylinder of unit radius presented in Chapters 9 and 10,

function $f(z)$ was represented by

$$f(z) = \lambda \log(z - z_0) + \text{single-valued components}, \tag{B.5}$$

which means that expression (B.4) for a cylinder of unit radius centred at z_0 can further be simplified to

$$T = 2\eta \,\text{Re}\left[2\pi \text{i} z_0 \lambda + \oint_{|z-z_0|=1} (z - z_0) g''(z) dz\right]. \tag{B.6}$$

References

[1] M.J. Ablowitz & A.S. Fokas, Complex variables, Cambridge University Press, (1997).

[2] I.D. Abrahams, The application of Padé approximants to Wiener-Hopf factorization, *IMA J. Appl. Math.*, **65**, 257–281, (2000).

[3] I.D. Abrahams, On the application of the Wiener-Hopf technique to problems in dynamic elasticity, *Wave Motion*, **36**, 311–333, (2002).

[4] I.D. Abrahams, A.M.J. Davis, S.G. Llewellyn Smith, Asymmetric channel divider in Stokes flow, *SIAM J. Appl. Maths*, **68** (5), 1439-1463, (2008).

[5] M. Abramowitz & I.A. Stegun, Handbook of mathematical functions, Dover, (1964).

[6] A. Atsumi, Stress concentrations in a strip under tension and containing an infinite row of semicircular notches, *Q.. J. Mech. & Appl. Math.*, **11** (4):478, (1958).

[7] A. Atsumi, Stresses in a plate under tension and containing an infinite row of semicircular notches, *Z.A.M.P.*, **8**, 466-477, (1957).

[8] J.R. Blake, A note on the image system for a Stokeslet in a no-slip boundary, *Proc. Camb. Phil. Soc.*, **70**, 303, (1971).

[9] V.T. Buchwald, Eigenfunctions of plane elastostatics I. The strip, *Proc. R. Soc. Lond. A*, **277**, (1964).

[10] V.T. Buchwald & H.E. Doran, Eigenfunctions of plane elastostatics II. Mixed boundary value problems of the strip, *Proc. R. Soc. Lond. A*, **284**, (1965).

[11] G. Carrier, M. Krook & C.E. Pearson,Functions of a complex variable: theory and technique, Classics in Applied Mathematics, SIAM, Philadelphia, (2005).

[12] A. Charalambopoulos, G. Dassios & A.S. Fokas, Laplace's equation in the exterior of a convex polygon. The equilateral triangle, *Q. Appl. Math.*, **68**, 645660, (2010).

[13] D.G. Crowdy, Frictional slip lengths for unidirectional superhydrophobic grooved surfaces, *Phys. Fluids*, **23**, 072001, (2011).

[14] D.G. Crowdy, Treadmilling swimmers near a no-slip wall at low Reynolds number, *Int. J. Nonlin. Mech.*, **46**, 577-585, (2011).

[15] D.G. Crowdy, Conformal slit maps in applied mathematics, *ANZIAM Journal*, **53**(3), 171–189, (2012).

[16] D.G. Crowdy, Exact solutions for cylindrical "slip-stick" Janus swimmers in Stokes flow, *J. Fluid Mech.*, **719**, R2, (2013).

[17] D.G. Crowdy, Surfactant-induced stagnant zones in the Jeong-Moffatt free surface Stokes flow problem, *Phys. Fluids.*, **25**, 092104, (2013).

[18] D.G. Crowdy, Fourier-Mellin transforms for circular domains, *Comput. Methods Funct. Theory*, (2015).

[19] D.G. Crowdy, A transform method for Laplace's equation in multiply connected circular domains, *IMA J. Appl. Math.*, (2015).

[20] D.G. Crowdy & A.M.J. Davis, Stokes flow singularities in a two-dimensional channel: a novel transform approach with application to microswimming, *Proc. R. Soc. A*, **469**, 20130198, (2013).

[21] D.G. Crowdy & A.S. Fokas, Explicit integral solutions for the plane elastostatic semi-strip, *Proc. R. Soc. Lond. A*, **460**, 1285-1310, (2004).

[22] D.G. Crowdy & E. Luca, Solving Wiener-Hopf problems without kernel factorization, *Proc. Roy. Soc. A*, **470**, 20140304, (2014).

[23] D.G. Crowdy & Y. Or, Two-dimensional point singularity model of a low-Reynolds-number swimmer near a wall, *Phys. Rev. E*, **81**, 036313, (2010).

[24] D.G. Crowdy & O. Samson, Stokes flows past gaps in a wall, *Proc. R. Soc. A*, **466**, 2727-2746, (2010).

[25] A.M.J. Davis, Periodic blocking in parallel shear or channel flow at low Reynolds number, *Phys. Fluids A*, **5**, 800, (1993).

[26] A.M.J. Davis & D.G. Crowdy, Matched asymptotics for a treadmilling low-Reynolds-number swimmer near a wall, *Q. J. Mechanics Appl. Math.*, **66** (1), 53-73, (2013).

[27] A.M.J. Davis & D.G. Crowdy, Stresslet asymptotics for a treadmilling swimmer near a two-dimensional corner: hydrodynamic bound states, *Proc. Roy. Soc. A*, **468**, 3765-3783, (2012).

[28] A.M.J. Davis & E. Lauga, Geometric transition in friction for flow over a bubble mattress, *Phys. Fluids*, **21**, 011701, (2009).

[29] A.M.J. Davis & M.E. O'Neill, Separation in a slow linear shear flow past a cylinder and a plane, *J. Fluid Mech.*, **81**, 551-564, (1977).

[30] A.M.J. Davis & M.E. O'Neill, Separation in a Stokes flow past a plane with a cylindrical ridge or trough, *Q. J. Mech. Appl. Math.*, **30** (4), 355-368, (1977).

[31] B. Deconinck, B. Pelloni & N.E. Sheils, Non-steady-state heat condition in composite walls, *Proc. Roy. Soc. A*, **470**, 20130605, (2014).

[32] B. Deconinck, T. Trogdon & V. Vasan, The method of Fokas for solving linear partial differential equations, *SIAM Rev.*, **56** (1), 159-186, (2014).

[33] M. Dimakos & A.S. Fokas, The Poisson and the biharmonic equations in the interior of a convex polygon, *Stud. Appl. Math.*, **134** (4), 456-498, (2015).

[34] J.M. Dorrepaal & M.E. O'Neill, The existence of free eddies in a streaming Stokes flow, *Q. J. Mech. & Appl. Math.*, **32** (95), (1979).

[35] T.A. Driscoll & L.N. Trefethen, Schwarz-Christoffel mapping, Cambridge University Press, Cambridge, (2002).

[36] H. Ebendorff-Heidepriem & T.M. Monro, Extrusion of complex preforms for microstructured optical fibers, *Opt. Express*, **15** (23), 15086-15092, (2007).

[37] A.H. England, Complex variable methods in elasticity, Wiley-Interscience, New York, (1971).

[38] A.S. Fokas, A unified approach to boundary value problems, CBMS-NSF Regional Conference Series in Applied Mathematics, No 78, SIAM, Philadelphia, (2008).

[39] A.S. Fokas, A unified transform method for solving linear and certain nonlinear PDEs, *Proc. Roy. Soc. Lond. A*, **453**, 1411-1443, (1997).

[40] A.S. Fokas, N. Flyer, S.A. Smitheman & E.A. Spence, A semi-analytical numerical method for solving evolution and elliptic partial differential equations, *J. Comput. Appl. Math.*, **227**, 59-74, (2009).

[41] A.S. Fokas, A. Iserles & S.A. Smitheman, The unified method in polygonal domains via the explicit Fourier transform of Legendre polynomials, *preprint* (2013).

[42] A.S. Fokas & A.A. Kapaev, A Riemann-Hilbert approach to the Laplace equation, *J. Math. Anal. Appl.*, **251**, 770-804, (2000).

[43] A.S. Fokas & A.A. Kapaev, On a transform method for the Laplace equation in a convex polygon, *IMA J. Appl. Math.*, **68**, 1-55, (2003).

[44] A.S. Fokas & S.A. Smitheman, The Fourier transforms of the Chebyshev and Legendre polynomials, *preprint* (2012).

[45] A.S. Fokas & E.A. Spence, Synthesis, as opposed to separation, of variables, *SIAM Review*, **54**(2), 291–324, (2012).

[46] B. Fornberg & N. Flyer, A numerical implementation of Fokas boundary integral approach: Laplace's equation on a polygonal domain, *Proc. Roy. Soc. A*, **467**, 2983–3003, (2011).

[47] S.R. Fulton, A.S. Fokas & C.A. Xenophontos, An analytical method for linear elliptic PDEs and its numerical implementation, *J. Comput. Appl. Math.*, **167**, 465-483, (2004).

[48] J. Happel and H. Brenner, Low Reynolds number hydrodynamics, Prentice-Hall, New Jersey, (1965).

[49] P. Hashemzadeh, A.S. Fokas & S.A. Smitheman, A numerical technique for linear elliptic partial differential equations in polygonal domains, *Proc. Roy. Soc. A*, **471**, 20140747, (2015).

[50] H. Hasimoto, Periodic fundamental solution of the two-dimensional Stokes equations, *J. Phys. Soc. Jap.*, **78**, 074401, (2009).

[51] H. Hasimoto, On the periodic fundamental solutions of the Stokes equations and their application to viscous flow past a cubic array of spheres, *J. Fluid Mech.*, **5**, 317, (1959).

[52] T. Ishibasi, Stresses in a semi-infinite plate with a circular notch under uniform Tension, Memories, Faculty Engng. Igiyushu Imp. Univ. 9, No. 2, **131**, (1940).

[53] D.J. Jeffrey & Y. Onishi, The slow motion of a cylinder next to a plane wall, *Q. J. Mech. Appl. Math.*, **34** (2), 129-137, (1981).

[54] J-T. Jeong, Slip boundary condition on an idealized porous wall, *Phys. Fluids*, **13**(7), 1884–1890, (2001).

[55] J-T. Jeong, Slow viscous flow in a partitioned channel, *Phys. Fluids*, **13**, 1577, (2001).

[56] J-T. Jeong, Two-dimensional Stokes flow through a slit in a microchannel with slip, *J. Phys. Soc. Japan*, **75** (9), 094401, (2006).

[57] J-T. Jeong, Two-dimensional Stokes flow through a slit in a vertical plate on a plane wall, *J. Phys. Soc. Japan*, **67** (12), 4074-4079, (1998).

[58] J-T. Jeong & C-S. Jang, Slow motion of a circular cylinder in a plane Poiseuille flow in a microchannel, *Phys. Fluids*, **26**, 123104, (2014).

[59] J-T. Jeong & M-U. Kim, Slow viscous flow around an inclined fence on a plane, *J. Phys. Soc. Japan*, **52** (7), 2356-2363, (1983).

[60] J-T. Jeong & M-U. Kim, Slow viscous flow due to sliding of a semi-infinite plate over a plane, *J. Phys. Soc. Japan*, **54** (5), 1789-1799, (1985).

[61] J-T. Jeong & M-U. Kim, Two-dimensional slow viscous flow from a converging nozzle, *J. Phys. Soc. Japan*, **57** (3), 856-865, (1988).

[62] J-T. Jeong & C.-G. Park, Slow viscous flow past a lattice of equal flat plates, *J. Phys. Soc. Japan*, **66** (6), 1660-1667, (1997).

[63] J.-T. Jeong & S-H. Yoon, Two-dimensional Stokes flow around a circular cylinder in a microchannel, *J. Mech. Sci. Technol.*, **28** (2), 573-579, (2014).

[64] D.D. Joseph, The convergence of biorthogonal series for biharmonic and Stokes flow edge problems, Part I, *SIAM J. Appl. Math.*, **33**, 337-347, (1977).

[65] D.D. Joseph & L. Sturges, The convergence of biorthogonal series for biharmonic and Stokes flow edge problems, Part II, *SIAM J. Appl. Math.*, **34**, 7-26, (1978).

[66] M-U. Kim, Two-dimensional slow viscous flow due to the motion of a cylinder on the center-line of a wedge, *J. Phys. Soc. Japan*, **46** (6), 1929-1934, (1979).

[67] M-U. Kim & M.K. Chung, Two-dimensional slow viscous flow past a plate midway between an infinite channel, *J. Phys. Soc. Japan*, **53** (1), 156-166, (1984).

[68] H.J. Ko and J.-T. Jeong, Two-dimensional slow stagnation flow near a slit, *J. Phys. Soc. Japan*, **63** (8): 3288-3294, (1994).

[69] W.E. Langlois, Slow viscous flows, Macmillan, (1967).

[70] E. Lauga, M.P. Brenner & H.A. Stone, Microfluidics: The no-slip boundary condition, Handbook of Experimental Fluid Dynamics, Chapter 19, C. Tropea, A. Yarin, J. F. Foss (Eds.), Springer, (2007).

[71] E. Lauga & T.R. Powers, The hydrodynamics of swimming microorganisms, *Rep. Prog. Phys.*, **72**, 096601, (2009).

[72] E. Lauga & H. A. Stone, Effective slip in pressure-driven Stokes flow, *J. Fluid Mech.*, **489**, 55-77, (2003).

[73] J. Lawrie & I.D. Abrahams, A brief historical perspective of the Wiener-Hopf technique, *J. Eng. Math.*, **59**(4), 351–358, (2007).

[74] M.J. Leitman & P. Villaggio, An extension of the complex variable method in plane elasticity to domains with corners: a notch problem, *J. Elasticity*, **81**, 205-215, (2005).

[75] C.B. Ling, On the stresses in a notched plate under tension, *J. Math. Phys.*, **26** (4), 284, (1947).

[76] C.B. Ling, Stresses in a notched strip under tension, *J. Appl. Mech., Trans. A.S.M.E.*, **69**, A-275, (1947).

[77] C-B. Ling & C-M. Hsu, Stresses in a perforated wedge, Trans. ASME, Ser. E, *J. Appl. Mech.*, **40** (3), (1973).

[78] P. Luchini, F. Manzo & A. Pozzi, Resistance of a grooved surface to parallel flowand cross-flow, *J. Fluid Mech.*, **228**, 87–109, (1991).

[79] J. Marshall, Function theory in multiply connected domains and applications to fluid dynamics, Ph.D. Thesis, Imperial College London, (2005).

[80] F.G. Maunsell, Stresses in a notched plate under tension, *Phil. Mag.*, **27**, 765, (1936).

[81] V.V. Meleshko, Steady Stokes flow in a rectangular cavity, *Proc. Roy. Soc. A*, **452**, 1999-2022, (1996).

[82] V.V. Meleshko & A.M. Gomilko, Infinite systems for a biharmonic problem in a rectangle, *Proc. Roy. Soc. A*, **453**, 2139-2160, (1997).

[83] V.V. Meleshko & A.M. Gomilko, Two-dimensional Stokes flow in a semicircle, *Int. J. Fluid Mech. Research*, **27** (1), 56-61, (2000).

[84] T. Miyazaki & H. Hasimoto, Separation of creeping flow past two circular cylinders, *J. Phys. Soc. Japan*, **49** (4), 1611-1618, (1980).

[85] H.K. Moffatt, Viscous and resistive eddies near a sharp corner, *J. Fluid Mech.*, **18** (1), 1-18, (1964).

[86] N.I. Muskhelishvili, Some basic problems of the mathematical theory of elasticity, Springer, (1977).

[87] B. Noble, Methods based on the Wiener-Hopf technique,Pergamon Press, London, (1958).

[88] J.R. Philip, Flows satisfying mixed no-slip and no-shear conditions, *J. Appl. Math. Phys. (ZAMP)*, **23**, 353-372, (1972).

[89] C. Pozrikidis, Boundary integral and singularity methods for linearized viscous flows, Cambridge University Press, Cambridge, (1992).

[90] C. Pozrikidis, Computation of periodic Green's functions of Stokes flow, *J. Eng. Math.*, **30**, 79-96, (1996).

[91] V.S. Protsenko, On two mixed problems of antiplane strain of an elastic wedge with circular holes, *PMM*, U.S.S.R., **52** (5), 629-635, (1988).

[92] S. Richardson, A 'stick-slip' problem related to the motion of a free jet at low Reynolds numbers, *Proc. Camb. Phil. Soc.*, **67**, 477-489, (1970).

[93] S. Richardson, On the no-slip boundary condition, *J. Fluid Mech.*, **59** (4), 707-719, (1973).

[94] S. Richardson, The die swell phenomenon, *Rheol. Acta*, **9** (2), 193-199, (1970).

[95] O. Samson, Low-Reynolds-number swimming in complex environments, Ph.D. Thesis, Imperial College London, (2010).

[96] O. Sano & H. Hasimoto, The effect of two plane walls on the motion of small sphere in a viscous fluid, *J. Fluid Mech.*, **87**, 673-694, (1978).

[97] A. Setchi, A.J. Mestel, K.H. Parker & J.H. Siggers, Low-Reynolds-number flow through two-dimensional shunts, *J. Fluid Mech.*, **723**, 21-29, (2013).

[98] A. G. Sifalakis, A. S. Fokas, S. R. Fulton & Y. G. Saridakis, The generalized Dirichlet-Neumann map for linear elliptic PDEs and its numerical implementation, *J. Comput. Appl. Math.*, **219**, 9–34, (2008).

[99] S.H. Smith, Stokes flow past slits and holes, *Int. J. Multiphase Flow*, **13** (2), 219-231, (1987).

[100] S. A. Smitheman, E. A. Spence & A. S. Fokas, A spectral collocation method for the Laplace and modified Helmholtz equations in a convex polygon, *IMA J. Num. Anal.*, **30**, 1184-1205, (2010).

[101] J-S. Son & J-T. Jeong, Stokes flow through a microchannel with protuberances of staggered arrangement, *J. Comp. Fluids Eng.*, **20** (4), 109-115, (2015).

[102] D.A. Spence, A class of biharmonic end-strip problems arising in elasticity and Stokes flow, *IMA J. Appl. Math.*, **30**, 107-139, (1983).

[103] E.A. Spence, Boundary value problems for linear elliptic PDEs, Ph.D. thesis, University of Cambridge, Cambridge, (2010).

[104] H.A. Stone & A.D.T. Samuel, Propulsion of microorganisms by surface distortions, *Phys. Rev. Lett.*, **77** (19), 4102-4104, (1996).

[105] J.W. Swan & J.F. Brady, Particle motion between parallel walls: Hydrodynamics and simulation, *Phys. Fluids.*, **22**, 103301, (2010).

[106] J.W. Swan & J.F. Brady, Simulation of hydrodynamically interacting particles near a no-slip boundary, *Phys. Fluids.*, **19**, 113306, (2007).

[107] L.N. Trefethen & M. Embree, Spectra and pseudospectra: the behavior of nonnormal matrices and operators, Princeton University Press, Princeton, (2005).

[108] S.A. Trogdon & D.D. Joseph, The stick-slip problem for a round jet I. Large surface tension, *Rheol. Acta*, **19**, 404-420, (1980).

[109] S.A. Trogdon & D.D. Joseph, The stick-slip problem for a round jet II. Small surface tension, *Rheol. Acta*, **20**, 1-13 (1981).

[110] E.O. Tuck, Matching problems involving flows through small holes, *Advances in Appl. Mech.*, **15**, 89-158, (1975).

[111] C.Y. Wang, Stokes flow due to the sliding of a smooth plate over a slotted plate, *Eur. J. Mech. B-Fluids*, **20**, 651-656, (2001).

[112] C.Y. Wang, Stokes flow through a channel obstructed by horizontal cylinders, *Acta Mech.*, **157**, 213-221, (2002).

[113] C.Y. Wang, Stokes slip flow through a lattice of parallel plates, *Can. J. Chem. Eng.*, **88** (3), 335-339, (2010).

[114] E. Weinel, Die Spannungserh6hung durch Kreisbogenkerben, *Z. angew*, *Math. Mech.*, **21**, 228, (1941).

[115] N. Wiener & E. Hopf, Über eine klasse singulärer integralgleichungen,*Sem-Ber Preuss Akad Wiss*, **31**, 696–706, (1931).

[116] S.F. Yeung, The use of comple variables to obtain stresses in a notched plate under tension, *Applied Scientific Research*, A, **14**, 172-176, (1965).

[117] S.-H. Yoon & J.-T. Jeong, Stokes flow through a microchannel obstructed by a vertical plate, *Eur. J. Mech. B-Fluid*, **34**, 64-69, (2012).